THE DEVELOPMENT OF NON-CONTACT LASER AND EMAT ULTRASOUND MEASUREMENT SYSTEMS FOR HOT STEEL

being a thesis submitted for the degree of
Doctor of Philosophy at the University of Warwick

by

Md Supar Rohani
B. Sc.Hons. (M'sia.), M. Sc. (Brunel)

Department of Physics
University of Warwick
November 1996

Contents

Summary

Non-contact laser and EMAT ultrasound systems have been developed for ultrasound measurements on hot steel. The pulsed lasers are capable of generating wide bandwidth ultrasound pulses and the transduction is entirely remote. The EMATs operate in close vicinity to the metal testpiece and can be used for both generation and detection of ultrasound. EMATs require no special surface preparation of the steel samples and the performance may even be enhanced by the presence of oxides on the surface. The EMAT can be operated either using a permanent magnet (P-EMAT) or a pulsed field electromagnet (E-EMAT); the latter is capable of producing a magnetic field over 1Tesla and would allow the easy removal of the ferromagnetic debris from the EMAT face. The EMATs were water cooled to allow operation at elevated temperatures. The EMATs were used to generate shear waves and as the detector they were sensitive to both the shear and longitudinal waves. Both types of EMAT are capable of making ultrasound measurements on steel up to a temperature of about 800°C in pulse echo mode when the same EMAT was used for both generation and detection.

A water cooled E-EMAT was used as the receiver of laser generated ultrasound. The system operated in send-receive arrangement where the EMAT is positioned on the generation side and measurement can be made from a single side has been made up to a temperature of 1000°C. The measurement was carried out by using a Nd:YAG laser as the generator. The E-EMAT also has been used to receive ultrasound generated by a pulsed CO_2 laser and could make ultrasound measurements up to a temperature of about 800°C. Besides, the laser-EMAT system was also used for epicentral measurements at elevated temperatures.

Ultrasound measurements by a shear wave EMAT on ferromagnetic steel have been made using the shear wave arrivals in a range of temperature up to about 750°C where the EMAT is sensitive to both shear and longitudinal wave. Above this temperature however, ultrasound measurement was based on longitudinal wave arrivals as the EMAT is no longer sensitive to shear wave. At a temperature close to the Curie point, T_c, of the sample, enhancement of longitudinal wave occurs. This may correspond to the reorientation and redistribution of the magnetic flux in a thin ferromagnetic layer on the bulk paramagnetic sample due to the cooling effect caused by the water-cooled EMAT or may be due to volume magnetostriction. We have monitored the magnetisation of the sample at elevated temperature and noted that the magnetisation of the sample reduces rapidly to zero as the temperature increases and approaches the T_c. The cooling effect on hot samples caused by momentary contact with the water cooled EMATs was measured and shown to be minimal and superficial.

The laser-EMAT ultrasound system could be used for thickness measurement on hot steels provided the velocity is known as a function of temperature. A series of measurements was carried out on steel samples in the laboratory to determine this data. The technique produces no significant damage to steel and has the potential of being rapidly scanned to test hot moving metals on the production line.

Acknowledgements

I am very grateful and would like to convey my special thanks to my supervisor, Professor Stuart Palmer for his guidance, enthusiasm, advice and friendship throughout my stay in this university. My special thanks also to Dr. Chris Edwards for his untiring assistance, guidance and expert advice.

I am very grateful to the Universiti Teknologi Malaysia, Malaysia, for providing myself with the opportunity to continue my study and financial support. I would like to thank Mr. Trevor Knox and Mr. Barry Whittaker of British Steel Plc.; and Mr. Lewis Morgan and Mr. John Burd of British Gas Plc., for provision of samples and access to industrial sites. I would like to thank Dr.Duncan Billson, the group technician Mr. John Reed and the workshop technicians for their willingness to provide assistance. I would like to thank my colleagues both within and outside the Physics Department for making my stay enjoyable.

Special thanks to my wife and children for their patience and courage during my studies.

Declaration

The work presented in this thesis is my own work except where specified otherwise. The work was carried out in the Physics Department, University of Warwick in the period from December 1992 to November 1996. No part of this thesis has been submitted previously to the University of Warwick nor other academic institution for admission to a higher degree.

Figure Captions

Chapter-1

Figure-1.1: The main production route of primary steel products. (after Knox, [1994])

Figure-1.2: Nondestructive testing and evaluation used in steel processing.

Chapter-2

Figure-2.1: Stress-strain relation in a cubic sample subjected to stress in x-direction.

Figure-2.2: Ultrasound propagation at a plane boundary.

Chapter-3

Figure-3.1: The interaction of electromagnetic wave (laser beam) with metal.

Figure-3.2: Generation of thermoelastic ultrasound source on metal by laser.

Figure-3.3: Generation of longitudinal wave from a buried and a finite thickness of thermoelastic source.

Figure-3.4: Generation of an ablative ultrasound source on metal.

Figure-3.5: Lorentz force interaction between the static magnetic field and induced current and the generation of ultrasound.

Figure-3.6: Shear wave generation by a spiral coil EMAT

Figure-3.7: Longitudinal wave generation by spiral coil EMAT

Figure-3.8: Two dimensional model for detection of shear wave by EMAT.

Figure-3.9: The predicted magnetic field dependence of the acoustic wave amplitude in polycrystalline iron generated by EMAT and detected by piezoelectric transducer (after Thompson, [1978]).

Figure-3.10: The theoretical prediction of the magnetic field dependence of the magnetostriction-strain coefficient and skin depth in a polycrystalline iron, to estimate EMAT transduction efficiency (after Thompson, [1978]).

Chapter-4

Figure-4.1: Water cooled permanent magnet EMAT (P-EMAT)

Figure-4.2: Permanent magnet EMAT with steel returning path.

Figure-4.3: Schematic diagram of pulse echo measurement using a permanent magnet EMAT.

Figure-4.4: Reluctance considerations using an E-shape core electromagnet to estimate the current required to generate a magnetic field 1.25T in a 5mm air gap between its limbs and the steel sample. The cross section area of the centre limb is $10cm^2$ and $5cm^2$ on each outer limb.

Figure-4.5: Water cooled pulsed field electromagnetic EMAT (E-EMAT)

Figure-4.6: Signal output of the field sensing coil; (a)- represents ($d\Phi/dt$), (b)-the magnetic field intensity; generated by pulsed field electromagnet on mild steel.

Figure-4.7: Basic electromagnet driver circuit.

Figure-4.8: Schematic block diagram of pulsed electromagnet driver.

Figure-4.9: Triggering sequences of the electromagnet driver and other related equipment e.g, EMAT driver, and pulsed lasers. This equipment is triggered at the negative edge of the electromagnet driver pulse where the maximum magnetic field is present on the surface of the sample.

Figure-4.10: Schematic diagram of experimental set-up for non-contact ultrasound measurement using E-EMAT.

Figure-4.11: Schematic diagram of experimental set-up for non-contact ultrasound measurement using CO_2 laser generator and E-EMAT detector.

Figure-4.12: Schematic diagram of experimental set-up for non-contacting ultrasound measurement using Nd:YAG laser generator and E-EMAT detector.

Figure-4.13: Pulse echo shear wave waveforms in aluminium and mild steel generated and detected by both P-EMAT and E-EMAT.

Figure-4.14: Send-receive shear waveform in aluminium showing an anisotropy effect. The shear wave pulse splits as it progresses indicating two wave components propagating at different velocity. The waveform was generated by CO_2 laser and detected by E-EMAT.

Figure-4.15: Epicentral shear wave waveform in mild steel showing an anisotropy effect. The waveform was generated by a P-EMAT and detected by E-EMAT.

Figure-4.16: Stand-off dependence of the pulse echo shear wave amplitude generated by P-EMAT on mild steel and aluminium.

Figure-4.17: Effect of oxide layer (magnetite) on the shear wave transduction efficiency in mild steel by E-EMAT. (A)-Clean surface, (B)-thin magnetite layer

Figure-4.18: Effect of hydrated oxide layer (red rust) on shear wave transduction efficiency of an E-EMAT: (A)-clean surface, (B)-thin layer of hydrated oxide on a rough corroded surface, (C)-in a sectioned of mild steel pipe after sand blasting.

Chapter-5

Figure-6.2: Variation of EMAT pulse echo shear wave amplitude in aluminium and mild steel samples with the square of magnetic field intensity.

Figure-6.3: Effect of (A)-magnetite layer, (B)-water corrosion scale on the variation of the ultrasound amplitude versus B_o^2, excited by E-EMAT in mild steel.

Figure-6.4: Effect of magnetite layer on sample surface on the variation of shear wave amplitude versus B_o^2, in mild steel generated by E-EMAT.

Figure-6.5: Measured and the predicted surface wave amplitude versus B_o curve for polycrystalline iron generated by EMAT, (after Thompson, [1976])

Figure-6.6: Magnetostriction curve of iron (after Bozoroth, [1951]).

Figure-6.7: Schematic diagram of the experimental set up for ultrasound and sample temperature mesurements due to cooling in close contact with a water cooled E-EMAT.

Figure-6.8: Schematic diagram of the delay timer.

Figure-6.9: Delay timer and EMAT in measuring position.

Figure-6.10: Reduction of the sample surface temperatures after contact with a water cooled E-EMAT in a pre-set period.

Figure-6.11: Magnetisation-temperature curve of mild steel measured using E-EMAT .

Figure-6.12: Pulse echo ultrasound waveforms in mild steel (10.5mm thickness) at elevated temperatures generated by E-EMAT.

Figure-6.13: Temperature dependence of E-EMAT pulse echo amplitude at elevated temperatures in mild steel.

Figure-6.14: Temperature dependence of; (a)-the predicted magnetic susceptibility, (b) predicted ultrasound transduction efficiency due to the paraprocesses and (c)-measured longitudinal wave amplitude generated by E-EMAT on mild steel above the Curie point, T_c.

CHAPTER-1

INTRODUCTION

1.1 Background

The production of primary steel products involves several stages (Figure-1.1), starting with liquid steel in either a basic oxygen furnace or an electric arc furnace followed by casting into slabs, billets or bloom. The billets and blooms then undergo hot rolling through different types of mill to form rods, rails, seamless pipes or tubes and other long products. In the same manner the slabs are hot rolled to form plates of different thickness. Some of the plates also undergo cold rolling into sheets. The products then undergo different manufacturing processes such as welding, machining, heat treatment, coating and grinding to make the final finished product. To ensure the quality of the final product, a careful selection of the primary materials, control of fabrication and manufacturing processes are made by integrating the inspection equipment into the production processes. Defects can arise or be modified at each process stage. These could be inherent defects in the raw materials or be introduced during the processing. The defects can be either internal such as slag inclusions, porosity and laminations, or external such as surface breaking defects and incorrect dimensions.

1.2 Non Destructive Evaluation in Steel Making Industries

Inspections are normally carried out on the final product at the end of the production line just prior to despatch at or near ambient temperature using various standard non-destructive test and evaluation (NDE) methods (Figure-1.2). This includes physical measurement, visual and optical inspection for the surface defects, electromagnetic methods for the surface breaking defects and radiography and ultrasound methods for the internal defects. Tests have been done at higher temperature to study the metallurgical structure allowing a control of the manufacturing processes.

Ultrasound has now probably superseded many of the above mentioned NDE techniques and become one of the most widely used for thickness gauging, detection of defects and material characterisation in steel production. Conventionally ultrasound test equipment uses piezoelectric transducers for generation and detection of high frequency acoustic waves in the specimen under test. Piezoelectric materials used have included single crystal materials such as quartz or lithium niobate, or polycrystalline ceramics such as barium titanate or lead zirconate-titanate (PZT). The transducers may be operated in contact with the test specimen, using grease to ensure good acoustic transmission, or spaced from it with a fluid, generally water as the coupling agent. Generally, for detection of defects, the pulse echo method is used. Very short pulses of ultrasound are launched into the specimen and, if any defects are present, a small part of the energy will be reflected back to the transducer, generating a signal which may be displayed as an 'A scan' trace on an oscilloscope. The position of the signal in the time domain indicates the distance of the defect from the transducer, and its amplitude gives some measure of the defect size.

End of line inspection is an effective measure of ensuring product quality so that defective or out of tolerance materials are not supplied to the customer. It also provides traceable records but has the disadvantage of imposing a considerable delay in detecting the onset of the faults that might have occurred at an earlier processing stage. This can reduce productivity due to the reduction in the yield of prime material and delay delivery of the full order since extra material may have to be processed to replace the scrap (Knox, [1994]). It is far better to ensure that the harmful defects are not introduced in the first place and to place the emphasis therefore on up stream inspection of the semi-finished product. However this often requires inspection in a hostile environment such as at high temperatures or in the presence of metallic dust, steam and water. Difficulties may also be

caused by the coarse grain material structure and poor surface finish.

To date there has been an increasing interest in inspection of the semi-finished product at elevated temperatures. Extensive studies have been carried out to develop high temperature ultrasound transducers which can be used in such hostile environments as on a production line (Whittington, [1978], [1987], Burns et al.,[1988]). A pulsed laser focused on the sample surface appears to be a suitable source for the remote generation of ultrasound pulses at the metal surface, (Scruby et al., [1982]; Dewhurst et al., [1988]; Edwards et al., [1989]) whereas electromagnet acoustic transducers or EMATs appear to hold promise as receivers (Edwards et al., [1990]). Both of these two devices are essentially non-contact and can be made to withstand high temperatures and do not require any special surface preparation (Edwards et al., [1994] and Idris et al., [1994]).

1.3 Scope of the Thesis

The thesis consists of seven Chapters, which describe the development of a high temperature water cooled EMAT receiver to be used with a pulsed laser for the measurement of the transit time of ultrasound propagation through a thick steel sample at elevated temperatures. The system will be operated in send-receive arrangement where the receiver is located on the generation side. The laser beam is focused on the sample surface through a hole in the centre of the EMAT. Such an arrangement provides remote generation and detection of ultrasound on a sample from a single surface. The thickness measurement will be made with reference to ultrasound longitudinal and shear wave velocity data, measured using a laser-EMAT system.

Chapter-2 describes a general overview of the ultrasound propagation in solids, and ultrasound behaviour with increasing sample temperature. Chapter-3 presents an overview of ultrasound measurements used for NDE at elevated temperature using

conventional and non-contacting techniques. A detailed account of laser generated ultrasound will be given to provide an understanding of the various generation mechanisms in metal and factors that influence the generation of ultrasound in metals. EMAT ultrasound transduction mechanisms are described in detail. The end part of the chapter discusses various developments and application of non-contact ultrasound techniques with a specific emphasis on laser-EMAT systems at elevated temperature.

The design of high temperature water cooled EMATs is described in Chapter-4. Initially a water cooled permanent magnet EMAT (P-EMAT) was developed to be operated both in pulse echo mode and as the epicentral receiver of the laser generated ultrasound. The design and the development of a water cooled EMAT where the magnetic field is generated by a pulsed electromagnet (E-EMAT) is also described. The optimisation of the EMAT and the electromagnet driver are described and initial pulse echo measurement results are given. The EMAT was then tested with pulsed lasers, both a Nd:YAG laser and a CO_2 laser in a send- receive arrangement. The last part of this chapter discusses the factors that affect the sensitivity of the system such as stand-off, surface oxides and EMAT rf coil dimensions.

The application of the system at elevated temperatures is described in Chapter-5. Measurements were made on mild steel samples using both types of EMAT in pulse echo mode, and using both types of EMAT as detectors for ultrasound generated by pulsed laser on epicentre and in send-receive arrangement. The temperature dependence of EMAT detected waveforms is discussed where the dominant detected wave arrivals change from shear wave pulses at low temperature into longitudinal wave at elevated temperature. As the temperature approaches the Curie temperature of the sample, the shear wave signal amplitude decreases and an enhancement of the longitudinal wave occurs at temperatures above T_c. At even higher temperatures the signal amplitudes fall as

a result of reduced transduction efficiency of the EMAT and increasing attenuation in the material. This chapter also discusses the cause of rapid velocity changes close to T_c.

Chapter-6 consists of three parts. The first part discusses the magnetic field dependence of EMAT transduction efficiency and variations in the sensitivity of the EMATs on different steel samples. Measurements are performed using a DC electromagnet so that the EMAT response could be studied as a function of applied magnetic field. Similar measurements are described for the E-EMAT. The EMAT transduction efficiency is enhanced by the presence of a surface oxide (magnetite) layer which exhibits a strong magnetostrictive effect. This effect is thought to be the dominant transduction mechanism in ferromagnetic materials at low fields. The second part of the chapter discusses the cooling effect of the introduction of a water cooled EMAT on the sample surface. This may be responsible for the formation of a thin layer of ferromagnetic phase on the surface of a bulk paramagnetic sample and the enhancement of longitudinal wave sensitivity at temperatures just above T_c. The third part of the Chapter discusses the temperature dependence of magnetisation in mild steel. Measurements are made using a non-contact technique to monitor the magnetic field of the E-EMAT. The magnetic field remains constant at about 1.4T from room temperature up to 770°C and then reduces dramatically to 0.35T at 800°C and above where the steel becomes paramagnetic.

Chapter-7 discusses conclusions drawn from the work of the thesis followed by suggestions for future work; mainly involving further studies of the non-contact ultrasound transduction on steel and various properties of steels that affect the EMAT transduction. This section will also outline the improvements of the laser-EMAT system to be used at elevated temperatures and suggestions for industrial applications.

1.4 References

Burns L. R., Alers G. A. and MacLauchlan D.T., Report in Prog. In. Quantitative NDE., ed.Thompson D. O. and Chimenti D. E., **Vol. 7B**, 1988, (Plenum New-York), pp.1677-1683.

Dewhurst R.J., Edwards C., McKie A.D.W and Palmer S. B., J. Appl. Phys. **Vol. 63**(4), Feb. (1988), pp.1225-1227.

Edwards C., Taylor G. S. and Palmer S. B., J. Phys D. Appl. Phys. **Vol. 22**, 1989, pp.1266-1270.

Edwards C. and Palmer S.B., IEEE Trans. On Magnetics, **Vol. 26**, no. 5, Sept. (1990), pp. 2253-2260

Edwards C., Dixon S., Idris A., Reed J. and Palmer S.B., Rev. in Prog. Of Quantitative Nondestructive Evaluation, Colorado, **Vol.14B**, (1994), pp.2253-2260.

Idris A., Edwards C. and Palmer S. B., Nondestr. Test. Eval., **Vol. 11**, (1994), pp.195-213.

Knox.T. J., INSIGHT, **Vol. 36**, no. 11, 1994, pp.849-853.

Scruby C. B., Palmer S. B., Dewhurst R. J. and Hutchins D. A.,. in Research Techniques in NDT, ed. R.S.Sharpe, **Vol. 5** 1982, chap. 8, pp. 281- 327. (Academic Press, London) 1982.

Whittington K. R., Phys. Technol., **Vol. 9**, 1978, pp.62-68.

Whittington K. R., Process Engineering, February 1987. pp.73-75.

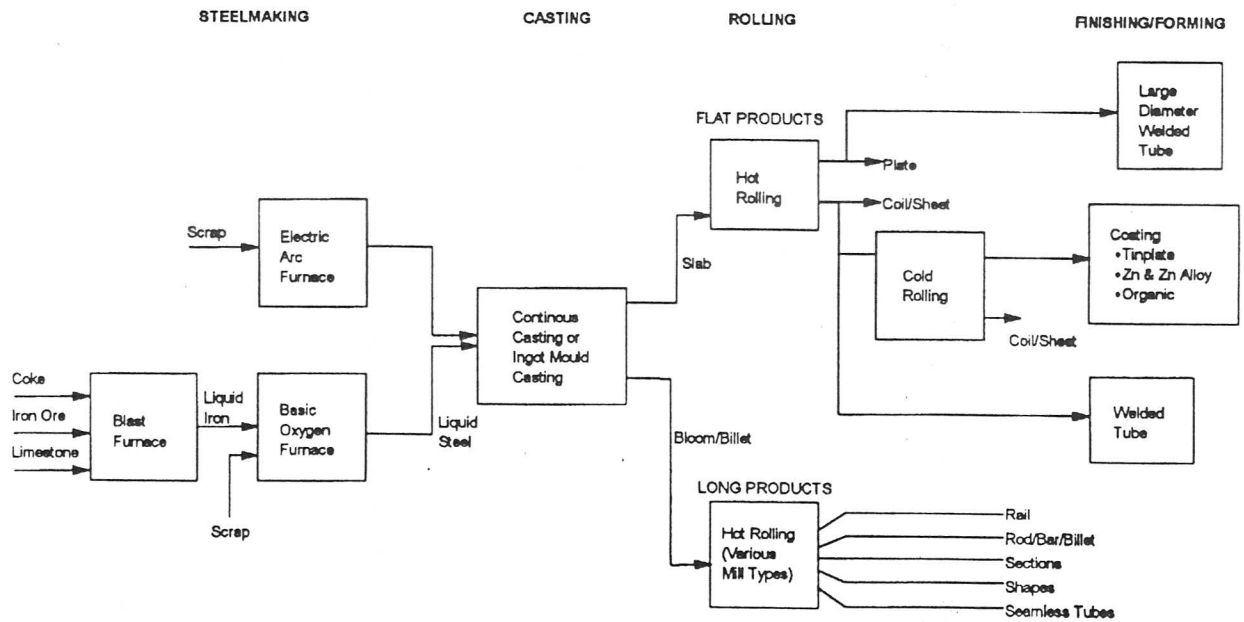

Figure-1.1: The main production route of primary steel products. (after Knox, [1994])

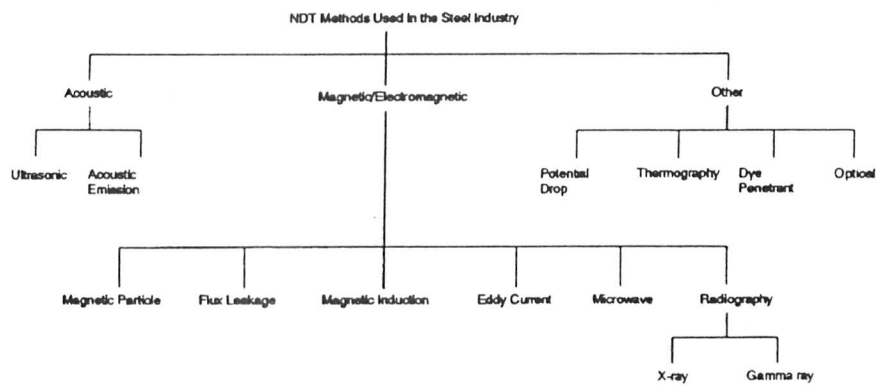

Figure-1.2: Nondestructive testing and evaluation used in steel processing.

CHAPTER-2

ULTRASOUND PROPAGATION IN SOLIDS

2.0 Introduction

Solids in practice exhibit bulk and shear elasticity and can propagate dilatation waves which involve periodic changes in the density of an element of the solid and also shear waves in which the element of solid changes its shape, but not its density. The elastic properties of a solid are usually anisotropic so that the velocity of a given type of wave depends on its direction of propagation. However a polycrystalline solid consists of particle grains with anisotropic properties. These grains are randomly orientated and the properties of the bulk of the solid are isotropic.

This chapter will provide a brief theory of ultrasound propagation in an isotropic elastic solid. It discusses the stress-strain relations that lead to the propagation of ultrasound. At the boundary, the wave will undergo reflection and transmission leading to the excitation of different wave modes of propagation. The nature of the wave propagation will be affected by both temperature and the nature of the medium. Increase in the temperature of the solid will reduce its rigidity and thus the wave velocity. It may also alter the grain size, change in phases and the structure of the material.

2.1 Stress and Strain relations

The propagation of ultrasound in elastic solids has been explained in many publications (Mason, [1958], Shutilov, [1988], Malecki [1969]). Utrasound propagation is accompanied by a periodic displacement of particles of the medium from their equilibrium position under the action of elastic forces. In the normal, unpertubed state, all particles in the medium are in certain equilibrium positions determined by the balance of intermolecular forces. If an elastic body is deformed, internal stresses are set up in the body which strive to eliminate the deformation or to restore the equilibrium state.

The stresses and strains acting on a body can be specified in terms of the resolved stresses and resolved displacements in a unit cube of material. Each stress acting on a face has three components along the coordinate axes. In Cartesian coordinate x, y, z axes, these stress components can be represented in the form of a tensor and can be written as;

$$\sigma_{ij} = \begin{bmatrix} \sigma_{xx} & \sigma_{xy} & \sigma_{xz} \\ \sigma_{yx} & \sigma_{yy} & \sigma_{yz} \\ \sigma_{zx} & \sigma_{zy} & \sigma_{zz} \end{bmatrix} \qquad \text{for i,j=x, y, z} \qquad (2.1)$$

The first index, i indicates the face or plane and the second index, j, indicates the direction along the axes. Since for each element, $\sigma_{ij}=\sigma_{ji}$, the tensor contains only six independent elements, three tensile components, σ_{xx}, σ_{yy} and σ_{zz} ; and three shearing components σ_{xy}, σ_{xz}, and σ_{yz}. The indices of these stress components can also be written as

$$\sigma_n \equiv \sigma_1, \sigma_2, \sigma_3, \sigma_4, \sigma_5, \sigma_6, \qquad (2.2)$$

where $\sigma_1 = \sigma_{xx}$, $\sigma_2 = \sigma_{yy}$, $\sigma_3 = \sigma_{zz}$, $\sigma_4 = \sigma_{yz}$, $\sigma_5 = \sigma_{xz}$ and $\sigma_6 = \sigma_{xy}$.

The strains can also be written in similar form,

$$\varepsilon_{ij} = \begin{bmatrix} \varepsilon_{xx} & \varepsilon_{xy} & \varepsilon_{xz} \\ \varepsilon_{yx} & \varepsilon_{yy} & \varepsilon_{yz} \\ \varepsilon_{zx} & \varepsilon_{zy} & \varepsilon_{zz} \end{bmatrix} \qquad \text{for i,j=x, y, z} \qquad (2.3)$$

where the component of strain is defined as

$$\varepsilon_{ij} = \left(\frac{\partial u_j}{\partial x_i} + \frac{\partial u_i}{\partial x_j} \right) \quad \text{for i,j=1,2,3 or x-,y-,z-in Cartesian coordinate.}$$

where u_i is the component of displacement of the body along the coordinate direction, x_j . The indices of these strain components can also be written as

$$\varepsilon_m \equiv \varepsilon_1, \varepsilon_2, \varepsilon_3, \varepsilon_4, \varepsilon_5, \varepsilon_6 \qquad (2.4)$$

where $\varepsilon_1 = \varepsilon_{xx}$, $\varepsilon_2 = \varepsilon_{yy}$, $\varepsilon_3 = \varepsilon_{zz}$ represent the tensile strains and $\varepsilon_4 /2 = \varepsilon_{yz} = \varepsilon_{zy}$, $\varepsilon_5 /2 = \varepsilon_{xz} = \varepsilon_{zx}$, $\varepsilon_6 /2 = \varepsilon_{xy} = \varepsilon_{yx}$ represent the shear strains.

For a small strain or deformation, the relation between the stresses and the resulting strains is linear and known as Hooke's law. In the limit of small deformation, components of the stress σ_n , at a given point of the body are linear and homogenous

functions of all components of strain ε_m, parallel to the principal axes. The stresses and strains relation is given in tensor form as

$$\sigma_n = C_{nm}\varepsilon_m \qquad \text{for n, m = 1, 2, 3, 4, 5, 6} \tag{2.5}$$

where the coefficients of form C_{nm} are linear elastic moduli or stiffness constants of the material. Since $C_{nm} = C_{mn}$, the 36 C_{nm} reduce to 21 independent constants. The existence of symmetry reduces the number of non-zero elastic moduli and the number of independent moduli. In an elastically isotropic solid, the elastic moduli are not dependent on any preferred direction and the behavior of the medium is determined by two independent moduli called Lame' constants λ and μ defined as follows;

$$\begin{aligned} &\lambda = C_{12} = C_{13} = C_{23} = C_{32} = C_{21} = C_{31} \\ &\mu = C_{44} = C_{55} = C_{66} \\ &C_{11} = C_{22} = C_{33} = \lambda + 2\mu \end{aligned} \tag{2.6}$$

If the components of stresses and strains are represented by two indices, the Hooke's law for an elastically isotropic solid can be expressed as;

$$\sigma_{ij} = \lambda\theta\delta_{ij} + 2\mu\varepsilon_{ij} \quad \text{for i,j =1, 2, 3,} \tag{2.7}$$

where in Cartesian coordinates, the indices i,j=1, 2, 3, can be substituted as x, y, and z axes, and $\theta = \varepsilon_{11} + \varepsilon_{22} + \varepsilon_{33}$ is the volume expansion, and δ_{ij} is the Kronecker delta function;

$$\begin{aligned} \delta_{ij} \quad &= 1 \text{ for } i=j \\ &= 0 \text{ for others} \end{aligned}$$

By substituting the definition in (2.2), (2.4) into (2.7), the stress-strain relations can also be written as;

$$\begin{aligned} &\sigma_1 = \lambda\theta + 2\mu\varepsilon_1 \,,\ \sigma_2 = \lambda\theta + 2\mu\varepsilon_2 \,,\ \sigma_3 = \lambda\theta + 2\mu\varepsilon_3 \\ &\sigma_4 = \mu\varepsilon_4 \,,\ \ \sigma_5 = \mu\varepsilon_5 \,,\ \ \sigma_6 = \mu\varepsilon_6 \end{aligned} \tag{2.8}$$

The x-, y-, z-, or 1-, 2-, 3-components of a force on a unit cube of infinitesimal dimension dx, dy and dz are given by;

$$F_i = \left(\frac{\partial \sigma_{i1}}{\partial x_1} + \frac{\partial \sigma_{i2}}{\partial x_2} + \frac{\partial \sigma_{i3}}{\partial x_3}\right) dxdydz = \frac{\partial \sigma_{ij}}{\partial x_j} dxdydz \quad \text{for i,j =1,2,3,} \qquad (2.9)$$

F_i determines the rate of change of the stresses along the edges of the unit volume.

2.2 Wave Propagation in Elastically Isotropic Solids

The equation of motion for a solid can be derived from Newton's law giving the relation between the mass, the acceleration and force. For the three directions of motion along the x-, y-, z- axes, the relation is given by

$$\rho \frac{\partial^2 u_i}{\partial t^2} dxdydz = F_i \quad \text{for i; 1=x, 2=y, 3=z.} \qquad (2.10)$$

where dxdydz is an infinitesimal unit of volume with density ρ, having displacements u_i along the three coordinate directions. Equation (2.9) gives the component of force in the x-direction (i=1) as shown in figure-2.1,

$$F_1 = \left(\frac{\partial \sigma_1}{\partial x} + \frac{\partial \sigma_6}{\partial y} + \frac{\partial \sigma_5}{\partial z}\right) dxdydz \qquad (2.11)$$

A similar expression applies to the other two components in the y- and z- directions. Substituting the stress-strain relation (2.8) into (2.10), the equations of motion in an isotropic medium are given by;

$$\begin{aligned} \rho \frac{\partial^2 u}{\partial t^2} &= (\lambda + \mu) \frac{\partial \theta}{\partial x} + \mu \nabla^2 u \\ \rho \frac{\partial^2 v}{\partial t^2} &= (\lambda + \mu) \frac{\partial \theta}{\partial y} + \mu \nabla^2 v \\ \rho \frac{\partial^2 w}{\partial t^2} &= (\lambda + \mu) \frac{\partial \theta}{\partial z} + \mu \nabla^2 w \end{aligned} \qquad (2.12)$$

where $\nabla^2 = \left(\frac{\partial^2}{\partial x^2} + \frac{\partial^2}{\partial y^2} + \frac{\partial^2}{\partial z^2}\right)$ and $\theta = \frac{\partial u}{\partial x} + \frac{\partial v}{\partial y} + \frac{\partial w}{\partial z} = \varepsilon_1 + \varepsilon_2 + \varepsilon_3$

This general wave motion in the medium can also be rewritten as

$$\rho \frac{\partial^2 u_i}{\partial t^2} = \frac{\partial \sigma_{ij}}{\partial x_j} \qquad (2.13)$$

where σ_{ij} are the components of the stress tensor, u_i are the components of the displacements along the coordinate axes $x_j = x, y, z$. These equations are true for both

isotropic and anisotropic media. If the solid is unbounded, both the longitudinal and shear bulk waves can propagate through it. The shear or transverse waves occur when the motion of the particles or polarisation of the stress wave is perpendicular to the direction of wave propagation, and longitudinal waves occur when the motion of the particles or the polarisation of the stress wave is along the wave propagation direction. On a solid with free boundary, the Rayleigh surface wave may also propagate. The ultrasound velocities of both longitudinal and shear waves in solids can be expressed as a function of their modulus of rigidity G, and the bulk modulus K, and written as:

$$\text{longitudinal wave velocity } \upsilon_l = \sqrt{\frac{K+\frac{4}{3}G}{\rho}} \qquad (2.14)$$

The shear wave velocity is expressed as $\upsilon_s = \sqrt{\frac{G}{\rho}}$ (2.15)

The waves velocities can also be expressed in terms of the Lame' constants λ and μ,

$$\upsilon_l = \sqrt{\frac{\lambda+2\mu}{\rho}} ,$$

and

$$\upsilon_s = \sqrt{\frac{\mu}{\rho}} \qquad (2.16)$$

The characteristics of the ultrasound wave field such as amplitude and frequency, depend on the size and nature of the source generating the changing stress field. If the source is a pulsating small sphere, it generates a stress field directed radially and the ultrasound propagates uniformly in all directions with a spherical wavefront. In an elastically isotropic non-absorbent material, the energy propagates out from a source in all directions with the intensity at any point at a distance r from the source, being directly proportional to the inverse square of the distance r. If P is the acoustic pressure and the propagation velocity υ, the wave motion can be written as;

$$\frac{\partial^2(rP)}{\partial t^2} = \upsilon^2 \frac{\partial^2(rP)}{\partial r^2} \qquad (2.17)$$

where the acoustic pressure P is the excess pressure caused by the passage of ultrasound that gives rise to the strain ε_{ij} and P is defined as

$$P = -K'\varepsilon_{ij} \qquad (2.18)$$

where K' is the appropriate modulus of elasticity.

An example of such a spherical wave source is a laser generated source. As the wave propagates sufficiently far from the source, the curvature of the wavefront is so small that one can effectively regard the wave as a plane wave. Plane wave ultrasound can be generated by a plane surface vibrating in a such manner that all points on the surface are in phase. An example is an EMAT, and one dimension wave propagation can be written as;

$$\frac{\partial^2 P}{\partial x^2} = \frac{1}{\upsilon^2}\frac{d^2 P}{dt^2} \qquad (2.19)$$

2.3 Effect of Rise in Temperature in Solids

The density and the elastic constants of a solid are directly dependent on the average of the interatomic separation. As the temperature rises, there is an increase in the average interatomic separation (thermal expansion) producing a reduction in the elastic constants and density. In addition, various structural and behaviour changes occur. The relationship between the density $\rho(T)$, of a solid, and temperature is given by (Silber et. al., [1970])

$$\rho(T) = \rho_{20}\,(1+3\alpha\Delta T)^{-1} \qquad (1.20)$$

where ρ_{20} is the density at 20°C, α is the linear coefficient of thermal expansion and ΔT is the difference in temperature referred to 20°C. For mild steel, over the temperature range between room temperature and 1000°C, the density changes by about 3% . The variation of the elastic moduli in mild steel has been studied by Dates et.al.,[1971], who showed that these quantities reduce gradually with increasing temperature up to about 750°C and

then begin to reduce rapidly at temperatures above 800°C. According to these studies, between room temperatures and about 750°C, both the shear and bulk moduli of a low carbon steel are expected to reduce by 35% and 39% respectively and, as a result, decrease the ultrasound velocities.

Increase in temperature may caused the grain size of the sample to increase and cause an increase in attenuation of the ultrasound. At higher temperatures the sample may undergo phase transitions such as a ferromagnetic-paramagnetic transition at the Curie temperature, changes in crystal structure from body-centred cubic into face-centred cubic resulting in a pronounced change in the nature of the ultrasound propagation i.e the velocities and the attenuation. Attenuation of ultrasound in solids will be discussed in section 2.5 of this chapter.

2.4 Effect of Boundaries on the Transmission of Ultrasound.

When ultrasound waves are incident on a boundary between two media, both reflection and transmission take place. The wave's energy is partitioned depending on whether the incident wave is either shear or longitudinal, on the incident angle at the interface and on the acoustic impedance Z, at the boundary, defined as the product between the wave velocity υ, and the density of the medium ρ, ($Z=\rho\upsilon$). A plane longitudinal wave of amplitude A_{lo}, incident on a boundary between two media 1 and 2 at an angle θ_{l1} (figure-2.2), will be reflected at an angle equal to the incident angle θ_{l1} with an amplitude A_{l1} and transmitted into the second media with amplitude A_{l2} and angle θ_{l2}. At the same time it generates a shear wave that is reflected back at an angle θ_{s1} with amplitude A_{s1} and is also transmitted into the second medium with amplitude A_{s2} at an angle θ_{s2} . The reflection and transmission of the ultrasound wave energy at the boundary is governed by Snell's Law in a similar way to the optical case,

$$\frac{\sin\theta_{l1}}{\upsilon_{l1}} = \frac{\sin\theta_{l2}}{\upsilon_{l2}} = \frac{\sin\theta_{s1}}{\upsilon_{s1}} = \frac{\sin\theta_{s2}}{\upsilon_{s2}} \qquad (2.21)$$

where θ_{l1} , θ_{l2} are the angle of reflection and refraction of the longitudinal wave relative to the normal in media 1 and 2 respectively and, θ_{s1} , θ_{s2} are the angle of reflection and refraction of the shear wave propagation in media 1 and 2 respectively. υ_{l1} and υ_{l2} are the longitudinal wave velocities in media 1 and 2, similarly υ_{s1} and υ_{s2} are the shear wave velocities in media 1 and 2 respectively. The shear wave is generated from mode conversion of the longitudinal wave, has a vertical plane of polarisation which is perpendicular to the boundary and is known as shear vertical (SV). This is due to the existence of a non-zero component of displacement normal to the boundary. At the boundary, the SV will be reflected and transmitted as a shear wave and also excite longitudinal waves. The plane of the polarisation of the shear wave remains unchanged. Since in the same medium $\upsilon_s < \upsilon_l$, then $\theta_{ls} < \theta_{ll}$, i.e., the shear wave is reflected at a smaller angle to the normal. If however the plane of polarisation of the incident shear wave is parallel to the boundary, it will not excite any normal components of displacement at the boundary, therefore it is reflected and transmitted as two pure shear waves with similar polarisation and displacement. This type of shear wave polarisation is known as shear horizontal (SH).

2.5 Ultrasound Attenuation in Polycrystalline Solids

In the previous section we have discussed wave propagation in a perfectly elastic solid. In such a solid, each stress component is a real linear function of the strain components. As a consequence, a small amplitude ultrasound plane wave propagates with undiminished intensity. Actually, ultrasound waves are attenuated in all real solids where the amplitude decreases exponentially as it progresses through the medium. The dissipation of ultrasound energy in a polycrystalline solid and particularly a metal is

generally due to elastic hysteresis, thermoelastic relaxation and scattering (Mason, [1958[). The details of this subject have been well documented e.g. Bhatia, [1967], Mason, [1958] and Papadakis, [1965].

The elastic hysteresis is caused by the time independent nonlinear stress and strain relationship. In a real solid, the passage of the ultrasound does affect it permanently and when the external forces cease to act, the strains partly remain there. The properties of the material change in such a manner that they cannot be restored by the action of the external forces (Malecki, [1969]).

Loss due to thermoelastic relaxation is dominant in metals at ultrasound frequencies below 1MHz which corresponds to the case where the ultrasound wavelength λ is several times greater than the diameter D of the individual grains. The loss occurs only with compressional waves that involve a change of volume. In the passage of a compressional wave, the compression of the solid causes the partial conversion of the mechanical energy into thermal energy and the compressed part becomes warmer than the extended parts. This causes the heat to flow from one grain to another and energy can be abstracted from the vibrational or mechanical energy. In a polycrystalline sample, the crystal grains vary in orientation and, as a consequence of elastic anisotropy, are compressed to differing degrees when a plane compressional wave is transmitted through the sample. As a result, the distribution of temperature changes due to the passage of the ultrasound is not uniform even though they are subjected to a uniformly acting pressure (since $\lambda >> D$, where D is the grain diameter). Depending on the random position in relation to the direction of the wave propagation, individual grains display a different stiffness and thermal conductivity in this direction. The loss is inversely proportional to the wave length. Thermal losses do not occur for shear waves, since their propagation does not involve any change in volume.

Scattering of ultrasound waves takes place whenever there exist regions of varying density or elasticity and scattering contributes a large part to the ultrasound attenuation in polycrystalline solids. In a polycrystal, the adjacent grains have different orientations and their anisotropic elastic constants cause an impedance mismatch between adjacent grains. Reflection thus can occur and the ultrasound will be diffracted or scattered depending on the grain size and the ultrasound frequency f or the wavelength λ. The resulting attenuation also is strongly dependent on the degree of anisotropy in the sample. Scattering can be devided into three different regimes depending on the ratio of the ultrasound wavelength λ and grain size D. Firstly the one that occurs when the acoustic wavelength is much greater than the average grain diameter is known as Rayleigh scattering, secondly when the wave length is approximately equal to the average grain diameter we have stochastic scattering and finally diffuse scattering occurs when the wavelength is less than or equal to the average grain diameter. The linear attenuation coefficient in the Rayleigh regime is proportional to the third power of the grain diameter and to the fourth power of the frequency of the ultrasound waves and is given by (Mason, [1958]);

$$\alpha(\text{neper per cm})=\frac{8\pi^4 D^3 f^4}{9\upsilon^4}(S) \ , \qquad (2.22)$$

when the wavelength is three times or more the grain size. S is the scattering factor related to the degree of anisotropy of the metal. Stochastic scattering regime occurs at shorter wavelengths, the attenuation changes less rapidly with frequency and is proportional to the average grain size and the second power of the frequency (Papadakis 1965). At much higher frequency where $\lambda << D$ in the diffuse scattering regime, the attenuation is independent of the frequency but inversely proportional to the average grain diameter. For most solids the longitudinal wave velocity is approximately equal to twice the shear wave velocity, therefore at a given frequency, it appears that the shear wave

attenuation is in general several times greater than that of the longitudinal wave.

In ferromagnetic material such as mild steel, domains exist inside a polycrystal or single crystal for which all the magnetic polarisations are in a single direction. Attenuation occurs as a result of ultrasound interaction with the magnetic domains leading to the rotation and growth of the domain wall (Mason [1958]). The ultrasound attenuation is found to increase rapidly in the vicinity of the Curie temperature T_c, where a transition from a ferromagnetic to paramagnetic phase occurs. The phase transition is also associated with the rapid reduction in ultrasound velocity at T_c for the iron and steels (Bozoroth, [1951]).

2.6 References

Bhatia A.B., Ultrasonic Absorption, (Oxford Press) , 1967. Chapter 11 and chapter.14.

Bozoroth , Ferromagnetism, (Van Nostrand Inc. Canada), 1951

Dates E.H.F., Atkins M. and Beaton G.V., Ultrasonics, Oct. (1971), pp. 209-214.

Malecki I., Physical Foundation of Tech. Acoustics, Pergamon Press, London, 1969.

Mason W. P., Physical Acoustics And The Properties Of Solids, (D Van Nostrand Co. Princeton), 1958, Chapter 8.

Papadakis E. P., Jour. of the Acoustical. Soc. of America, **Vol.** 37, no. 4, April 1965, pp.703-710.

Shutilov V.A., Fundamental Physics Of Ultrasound, (Gordon and Breach Science Pub.) 1988

Silber F. A. and Ganglbauer C., Nondestructive Testing, 1970, pp. 492-432.

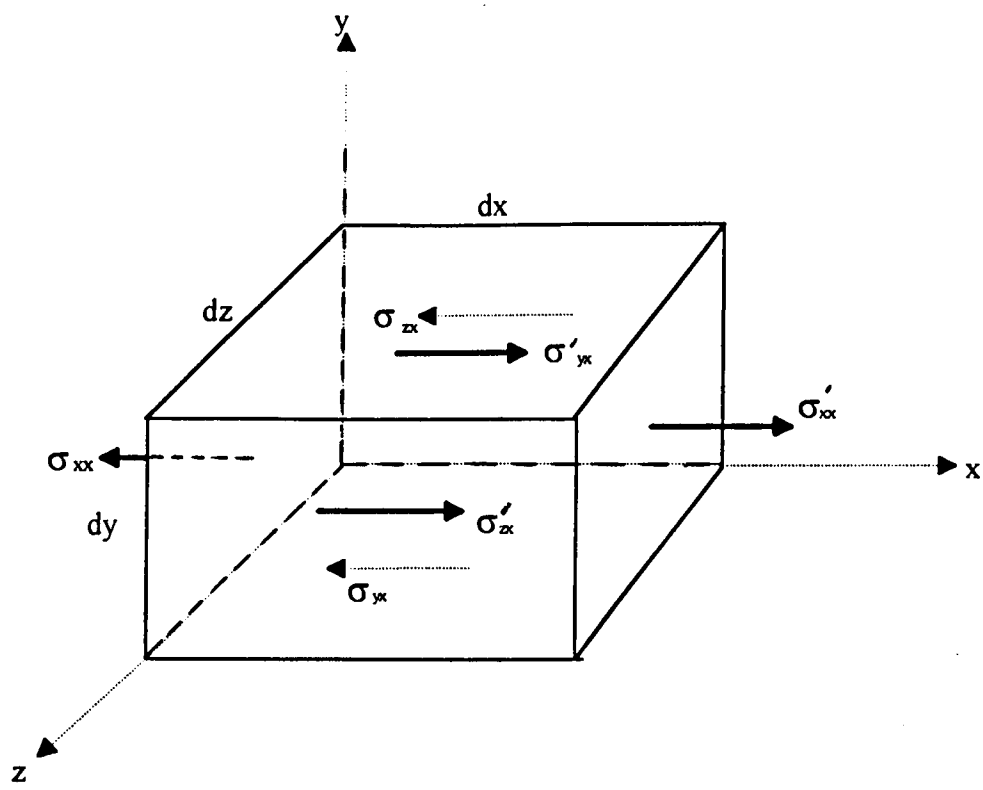

$$\sigma'_{xx} = \sigma_{xx} + \frac{\partial \sigma_{xx}}{\partial x} dx$$

$$\sigma'_{yx} = \sigma_{yx} + \frac{\partial \sigma_{yx}}{\partial y} dy$$

$$\sigma'_{zx} = \sigma_{zx} + \frac{\partial \sigma_{zx}}{\partial z} dz$$

Figure-2.1: Stress along x direction acts on a unit cube of dimension dx, dy, and dz causing tensile and shear strain components along x axis.

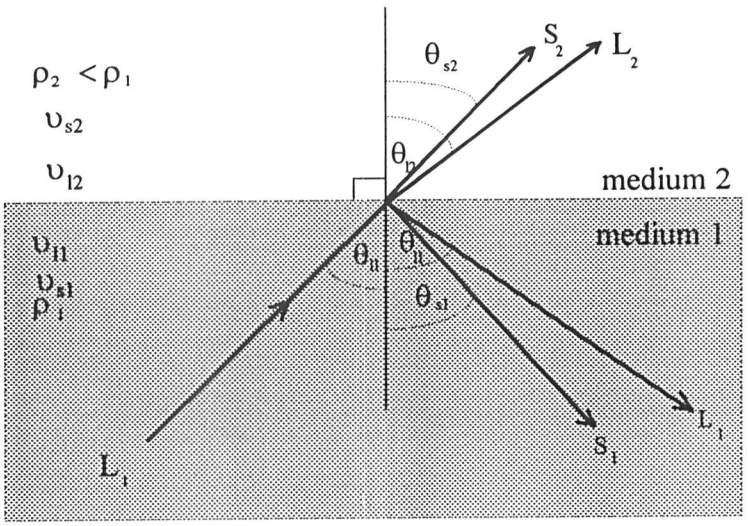

(A)

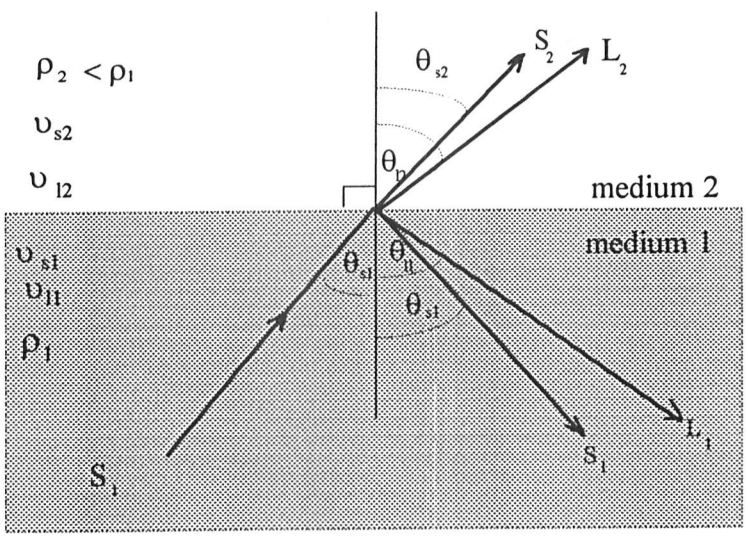

(B)

Figure-2.2: Ultrasound behaviour at a plane boundary between two media, (A) incident longitudinal L, (b) incident shear verticle SV, waves at the .boundary

CHAPTER-3

Non-Contact Ultrasound : Physical Principles, Techniques and Applications

3.0 Introduction

Ultrasound has been widely used as a standard non-destructive method in industry, for probing the surface and the interiors of solids; to locate defects and measure material properties. Conventionally, measurement is carried out at or near ambient temperature. The generation and detection of ultrasound are usually accomplished using transducers containing a piezoelectric element such as quartz or lead zirconate titanate (PZT). The construction of these transducers is generally simple, relatively cheap and, in a majority of applications, they are able to couple sufficient ultrasound energy into the sample under test. The transducers also provide a relatively efficient means of producing acoustic energy when compared with the other methods such as electrodynamics, magnetostrictive and optical techniques. However, conventional ultrasound techniques face severe limitations at elevated temperatures, where testing would offer several advantages in terms of the product quality and control of production processes.

Realising the need to carry out ultrasound inspection at higher temperatures, extensive studies have been carried out to develop high temperature ultrasound transducers for various industrial applications. A wide range of ultrasound transducer systems for high temperature use have been developed to study elastic constants in metal (Brammer et al., [1970]), phase transformations (Lavender, [1971]), ultrasound attenuation (Darbari et al., [1968], Papadakis et al., [1972]). In these reports, the ultrasound transduction was carried out by piezoelectric transducers coupled to the sample surface by a delay line. In recent years, non-contact ultrasound transducers to be used at elevated temperature have been developed using either electromagnet acoustic transducers (EMATs), optical transduction using pulsed lasers or the combination of both. These have been reported in several publications such as wave velocity measurements, (McKie,

[1987]); monitoring the solid and liquid metal, (Idris et al., [1994]); thickness measurement, (Maxfield et al., [1987]; Whittington, [1978]; Boyd et al., [1988]), flaw detection (Kubota et al., [1988]), measurement of internal temperature distribution (Wadley et al., [1986]).

This chapter firstly discusses in brief the different methods of ultrasound transduction in metals particularly at elevated temperature. Secondly, it reviews various work regarding non-contacting ultrasound transduction and measurement at elevated temperature using pulsed lasers, EMATs and in particular combined pulsed laser-EMAT systems.

3.1 The Shortcomings of Piezoelectric Transducers

The methods and the instrumentation of conventional ultrasound techniques used in NDE have been described in detail by Krautkramer, [1983]. With these techniques, the piezoelectric transducers are usually coupled to the test sample with a liquid couplant such as water or grease, to allow maximum transmission of ultrasound energy. However, in the metal processing industries such as the steel making industry, there is a need for defect detection and physical dimensioning. This could be done by ultrasound inspection but for maximum benefit it should be carried out at the early stage of processing when the metal is still hot. High temperature ultrasonic inspection could detect the presence of defects and prevent further processing of the defective materials.

Ultrasound measurement at elevated temperature using conventional contact piezoelectric transducers becomes difficult and most ultrasound couplants are not suitable to be used for temperatures above 300°C as they tend to evaporate or undergo chemical degradation. At elevated temperatures the materials used for the construction of the transducers such as epoxy-resin, solder and plastics, begin to deteriorate therefore

alternative construction procedures and design are necessary. In addition, if the Curie temperature of the transducer is exceeded (370°C for PZT), the piezoelectric nature of the material is destroyed. When the temperature approaches the Curie temperature, the amplitude of the ultrasound drops and the pulse shape becomes distorted. The effect may become progressively worse if the transducer is operated close to the Curie temperature for a long period. Various piezoelectric transducer designs and couplings including the use of wave guides, wheels, molten salt and water-jets have been investigated, and these facts have been pointed out in the literature (Parkinson et al.,[1977]; Whittington, [1978], and Andrews, [1982]) to fulfil various industrial applications. However, they all present problems of data interpretation and inflexibility. Therefore, to overcome these problems, non-contacting ultrasound systems have to be considered.

3.2 Non-contacting Ultrasound Techniques

In these techniques, the ultrasound transduction normally occurs without any physical contact or liquid couplant between the transducers and the surface under test. The ultrasound sources can be located at or near the surface of the sample and the presence of the transducers does not disturb the elastic wave propagation in the material by loading the surface. The techniques allow rapid scanning on the sample. There are several techniques for the remote generation and detection of ultrasound in metals and the pulsed laser and EMAT in particular have been developed.

The use of pulsed lasers for the remote generation of broadband ultrasound pulses in solid has been reported in many publications since the first publication by White in 1963, (Edwards et al, [1990]; Scruby et al., [1982 and 1990]; Taylor, [1990]). The laser can be positioned up to several metres away from the test piece. The advantages for probing samples at elevated temperature are obvious.

The applications of EMATs at elevated temperature on non magnetic metal have been reported by Whittington, [1989] and Idris, [1995]; on steel by Parkinson et al., [1977]; Maxfield et al, [1987] and Lee et al., [1992]. Pulsed laser and EMAT techniques and their applications will be described in detail in the following section. Other methods of non-contact ultrasound transduction include capacitance transducers (Hutchins et al., [1985]), spark sources (Cooper et al., [1985]) and air-coupled transducers (Hutchins et al., [1994] and Farlow et al., [1994]).

Capacitance transducers can be used as detectors. A typical device for bulk wave detection consists of a flat metal plate positioned close to (typically a few tens μm) and parallel to the specimen surface. Any change in the dielectric (air) filled gap between the surface and the transducer due to an acoustic disturbance will cause change in the capacitance of the system. The primary restriction on the use of this transducer is the need for a small gap between the transducer plate and the sample surface. Although this is not a problem under laboratory conditions (low vibrations and polished samples), they are almost impossible to use on unprepared samples in an industrial environment.

A spark source transducer involves discharging a high voltage capacitor bank from an electrode to the sample surface (Cooper et al., [1985]). The momentum transfer from ions in the spark provides a normal force and generates ultrasound in the metal in its proximity. This method is not widely used because the spark discharge is hazardous.

Air coupled piezoelectric transducers have been developed for both generation and detection of bulk waves, (Farlow et al., [1994] and Hutchins et al., [1994]). However such transducers are generally operated at low frequency, in the range of 500-700 kHz, to minimise the attenuation in the air (Farlow et al., [1994]). The transducers are able to generate large amplitude ultrasound in the air. However there is a large impedance mismatch with solids and they are only well-suited to materials with relatively low acoustic

impedance such as graphite composites, plastics or metal composites (Farlow et al., [1994]). On metals where there is a large impedance mismatch at the metal-air interface, only a small fraction of the airborne ultrasound penetrates into the sample. During the detection, ultrasound intensity will be further reduced at the interface making transduction almost impossible particularly at elevated temperature.

3.3 Laser Generated Ultrasound.

The generation of ultrasound pulses in solids by laser has been established as a versatile laboratory NDE technique to examine materials defects (Burns et al., [1988]), thickness monitoring (Edwards et al., [1994]) and to assess a range of inherent properties such as internal structural changes, (Greenough et al., [1987]) and anisotropy (Allen et al., [1984]). Laser generated ultrasound also has been used to determine the elastic constants of metals, metal matrix composites and ceramics at elevated temperature, (Aussel et al., [1989]). The technique also has been used to monitor the partial melting in thixoforgeable metal (Idris et al., [1994]). The generated ultrasound transients are broadband (DC-20MHz,) with rise-times 10-100ns, depending on the type of laser used. These features enable highly accurate timing measurements to be made yielding precise determination of the elastic constant, (Dewhurst et al., [1988]). The short ultrasound pulses propagating in the specimen, give a high resolution when inspecting layered composite materials or in resolving internal material structure. The unique feature of laser generation is its total remoteness from the specimen surface which is unperturbed by the presence of a generating transducer. This gives an additional benefit that the specimens under test may be moving in the case of on-line monitoring, hot as for the inspection of newly rolled steel or it may be radioactive, where it is too hazardous for direct contact methods. The main disadvantage of the laser source is that it costs more than conventional

piezoelectric transducers, tends to damage the surface and needs separate sensitive detectors.

3.3.1 Physical Principle of Laser Generated Ultrasound

The generation of ultrasound in metal, by pulsed laser is caused by the interaction of the optical pulse with the metal. The interaction takes place on the metal surface and the acoustic waves propagate directly from the source at the surface. The laser source can generate a number of ultrasound modes which propagate in the solid simultaneously. In bulk material, both longitudinal and shear waves can propagate together with surface waves at the solid boundaries. The dominant wave mode generated is dependent on the ultrasound's generation mechanism, selected by varying either the incident optical power density or the condition of the irradiated surface.

Several reviews of this subject exist in the literature (Scruby et al., [1982]; Scruby et al., [1990] and Davies et al., [1993]) and they report the generation mechanisms in some detail. Laser wavelengths used to generate ultrasound in metals most commonly lie in the mid-infrared (λ~10.6μm in the case of CO_2 laser) or near infrared bands(λ~1.06μm in Nd:YAG laser). A pulsed laser emits a burst of coherent electromagnetic radiation. When it is incident on a metal surface, (figure-3.1), some of the incident energy is absorbed by the resistive loss in the metal and converted into heat and the remainder is reradiated back as the reflected pulse or scattered from the surface. The absorption and reflection of the electromagnetic radiation take place near the surface within a layer thickness of the order of the classical skin depth, δ, given by $\delta = (2/\omega\sigma\mu_r\mu_o)^{-1/2}$, (Jackson, [1974]), where σ is the material conductivity, μ_r is the material relative permeability, $\mu_o = 4\pi \times 10^{-7}$ Hm^{-1} is the permeability of the free space, and ω is the angular frequency of the electromagnetic wave. For a Nd:YAG laser (λ=1.06μm), the skin depth is ~5nm in

aluminium assuming $\sigma \sim 38 \times 10^6 (\Omega m)^{-1}$ and relative permeability $\mu_r = 1$ and less than 3nm in iron due to its higher permeability ($\mu_r \sim 1000$). From the classical electromagnetic theory, the reflection coefficient of the laser energy at the metal surface is defined as the ratio of the reflected energy E" to the incident energy E and is given by

$$R = \frac{E''}{E} = \frac{2 - 2t + t^2}{2 + 2 + t^2} \qquad (3.1)$$

where $t = \mu_o \sigma \delta c$, and c is the velocity of light. For a metal where σ in order of $10^7 (\Omega m)^{-1}$, $t >> 1$ for all frequencies up to the visible, so that the reflection coefficient can be approximated to

$$R \sim 1 - \frac{4}{t} \qquad (3.2)$$

The absorbed energy E' is given by

$$E' = (1 - R)E = \frac{4}{\mu_o \sigma \delta c} E \qquad (3.3)$$

This shows that the absorbed energy at the metal surface depends on the laser wavelength and is also affected by the surface roughness and the presence of oxidation on the metal surface. On a polished metal surface, the typical reflectivity for 1.06μm radiation is 90% on aluminium and slightly lower on steel. In practice however, the surface of the sample is likely to be roughened, oxidised or contaminated in some other way. These factors all have the effect of increasing the absorbed energy and hence the efficiency of ultrasound generation.

The absorbed energy on the metallic sample surface mostly takes the form of heat that is confined in a small thickness determined by classical skin depth and surface area similar to the irradiating laser beam. As a result, the temperature of the irradiated surface rises with a rise-time comparable to the laser pulse intensity (White, [1963]). A pulsed laser can usually deliver instantaneous optical powers of more than 1MW, but only for the duration of the pulse. At normal pulse repetition rates, (5Hz with Nd:YAG laser), the average power incident on the surface remains low, typically in the range of 1W or less, so

that bulk heating can be neglected. It has been pointed out in many publications (e.g.. Scruby et al., [1982]) that the ultrasound generation in metals can be categorised into two distinct regimes depending on the laser power density irradiating the surface namely thermoelastic and ablation regimes. As an understanding of these generation mechanisms is essential for this thesis, it will briefly be described in the following section.

3.3.1.a Thermoelastic Source

At relatively low incident power densities, typically $<10^7 Wcm^{-2}$, the laser energy is partially absorbed at the metallic surface and produces localised transient heat. Initially the heat is deposited in a confined volume determined by the electromagnetic skin-depth δ of 2-5nm and the diameter of the laser beam (Figure-3.2). The heat is rapidly distributed throughout the material by thermal conduction. Within the time-scale of the incident laser pulse, 30ns, the heat penetrates to the thermal skin depth determined by $(4K\tau/\rho C)^{-1/2}$, where K is the thermal conductivity, ρ is the density, C is the specific thermal capacity of the material and τ is the laser pulse duration. The thermal penetration depth is typically in the range 0.5-10μm (Ready, [1965]), and causes local heating without changing the phase of the material creating a temperature gradient. The surface temperature increases linearly with the incident laser power density. Thermal expansion in this thin disc of the material gives rise to a stress distribution leading to the propagation of a stress wave, (Figure-3.2). The wave propagates away from the centre of the irradiated surface. Since the thickness of the thermal skin layer is small compared to its diameter, and the thermoelastic source is located at the surface, the thermoelastic strains produce radial stresses parallel to the surface and a zero net stress component acting normal to the surface. As a result, it produces mainly shear waves. If however the thermoelastic source is buried beneath the surface or the thermoelastic source has non-zero thickness, (Figure-3.3), whereby the

thermal penetration depth is of the same order as the beam diameter, the material is able to expand upwards perpendicular to the surface (Dewhurst et al., [1982]). This may propagate both shear and longitudinal waves in the material. In the thermoelastic regime, the deposition of the laser energy does not damage the sample surface.

3.3.1b Ablation Source

The temperature of the laser irradiated surface increases linearly with the laser power density. As the laser power density is increased, say $>10^8 Wcm^{-2}$, either by increasing the energy per pulse or by focusing a constant energy beam into a smaller spot on the surface, the optical radiation is sufficiently intense to deposit an amount of energy that exceeds the threshold of the vaporisation of the metal. The absorbed energy causes ablation of the metal from its surface and forms a plasma. The removal of the metal from the surface produces a net impulsive normal stress against the sample in reaction to recoil force caused by the transfer of momentum from the surface (Figure-3.4), leading to the propagation of the longitudinal wave. As the laser power density is further increased from the "weak" plasma (pulse like force) the time duration of the normal force increases and tends towards a Heaviside function producing a "strong" plasma (step like force) (Dewhurst et al., [1982]). The ablation leaves a small pit on the surface of the material under test. In the work presented here, the laser source was generated either in the thermoelastic regime or in a mild ablative mode so that both shear and longitudinal waves could be produced with measurable amplitudes.

3.3.1c Generation By CO_2 Laser

Ultrasound generation by CO_2 laser is slightly different from those described above as the laser wavelength of 10.6μm is at least one order of magnitude longer than those typically used to generate ultrasound. A detailed study of the mechanism has been made by

Edwaards et al.,[1989] and Taylor, [1990]. At such wavelengths, the incident optical energy on a metal surface is almost totally reflected (the absorbed energy is three times less than for 1.06μm radiation). Typical figures for the absorption coefficient at this wavelength (10.6μm) on clean metal surfaces are ~0.01 on aluminium and ~0.02 on iron (Kaye & Laby, [1986]) and the ability of the CO_2 laser to generate ultrasound by an absorption mechanism is small. Any observed transient stress field may originate from the action of the plasma above the surface. Although the CO_2 laser delivers photon energies less than those produced by the Nd:YAG laser by an order of magnitude, it is capable of producing much higher total energy (4J available in our Laboratory). Since CO_2 laser pulse duration (typically of the order~100ns) is much longer than that of the Nd:YAG laser, the 1J of energy supplied by the CO_2 laser is sufficient to generate a significant thermoelastic ultrasound source arising from an absorption mechanism and comparable to that produced by 3-5mJ Nd:YAG laser.

A much higher optical energy density can be obtained by focusing the laser beam onto a smaller spot on the surface of the sample. Since the laser wavelength, 10.6μm, is well outside the visible spectrum, normal quartz or crown glass lenses may not be used to manipulate the beam as they are opaque at this wavelength. Focusing must be carried out with suitable optics such as zinc selenide or germanium lenses, with anti-reflection coatings to reduce reflection losses. At the focal point, the high intensity of photons interact with the air molecules and ionisation leads to a cascade of high energy electrons and ions resulting in plasma breakdown of the air. The presence of the target metal, dust particles or humidity in the air reduces the power density required for breaking down of the surrounding gas from that required for ionisation of clean dry air. The plasma breakdown generates high pressures and stresses, creating a detonation wave in the air that strikes the surface of the sample. This causes a normal reactive force on the surface which

in turn acts as a source of ultrasound in the solid sample (Edwards et al 1989). The force exerted on the surface is impulsive and resembles those generated by the ablation of the metal surface, but it does not damage the sample surface. When the beam was partially focused on the surface of the metal covered with an oxide layer, the deposition of high laser energy causes the ablation of the oxide layer on the surface leads to the generation of impulsive force normal to the surface and thus propagates the longitudinal wave.

3.3.2 The Effect of Surface Coating and Roughness

The first effect of the presence of a surface coating on metal, such as an oxide layer or rust on steel, is to change the reflectivity of the surface and thus increase the absorbed energy. At low power incident energy densities, local temperatures rise leading to an increase in the thermoelastic stresses and the ultrasound intensity. Secondly, they will alter the nature of the source by increasing the absorptivity of the surface, providing enough energy to vaporise the surface coating, causing a normal reaction on the surface similar to the metal ablation. As a result both stress components parallel and normal to the surface exist and propagate both shear and longitudinal waves in the sample. In ultrasound generation using a CO_2 laser, the presence of a surface coating and roughness may increase the absorptivity of the incident laser energy into the sample surface and lead to surface ablation. This occurs at a lower optical energy density than that required for the break down of the surrounding gas. At higher energy density however, it may be enough to cause the formation of plasma and detonate an air blast wave (Taylor, [1990]). Such surface coating and roughness provides a potential reservoir for easily created electrons to seed the formation of a plasma. In general the presence of a surface coating such as rust, oxide and roughness on the sample surface enhances the ultrasound generation, particularly the longitudinal wave at lower incident laser energy density.

3.3.3 Effect of Rise of the Sample Temperature

Increase in the bulk temperature of the sample may cause the threshold for transition from thermoelastic to ablation regime to occur at a lower power density when less energy is required to raise the temperature of the metal to its boiling point (Dewhurst et al., [1988]). Furthermore, heating may develop an oxide layer that reduces the reflectivity of the sample surface and hence increases the energy absorbed in the surface of the sample. As a result, the thermoelastic stress generated on the surface increases. In the ablation regime, the increase in sample temperature enhances the ablative source strength where more energy is available to raise the temperature of the surface to its boiling point and cause ablation.

3.4 Electromagnetic Acoustic Transducers (EMATs).

Electromagnetic Acoustic Transducers (EMATs) offer a cheaper means for non-contact generation and detection of ultrasound on metals. Whereas the laser approach is truly remote, EMATs have to be operated close to the metal surface as the sensitivity decreases exponentially with stand off. EMATs can be made to withstand high temperature and are relatively easy to use in industrial environments for measurements on hot and/or moving samples. The EMAT is basically an inductive device with a small resistive element of approximately 2-2.5Ω and a small capacitance. For the generation of broadband ultrasound, it is excited by a sharp driving pulse of current through the EMAT rf coil. The amplitude of the ultrasound generated is proportional to the amplitude of the exciting current pulse. Therefore to generate ultrasound at a fixed driving voltage, it is essential to have an EMAT coil with a low impedance so that more current can be driven through it. At the same time, it should induce a large current into the metal sample surface. The larger amplitude of the induced current will give rise to a larger ultrasound

amplitude. As the ultrasound generator, it is desirable to have the EMAT coil with a low inductance.

In non magnetic metals, EMAT transduction occurs by a Lorentz force interaction (Frost, [1979], Dobbs et al., [1976]); between a static magnetic field $\mathbf{B}_o$ (supplied by either a permanent or an electromagnet) and a high frequency induced eddy current **J** created by pulsing a current through an rf coil, positioned in the vicinity of the metal surface. This produces a force with a direction perpendicular to both the static magnetic field and the induced current direction which couples to the atomic lattice, generating an elastic disturbance that is a temporal reproduction of the rf current pulse (Figure-3.5). In ferromagnetic materials, an additional generation mechanism due to the magnetostriction effect is also possible, (Thompson, [1976 and 1978]; Dobbs et al., [1976]), making the transduction mechanism more complicated, being dependent on the metallurgical, electrical and magnetic properties of the sample. The transduction mechanism is also affected by the presence of oxides; in particular magnetite on steel can result in enhanced sensitivity.

In EMAT operation, the electromechanical conversion takes place directly within the eddy current skin depth, and no mechanical coupling to the sample under test is needed. The metal surface acts as it own transducer, and there is no acoustic mismatch between the transducer and the sample. An additional benefit of the EMAT is that it can be made to have a wide bandwidth (0.5-10MHz in this application) and thus it can generate several different ultrasound wave modes, by varying the combinations of the direction of the magnetic field and induced eddy current or the coil design, some of which are not readily generated by a conventional ultrasound transducer. A spiral pancake coil with the magnetic field perpendicular to its plane, generates shear waves that are polarised in the radial direction, (Figure-3.6). It is useful for thickness measurements (Maxfield et al.,

[1987]); and for the determination of interfacial reflection coefficients, (Dixon, [1994]). Other EMAT designs for the generation of various wave polarisations have been described by Frost, [1979] and Hutchins et al., [1985].

3.4.1 Physical Principle of Ultrasound Transduction by an EMAT.

Ultrasound transduction in metal by an EMAT has been described in detail in many publications, e.g. Grubin, [1970], Dobbs et al., [1976]; Kawashima, [1976] and [1984]; Banik et al., [1977]. The EMAT for generating a radially polarised shear wave is shown in figure-3.6. It consists of a flat pancake spiral coil positioned in the vicinity of the sample surface at distance, x, carrying pulsed rf current as a function of time $I\exp(j\omega t)$ at a desired ultrasound frequency ω . A static magnetic field $\mathbf{B}_o$, is applied with direction perpendicular to the coil plane. When an rf electromagnetic wave is incident on the metal surface, the dynamic eddy current $\mathbf{J}\exp(j\omega t)$ and an alternating magnetic field are set up in a thin skin layer beneath the sample surface. In a metal at room temperature, the electromagnetic wave penetrates to a depth determined by the classical skin effect, which is small with respect to the sample thickness. The eddy current density below the sample surface decreases exponentially with the depth, z, from the surface given by $\mathbf{J}_o\exp(-z/\delta)$, where $\mathbf{J}_o$ is the current density at the surface, δ is the electromagnetic skin depth, which can also be written as $\delta^2=2/[\mu_o(1+\chi)\sigma\omega]$, where χ is the magnetic susceptibility, (i.e., $1+\chi=\mu_r$), and σ is the electrical conductivity, it represents the depth at which the current density has dropped by a factor 1/e of the density at the surface $\mathbf{J}_o$. In aluminium, δ is about 25μm at 10MHz, whereas the acoustic waves length λ is about 300-600μm. The eddy current density on the sample surface also decreases exponentially with the rf coil stand-off, x, from the sample surface, given by the factor $\exp.(-4\pi x/D)$, where D is the coil diameter. The stand-off, therefore has to be minimised in order to maximise the EMAT transduction.

In the free electron model of a metal (Smith, [1979]), the metal consists of conduction electrons and a lattice of positively charged ions. The electrons move freely in the background of these positive ions except for infrequent collisions with the impurities in the lattice. The induced rf field in the skin layer accelerates the conduction electrons, transferring their excess momentum to the lattice through collisions. The resulting force on the ions is called the collision drag force. The induced rf field also exerts a Lorentz force on the lattice in the skin layer. If these two forces are dynamically unbalanced, they will excite propagating acoustic waves. In the absence of a static magnetic field, this happens only if the electronic mean free path between collision with ions, $l >> \delta$. These two forces are then spatially separated and produce a shear on the lattice. The generated shear wave will polarise parallel to the electric field in the skin layer. If however, $l<\delta$, the two forces locally cancel each other and there is no acoustic generation (Banik et al., [1977]).

In the presence of a static magnetic field $\mathbf{B}_0$, normal to the surface of the sample, the electrons experience a Lorentz force given by vector relation $\mathbf{F} = \mathbf{J} \times \mathbf{B}_0$. The force $\mathbf{F}$ acts perpendicular to the field $\mathbf{B}_0$ and the eddy current density $\mathbf{J}$ beneath the sample surface. The momentum acquired is then given up to the lattice through the process of collisions and creates unbalanced dynamic forces in the surface layer. This results in the generation of elastic waves with amplitude linear in $\mathbf{B}_0$ and polarised in the direction perpendicular to the electric field. If however the magnetic field is parallel to the surface of the sample and the plane of the rf coil, (Figure-3.7), the generated stress field launches a longitudinal wave. As the generated stress field is the precise temporal reproduction of the rf current, the EMAT generates bulk waves with a plane wave-front. The amplitude of the ultrasound wave generated from the Lorentz force interaction at a distance $z>>\delta$, is given by Grubin, [1970];

$$\xi = \frac{BB_o}{\mu_o \rho \upsilon (1+\beta^2)^{\frac{1}{2}}} \qquad 3.4$$

where ρ, is the material density, υ is the wave velocity, B is the rf magnetic field and B_o is the external magnetic field ($B_o = \mu_o H_o$), β is the skin depth parameter, $\beta = k^2\delta^2/2$ and $k = \omega/\upsilon$ is the ultrasound wave number. The amplitude of the ultrasound wave depends directly on the amplitudes of both static and rf magnetic fields and inversely on the density, sound speed and frequency. It also depends on the skin depth parameter β.

The transduction efficiency η defined as the ratio of the generated acoustic power, P, to the electromagnetic power, Q, entering the surface, for both nonmagnetic and magnetic metal arises from the Lorentz force mechanism is given by Grubin , [1970]:

$$\eta = \frac{P}{Q} = \frac{2B_o^2}{\mu_o \mu_r \rho \omega \upsilon \delta (1+\beta^2)} \qquad 3.5$$

Therefore the transduction efficiency at a given acoustic frequency and $\beta^2 << 1$, is inversely proportional to the skin depth.

3.4.2 Physical Principle of the EMAT Receiver

The interaction between the induced eddy current beneath the sample surface and the applied magnetic field is a reversible process with a similar mechanism applying for the detection of the ultrasound by an EMAT. As a detector, it should be able to induce a large current from the metal sample surface, and therefore preferably requires a higher impedance as the induced signal is proportional to the number of turns of the coil. In this explanation we adopt that of Kawashima, [1984], who initially used a plane shear wave description. In figure-3.8, the incident ultrasound wave propagates normal to the surface along the z-axis, $\mathbf{B_o}$ is the applied external magnetic field in the direction normal to the surface of the sample, $\xi'(y,z,t) = d(\xi(y,z,t)/dt$ is the particle motion velocity. Sinusoidal oscillating ultrasound waves S(z,t) in the metal proceed to the surface and are reflected back.

The sinusoidal oscillation of the metal particle $\xi(y,z,t)$ is given by the superposition of both incident and reflected waves;

$$\xi(y,z,t) = \mathbf{S}_o(e^{-jkz} + e^{jkz})e^{j\omega t} \qquad (3.6)$$

where z is the distance into the sample, k is the ultrasound wavenumber and $\mathbf{S}_o$ is the amplitude. The interaction between the external magnetic field $\mathbf{B}_o$ which is perpendicular to the sample surface and also perpendicular to the particle oscillation, $\xi(y,z,t)$, induces an eddy current density $\mathbf{J}(z,t)$ a skin layer thickness, where

$$\mathbf{J} = \sigma\frac{d}{dt}\xi(y,z,t)\mathbf{B}_o. \qquad (3.7)$$

As a result, the current density $\mathbf{J}$ is associated to the dynamic magnetic field $\mathbf{H}$ in the metal, as given approximately by $\mathbf{J} = \nabla\times\mathbf{H}$. The field $\mathbf{H} = \frac{1}{\mu_o}\nabla\times\mathbf{A}$, with $\mathbf{A}$ the time varying vector potential outside of the specimen which can be detected as a voltage in a pickup coil, (i.e. EMAT receiver) positioned in the vicinity of the specimen under test. The vector potential $\mathbf{A}(z_1,t)$ in the air, in the direction normal to the metal surface at a distance z_1 above the sample, can be written as:

$$\mathbf{A}(z_1) = 2\mathbf{S}_o\mathbf{B}_o\frac{1}{1-\frac{1}{2}jk^2\delta^2} \qquad (3.8)$$

The receiver voltage *V(t)*, due to the sensing of the electric field strength $\mathbf{E}=-j\omega\mathbf{A}$ by the EMAT coil of area W and consisting of N turns per metre placed in the close vicinity of the sample, is given by;

$$V(t) = -NWj\omega\mathbf{A}(z) \qquad (3.9a)$$

$$= -2NWj\omega S_o B_o\frac{1}{1-\frac{1}{2}jk^2\delta^2} \qquad (3.9b)$$

In the above description, we ignored effects due, for example, to temporal variations in both electrical displacement and induction field vectors, non-linear reaction fields arising from coupling between the elastic and electromagnetic fields and propagation of electromagnetic waves in metal. The description can be generalised to include these effects as well as others such as magnetostriction (Frost, [1979]). For the case of a pulsed ultrasound wave $\mathbf{S}_p(z,t)$ with the amplitude at the surface $\mathbf{S}_p(0,t)$, by neglecting the factor

$(k\delta)^2 = 2\beta^2$ and taking the factor $2j\omega S_o$ as $\frac{d}{dt}(2S_p(z,t))$, the equation can be approximated to;

$$V_p(t) = -NWB_o\frac{d}{dt}(2S_p(0,t)) \qquad (3.10)$$

This indicates that the voltage pickup by the EMAT receiver is proportional to the time derivative of the surface motion, making it a velocity sensor.

3.4.3 EMAT Transduction in Magnetic Metals

In magnetic materials, an additional dynamic magnetoelastic force has to be taken into consideration besides the Lorentz force interaction described above. The presence of an alternating magnetic field on the surface of the sample generates an alternating stress and thus generates ultrasound in the sample through the magnetostrictive interaction between the alternating magnetic field and the magnetic domains. The transduction of ultrasound in mild steel by this mechanism has been described by Thompson, [1976 and 1978], for a surface wave, generated using a meander line EMAT and detected by a piezoelectric transducer, however a similar treatment can be used for bulk waves. The transduction efficiency from this mechanism is strongly dependent on the external magnetic field as the magnetostriction coefficient is dependent on the external magnetic field $\mathbf{B}_o$. The contribution of magnetostriction to the transduction efficiency is dominant at lower field and exhibits a maximum at an external field about 0.3T.

The magnetostrictive effects on mild steel are affected by the metallurgical and thermal history of the sample, therefore influencing the EMAT transduction efficiency in magnetic materials. A model of the field dependence of the magnetostrictive generation has been investigated by Thompson, [1978]; and it is determined by the changes in two parameters, the skin depth δ and magnetostrictive-strain coefficients. The signal amplitude is proportional to their product. The increase in generation efficiency when the field intensity approaches 0.3T is caused by the increase in the magnetostrictive coefficient and

a small change in magnetic permeability which results in a small change in δ. At lower fields, below 0.3T, the permeability increases rapidly causing decreases in δ and the transducer efficiency diminishes. This occurs due to increased shielding by the eddy currents which allows less of the material to participate in the generation process. Within the magnetostrictive regime, the magnetostrictive generation is proportional to δ, and decreases in electrical conductivity and magnetic permeability cause an increase in transduction efficiency.

The efficiency of the Lorentz force mechanism on the other hand is independent of the skin depth and electrical conductivity as long as the δ is small with respect to the wavelength. At higher field intensities, δ increases but the magnetostictive-strain coefficient decreases rapidly, making their product significantly smaller. In this high field region, the Lorentz force is dominant and the magnetostrictive and other magnetic forces can be neglected.

3.5 Literature Review on the Applications of the Techniques

The development of non-contacting ultrasound measurement systems to be used in hostile environments and for rapid scanning have received great interest. Ultrasound transduction at elevated temperatures is particularly difficult as the conventional piezoelectric transducers face degradation and loss of sensitivity. This section will describe the development and applications of non-contacting ultrasound transduction at elevated temperatures.

3.5.1 Optical Transduction of Ultrasound at Elevated Temperature

Brammer and Percival in 1970 reported the application of a pulsed laser technique for the determination of elastic constants of a 2024 aluminium alloy over a temperature

range 22-500°C. The ultrasound was generated by Q-switched ruby laser pulses of 5J energy and 15ns duration incident at one end of the rod. The transit time of the ultrasound waves along the rod was measured with a piezoelectric transducer (tourmaline) bonded onto the opposite end of the rod. The laser was fired after temperature equilibrium along the sample length was attained. Two consecutive longitudinal pulse arrivals were measured where the first arrival corresponded to the direct longitudinal pulse propagating along the length of the rod. The second arrival corresponded to the longitudinal wave that had undergone mode conversion into the shear wave propagated across the sample diameter and mode converted back into longitudinal wave upon reflection on the opposite surface. The second longitudinal pulse was measured and delayed from the first by a time related to the rod diameter and also the shear wave velocity in the material. In this experiment, both the material elastic constants were obtained simultaneously from a single measurement.

Calder and Wilcox, [1978]; developed a remote system for ultrasound defect detection at elevated temperature using a pulsed laser generator and laser interferometer as the detector. They used a 15J Q-switched neodymium-glass laser of pulse length 30ns as the ultrasound generator and for detection, they used a Michelson type interferometer, employing a single frequency argon laser operated at wavelength λ=514.5nm and power levels of the order of 0.1W. Measurements were made on the epicentre. The sample surface on the detection side was polished to a reasonable reflective surface to act like a moving mirror of the interferometer. Measurements were made on aluminium, stainless steel, copper, brass, tantalum and molybdenum. The samples were situated inside a clamshell oven with an opening on both ends giving optical access for both the generating and receiving laser beam.

McKie, [1987], has made precise ultrasound velocity measurements at elevated temperature using a pulsed laser generator and interferometric detector. The ultrasound source was a Q switched Nd:YAG laser of 25ns pulse duration with 65mJ energy. The measurement was made on polycrystalline materials namely, iron, dural, aluminium, stainless steel and graphite. The samples were polished to form a mirror in the sample arm of a modified Michelson interferometer, and located in the centre of a temperature controlled furnace. The measurement was made with the ultrasound source and the detector on epicentre. The system was capable of making measurements up to 1000°C with absolute accuracy in ultrasound velocity of $\pm$ 1%.

Another application of the optical transduction of ultrasound at elevated temperature has been reported by Monchalin et al., [1986], to determine both the shear and longitudinal wave velocities in ceramic and metal/ceramic composites at temperatures up to 1000°C. The samples were located in a vacuum chamber to prevent oxidation and the measurement was made on epicentre. The ultrasound was generated by a Q-switched Nd:YAG laser providing 8ns pulses with maximum energy 750mJ. The detector was a heterodyne interferometer using 1.0W single mode argon laser which permits samples with optically rough surfaces to be probed.

3.5.2 EMAT at Elevated Temperature Measurements

Application of EMATs for generation and detection of ultrasound at elevated temperature has been reported. Parkinson et al., [1977] have carried out experiments using a shear wave EMAT to measure the variations of wave velocity, attenuation and signal amplitude in steel bars over the temperature range 20°C to 900°C. The technique used a through-transmission arrangement. The magnetic field for the EMAT operation was produced by a dc electromagnet. The separation between the EMAT surface and test

surface was approximately 1.5mm. The results show that the shear wave amplitude decreased rapidly by more than 20dB above 740°C, and disappeared at 750°C. It was also observed that the EMAT generated a strong longitudinal wave in the temperature range 760°C-800°C, and exhibited a peak amplitude (~20dB above the shear wave signal level at room temperature) at about 780°C. The longitudinal wave disappeared at temperatures above 800°C. The authors noted that the generation of the longitudinal wave occurred due to the reorientation of the magnetic flux that entered the sample in a direction that was favourable for the generation of longitudinal waves. Furthermore, in this temperature range, when steel becomes paramagnetic, the surface temperature is likely to be slightly lower than the interior temperatures, a thin layer of ferromagnetic material exists at the surface and acts to concentrate the magnetic field parallel to the surface. They concluded that shear waves are preferable for the thickness measurement on hot steel for temperatures ranging up to 750°C and that measurement would have to be accompanied by an independent temperature measurement of the sample because of the dependence of shear wave velocity on temperature. It was suggested that, for temperatures above 760°C-800°C , the inspection could be easily achieved using the anomalous longitudinal waves generated by a shear wave EMAT. The authors have also developed a prototype EMAT inspection unit for use on a steel production line. Two EMAT coils were placed side by side under the separate pole piece for transmitting and receiving function. The system was water cooled and has been tested up to 500°C at a scanning speed of $1 ms^{-1}$.

Whittington, [1978] has described the application of EMAT for defect detection on hot steel. The shear wave EMAT was used when working below the Curie temperature (about 760°C) and operated in send-receive arrangement with the transmitting and receiving coils positioned side by side. The attenuation of the shear waves is very high above this temperature, so that a higher temperature system would use longitudinal waves.

The longitudinal wave EMAT designed for higher temperature operation uses concentric transmit and receive coils, arranged between the electromagnet pole-pieces.

An experiment using an EMAT to study the effect of temperature on the transduction of a longitudinal surface wave in steel samples has been reported, (Cole, [1978]). The transducer comprised an E-cored dc electromagnet with transmitting and receiving coils arranged between the pole pieces. The coils consisted of four elements in the form of identical grids, each having 3 turns of 0.5mm diameter platinum wire. These 4 coil elements were in anti-phase arrangement The wavelength was 9mm for a 250kHz operating frequency at 800°C. It was noted that the surface waves can be generated on mild steel up to 1000°C and an enhancement region exists when the bulk of the material is non-ferromagnetic but the surface layer is ferromagnetic. This caused the magnetic flux to concentrate in the ferromagnetic surface layer.

Whittington, [1989] carried out experiments using EMATs for generation and detection of Lamb waves on hot aluminium strip. The author used an rf excitation shear EMAT in the frequency range 300kHz - 3MHz, and caused the plate to resonate in its thickness at specific harmonic frequencies. By measuring the resonance frequency, the sample thickness can be determined if the shear wave velocity is known. At the fundamental resonant frequency, a standing wave will be set up with two nodes positioned at the faces of the plate, such that the thickness of the plate represents the half-wavelength of the ultrasound signal. At the n-th harmonic resonant frequency, n half wavelengths represent the plate thickness. In the experiment, the plate was heated up to 500°C and the rf signal was swept to generate shear waves in the range 300kHz-3MHz, and when the n-th harmonic resonance was observed, the rf frequency f was measured and thus the velocity could be determined (velocity = 2f/n). From here the relation between the shear wave's velocity and the temperature could be established.

Boyd et al., [1988], have developed a through transmission EMAT pulser and receiver system for the thickness measurement of steel billet of cross section dimension 100mm x100mm, in a steel mill. The measurement was made using a longitudinal wave at temperatures up to about 1100°C. The EMATs were water-cooled and have been used for continuous operation to test samples at temperatures below 600°C.

The application of an ultrasonic longitudinal wave generated and detected by a water- cooled electromagnetic EMAT is reported by Yamaguchi et al., [1984] for the inspection of hot steel billet. The EMAT-EMAT system operated in through-transmission. Between the poles of the electromagnet, there were six sensors of transmitter and receiver coils arranged on six circumferential points of the sample. These EMATs were water-cooled and operated with a magnetic field of more than 1T on the sample surface, 10mm beneath the magnet poles. The transmitter was operated at about 250Hz, 30A peak to peak 200ns. The approach was able to detect simulated flaws of side drilled holes 4mm diameter in hot steel billet, 180mm thick at 860°C and 10mm diameter side-drilled holes in 250mm thick steel slab at 930°C. Improvement of the EMAT electronic system has been reported by Kubota et al., [1988].

Lee et al., [1992] studied the temperature dependence of the ultrasound velocities and attenuation in ferromagnetic steel and stainless steel samples at elevated temperatures. Measurements were made up to 800°C using water-cooled permanent magnet shear and longitudinal EMATs. The result showed that for both type of samples, the longitudinal and shear wave velocities decreased linearly with the increasing temperature.

3.5.2 The Application of Laser-EMAT System at Elevated Temperatures

The applications of laser-EMAT combinations at elevated temperature have also been studied. Burns et al., [1988] have developed a compact longitudinal wave EMAT

receiver for use with a pulsed laser as the ultrasound generator. The magnetic field required for EMAT operation was provided by a magnetising pancake coil, consisting of 50 turns of 3mm copper tape wound with an internal diameter of 6mm and outer diameter of 40mm and housed in a water-cooled chamber that had been grounded. The magnetising coil was energised by a current pulse with amplitude 1400A and pulse duration 30μs, this produced a tangential field beneath the coil of approximately 0.8T near to a steel sample. A pancake EMAT coil was laid beneath the magnetising coil and protected from the radiant heat by an alumina plate. The system has been demonstrated on stainless steel samples with thickness of up to 250mm at temperatures up to 500°C; the measurement was carried out in through-transmission arrangement.

Boyd and Sperline, [1988]; have used a laser-EMAT system to measure acoustic velocity in stainless steel samples up to 750°C by continuous EMAT contact and up to 1300°C by momentary EMAT contact. They developed a system using a liquid dye Q-switched pulsed ruby laser for the ultrasound generator and longitudinal pulsed EMAT as the receiver in a through-transmission arrangement. The measurement was carried out with the EMAT on the epicentre.

In another study, Wadley et al., [1986]; used a laser generator and EMAT detector to determine the internal temperature distribution in a steel billet at elevated temperatures. The samples were heated to a temperature of about 700°C in an induction furnace before being transferred to the experimental table. The ultrasound was generated by a Q-switched Nd:YAG laser capable of producing energy about 850mJ. A water-cooled EMAT with sensing coil of dimension 4mm x 4mm was placed at 1mm stand-off and measurements were made in a through-transmission arrangement. Thermocouples were mounted at various positions on the sample to provide continuous internal temperature monitoring. The average sample temperature was determined using a calibrated relationship between

the ultrasound velocity and temperature. The velocity data then was used to compute a tomographic reconstruction of the internal temperature distribution of the sample. The measured and the reconstructed temperature data are in agreement to within about 20°C in the cylindrical sample and within 10°C for the square sample. Data were obtained at temperatures as high as 750°C.

A non-contacting ultrasound system using a pulsed laser generator and magnetomechanical sensing coil detector has been developed to monitor the structural changes in metallic amorphous ribbon, (Greenough et al., [1987]). The ultrasound was generated from an ablative line source and a detector monitored the waveform at some distance from the source. The quality of the ribbon was assessed by either changes in the wave velocity or the signal amplitude. The system was capable of showing the velocity changes in Metglass 2605SC from $4940ms^{-1}$ to $5830ms^{-1}$ as the materials became progressively less amorphous.

Carlson et al., [1993]; have developed a computerised Nd:YAG laser-EMAT system to be used for concurrent defect detection in solidified weld metal. The EMAT operated with a permanent magnet and was sensitive to incident shear waves at 45° with a frequency range of about 0.5 to 2MHz. During the operation, the laser beam was irradiated onto the weld pool and the EMAT was scanned in parallel to the weld bead at the top surface of the parent metal. The EMAT detected the ultrasound pulses generated by the pulse laser ablation on the solidified weld metal, after being reflected and/or mode converted at the bottom surface of the sample. The technique has been tested on the preheated sample at 93°C and was capable of detecting defects on pass-by-pass basis when joining thick section plate using gas metal arc-welding (GMAW). The information obtained from this measurement will be used as a feedback device to the welding process.

Billson et al., [1993]; have described the shear wave measurement to monitor phase transition in zircalloy using a laser generator and EMAT receiver. The system operated in through-transmission arrangement on the hydrided and unhydrided samples during cooling. They plotted the measured shear wave transit time with the temperature and deduced the material's phase transition from the change in the gradient of the curve of the hydrided sample. Such change did not occur in the unhydrided sample thus it did not undergo phase transition during the cooling process.

More recently Idris, [1995]; used laser generator and EMAT receiver to monitor the partial melting of thixoforgeable materials such as aluminium silicon alloys and also other metals with higher melting points such as Cu-Sn alloy, mild steel, and tool steel. In this work, the ultrasound was generated by Nd:YAG laser and a water-cooled permanent magnet shear EMAT as the receiver. The system operated in through-transmission arrangement and the EMAT was only introduced onto the sample surface momentarily to capture the waveform. The system was capable of making measurements not only in the partially molten state but also in the fully molten state with the temperature 1140°C in mild steel. The author also used a pulsed CO_2 laser to generate ultrasound in mild steel and this was detected by the EMAT on epicentre. The system can be operated up to temperatures of about 900°C.

The capability of the laser-EMAT system for non-contact ultrasound measurements at high temperature has been reported by Edwards et al., [1994]. The measurement was carried out on a 50mm thick low carbon steel heated in a large cylindrical bore electric furnace. A 100mJ Nd:YAG laser and a concentric water-cooled permanent shear EMAT with a 3.5mm diameter hole, were used as ultrasound generator and the receiver respectively. The system was made in hand-held size and operated in send-receive arrangement where the sample was assessed from a single side at sample temperatures up

to 605°C. In a separate paper, Edwards et al.,[1995] described the application of send-receive EMAT system to monitor steel kettle's wall thickness on a galvanising tank. A water-cooled permanent magnet shear EMAT was used. The measurement was carried out in situ at temperatures of about 450°C without the need to shut off the galvanising operation. The system is capable of revealing the actual remaining steel wall thickness and the steel-zinc complex layer and thus provides an effective means for wall thickness monitoring. Another laser-EMAT measurement at elevated temperature up to 1200°C has been reported by Billson et al., [1995]. The measurement was carried out on 12mm wall thickness mild steel extruded pipe. A CO_2 laser and a concentric water-cooled permanent magnet shear EMAT was used as the ultrasound generator and receiver respectively. The laser beam was focused onto the sample surface using a germanium converging lens (focal length 200mm).

3.6 Discussion

In the preceding section, various non-contact ultrasound systems and their applications at elevated temperature in particular, have been described. EMATs are perhaps the most well known transducer design for non-contact ultrasound measurement on conducting surfaces. The EMAT does not suffer from couplant problems but it still has to be operated very close to the surface of the sample and suffers sensitivity variation due to changes in stand off as both the static and dynamic magnetic field strengths decrease with the increase in stand off. Although ultrasound transduction by EMATs is relatively inefficient compared to piezoelectric transducers, its non-contact nature has advantages at elevated temperatures. EMATs have been used for thickness measurement on hot steel in production line and are also useful in the presence of relative motion between the sample and the transducer. An advantage of EMATs is that their characteristics may be changed

simply by interchanging the coil geometry and/or the direction of the magnetic field and, for high temperature operations, it can easily be water-cooled. These devices can be used as the detector and they can be constructed to have a wide bandwidth.

Ultrasound measurement at elevated temperatures is limited by the intense heat that will destroy the transducers and also the need to deliver a high intensity of ultrasound into the sample that exhibits a high ultrasound attenuation to observe a discernible effect. Pulsed lasers have several advantages as an ultrasound generator, where they are able to generate both longitudinal and shear waves in bulk solid materials at a reasonable amplitude. The generated ultrasound pulses exhibit very wide bandwidths of the same order of the laser pulse duration and their spectra carry appreciable ultrasound energy ranging from audible frequencies to tens of megahertz which are not flat but fall slowly and monotonically with increasing frequency. The generated ultrasound takes the form of short and well-defined monopolar pulses without any reverberation. It can be operated totally remote from the sample surface and this eliminates any problems of coupling to the sample, hence it can be used in hostile environments and allow rapid scanning. On a rough surface due to oxide layer or surface coating, most of the incident laser energy will be absorbed and enhance the ultrasound generation.

The combination of laser generation and reception of ultrasound offers entirely remote transduction and has a good sensitivity comparable to EMATs. Their remote nature and the small diameter of both the laser irradiating beam and the irradiated area of the sample, mean that the techniques can be used for applications with awkward or limited access. However there are potential disadvantages of laser reception systems. They are at their most sensitive when the sample surface is highly polished. They rapidly lose sensitivity as the surface becomes roughened or dirty and absorbs the light. Such polished surfaces are hardly encountered in industrial environments, in particular at elevated

temperature. It is difficult to maintain maximum reflectivity as the sample tends to oxidise and the surface becomes tarnished. McKie, [1987] and Dewhurst et al., [1988] noted that the ultrasound waveforms detected by laser interferometer at elevated temperature exhibit weak and broad features and hence the transit time could not be determined accurately.

Laser generation and EMAT detection ultrasound systems are relatively insensitive to the surface finish or roughness and sample vibration therefore, this approach has an advantage over the laser detection systems although they are not an entirely remote system. The systems are insensitive to alignment problems and ease of scanning. The measurements have been made on hot steel up to a temperatures as high as 1100°C with the EMAT detector positioned on epicentre.

3.7 Conclusions

Various aspects of non-contact ultrasound transduction have been described with particular emphasis on elevated temperature applications. Each particular system has its limitations and advantages. Laser-EMAT systems have the advantage of being relatively low cost, with robust detectors which could be applied to ultrasound measurements on hot steel at elevated temperature. A send-receive arrangement, where the detector and the ultrasound source are positioned on the same side of a hot steel sample, is the ultimate aim of this thesis.

3.8 References

Allen D. R. and Sayers C. M.,Ultrasonics, **Vol. 22**, 1984 pp.179-186.

Andrews K.A., in Ultrasonic Testing, Edited by Szilard J., (John Wiley & Sons New York), 1982 pp. 411-436.

Aussel J. D and Monchalin J. P., Ultrasonics, **Vol. 27**, May 1989, pp.165-177.

Banik N. C. and Overhauser A. W., Physical Review B, **Vol. 16**, no. 8, 1977, pp.3379-3388.

Bilson D., Hutchins D., Jour. Nondestr. Test. **Vol.10**, 1993.

Bilson D., Edwards C., Rohani M.S., Palmer S.B., Paper Presented in Institute of Metal's meeting , May 1995.

Boyd D. M. and Sperline P. D., in Progress In Quantitative NDE, ed. D.O Thompson and D.E Chimenti., **Vol. 7B**, 1988, (Plenum New York), pp. 1669-1676.

Boyd D. M. and Sperline P. D., In Plant Demonstration of High Temperature EM Pulser and Pulsed EMAT Receiver: Final Report." Pasific Northwest Lab., Richland USA 1988.

Brammer J.A and Percival C.M., Experimental Mechanics, June, 1970, pp.245-0250

Burns L. R., Alers G. A. and MacLauchlan D. T., Prog. In Quantitative NDE, ed. Thompson D.O. and Chimenti D.E., **Vol. 7B,** 1988 , (Plenum , New York), pp.1677 1683.

Calder C.A. and Wilcox W.W., Edited by Smith G.V., (ASME) 1978, pp.169-181.

Carlson M. N., Johnson A.J., and Larsen E.D., Prog. Review In Quantitative NDE., **Vol. 12A**, (Plenum), New York, 1993, pp.949-956.

Cole P. T., Ultrasonic, July 1978, pp.151-155.

Cooper J. A., PhD Thesis, University of Hull, 1985.

Darbari G. S., Singh R. P. and Verma G. S., J.of Appl. Phys., **Vol. 39**, no.5, April 1968, pp.2238-2243.

Davies S. J., Edwards C., Taylor G.S. and Palmer S.B., J. Phys. D: Appl. Phys. **Vol. 26,** (1993) pp. 329-348

Dewhurst R. J., Hutchins D. A., Palmer S. B. and Scruby C. B., J. Appl. Phys., **Vol. 53,** no. 6, 1982, pp.4064-4071.

Dewhurst R.J., Edwards C., McKie A.D.W and Palmer S.B., J. Appl. Phys. **Vol. 63** (4), 15 Feb. (1988), pp.1225-1227.

Dixon S., PhD Thesis, University Of Warwick, 1994

Dobbs E. R., in Physical Acoustic, ed. W.P Mason and R.N Thruston. **Vol.7**, 1976, (Academic Press, New York), pp.197).

Edwards C., Taylor G. S. and Palmer S. B., J. Phys D. Appl. Phys. **Vol. 22**, 1989, pp.1266-1270.

Edwards C., Nurse G., Dewhurst R. J. and Palmer S.B., British Journal of NDT, **Vol. 32,** No.2, 1990 pp.76-78

Edwards C., Dixon S., Idris A., Reed J. and Palmer S.B., in Rev. in Prog. of Quantitative Nondestructive Evaluation, **vol.14B**, Colorado, (1994), pp.2253-2260.

Edwards C., Dixon S. and Palmer S. B., INSIGHT , **Vol. 37**, 1995.

Farlow R and Hayward G., INSIGHT **Vol. 36**, no.12, Dec. 1994, pp. 926-935.

Frost H. M., in Physical Acoustic, ed. W.P Mason and R.N Thruston. **Vol. 14**. 1979, (Academic Press, New York), pp. 179-275.

Greenough, Dewhurst R. J. and Edwards C., J. Appl. Phys.**Vol. 62**, pp.4728-4731, 1987.

Grubin H. L., IEEE Trans. on Sonic and Ultrasonics, **Vol. SU-17,** No. 4 1970, pp.227-229.

Hutchins D. A. and Macphail J. D., J. Phys. E, **Vol.18,** pp.69-73, 1985

Hutchins D. A and Wilkins D. E., J. Appl. Phys. Vol. 58 no. 7, pp.2469-2477, 1985.

Hutchin D.A., Wright W.M.D. and Hayward G., IEEE Trans. Ultrson., Ferroelectric, and Freq. Control, **Vol. 41**, no. 6, Nov. 1994, pp.796-805.

Idris A. Edwards C. and Palmer S. B., Nondestr. Test. Eval., **Vol. 11,** (1994), pp.195-213.

Idris A.; Ph D Thesis, Warwick University, 1995

Jacksons J. D., Classical Electrodynamic, 1974, Chapmann-Hall. London.

Kawashima K., J. Acoust. Soc. Am., **Vol. 60,** No.5, Nov. 1976.

Kawashima K., IEEE Trans. on Sonic and Ultrasonics, **Vol. SU-31**, No.2, 1984, pp. 83-94.

Kaye G. W. C. and Laby T. H., Tables Of Physical and Mechanical Constants, (Longman London) 1986

Krautkramer J. and Krautkramer H., Ultrasonic Testing of Materials, 3rd. Edition, Springer-Verlag, (1983).

Kubota J., Sasaki S., Sato.I., Ito S., Kadowaki T., Yamaguchi H., Fujisawa K. and Murayama R., Material Evaluation, **Vol. 46**, March 1988, pp.523-526.

Lavender J.D., Journal of Research, SCRATA, **Vol.12**, March, 1971, pp.31-35

Lee S.S and Ahn B.Y., Nondestr. Test. Eval., **Vol. 7,** (1992), pp.253-261.

Maxfield B. W., Kuramoto A. and Hulbert J. K., Material Evaluation, **Vol. 45,** Oct.1987, pp.1166-1183.

McKie A.: Ph D Thesis , University of Hull , (1987)

Monchalin J.P. and Heon R., Materials Evaluation, **Vol. 44,** Sept.(1986), pp.1231-1237

Papadakis E. P., Lynnworth L. C., Fowler K. A. and Carnevale E. H., J. Acoust. Soc. Am., **Vol. 52,** no. 3, (part 2), 1972, pp.850-857.

Parkinson G.J and Wilson D.M., Brit. Jour. of NDT, July 1977, pp.1184-1189.

Ready J. F., J. Appl. Phys. **Vol. 36** (2) pp.462-468, 1965

Scruby C. B., Palmer S. B., Dewhurst R. J. and Hutchins D. A., J. Appl. Phys. **Vol. 51,** 1980, pp.6210-6216.

Scruby C. B., Palmer S. B., Dewhurst R. J. and Hutchins D. A., in Research Techniques in NDT, ed. R.S.Sharpe, **Vol. 5** 1982, chap. 8, pp. 281- 327. (Academic Press, London) 1982.

Scruby C. B. and Drain L., Laser Ultrasonics: Techniques and Applications, Adam Hilger, Bristol 1990

Smith R.A., Wave Mechanics In Crystalline Solids, Ch.2. Butterworth, London, 1979.

Taylor G. S., The TEA-CO_2 Laser As A Means Of Generating Ultrasound In Solid, PhD Thesis , University Of Warwick, 1990

Thompson R. B., Appl. Phys. Letters, **Vol. 28**, no. 9, 1976, pp.483-485

Thompson R. B., IEEE Trans. on Sonic and Ultrasonics, **Vol.SU-25**, No.1, 1978, pp.7-15.

Wadley H. N. G., Norton S. J., Mauer F. and Droney B., Phill. Trans. R. Proc. Lond. **A 320,** pp.341-361 (1986).

Whittington K. R.. Phys. Technol. **Vol. 9**, (1978) pp. 62-68.

Whittington K .R., British Journal NDT, **Vol. 31,** no.3 March 1989, pp.140-144.

White R. M., Jour. Appl. Phys. **Vol.34,** no.12, 1963, pp.3559-3567.

Yamaguchi H., Hashimoto K., Ikishawa H., Kadoki T., Sato I., in Rev. Prog. In Quantitative NDE., ed. D.O. Thompson and D.E Chimenti, **Vol. 3,** Plenum, New York (1984), pp. 734-737

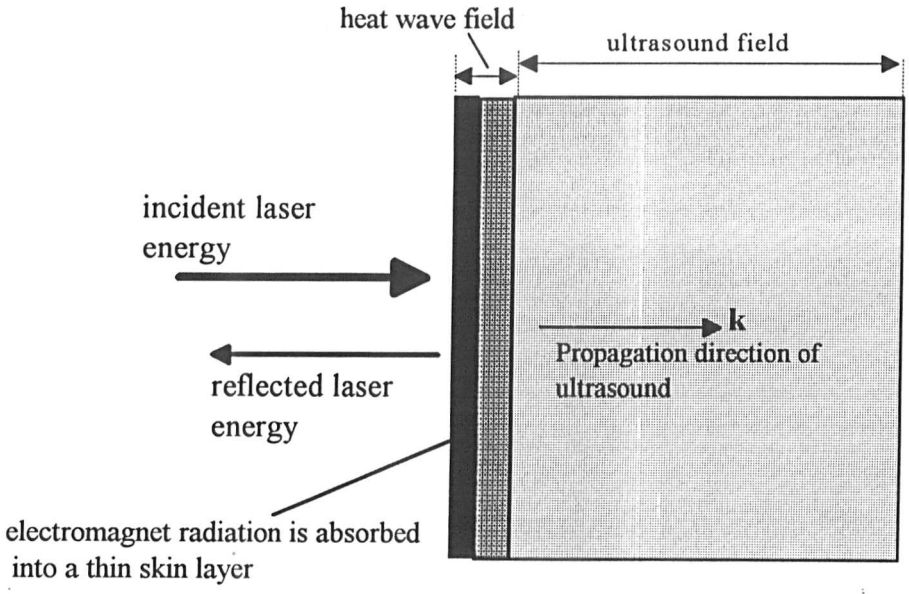

Figure-3.1: The incident pulsed elctromagnetic radiation from the laser is absorbed into a thin layer of the sample surface. Evaporation of the surface material and/or thermal expansion occurs depending on the laser energy density, causing the generation of a stress wave and thus the ultrasound into the material.

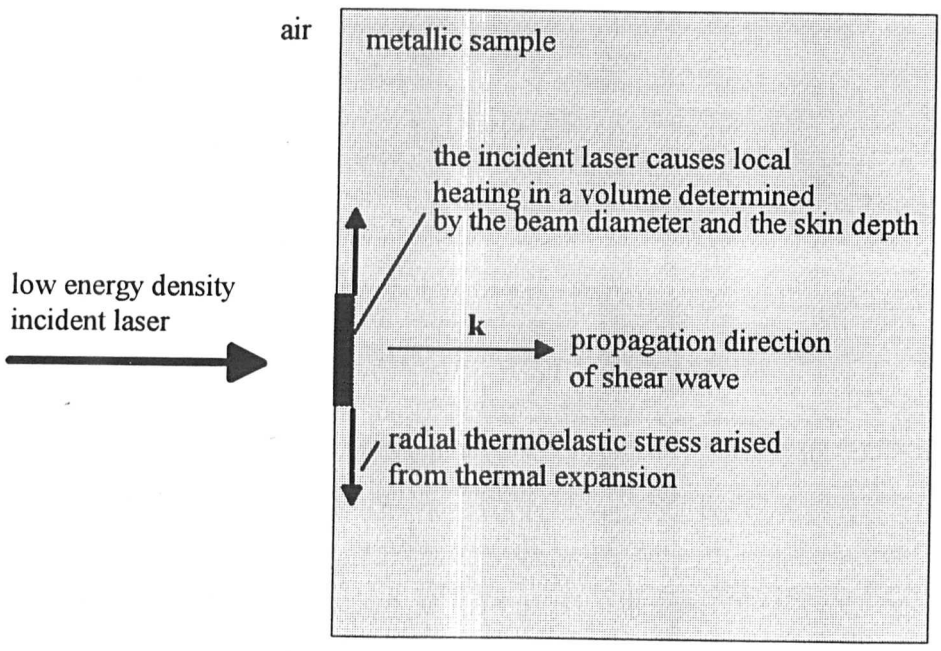

Figure-3.2: The incident low energy density pulsed laser causes local heating at the surface, creating a radial thermoelastic stress parallel to the surface and with zero net normal component. The stress wave then propagates into the sample . as a shear wave.

(a) Buried under the surface

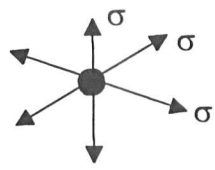

(b) On the surface with neglectable thickness

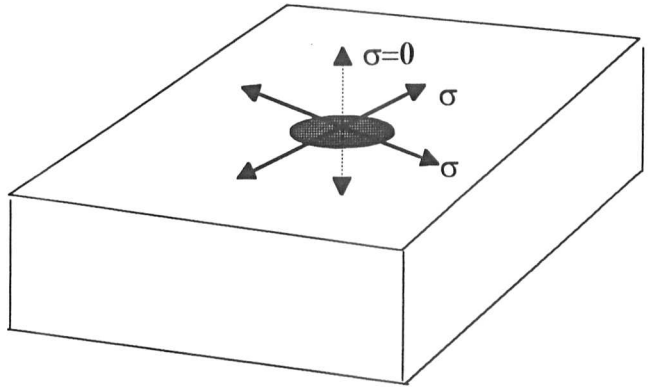

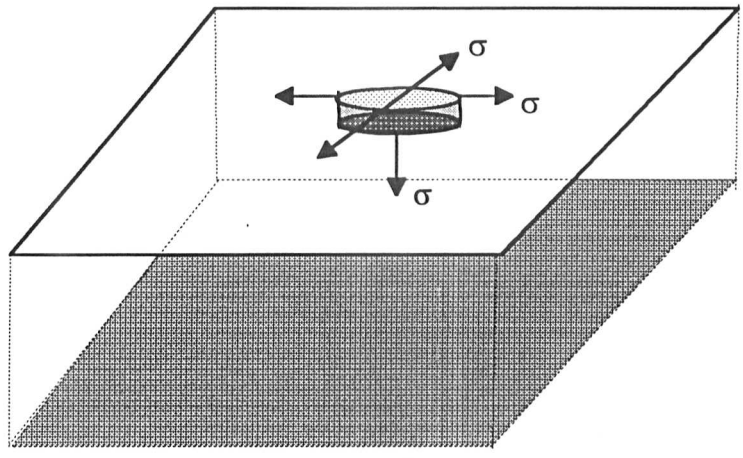

(c) Exhibits a finite thickness beneath the surface

Figure-3.3: If the thermoelastic source is buried (a) or has a finite thickness beneath the surface (c), it will produce a net component of stress normal to the surface and generates a longitudinal wave besides the shear wave. If the thermoelastic source lies on the surface with neglectable thickness (b), it will excite a shear wave (After Dewhurst et al.,[1982])

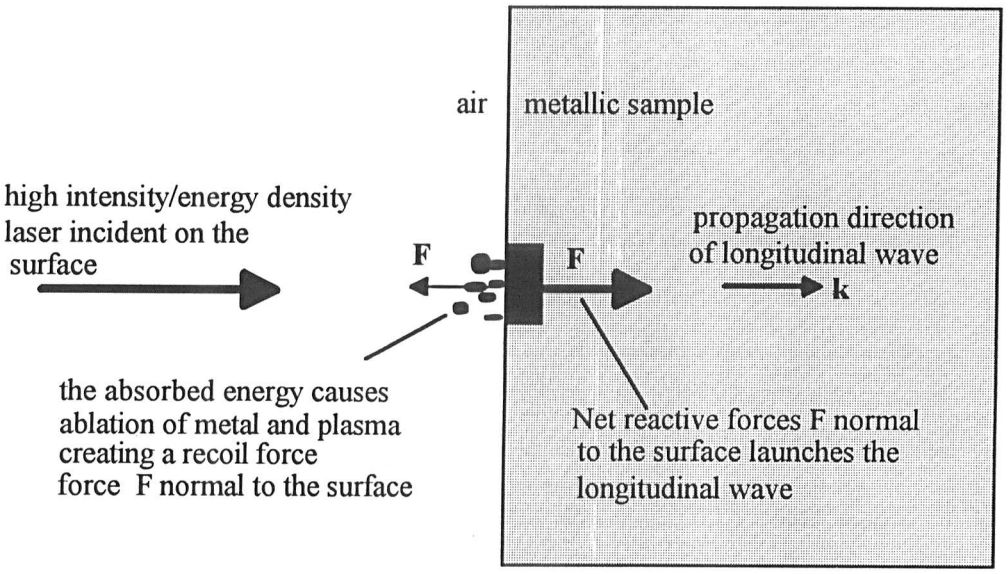

Figure-3.4: The incidence of a high energy density laser causes ablation or vaporisation of the material at the surface and creates a net recoil force normal to the surface, generating an ablative ultrasound source that launches a longitudinal wave.

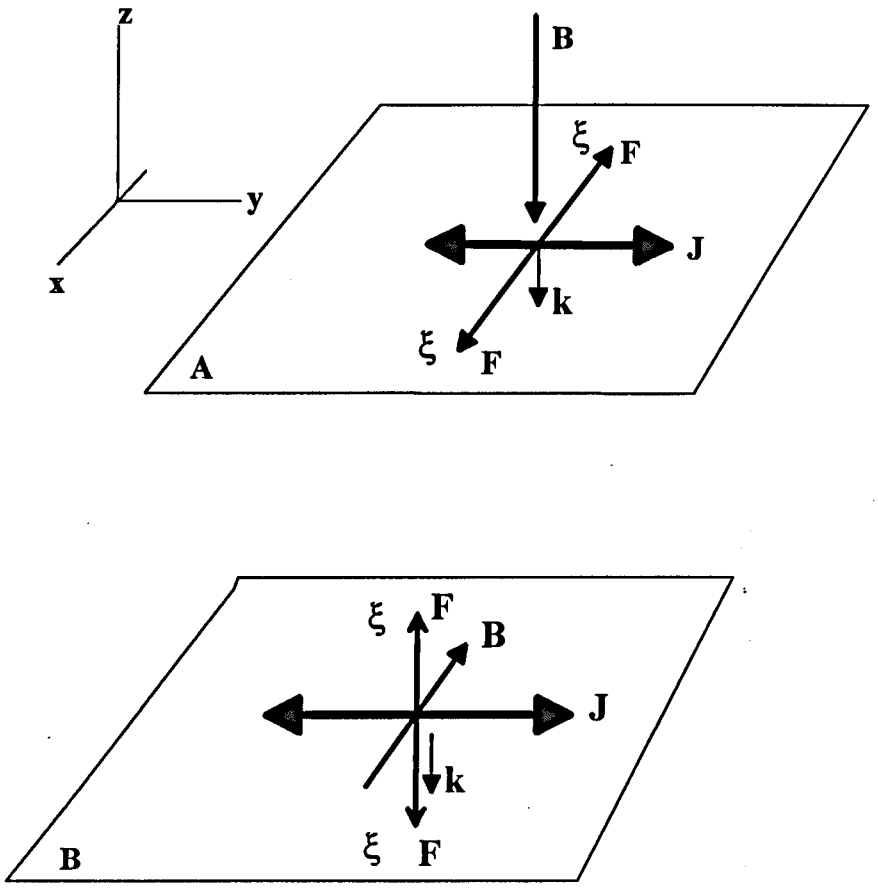

Figure-3.5: Lorentz force interaction between the static magnetic field **B** and the alternating current **J** polarised in the xy plane, and propagates along -z direction. (A) If the magnetic field is normal to the surface, it generates a shear wave with particle oscillation ξ tangential to the surface. (B) If the magnetic field is parallel to the surface along the x-axis, it will generate a longitudinal wave with particle oscillation ξ normal to the surface or in out of plane. .

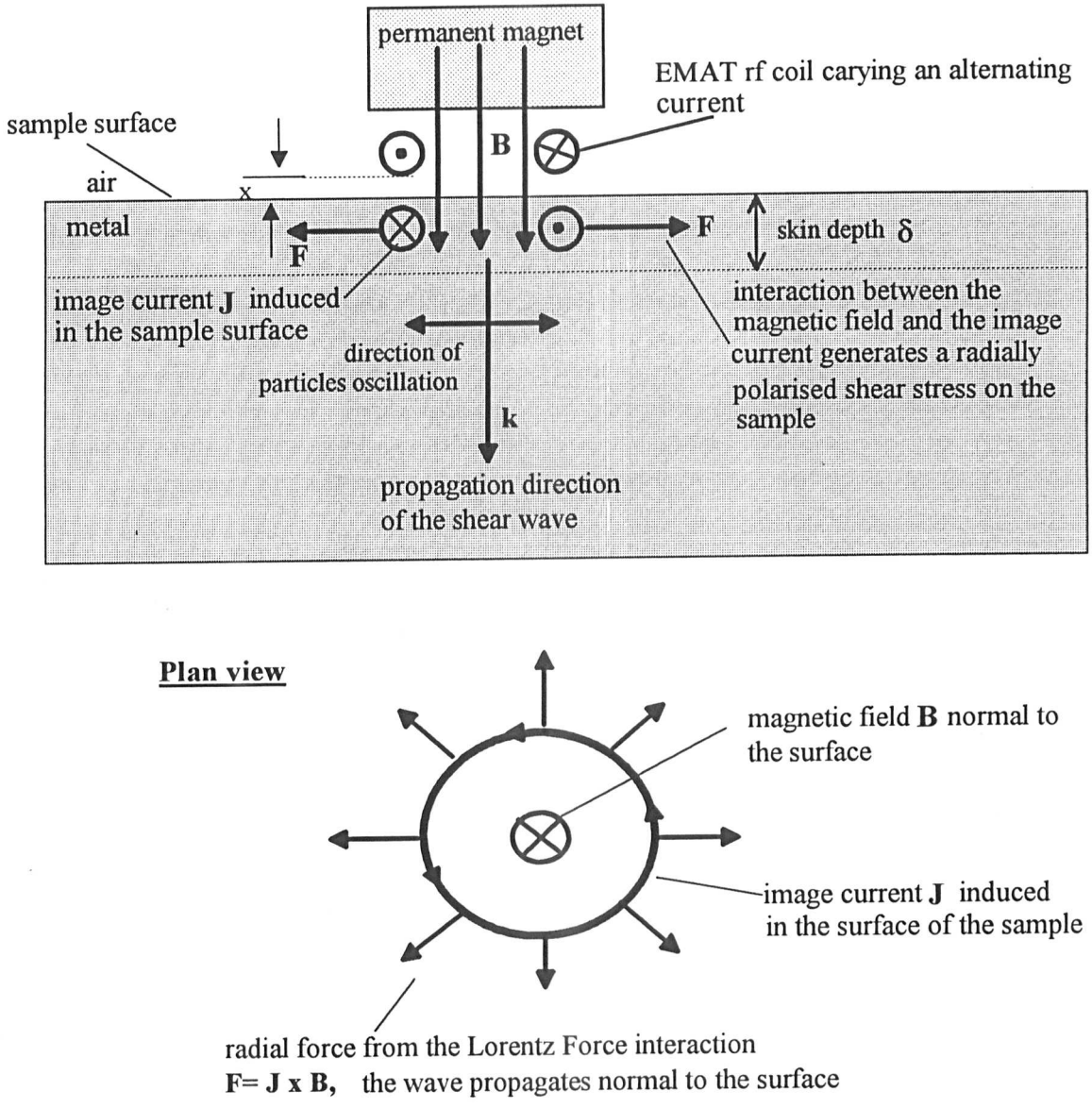

Figure-3.6: Shear wave generation in metal through Lorentz force interaction between the induced image current and the magnetic field. EMAT coil carrying. an rf current in the x-y plane, induced image current **J** in the sample subsurface and distributed in a similar configuration to the rf coil. The image current penetrates the sample with an amplitude decay within the depth of penetration δ of the metal and propagates along the z-axis. Interaction between the image current **J** and the magnetic field **B** normal to the surface generates a shear wave polarised radially and propagating along the z-axis.

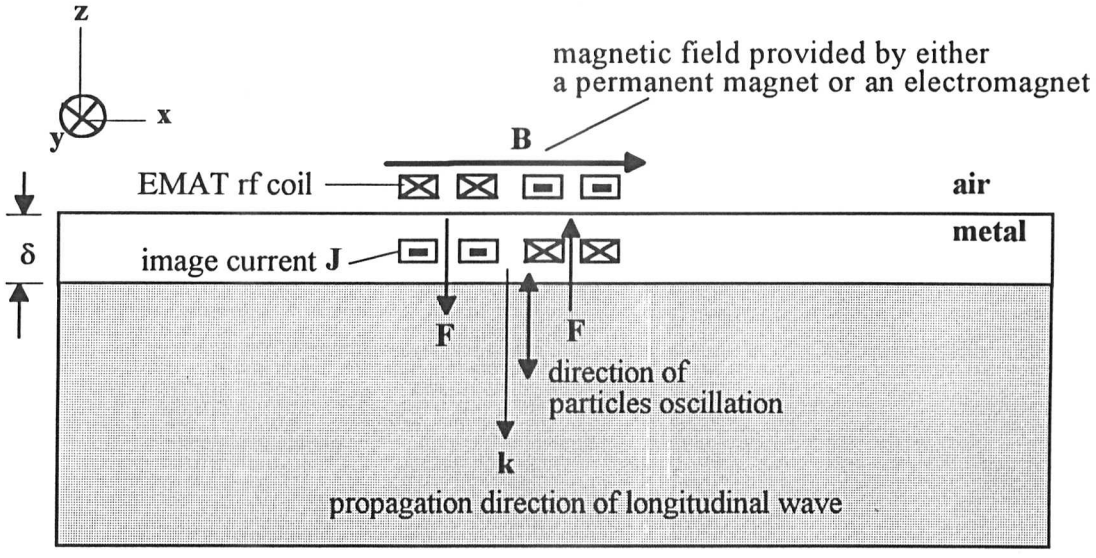

Figure-3.7: Longitudinal wave generation in metal through Lorentz force interaction between the induced image current and the magnetic field. The magnetic field is along the y-axis interacts with the image current lying in the xy-plane producing an alternating force along the z-axis and propagating in the -z direction.

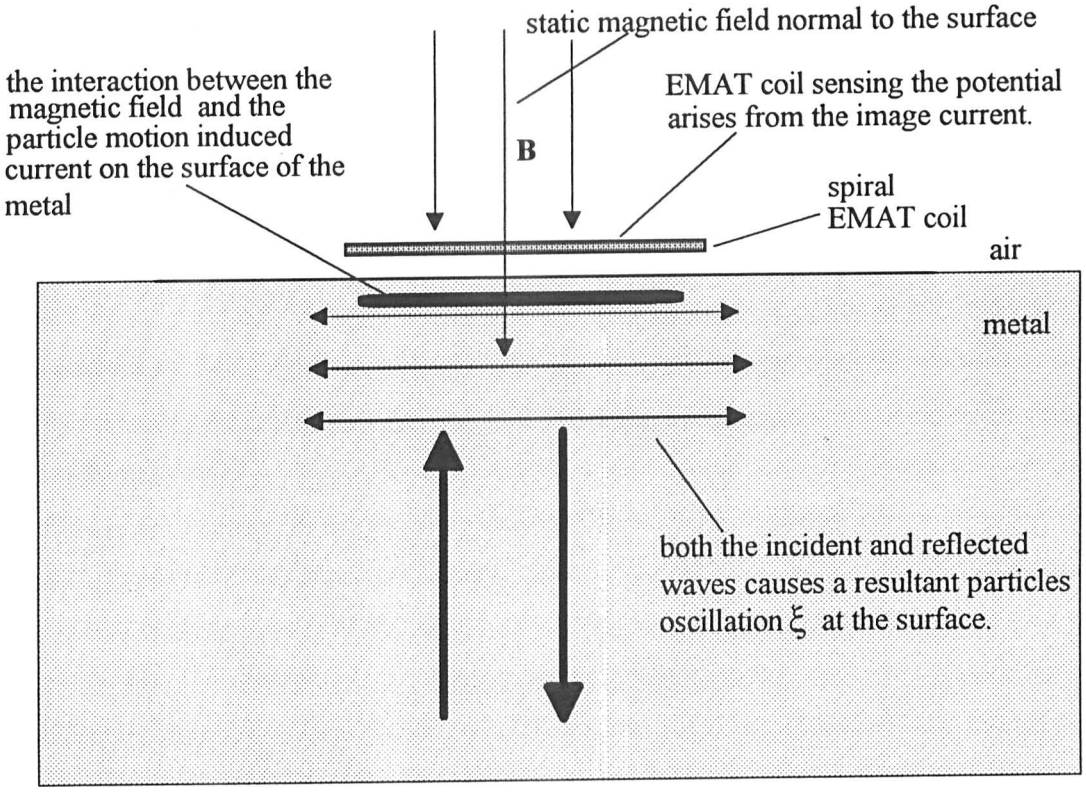

Figure-3.8: Two dimensional model for the detection mechanism by a shear wave EMAT. The interaction between the particle oscillation at speed $d\xi/dt$ with magnetic field **B** ,causes an induced current **J** on the surface that will be detected by EMAT rf coil.

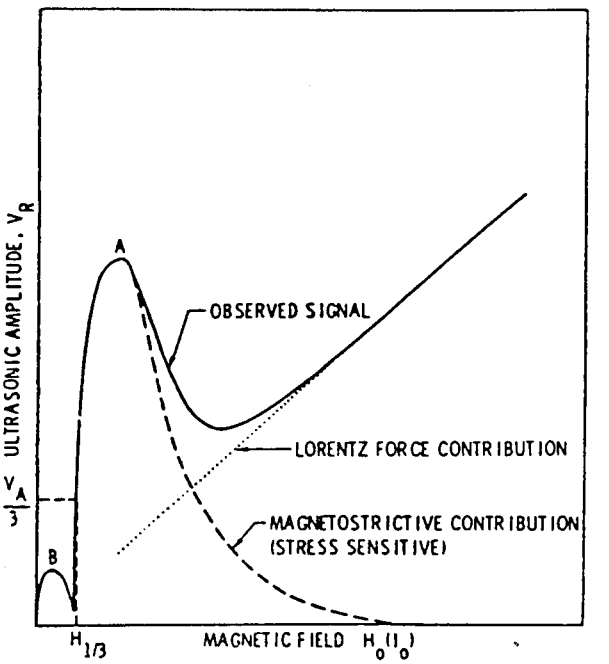

Figure-3.9: The predicted magnetic field dependence of the acoustic wave amplitude in polycrystalline iron generated by EMAT and detected by piezoelectric transducer (after Thompson, [1978]).

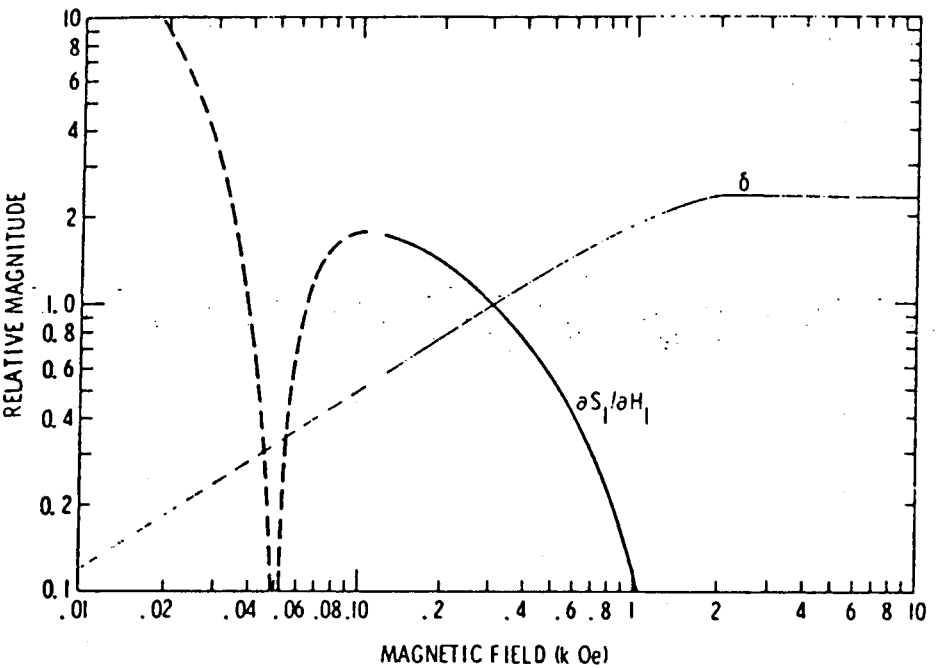

Figure-3.10: The theoretical prediction of the magnetic field dependence of the magnetostriction-strain coefficient and skin depth in a polycrystalline iron, to estimate EMAT transduction efficiency (after Thompson, [1978]).

CHAPTER-4

The Development Of High Temperature EMATs

4.0 Introduction

Various techniques for non-contact ultrasound measurements in solids have been developed recently. The application of EMATs and the combination of pulsed laser-EMAT systems have been discussed in the previous chapter. Measurements have been carried out at elevated temperatures (Idris, [1995], Lee at.al., [1992]) and on moving hot steel (Burns et.al., [1987]). This chapter will describe the design of a water-cooled P-EMAT for ultrasound measurements at high temperature followed by the design and operation of an E-EMAT. Secondly we will discuss the use of the E-EMAT as the ultrasound receiver for laser generated ultrasound. In this technique the EMAT, located on the generation side will be used to measure the transit time taken for the ultrasound propagation within the sample. The ultrasound will be generated by pulsed lasers and in particular a Nd:YAG laser, (LUMONICS HY400) with wavelength 1.064μm and a Transverse Excitation Atmospheric (TEA), CO_2 laser, (COHERENT Laserbrand M15 Mk IV) with wavelength 10.6μm.

4.1 Permanent Magnet EMAT (P-EMAT)

A P-EMAT used in the work reported in this thesis is shown in figure-4.1. The magnetic field required for the EMAT operation was produced by a NdFeB (Neodymium Iron Boron) permanent magnet, manufactured by Magnetic Development Ltd., with dimensions: 25mm diameter and 7mm thick. It produces a normal static magnetic field of 0.3T at the surface of the magnet and this increases to 0.5T when it is placed on a ferromagnetic sample, such as mild steel. The field intensity can be enhanced by backing with a 10mm thick, 25mm diameter mild steel buffer behind the magnet. The buffer

decreases the demagnetising factor, (Crangle, [1991]), guiding the magnetic flux perpendicular to the sample surface and thus increases the field intensity to about 0.7T when it is located on the mild steel sample or 0.35 T at the surface of the magnet. The magnetic field drops from 0.35T on the surface to 0.25T at a distance 1mm away from the surface. This distance is significant since it is equal to the thickness of the printed circuit board (PCB) onto which the EMAT coil is etched. The magnetic field from the permanent magnet could be further enhanced up to about 0.75T on ferromagnetic samples by making a closed magnetic circuit as shown in figure-4.2. This, however does not significantly increase the signal to noise ratio of the EMAT signal but does increase the attractive force between the EMAT and steel sample resulting in difficulties when scanning the EMAT.

We used a spiral pancake EMAT rf coil, which consisted of 18 turns and was of 16mm diameter, etched on one side of a double sided printed circuit board (PCB) 1.0mm thick. It will generate shear waves that are polarised in the radial direction suitable for thickness measurement or detection of laminar defects. Such an EMAT also can detect the arrival of longitudinal waves. The PCB track coil is more efficient than a wire coil of equal resistance and length since the track is broader than the thickness of the conductor on the PCB. At the desired ultrasound frequency (approximately 0.5-10MHz), the ac current will only flow within a thin skin layer with depth determined by the classical electromagnetic theory. A flat strip of conductor is therefore more efficient than a round thicker wire of equal dc resistance since the flat coil has a larger area to volume ratio. The other side of the conducting layer of the PCB was left unetched to provide an electromagnetic screen between the coil and the magnet, reducing unwanted ultrasound generation in the magnet which itself is both an electrical conductor and magnetostrictive. The ultrasonic echoes in the magnet are similar to the normal ultrasound signal detected by the EMAT in metals and therefore it becomes essential to screen them out if the EMAT is

used as both the generator and receiver. If the screening is not present the magnet signals could be wrongly interpreted as defect signals, particularly in highly attenuating samples or on metals with a poor transduction efficiency.

The magnet and the steel backing assembly were contained in a brass housing and the coil was bonded on the surface of the magnet using a thin layer of super glue. The electrical terminals of the coil were taken out through a hole drilled at the centre of the magnet and the steel backing to a BNC connector. To minimise the electromagnetic interference, double-screened coaxial cables were used to connect the EMAT to the other devices e.g., EMAT driver or the preamplifier. For general laboratory use the EMAT coil was protected by a 100μm thin layer of hard plastic so that it could be scanned over the surface of samples. However for EMATs to be used in more hostile environments, e.g. at high temperature, a ceramic material such as an 0.5mm thick alumina disc or mica plate was bonded on the EMAT face for protection. To allow the EMAT to withstand high temperature, the brass housing is water-cooled to dissipate heat and to keep the magnet below its Curie temperature (about 100 °C), beyond which the magnetic field strength will be diminished. During measurements at elevated temperature, in order to minimise the heating of the magnet and to avoid excessive cooling on the specimen, the EMAT is only introduced into the furnace to capture the ultrasound waves and pulled out again once the waveform has been recorded.

At elevated temperatures, (above 600°C), prolonged contact between EMAT and the sample destroys the EMAT coil, as the water-cooled magnet is unable to efficiently remove the heat from the coil through the thick PCB. To avoid this a hand wound wire coil was directly bonded onto the surface of the magnet. This allows the EMAT to remain in contact with a hot sample surface over a longer period. As the EMAT was to be used as a detector for the laser generated ultrasound, additional screening was not needed.

We used a P-EMAT with a concentric coil for the initial studies on a send-receive laser-EMAT system. The coil was hand wound from 0.2mm diameter enamel insulated copper wire, the flat spiral coil had inner and outer diameters of 12mm and 29mm respectively and was bonded directly beneath the magnet surface. The magnet is a doughnut shape with inner and outer diameter 10mm and 35mm respectively. The static magnetic field intensity measured on its face is 0.3T. The experimental set up for the pulse echo ultrasound measurement using a P-EMAT is shown in figure-4.3.

4.2 Pulsed Field Electromagnetic EMAT (E-EMAT)

P-EMATs have been used to generate and detect ultrasound and shown to be efficient in both magnetic and non-magnetic metals. These EMATs are small and can be used for high temperature measurements as described above. However there are some limitations with permanent magnet EMATs. The magnetic field is fixed and cannot be increased whereas in some mild steel samples, a higher magnetic field may be desirable. If the EMAT is to be used on a ferromagnetic sample for a prolonged period, magnetic debris and swarf would tend to stick on the EMAT face resulting in a poor performance. A pulsed field electromagnet is an alternative means to generate a high intensity, controllable magnetic field for the EMAT. This approach also allows the easy removal of the magnetic dirt from the EMAT surface between the pulses.

Electromagnetic EMATs are normally bulky and cumbersome compared to permanent magnet EMATs, however it is possible to generate higher magnetic fields than are possible using permanent magnets. Maxfield et.al.,[1983] have reviewed the design of the EMAT using steel-cored electromagnets. A steel-cored electromagnetic EMAT system also has been described by Kubota et.al.,[1988], where the prototype system was tested on a steel production line. Burns et.al.,[1988], carried out an experiment using an air-cored

electromagnetic EMAT to detect longitudinal waves generated by pulsed laser on hot steel. In their work, the pulsed magnetic field was generated by a pancake spiral coil of thick copper wire and energised by a pulsed current.

For the purpose of this thesis, we opted for the ferromagnetic core approach to generate a pulsed magnetic field with direction normal to the surface of the sample using a water-cooled electromagnet. The intensity of the field could be varied allowing easy monitoring of the magnetisation of the sample, in particular at elevated temperatures.

4.2.1 Design Principles

It has been estimated (from reluctance considerations), that an E shape, steel core electromagnet (relative magnetic permeability μ_r=1000), with cross section area 10cm^2 at the centre leg and 5cm^2 on the outer legs as shown in figure-4.4, could generate a magnetic field about 1.25T in the 5mm air gap between the centre pole and the mild steel (relative permeability μ_r=100). For this it requires a magnetising current of about 10000 ampere-turns. Therefore if the electromagnet energising coil consists of 800 turns, it requires a current of about 12A to generate the desired field. For a small electromagnet such as a 100VA transformer kit, it will be able to accommodate a maximum continuous current of about 0.5A from a 240V supply. The electromagnet could accommodate a higher current in pulsed mode depending on the pulse duration and its duty cycle. A large magnetising current pulse could be delivered to the electromagnet by driving the current from a capacitor bank discharged through a high speed switching device. Switches most commonly used are thyristors, power MOSFETs and thyratrons. These devices are capable of withstanding a high voltage in the off-state and large currents in the on-state.

The electromagnet will be synchronised with the EMAT driver to excite the EMAT rf coil when there is sufficient magnetic field on the surface of the sample. The duration of

the generated magnetic field pulse should be longer than the desired duration of the ultrasound propagation in the sample. The duration of the pulse also determines the peak intensity of the magnetic field. The electromagnet may also need to be synchronised with other components of the system such as the EMAT driver, or pulsed laser so that the E-EMAT could be used as the ultrasound receiver in both send-receive or through-transmission arrangement. The E-EMAT receiver should operate at the repetition rate of the ultrasound generator. The details of the electromagnet driver will be described in the following section.

4.2.2 The E-EMAT Design

The construction of the E-EMAT is shown in figure-4.5. It consists of an electromagnet made from a 100VA transformer-kit with E-shape core of laminated silicon steel with the centre pole dimension 29mm x 29mm and 14.5mm x 29mm on the other legs. The electromagnet dimension is 85mm x 60mm and 65mm height. The energising coil consists of 4 parallel, 200 turns of 0.2mm diameter enamel-insulated copper wire coils, wound around the centre pole. The electromagnet produces a magnetic field normal to the sample surface from the centre pole with the other poles providing the return path and at the same time maximising the generated magnetic field by completing the magnetic circuit. The air gap between the electromagnet poles and the sample surface needs to be minimised to reduce the reluctance of the non-magnetic portion of the magnetic circuit. The poles protrude into a brass water jacket 10mm thick which forms the front base of the EMAT assembly. This is the maximum thickness that will accommodate the energising coil and provide sufficient room for a water cooling groove to be made in the brass base. This assembly is housed in an aluminium case with dimension 100mm x 85mm on the front face and 75mm in height. The brass jacket is water-cooled to remove heat from the EMAT

assembly. The water inlet and outlet are connected to the mains water supply where the water flow rate can be altered accordingly.

A 6mm diameter hole was drilled through the centre of the electromagnet to allow the laser beam access to the sample surface. The beam diameter of the Nd:YAG laser is 3mm and can easily be reduced down to less than 0.5mm when focused using a converging lens. A bigger conical hole tapering from a diameter 15mm at the rear to 7mm at the front surface was made in the electromagnet later to accommodate the larger CO_2 laser beam. The dimension of the CO_2 laser beam is 25mm x 25mm at the laser window and can only be reduced down to 3mm x 3mm using a suitable lens (antireflection coated meniscus germanium lens). The focal-length of this lens is 200mm, and a great care should be taken not to focus the CO_2 laser beam down by positioning the lens half of its focal-length away from the metal surface. The high reflectivity of the laser beam from the metal surface, i.e.; 98% at λ=10.64μm on polished aluminium, will cause the reflected beam to be focused back onto the lens, removing the antireflection coating and damaging the lens. The CO_2 laser beam power can be reduced by using a metallic diaphragm aperture positioned in front of the window. The EMAT and the related optics need to be securely aligned on an optical bench with some allowance to adjust the position of the converging lens with respect to the surface of the sample whilst remaining parallel to the surface.

The EMAT is designed to generate the radially polarised shear wave. As a receiver, the EMAT is also sensitive to longitudinal waves propagating in the sample. These have been described elsewhere (e.g.. Frost, [1979], Maxfield et al., [1987], Lee et al., [1992], Edwards et al., [1990] and Idris, [1995]). The detection of a longitudinal wave occurs because there are some components of the magnetic field in the direction parallel to the sample surface and the EMAT coil and also because laser generated longitudinal waves have tangential components in the longitudinal wavefront. The EMAT coil is an

annular pancake type, consisting of 40 turns, hand wound from 0.2mm diameter enamel insulated copper wire with the outer diameter 29mm and 12mm inner diameter. It is bonded concentrically with the electromagnet centre pole by a thin layer of super-glue to maximise heat transfer between the coil and the electromagnet pole. No metallic screen is required as there is a negligible eddy current induced on the laminated steel core. The EMAT has an inductance of 36μH and resistance 0.8Ω , giving a total impedance of 37Ω at 1MHz, (neglecting stray capacitance). The EMAT is matched to a preamplifier with an input impedance of about 50Ω at a high frequency so that it can be connected by normal coaxial cables.

A single turn of diameter 25mm from 0.2mm enamel insulated copper wire is then, bonded outside the EMAT coil to monitor the magnetic field, the output represents the time derivative of the magnetic field ($d\Phi/dt$). By integrating the waveform V(t) over the pulse duration τ, the actual magnetic flux Φ, through the loop at a particular instance could be determined by;

$$\Phi. = \int_0^{\tau} V dt \qquad (4.1)$$

The magnetic field intensity B in Tesla generated by the electromagnet is given by;

$$B = \frac{1}{A}\int_0^{\tau} V(t)d \qquad (4.2)$$

where A is the area of the field sensing coil in m^2.

A 0.5mm thick alumina disc is bonded on the surface of the coil using araldite to protect the coil from any damage. Prior to this, the electromagnet core was skimmed off to remove a thickness of 1mm to accommodate the EMAT coil and the alumina disc so that the EMAT surface and the other poles lie in the same plane.

The positioning of the electromagnet in the brass base reduces its inductance and thus the generated magnetic field from about 1.2T to 0.7T in mild steel compared to when

it stands alone on the sample before any modification takes place. In this measurement, the electromagnet is energised by a high current 2ms driving pulse at 1Hz repetition rate. The reduction of the magnetic field occurs when the volume of the electromagnet's high permeability core has been reduced to accommodate the space for the brass base and also a hole at the centre of the electromagnet for the access of the laser beam. A further contribution to the reduction is the induced eddy current in the brass base. To reduce this effect, a saw cut was made across the brass base around the centre pole so that the eddy-current path is no longer continuous. The reduction in generated magnetic field can be compensated for by increasing the duration of the pulsed current energising the electromagnet, a 3ms pulse is found to give a field of 1.2-1.3 T on steel samples.

The electromagnet has 48mH inductance and 2.6Ω resistance and total impedance of 147Ω measured when it is off the ferromagnetic samples. This value is large enough to keep the current from the driver below the current limit of any of the components. The waveform of the time varying magnetic field generated by the electromagnet is shown in figure-4.6, where the electromagnet was driven with a 3ms energising pulse for the reasons stated.

4.2.3 Electromagnet Driver

The electromagnet driver design is shown in figure-4.7, and it is based on the pulsed excitation EMAT driver circuit. It generates a pulsed current of a few tens of amperes amplitude through the electromagnet. The capacitor C is first charged through the current limiting resistor R to a high voltage V. When the switch S is closed, the capacitor is discharged through the electromagnet. The switching element S should be capable of withstanding the high voltage V in the off-state and large current peaks in the on-state.

The schematic diagram of the electromagnet driver circuit is shown in figure-4.8. The capacitor C is 500μF 800V and charged up to a maximum of 560V by a step-up transformer which is fed from a variable supply (VARIAC 0-240V). The high-speed switch S is controlled by a square wave driving pulse of duration 3ms and repetition rate 1Hz, amplitude 12V in high state and 0V when it is low, generated by a 555 timer. The switch S is turned into the on-state at the positive edge of the driving pulse and turned into the off-state at the negative leading edge so that the electromagnet is turned on when the driving pulses are in the high state. In the on-state, the switch passed a time varying current (saw-tooth waveform) with the maximum of about 20A through the electromagnet and generating a time varying magnetic field with a maximum intensity of about 1.2T on a mild steel sample at the negative edge of the driving pulse. This magnetic field intensity corresponds to the 240V output supply of the VARIAC. The relative sequence of this operation is shown in figure-4.9.

We firstly used a BUK345 power MOSFET as the fast switch however, it could not withstand all operating conditions. This was then replaced with a BUZ334, a higher power rating MOSFET and was used for all the subsequent work. The maximum continuous current rating is 12A at 600V but for the pulsed current, the maximum current is almost 5 times higher depending on the pulse duration and its duty cycle (i.e. the ratio between the pulsed duration and pulse period). At a few millisecond duty cycle (3ms duty cycle in this work), the maximum current was 48A. There are other higher power rating devices such as thyratrons or thyristors available in the market but unfortunately they either have slower switching than MOSFETs or are very expensive. The cost for a thyratron is about 1000 times greater than that for the MOSFET and therefore is not justifiable.

The pulse duration of 3ms is selected in order to provide sufficient magnetic field for the EMAT operation where the magnetic field intensity is proportional to the pulse duration. We tried to work with a shorter magnetic pulse duration, however the resulting magnetic field was far too small even if compared to that produced by a permanent magnet. On the other hand if the pulse duration was too long, the power limit of the MOSFET would be exceeded. The repetition rate of 1Hz allowed the capacitor bank to be fully charged and then discharge a current large enough to generate the required magnetic field. The repetition rate was also compatible with the maximum repetition rate of the CO_2 laser and the Nd:YAG laser (maximum repetition rate 10Hz at duty cycle).

The MOSFET is protected from the large reverse voltage from the collapsing magnetic field in the electromagnet by inserting Zener diodes (1N4007) across the gate-source terminals and also across the electromagnet terminal. This provides a low impedance grounding route of the relatively high current and prevents it from flowing in the reverse direction from source to gate terminal. Additional protection is given by a 5A fast blow fuse at the source terminal and the current flowing through the electromagnet could be monitored across the point A-B shown in figure-4.8.

The firing of the pulsed laser was normally made by an external trigger switch so that it can be operated in continuous mode according to its designated repetition rate or in single shot mode using an external push button switch. The TEA-CO_2 trigger switch requires a pulse of a 3ms width and 9-12V amplitude and fires at its negative leading edge, therefore it could be synchronised directly to the electromagnet driver through the 9-12V trigger output socket (figure-4.8). The Nd:YAG laser could be triggered by a short pulse of a few tens of microseconds duration, 5V amplitude, and laser firing occurs on its positive edge with the maximum repetition rate of 10Hz. The Nd:YAG laser therefore could not be triggered directly by the same trigger output of the electromagnet driver.

However it requires a delayed trigger output to trigger the laser to fire. The delayed trigger output (100μs duration, 5V) was generated using two stages of the 555 timer chip.

The above describes the continuous operation (1Hz rep. rate) of the E-EMAT where the electromagnet driver trigger switch is in INTERNAL position, (figure-4.8). The electromagnet driver may accommodate up to 240V of VARIAC output or 600V across the capacitor charging supply. However in this operation, the capacitor bank may only be charged up to 50% of its full load and therefore discharged current at much lower than the maximum limit of the MOSFET current. The electromagnet and its related instruments also can be triggered in a single shot externally by positioning the electromagnet trigger switch to position EXTERNAL. The pulse generator may be triggered by a push button switch or other, connected at the external trigger output socket. At a sufficiently low repetition rate (once every 2 minutes), the capacitor bank fully charges at much lower voltage, (we limit the supply to 120V of VARIAC output or equivalent 240V charging output so that it will not exceed the current limits of the components). In a single excitation, the electromagnet could generate a higher field at a lower charging voltage, where it is able to generate magnetic fields of about 1.4T on mild steel sample and about 0.45T on aluminium. In the external trigger mode, the electromagnet could be excited after a pre set time, e.g. after positioning the EMAT on the sample surface.

4.2.4 Operation of E-EMAT

The EMAT driver is synchronised to the electromagnet driver and delivers a pulse of current to excite the EMAT at the negative leading edge (or a few microseconds earlier) to ensure that the ultrasound generation occurs within the operation range of the pulsed field EMAT, (Figure-4.10). The transit time of ultrasound propagation in the sample (a few tens of microseconds) is negligibly small compared to the time constant of

the magnetic field decay (a few tens milliseconds). To surpress ultrasound signal from any pickup noise, the EMAT normally is connected by a double screened cable and undergoes band-pass filtering. The captured ultrasound signals are displayed on the Lecroy 9310 digital oscilloscope and stored on a disk for further analysis. The oscilloscope is externally triggered from the electromagnet driver trigger output.

Equipment set-up for the detection of ultrasound generated by a TEA-CO_2 laser by the pulsed electromagnetic EMAT receiver is shown in figure-4.11. The firing of the laser is synchronised with the magnetic field at a repetition rate of 1Hz, triggered at the negative edge of the electromagnet driver trigger output and could be controlled by a switch S_1 along the line so that the laser may be fired whenever it was required. The equipment set-up for the detection of ultrasound generated by a pulsed Nd:YAG laser is shown in figure-4.12. The firing of the laser is triggered by a delayed output pulse of 100μs duration and amplitude 5V, at a repetition rate of 1Hz. The pulse is generated at about the negative edge of the electromagnet driving pulse as shown in figure-4.9. The oscilloscope is triggered by the signal output of a photodiode which responds to the incident laser reflected from a beam splitter. In both experimental set-ups, the laser beam and the EMAT first have to be aligned accurately so that the EMAT is positioned at the epicentre in a through transmission arrangement or the beam passes through the centre of the EMAT in send-receive arrangement.

4.3 High Temperature Operations

Both types of EMAT have been evaluated at high temperatures in pulse echo mode of operation. Measurements were made on a steel sample at a temperature of about 700°C. The EMAT was brought in momentary contact with the sample. The detail of these experiments will be discussed in Chapter -5.

4.4 Results and Discussion

4.4.1 Send-receive EMAT

Figure-4.13 shows the pulse echo ultrasound waveforms generated by both types of EMAT on aluminium and mild steel. In aluminium, the waveform generated by the P-EMAT shows 3 small pulses in between large shear wave pulses. These pulses arise from the mode conversion of the shear wave into the longitudinal wave at the free boundaries, noted as LS, LS2L, 2S2L, LS2S along with the large shear wave arrivals noted as 2S, 4S, 6S etc. The subsequent echoes arise from multiple reflection of these pulses at the free surface. The weak longitudinal wave is excited because there exists a component of stress normal to the sample surface and also a tangential component of the magnetic field in the direction parallel to both the sample surface and the plane of the coil. A similar waveform was generated by the E-EMAT, however, the mode converted signal is hardly observed. The waveforms on mild steel exhibit low frequency noise and are smaller in amplitude, corresponding to a lower transduction efficiency compared to aluminium caused by lower conductivity and higher material density. The waveform has a paralysis time (about 2.5μs with P-EMAT and 3.5μs with E-EMAT) since the same coil is used to both generate and detect signals with large amplitude differences. In generation, the coil is excited by placing a 800V pulse across the coil and in detection, only a few tens of microvolts appear across the coil. In the case of an EMAT in pulse-echo arrangement, a trade-off has to be made between the duration of the paralysis time and the sensitivity. In the case of the same coil used for both generation and the detection, the existing paralysis duration of the EMAT pulser-receiver is 2.5μs, which is the shortest deadtime with a acceptable sensitivity that has been reported.

Figure-4.14 shows that, in an aluminium sample, the successive shear wave pulses begin to split into two components arising from anisotropy within the sample as a result of

the working processes that have been performed on the metal. A similar effect also arises in steel samples as shown in figure-4.15. The plate samples consisted of an aggregate of metallic grains orientated in a specific direction which cause the shear wave with a radial polarisation to be beam steered into two orthogonal polarised beams. This is because of the waveguiding within the sample as the propagation velocities have functional dependence on the propagation direction and wave polarisation (Musgrave, [1970]). In an anisotropic metal plate, the shear EMAT will generate a radial stress and cause an inhomogeneous radial strain. This in turn gives rise to the polarised shear waves that propagate in two orthogonal directions, perpendicular and parallel to the direction of grain alignment. The propagation velocity will be different for each of these polarisation directions. This effect is known as acoustic birefringence and is analogous to optical birefringence.

Figure-4.16 shows the effect of stand-off, x, on the ultrasound transduction in aluminium and mild steel samples using a permanent magnet EMAT. It is shown that the signal amplitude reduces by $15dBmm^{-1}$. Two factors contributed to the reduction in the EMAT transduction efficiency, namely the reduction of the magnetic field and the induced current density on the sample surface on the generation side or the induced current on the EMAT coil during detection. Both quantities reduced exponentially with stand-off, x, i.e., exp(-bx) where b is a positive constant. The stand-off factor due to the magnetic field is given as exp(-2x/D) where D is the diameter or the width of the magnet pole. The stand-off factor is given as $\exp(-4\pi x/D_c)$ where D_c is the diameter of the spiral pancake coil. Therefore, a smaller coil diameter exhibits a larger stand-off factor than a larger coil (Maxfield et.al., [1987]).

4.4.2 Effect of Oxide Layer on Ultrasound Transduction by EMAT

The effect of oxide layers on steel on the ultrasound transduction by an EMAT is shown in figure-4.17. Waveform-A was obtained on an oxide free surface and waveform-B from the surface with a thick oxide layer. The oxide layers (mainly magnetite) enhance the signal amplitude compared to that on a clean surface. The magnetite layer also introduces an additional resonance to the waveform which may arise from the ultrasound reverberation within the layer and a distributed source in the layer thickness. The enhancement depends on the degree of the adhesion of the layer upon the surface. If this layer is poorly adhered to the underlying metal any acoustic energy will remain trapped in the layer and will not be transmitted in the metal. It has been reported that there is an optimum thickness of this oxide layer to enhance the ultrasound transduction, typically up to1mm thick (Maxfield et.al., [1983]). The details of this effect will be discussed in chapter-6.

Figure-4.18 shows pulse echo ultrasound waveforms in mild steel generated by the E-EMAT. The first waveform was obtained from a section of a corroded pipe sample, with surface covered with a red rust layer due to water corrosion. The subsequent waveform was obtained after the surface was ground down to bare metal. These waveforms show that the presence of a hydrated red rust layer on surface does not enhance the signal amplitude. The third waveform was obtained from a section of a different water corroded mild steel pipe. The surface was cleaned using a sand blasting process to remove the oxide layer. The sample exhibits poor ultrasound transduction using a P-EMAT, however an E-EMAT generates ultrasound of appreciable amplitude due to a higher static magnetic field intensity. The waveforms shown in figure-4.17 and figure-4.18 indicate that EMAT transduction on mild steel varies from one sample to another depending on the particular sample and the presence of surface oxides.

4.4.3 Nd:YAG Laser-EMAT System

Figures 4.19 and 4.20, show send-receive waveforms detected by an E-EMAT operating on aluminium and mild steel samples of different thickness. The ultrasound was generated by a pulsed Nd:YAG laser in the thermoelastic regime. The waveforms show the arrivals of the shear wave pulses noted as 2S, 4S, 6S and also the arrivals of weak mode converted signals noted as LS, LS2L, 2S2L and LS2S and their reflection pulses. These pulses may overlap each other as the velocity of the longitudinal wave is about twice that of the shear wave. In a thick sample the waveforms show the arrivals of the shear wave pulses with weak mode converted pulses, however for thinner samples, the amplitude of the mode converted pulses and in particular the LS and its reflection pulses increases. In thin samples of either aluminium or mild steel, the 1st and 2nd pulse arrivals may not be seen as they arrive within the dead time of the EMAT and the waveform is dominated by principle echoes and the related mode converted arrivals.

4.4.4 TEA-CO_2 Laser-EMAT System

Figure-4.21 shows the send-receive ultrasound waveforms generated by a TEA-CO_2 laser on aluminium. The detected waveforms are similar to those generated by a Nd:YAG laser. The ultrasound sources generated by both pulsed TEA-CO_2 laser and the Nd:YAG laser were in the thermoelastic regime producing a point ultrasound source that propagates shear waves with a spherical wavefront into the bulk of the sample. At the backwall of the sample, the wave undergoes reflection and also mode conversion into a longitudinal wave before propagating back towards the receiver. As the wave traverses the sample, the wavefront becomes flatter and after reaching a certain path-length, the waves become effectively plane waves compared to the dimensions of the detector. The mode converted arrivals become more pronounced as the sample thickness decreases and the

relative size of the EMAT coil becomes large compared to the thickness of the sample. Figures-4.20 and figure-4.21 show that with a 2.5μs dead time, the send-receive laser-EMAT system, is restricted to thickness measurement on plates thicker than 4mm using shear waves if the first echo has to be detected. Thinner plates can be measured with multiple echoes although this can be ambiguous if lamellar defects are present in the plates.

Figure-4.22, shows how the width of the concentric EMAT coil affects the nature of the ultrasound waveforms generated as a point source in aluminium and mild steel of thicknesses 20mm and 15.5mm respectively. A similar result from stainless steel of 25mm thickness, is shown in figure-4.23. The ultrasound was generated using a pulsed laser in a thermoelastic regime and detected by the E-EMAT in send-receive arrangement. Two EMAT receivers with different coil widths were used, one with 29mm outer diameter and 12mm inner diameter, denoted as 29/12mm and the other with 20mm outer diameter and 6.5mm inner diameter, denoted as 20/6.5mm. The wider EMAT coil gave a higher signal amplitude as it has a larger number of turns, {i.e. as receiver, the signal amplitude is directly proportional to the number of coil windings, (Kawashima, [1984])}, however it caused the pulses to be broad compared to the thinner coil. The width of the 1st shear pulse arrivals measured using the two different EMAT coils are 1359ns and 740ns in mild steel, 1380ns and 970ns in stainless steel and 1035ns and 890ns in aluminium. The broadening of the signal arrivals arises because the EMAT signal response is the convolution of the response of each element of the EMAT and therefore the wider the EMAT coil, the larger the time differences between the responses at the inner and the outer edge of the coil. This signifies the difference in the ultrasound path-length between the inner and the outer edges of the coil. The width of the second pulse arrivals detected by the 29/12mm coil are 1075ns in mild steel, 1035ns in stainless steel and 1220ns in aluminium. The former two are reduced since the wavefront is more planar and in

aluminium the broadening arises from anisotropy effects where the shear waves of different polarisation begin to split.

In a send-receive measurement using a laser generator and an EMAT receiver, an increase in the stand-off x, does not show such dramatic reduction of the signal amplitude (Figure-4.24). The waveforms were detected using the E-EMAT with an annular coil with outer and inner diameter 29mm and 12mm respectively. In aluminium the signal amplitude dropped by 9.3dB for a 2.5mm stand-off and 7.6dB for a 4mm stand-off in mild steel. Such a small reduction in the signal amplitude compared to that shown in figure-4.16, may be caused by the size of the EMAT coil as the annular coil consists of a higher number of turns compared to the pancake spiral coil. The stand-off performance of a laser-EMAT system is only affected by the reduction in the sensitivity of the EMAT detector whereas in the EMAT-EMAT system, the performance of both the generator and detector are affected.

Figure-4.25 shows the send-receive ultrasound waveforms generated by the CO_2 laser on mild steel and detected by an E-EMAT. The laser beam was partially focused on the surface of the sample, and the laser energy density deposited on the sample surface was altered by varying the aperture diameter of the laser window. At low energy density (aperture diameter 12mm), the waveform was dominated by the shear arrivals which corresponded to the thermoelastic source. At a higher energy density (aperture diameter 20mm) surface ablation occurs on the sample surface and creates a plasma which expands at supersonic speeds and results in a normal force on the sample generating strong longitudinal waves. The increase in laser energy density deposited on the sample surface introduced an additional low frequency noise in the signal waveform. As the laser energy increased further, it caused the ionisation of the air and plasma breakdown to occur on the sample surface and caused saturation in the EMAT response. In contrast, these effects did

not affect the response of the EMAT receiver on epicentre as shown in figure-4.26, where the ultrasound waveforms generated in a similar condition as those described in figure-4.25.

The saturation effect in EMAT receiver response can be reduced by allowing only about 50-70% of the CO_2 laser output incidence onto the surface of the sample so that we could detect the ultrasound wave pulses with a good signal to noise ratio. When the beam was only partially focused, it formed a thermoelastic stress source and the presence of the oxide layer enhanced the generation of the ultrasound. When the beam was focused onto the surface, it created a plasma which built up in the confined region inside the EMAT. The presence of the dust in the region will seed the formation of the plasma (Taylor, 1990]). At low energy densities, the surface ablation led to the generation of a plasma that could be reliably made on the surface of the sample. As the incident energy was increased, the plasma breakdown tended to occur above the surface in the body of the EMAT, giving a poor ultrasound source and saturating the receiver response.

If the EMAT could be used with the Nd:YAG laser only, the diameter of its centre hole could be reduced down to about 5mm diameter. This would make the inductance of the electromagnet higher and therefore it could be driven for a shorter duration (2ms has been tried earlier). This would also allow the electromagnet to be made smaller .

4.4.5 High Temperature Operations

The performance of both types of EMAT has been evaluated for high temperature operations in pulse echo mode. Measurements were made on a mild steel sample at a temperature of about 700°C. The water-cooled EMAT was brought in momentary contact with the sample. The detected waveforms (figure-4.27), were dominated by the shear wave arrivals of appreciable amplitude. Momentary contact (about 2-3 seconds) between

the water-cooled EMAT and the sample at high temperature did not indicate any damage to the EMAT. As the contact was prolonged, (about 5s), the intense heat burnt the residual araldite on the EMAT face, however this did not affect its performance and the alunmina face was still intact on its place. When the contact was made still longer, the intense heat burnt the araldite layer and detached the alumina face. It is anticipated that as the temperature goes higher, the EMAT should only be brought in momentary contact with the sample.

4.5 Conclusions

It has been demonstrated that the E-EMAT with a concentric coil, can be used to generate and detect pulse echo ultrasound with an efficiency comparable to the P-EMAT. It can be operated in send-receive arrangement to detect the ultrasound wave generated by either the Nd:YAG laser or CO_2 laser, both at 1Hz repetition rate. The magnetic field for its operation is driven by a pulsed current of duration 3ms from a discharged capacitor bank (800V 500μF), producing a magnetic field intensity of about 1.3T on the surface of a ferromagnetic sample and 0.3T on non-magnetic samples. The system exhibits about 2.5μs dead time restricting operation to sample thicknesses greater than 4mm if the first shear wave arrival is to be detected. Thinner samples can also be measured using multiple echoes. Ultrasound measurements at elevated temperatures using both types of EMAT are feasible. Non-contact measurements could be made with a water-cooled EMAT.

4.5 References

Burns L.R and Allers G.A., Material Evaluation, **Vol. 45**, October 1987, pp.1184-1189.

Burns L. R., Allers G. A. and MacLauchlan D. T., in Rev. Prog. In Quantitative NDE, ed. Thompson D.O. and Chimenti D.E., **Vol. 7B**, (1988), (Plenum, New York), pp.1677-1683.

Crangle J., Solid-state Magnetism , Arnold (1991), pp. 157-158

Edwards C., Nurse G., Dewhurst R. J. and Palmer S. B., Brit. Jour. of NDT, **Vol. 32**, No. 2, Febuary 1990, pp.76-78.

Edwards C., Dixon S., Idris A., Reed J. and Palmer S.B., in Rev. in Prog. of Quantitative Nondestructive Evaluation, **Vol. 14B,** (1994). pp.2253-2260.

Frost H.M, in Physical Acoustic, Ed. Mason W.P., **Vol. XIV**, pp.179-275, Academic Press. 1979.

Idris A, Ph.D Thesis, Warwick University.(1995)

Kubota J., Sasaki S., Sato.I., Ito S., Kadowaki T., Yamaguchi H., Fujisawa K. and Murayama R., Material Evaluation, **Vol. 46,** March 1988, pp.523-526.

Kawashima K.,. IEEE Trans. on Sonic and Ultrasonics, **Vol.SU-31**, No.2, 1984, pp. 83-94.

Lee S.S and Ahn B.Y., Nondestr. Test. Eval., **Vol. 7,** (1992), pp.253-261.

Maxfield B.W., and Fortunko C. M., Materials Evaluation, **Vol. 41,** No.12, Nov.1983, pp.1399-1408.

Maxfield B. W., Kuramoto A. and Hulbert J. K., Material Evaluation, **Vol. 45,** Oct.1987, pp.1166-1183.

Musgrave M. J. P., Crystal Acoustics, . (Holden-Day, San Francisco) , 1970.

Taylor G. S., PhD Thesis, Warwick University, (1990)

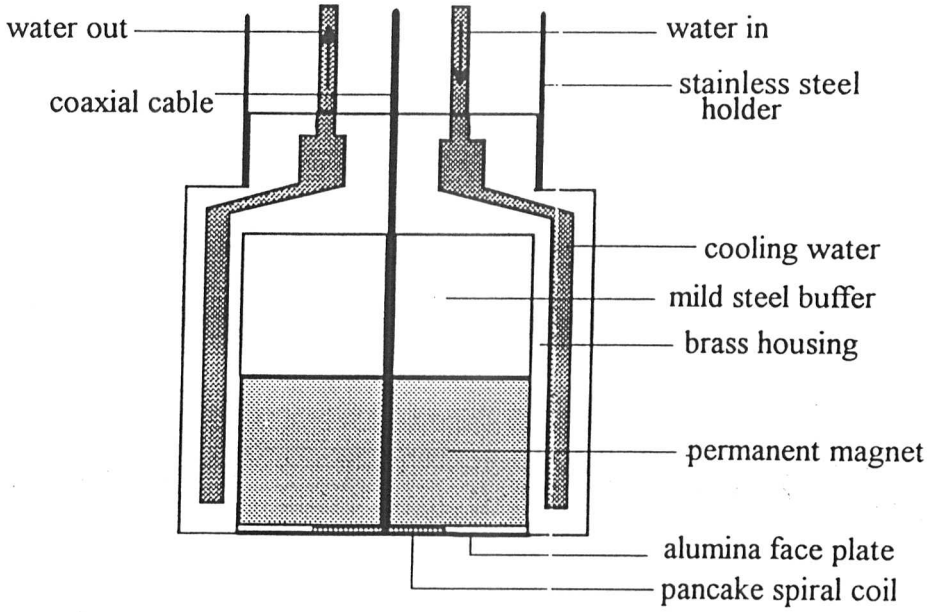

Figure-4.1: Water cooled permanent magnet EMAT (P-EMAT)

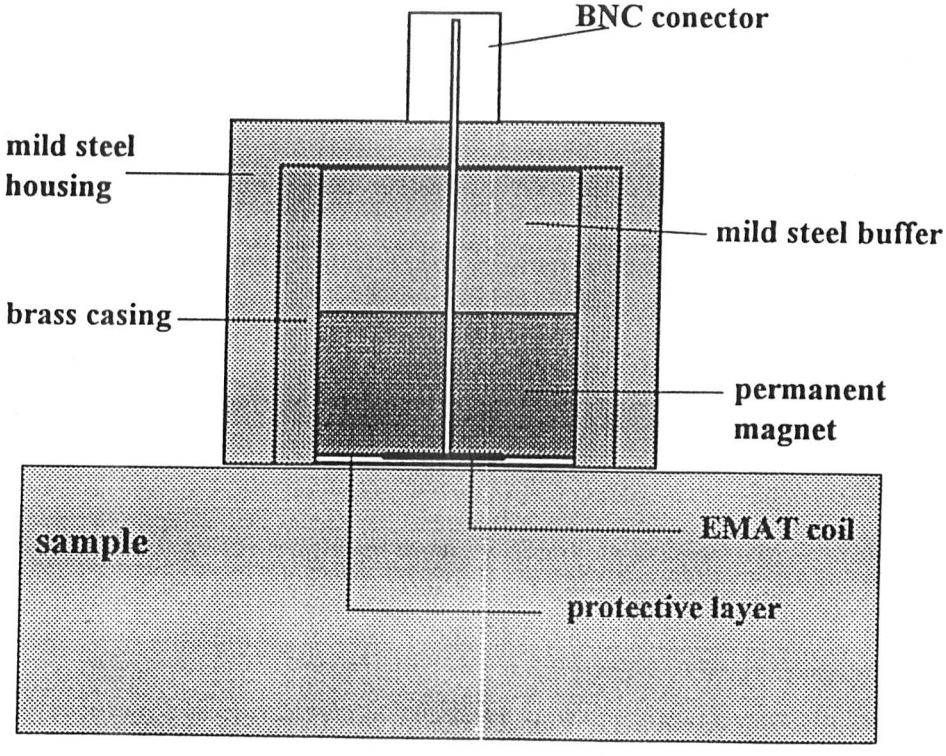

Figure-4.2: Permanent magnet EMAT with steel returning path

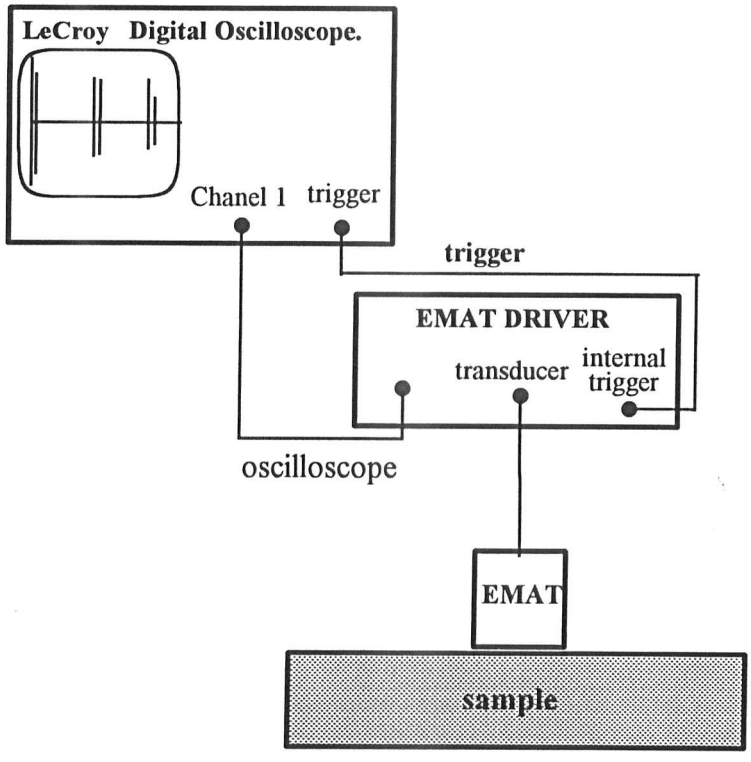

Figure-4.3: Experimental set up using a permanent magnet EMAT

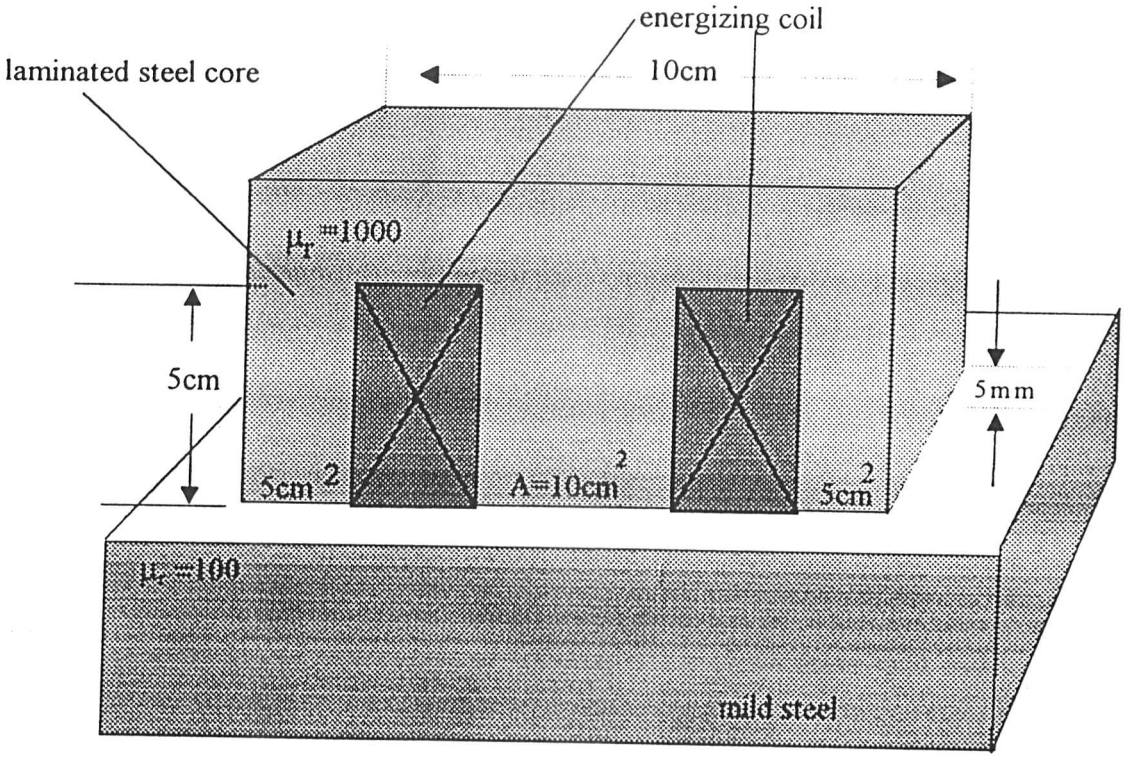

Figure-4.4: Reluctance considerations using an E-shape core electromagnet to estimate the current required to generate a magnetic field 1.25T in a 5mm air gap between its limbs and the steel sample. The cross section area of the centre limb is $10cm^2$ and $5cm^2$ on each outer limb.

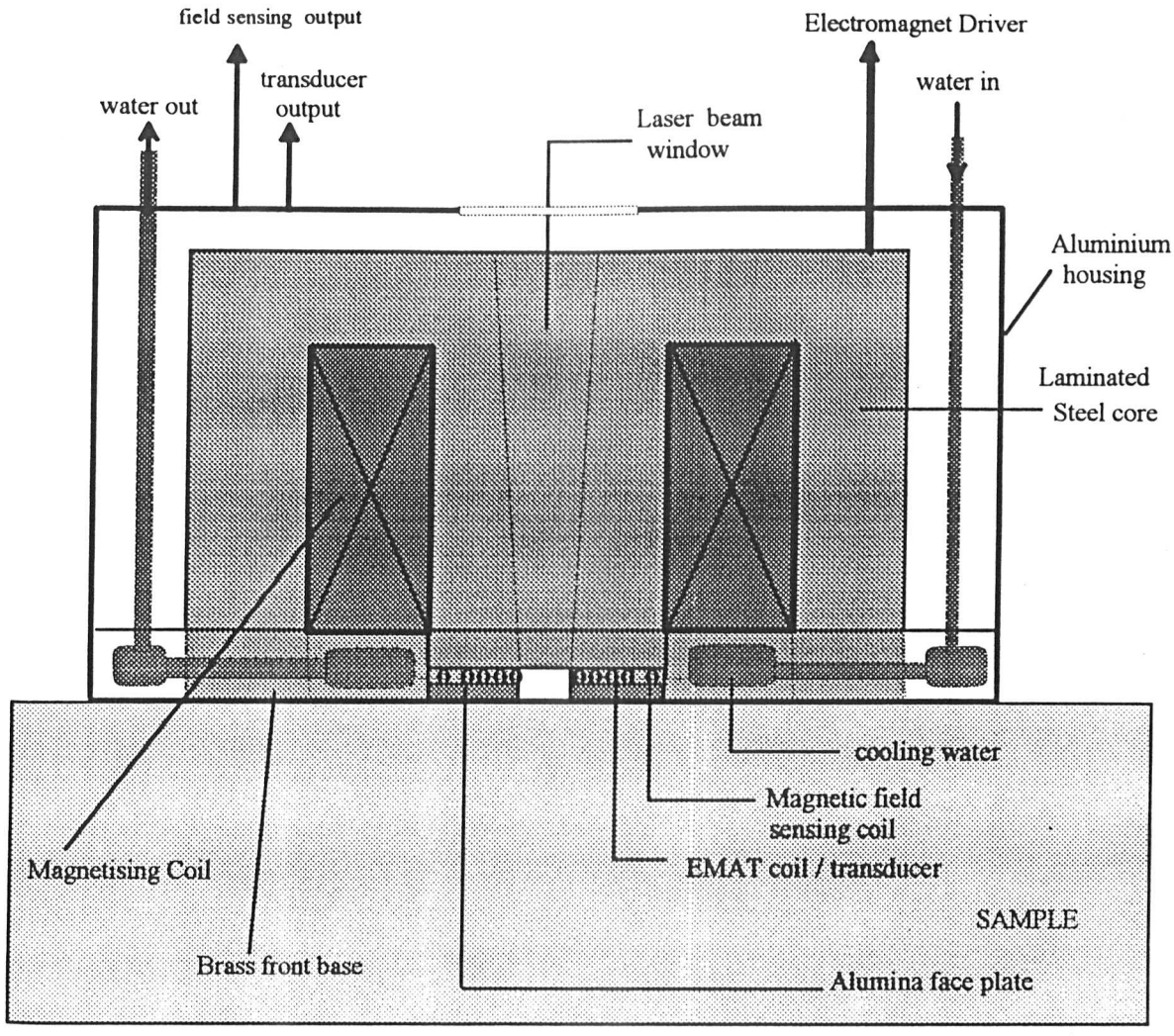

Figure-4.5: Water-cooled pulsed field EMAT.

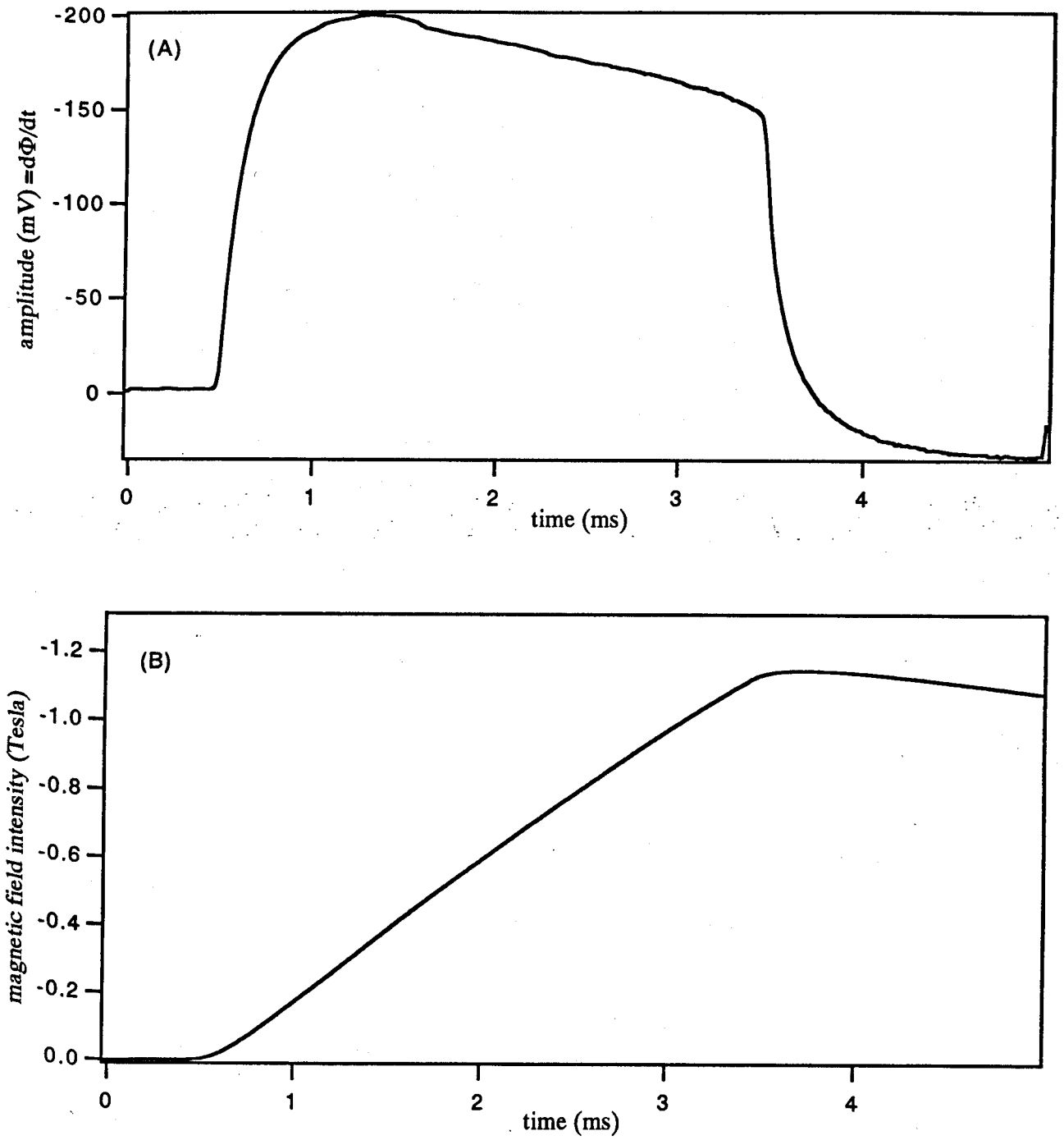

Figure-4.6: Signal output of the field sensing coil, (A) represents (dΦ/dt), (B)-the corresponding magnetic field intensity (Tesla), generated by pulsed field EMAT

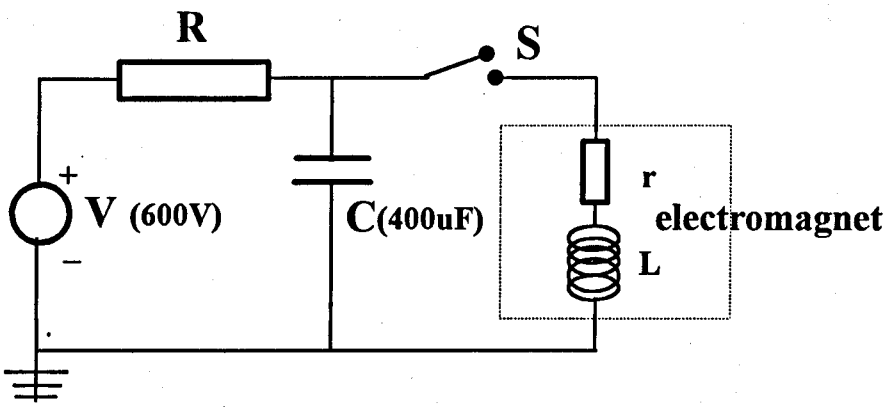

Figure-4.7 Basic electromagnet driver circuit

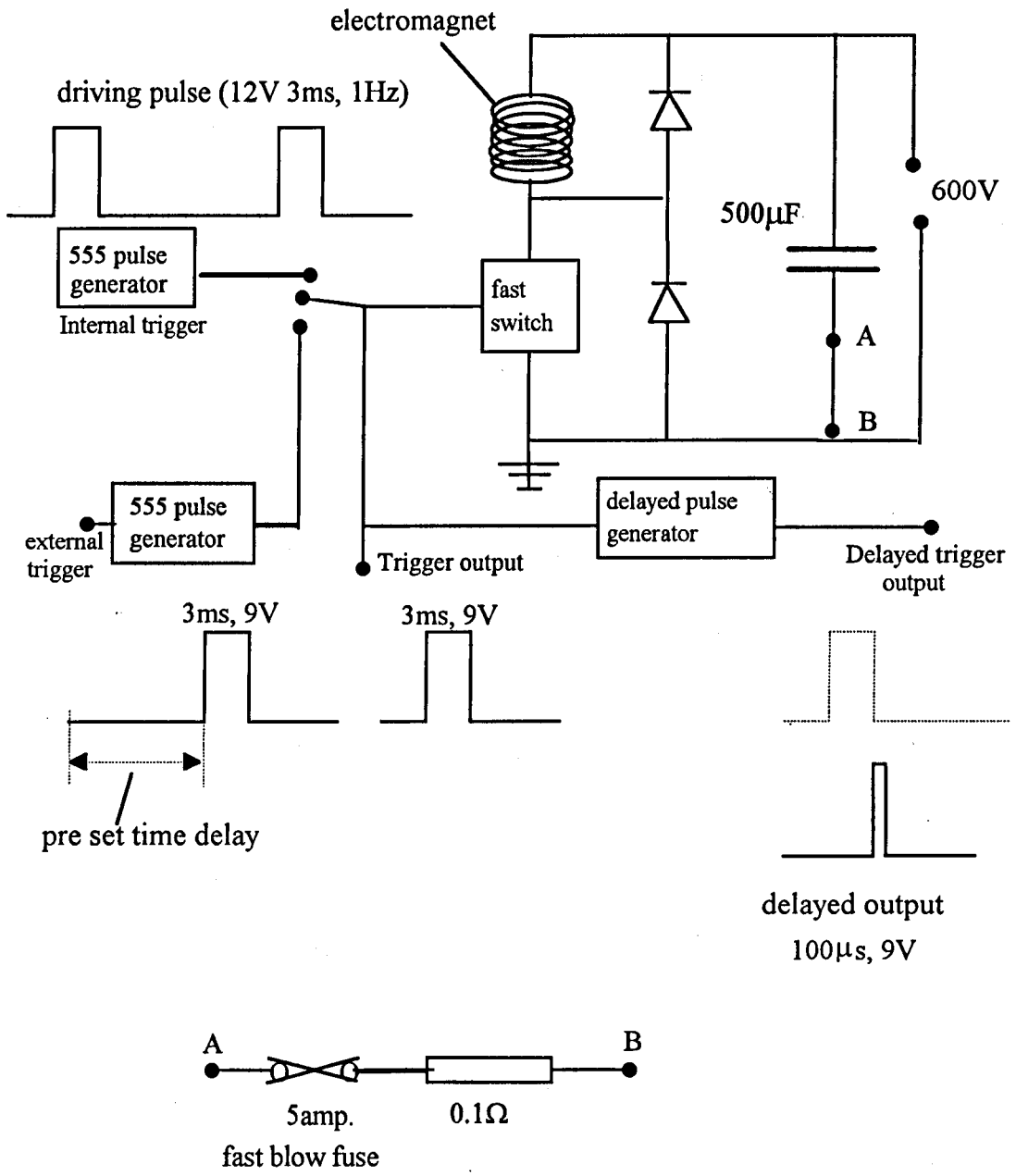

Figure-4.8: Schematic diagram of the pulsed electromagnet driver

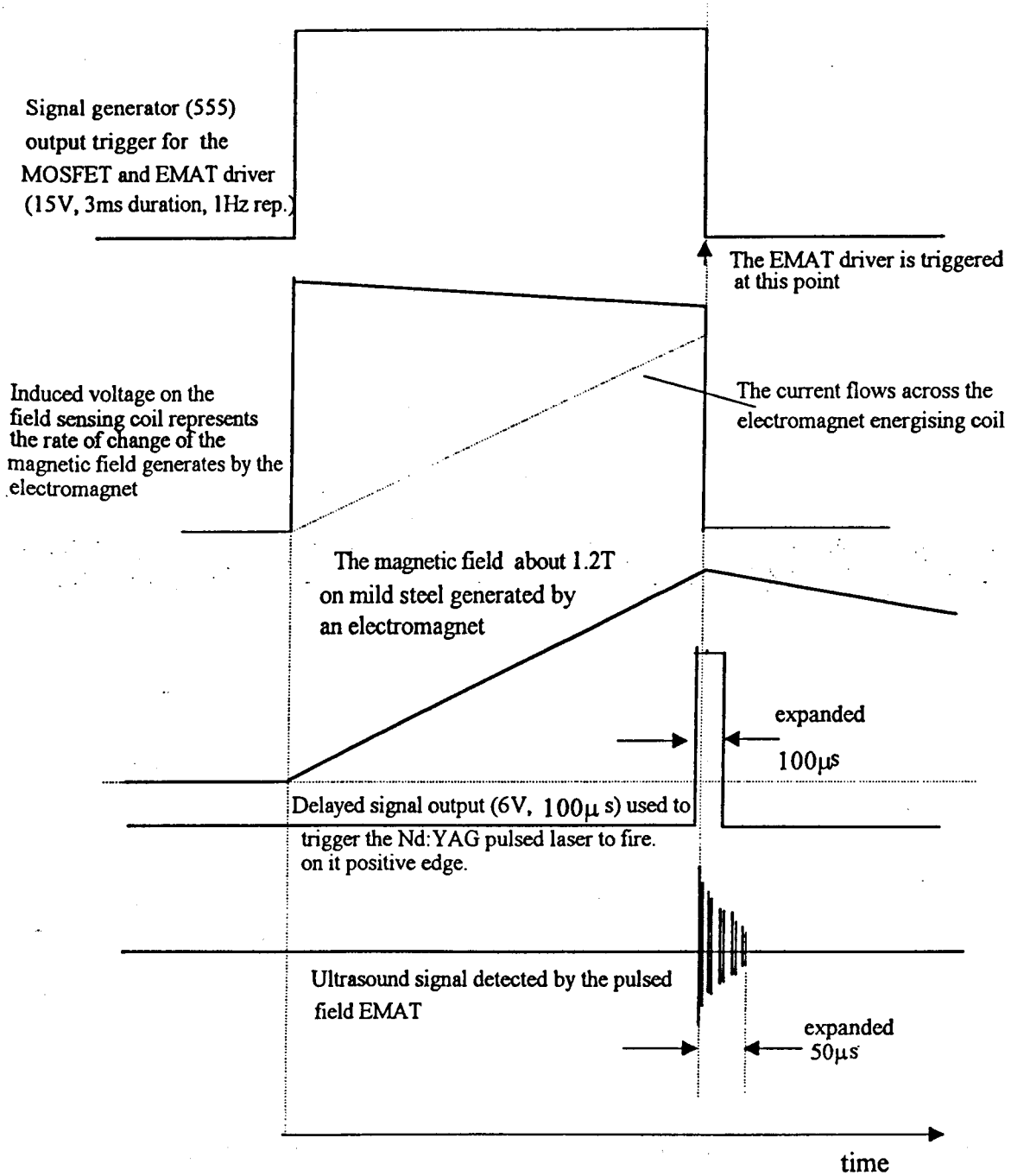

Figure-4.9: Triggering sequences of the electromagnet driver and other related equipment e.g, EMAT driver, and pulsed lasers. This equipment is triggered at the negative edge of the electromagnet driver pulse where the maximum magnetic field is present on the surface of the sample.

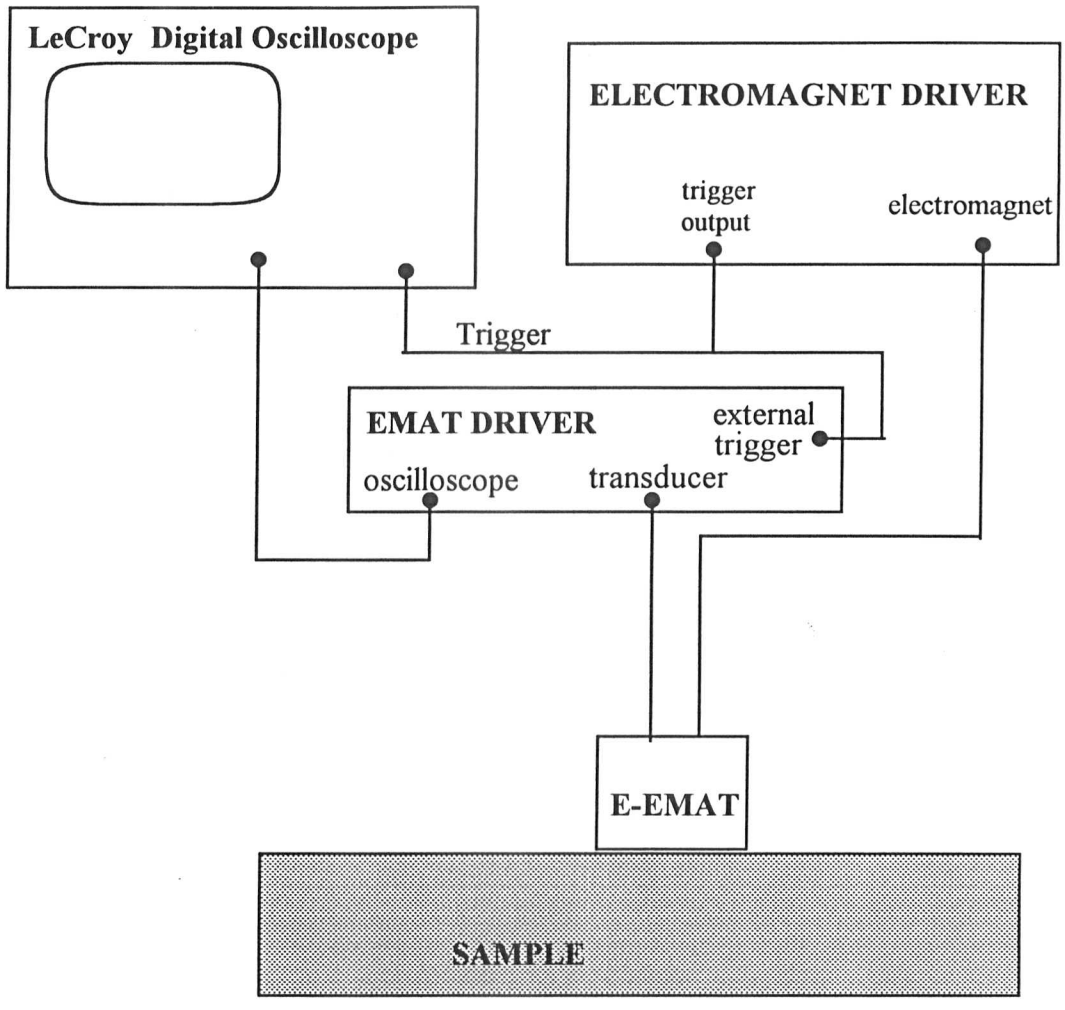

Figure-4.10: Schematic diagram of experimental set up for non-contact ultrasound measurement using E-EMAT.

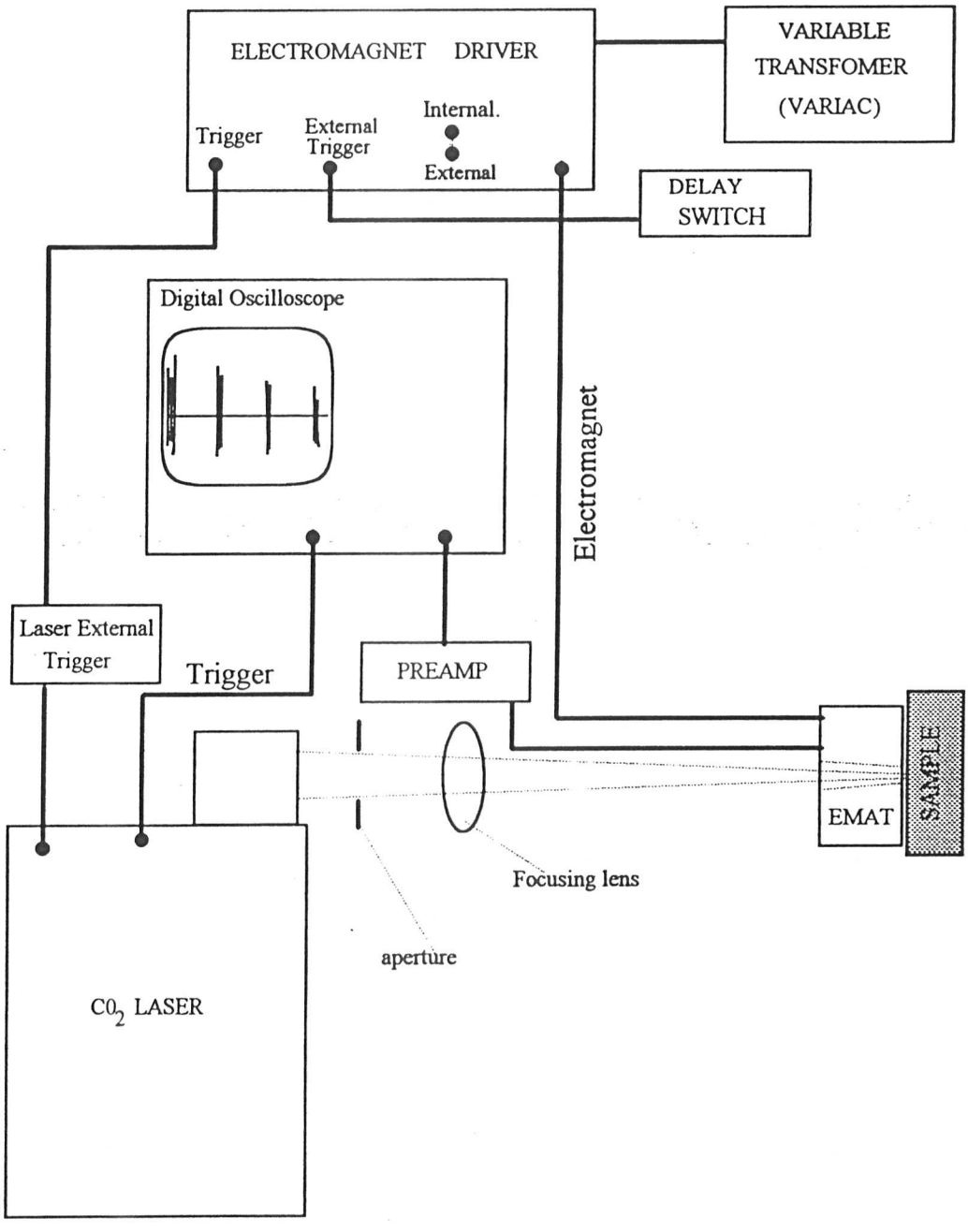

Figure-4.11: Schematic diagram of experimental set-up for non-contact ultrasound measurement using CO_2 laser generator and E-EMAT detector.

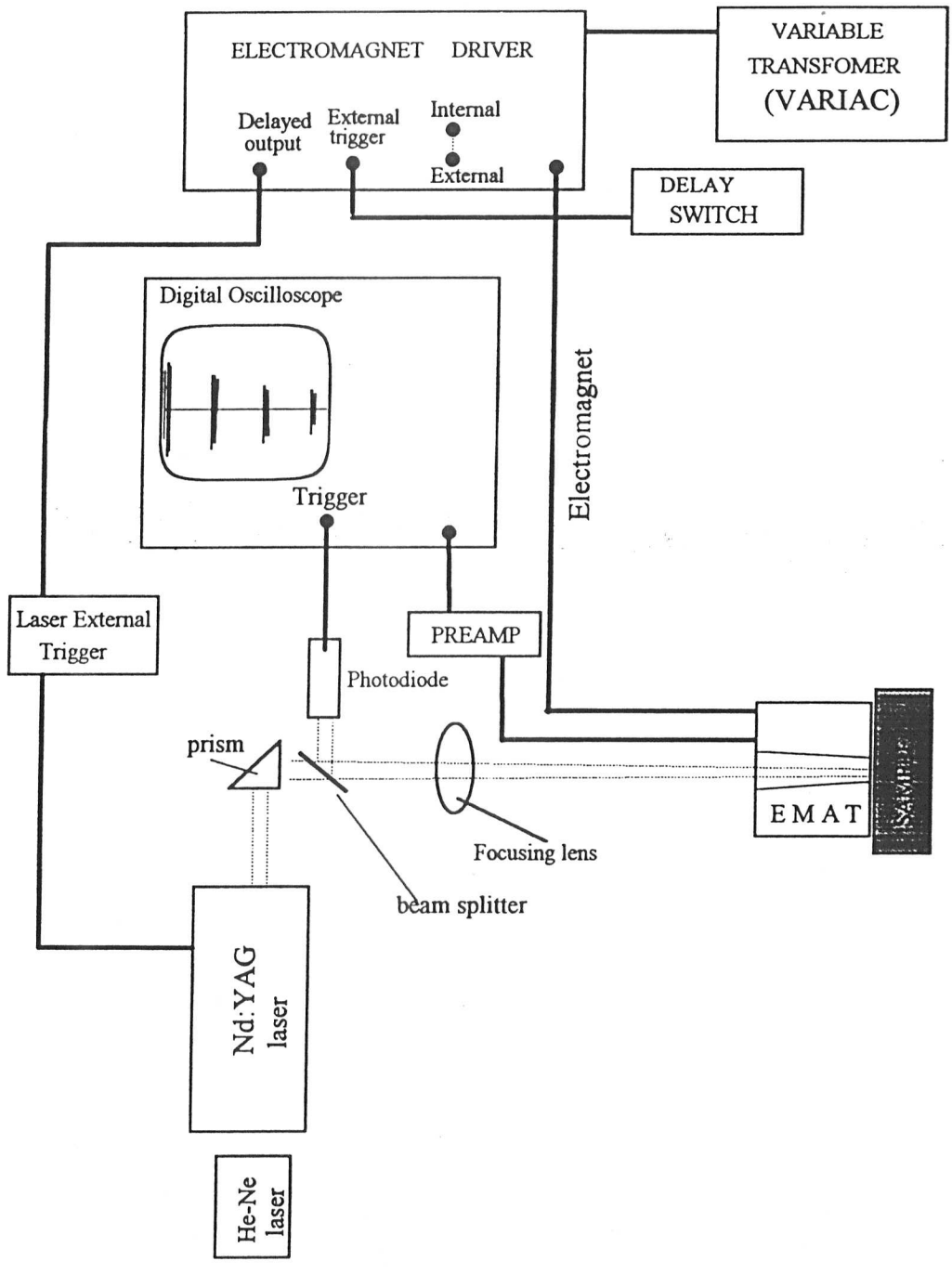

Figure-4.12: Schematic diagram of experimental set-up for non-contacting ultrasound measurement using Nd:YAG laser generator and E-EMAT detector.

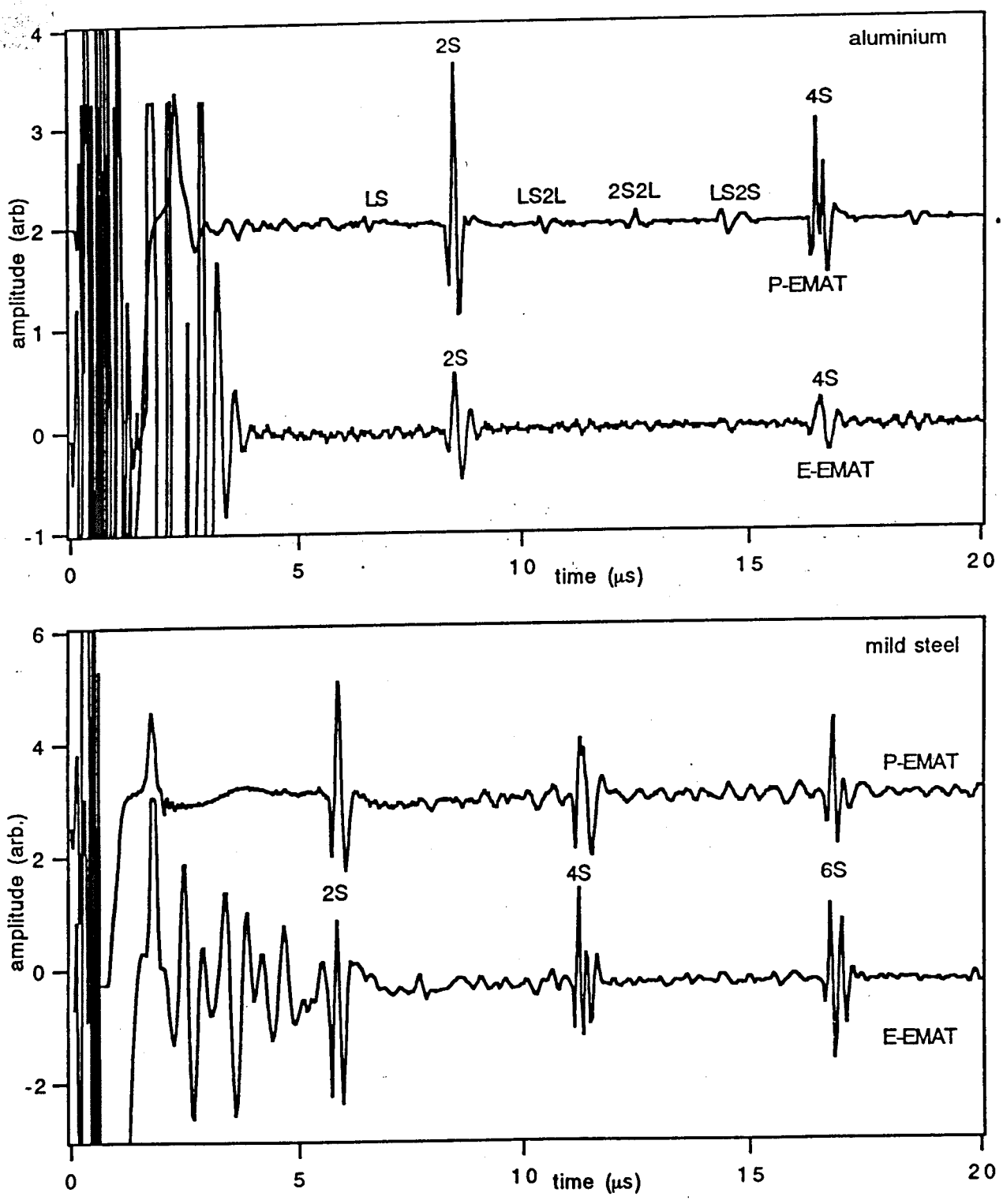

Figure-4.13: Pulse echo shear wave waveforms in aluminium and mild steel generated and detected by both P-EMAT and E-EMAT.

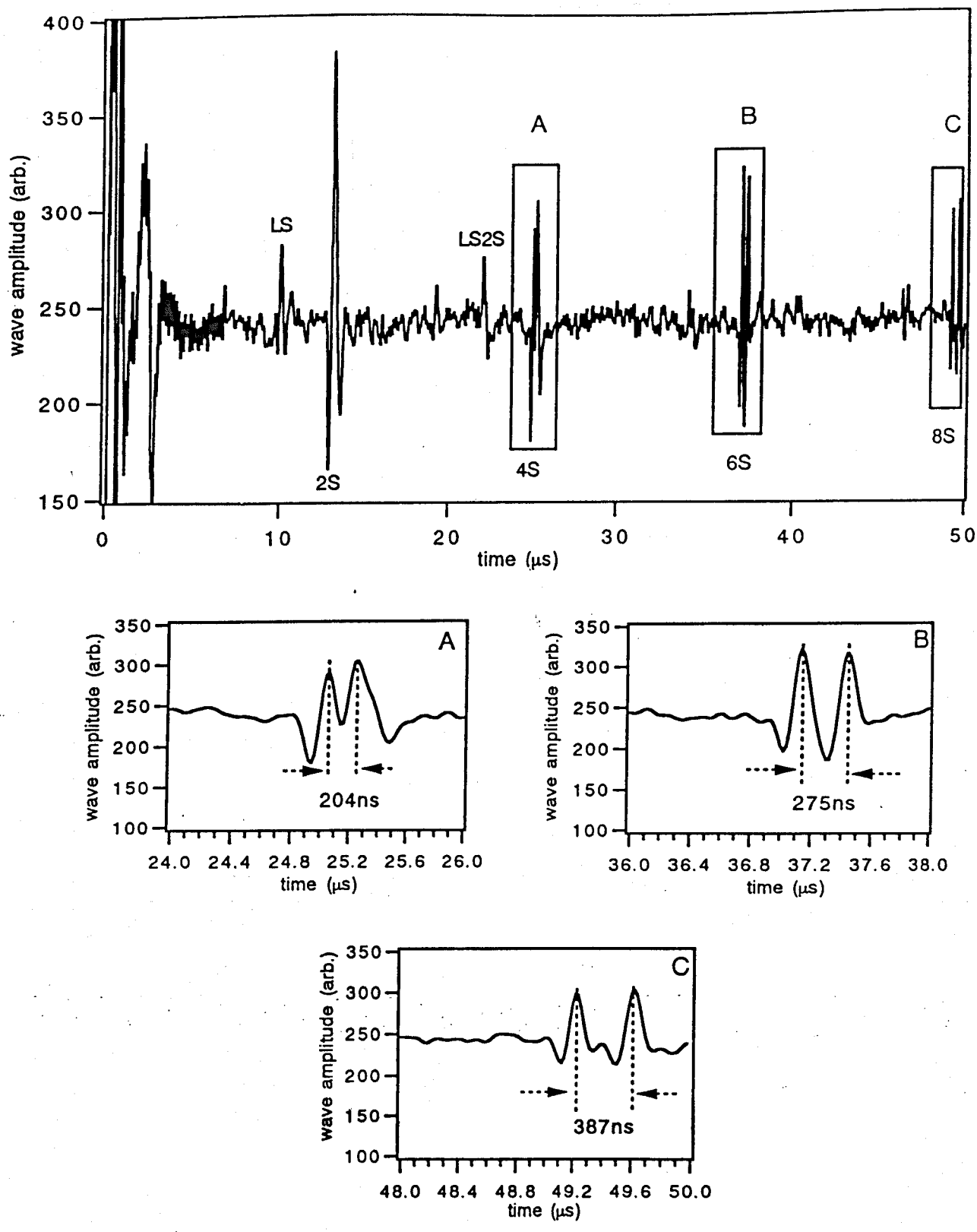

Figure-4.14: Send-receive shear waveform in aluminium showing an anisotropy effect. The shear wave pulse splits as it progresses indicating two wave components propagating at different velocity. The waveform was generated by CO_2 laser and detected by E-EMAT.

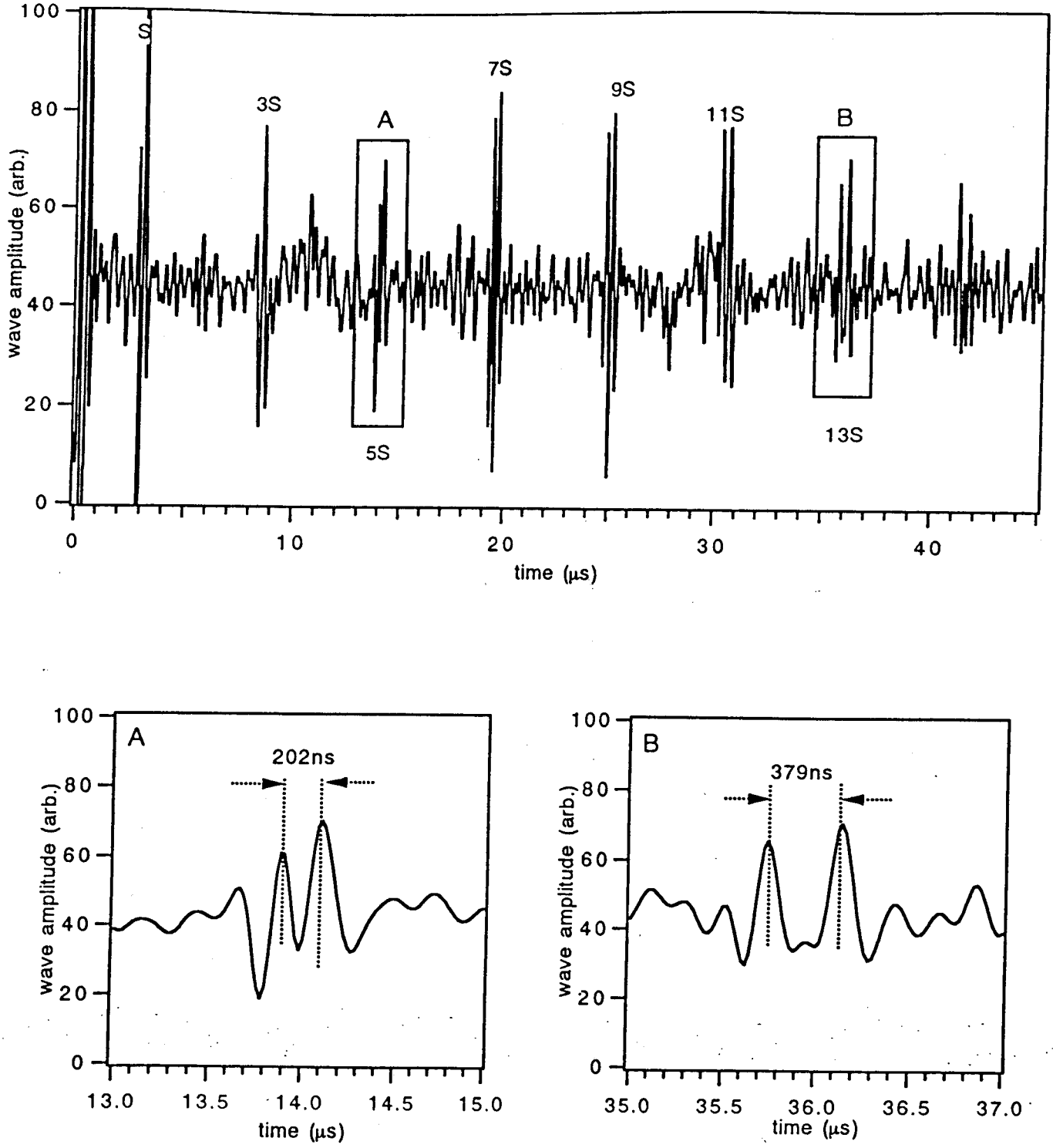

Figure-4.15: Epicentral shear wave waveform in mild steel showing an anisotropy effect. The waveform was generated by a P-EMAT and detected by E-EMAT.

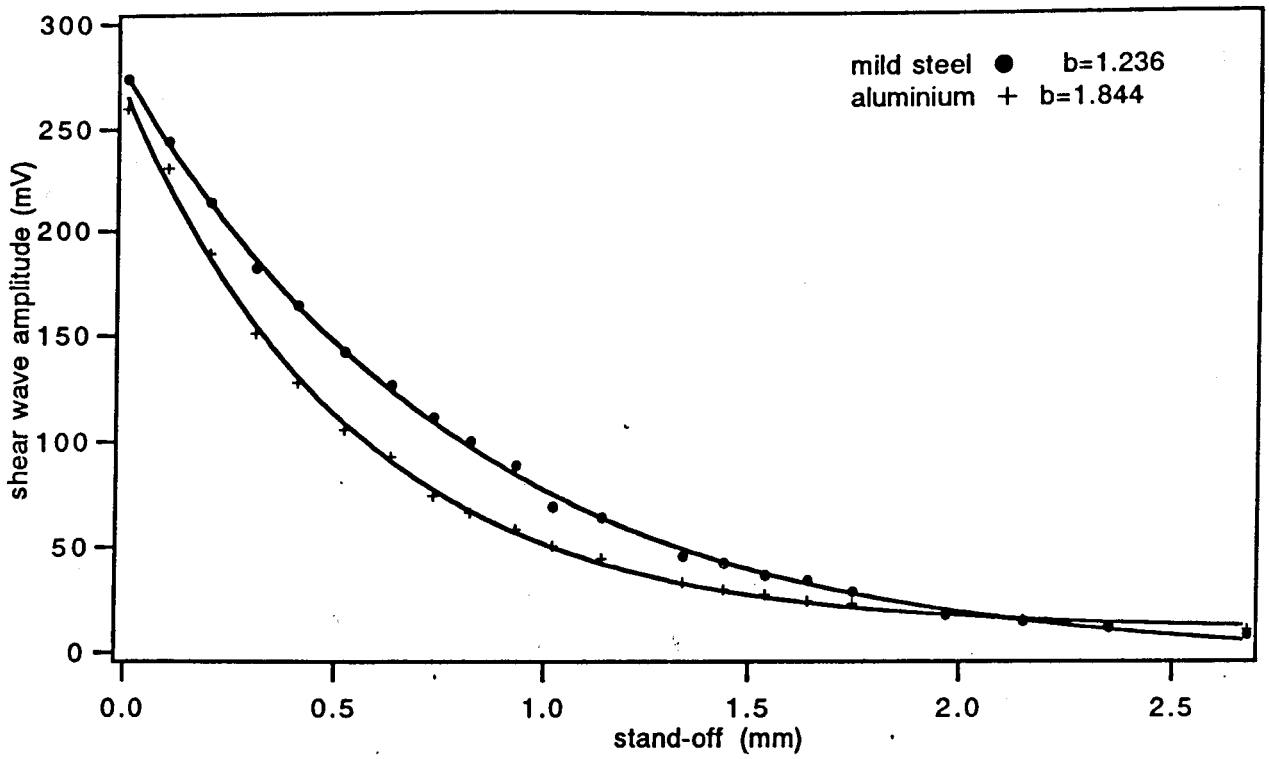

Figure-4.16: Stand-off dependence of the shear wave generated and detected by P-EMAT on mild steel and aluminium.

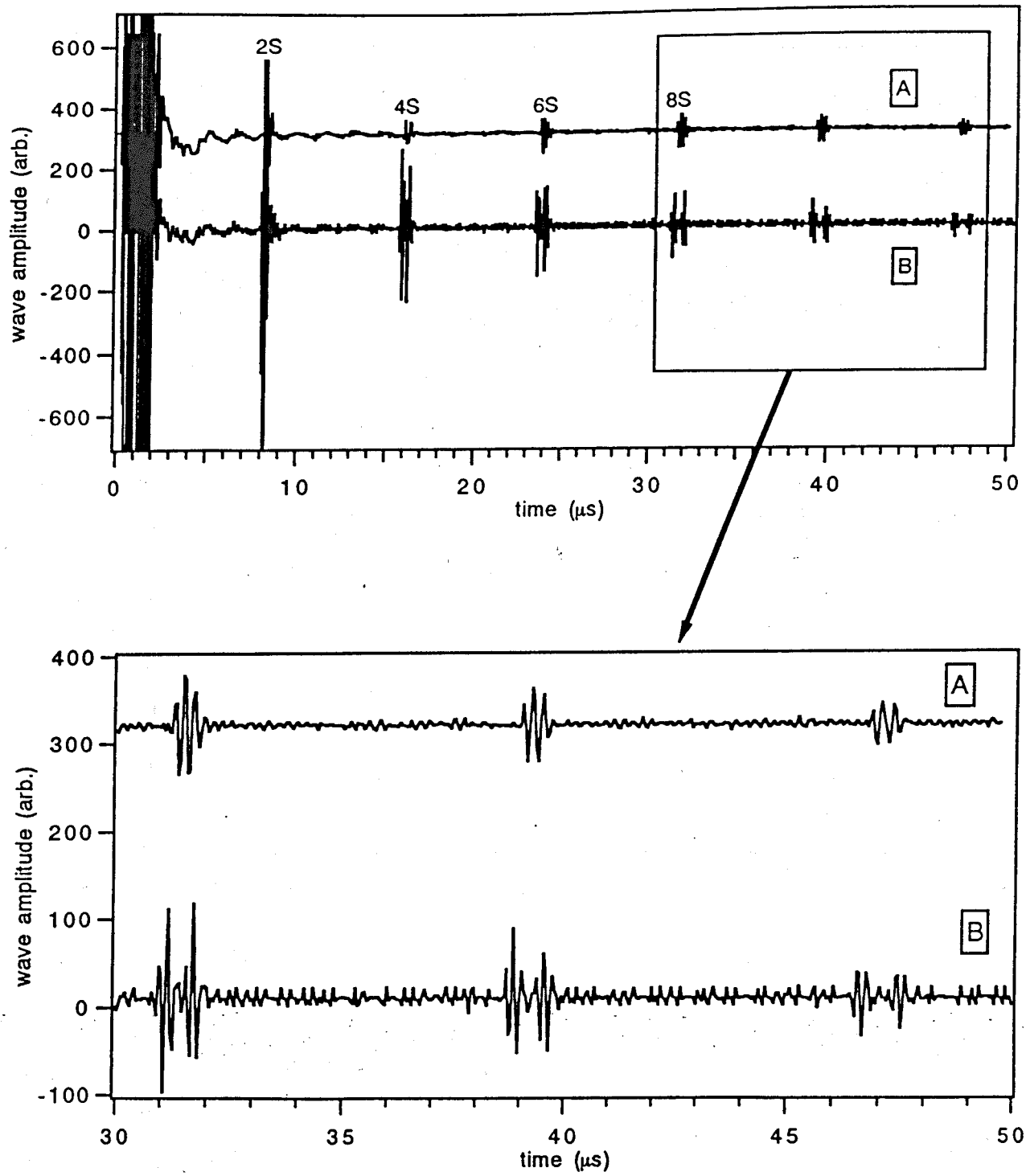

Figure-4.17: Effect of oxide layer (magnetite) on the shear wave transduction on mild steel by E-EMAT. (A)-Clean surface, (B)-thick magnetite layer (about 100μm).

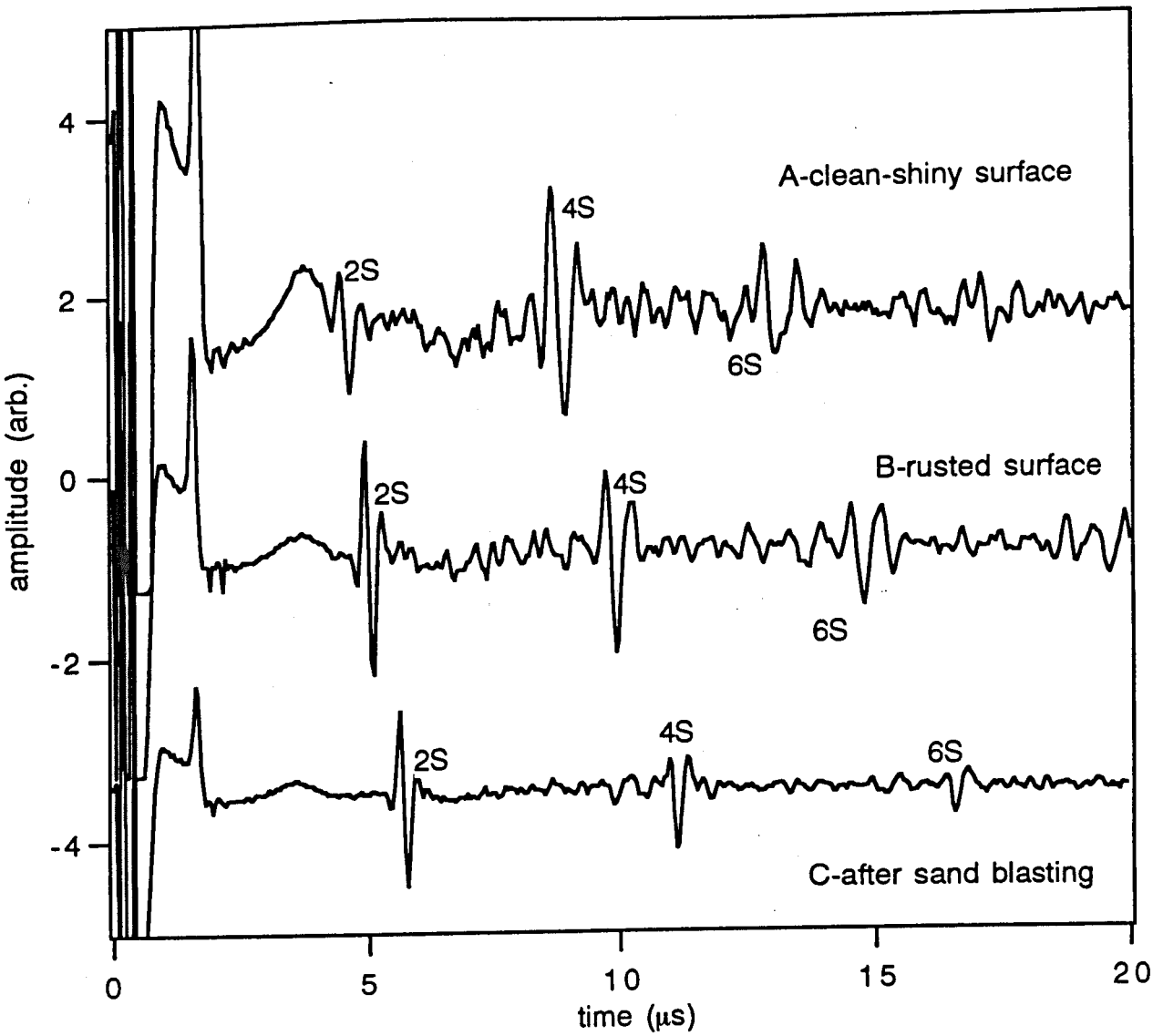

Figure-4.18: Effect of hydrated oxide layer (red rust) on shear wave transduction efficiency of an E-EMAT: (A)-clean surface, (B)-thin layer of hydrated oxide on a rough corroded surface, (C)-in a sectioned of mild steel pipe after sand blasting.

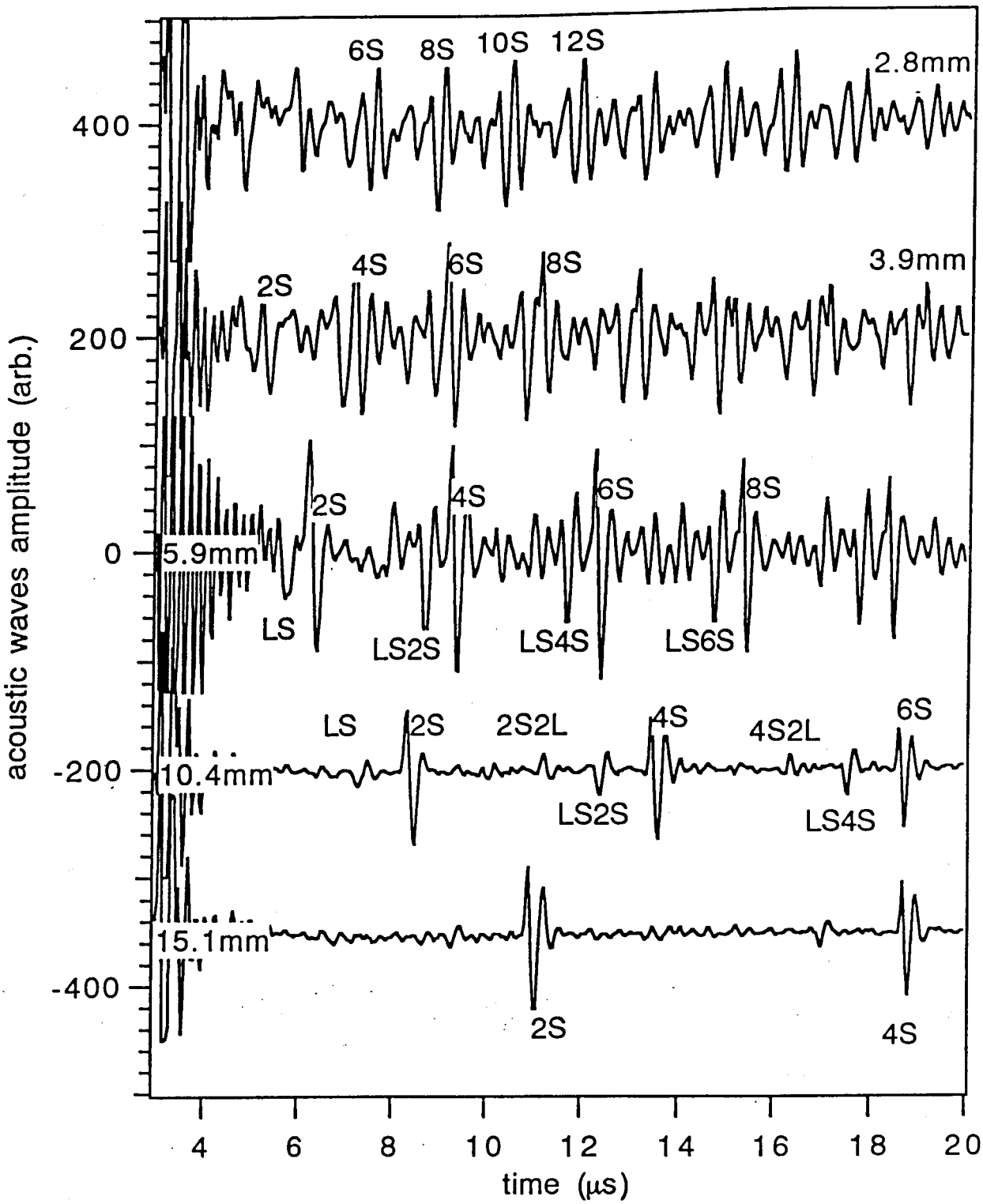

Figure-4.19: Send-receive ultrasound waveforms on mild steel step wedges, generated by Nd:YAG laser and E-EMAT detected. The waveforms have a different time delay of about 3μs to show the relative pulse arrivals.

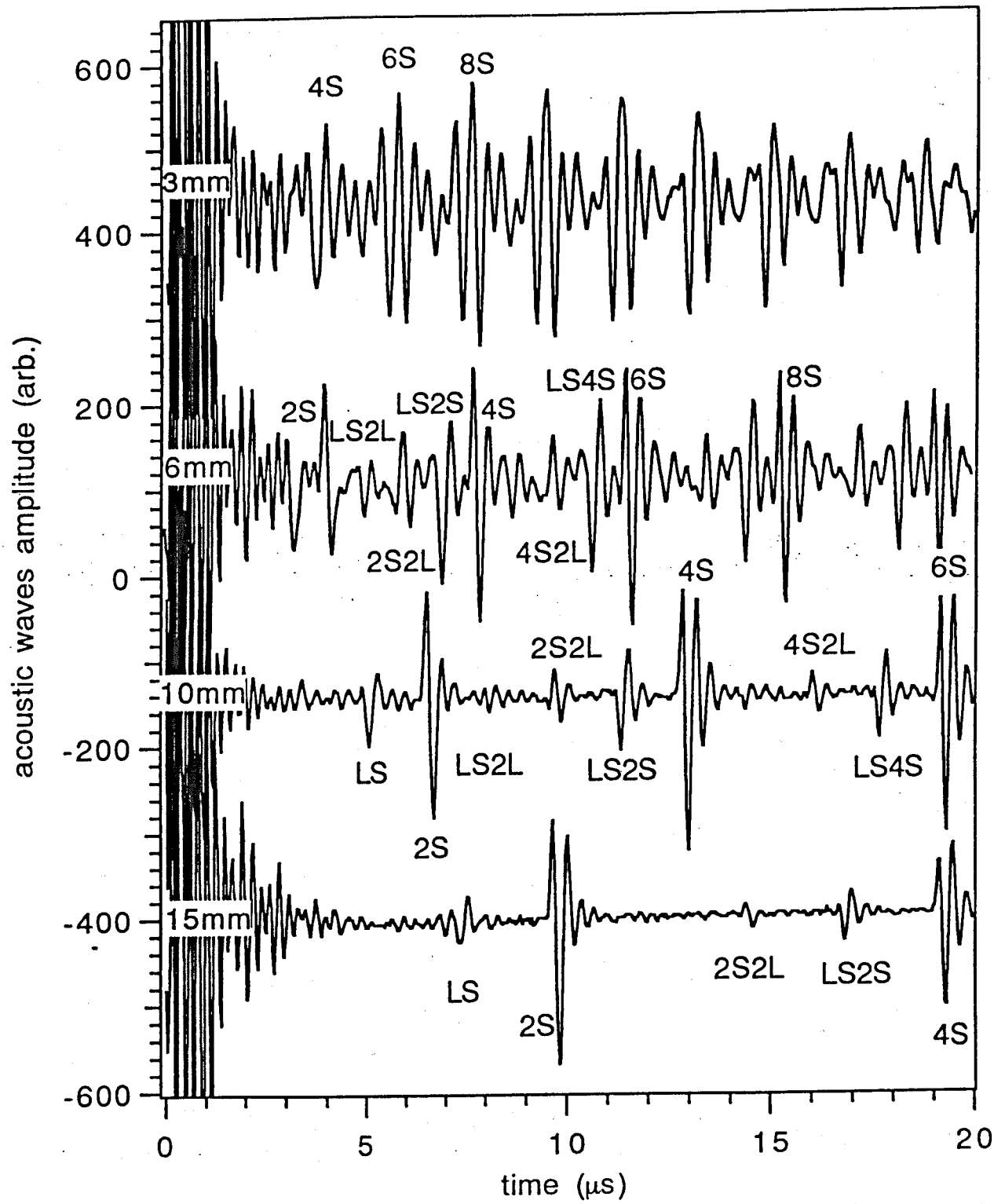

Figure-4.20: Send-receive ultrasound waveforms on aluminium step wedges, generated by Nd:YAG laser and detected by E-EMAT.

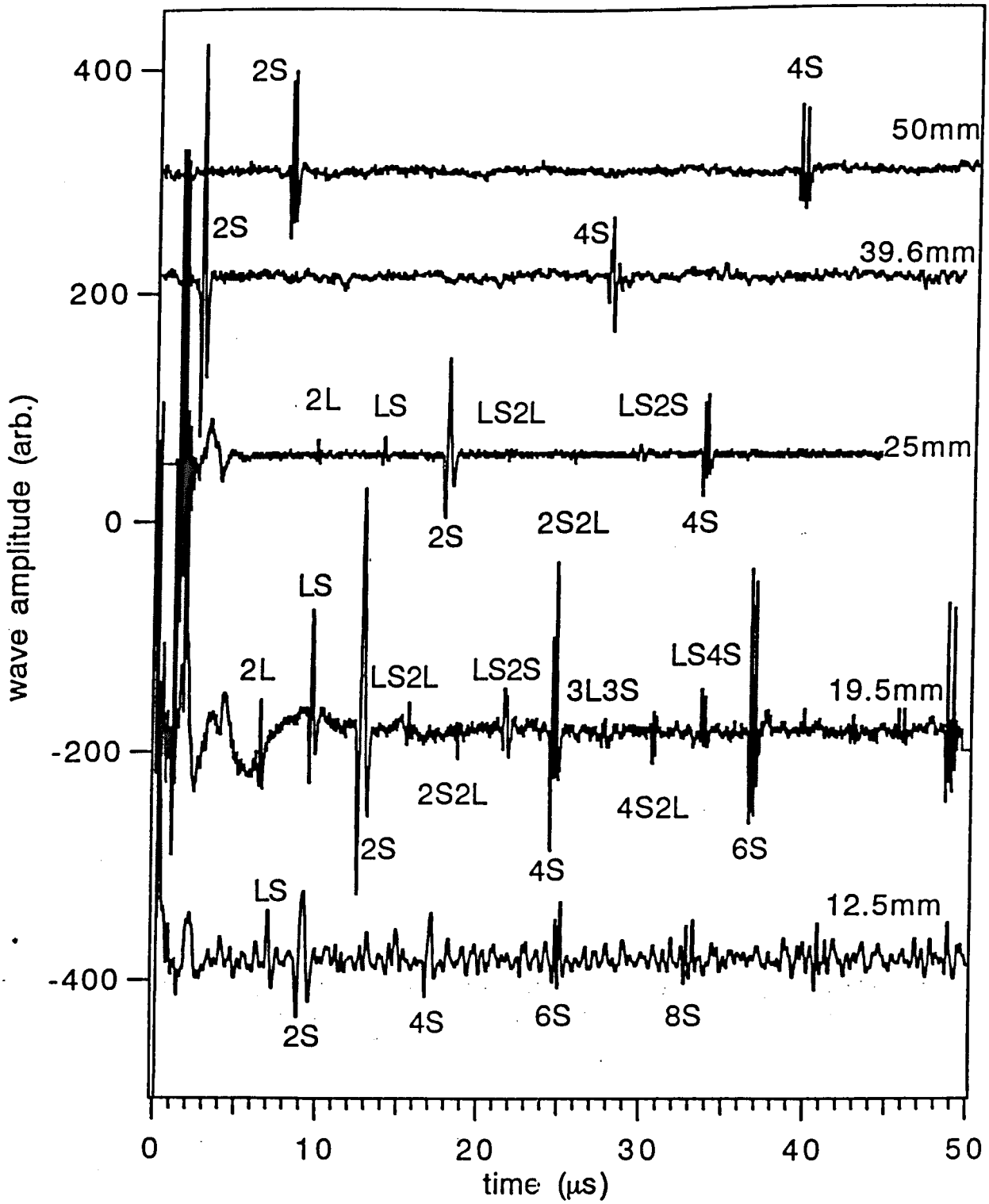

Figure-4.21: Send-receive ultrasound waveforms on aluminium of different thickness, generated by CO_2 laser and detected by E-EMAT. The waveforms of 50mm, 39.6mm and 25mm samples have time delay so that both 2S and 4S pulse arrivals could be displayed.

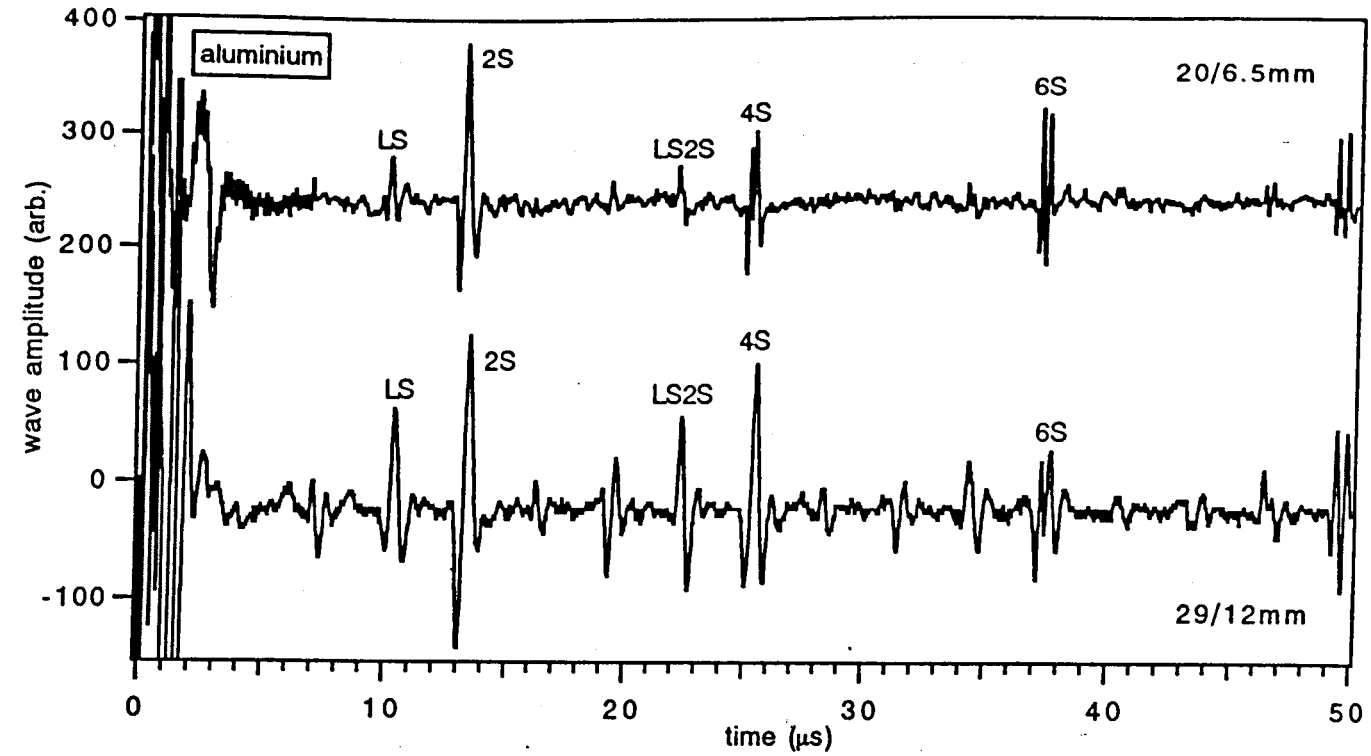

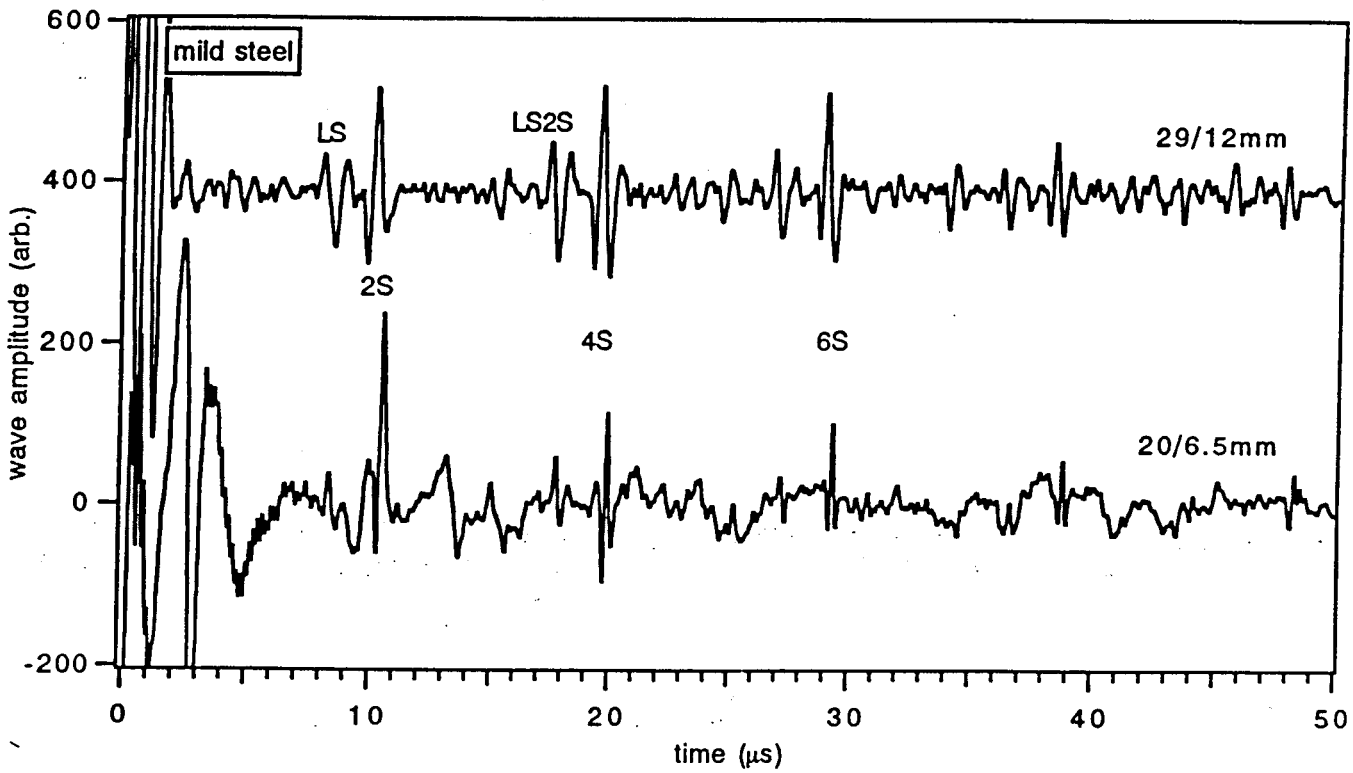

Figure-4.22: Effect of width of the annular EMAT coil on the send receive ultrasound waveforms in aluminium and mild steel, generated by a Nd:YAG laser and detected by E-EMAT.

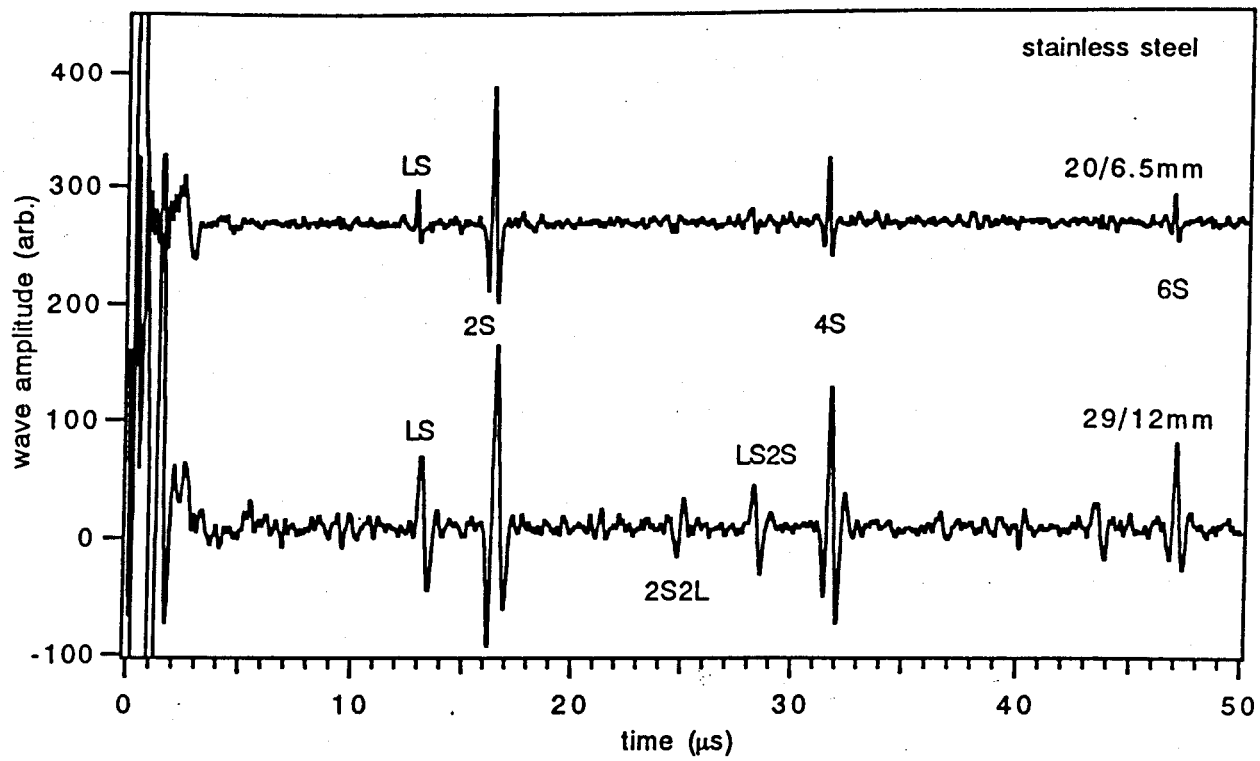

Figure-4.23: Effect of width of the annular EMAT coil on the send-receive ultrasound waveforms in stainless steel, generated by a Nd:YAG laser and detected by E-EMAT.

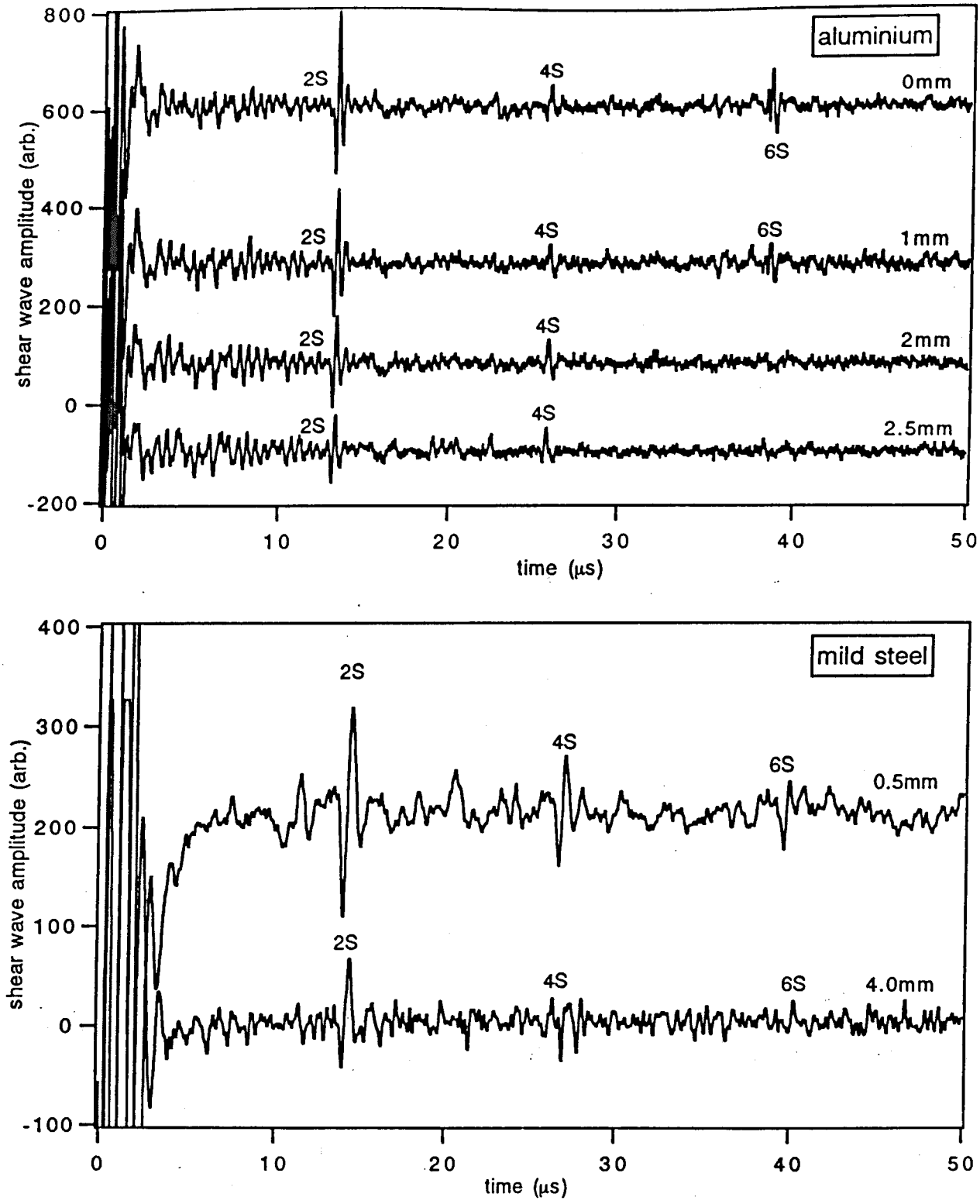

Figure-4.24: Effect of stand off on send-receive ultrasound waveforms in aluminium and mild steel, generated by a CO_2 laser and detected by E-EMAT.

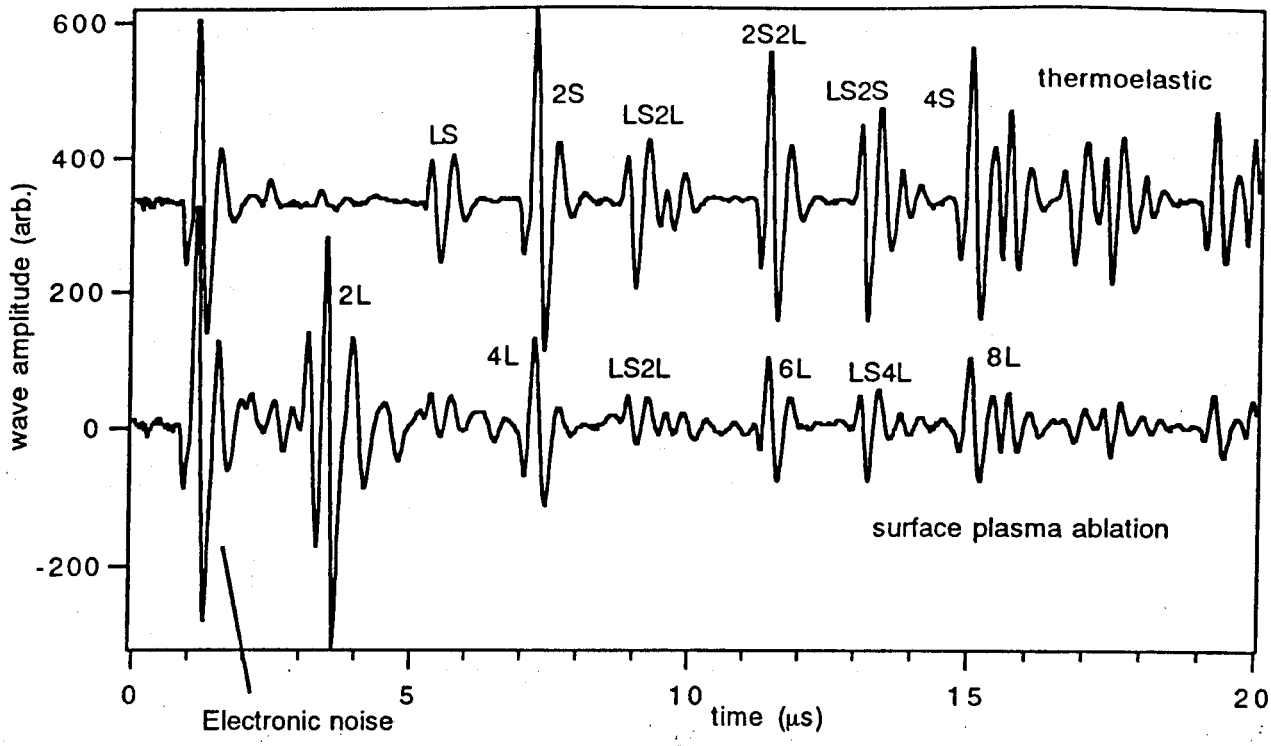

Figure-4.25: Send-receive ultrasound waveforms generated in mild steel by a CO_2 laser at different energy density and detected by E-EMAT. At low optical energy density, the incident energy generates a strong thermoelastic source and thus the shear wave. At sufficiently high energy density, the incident energy causes plasma ablation on sample surface and launches a longitudinal wave besides a weaker shear wave.

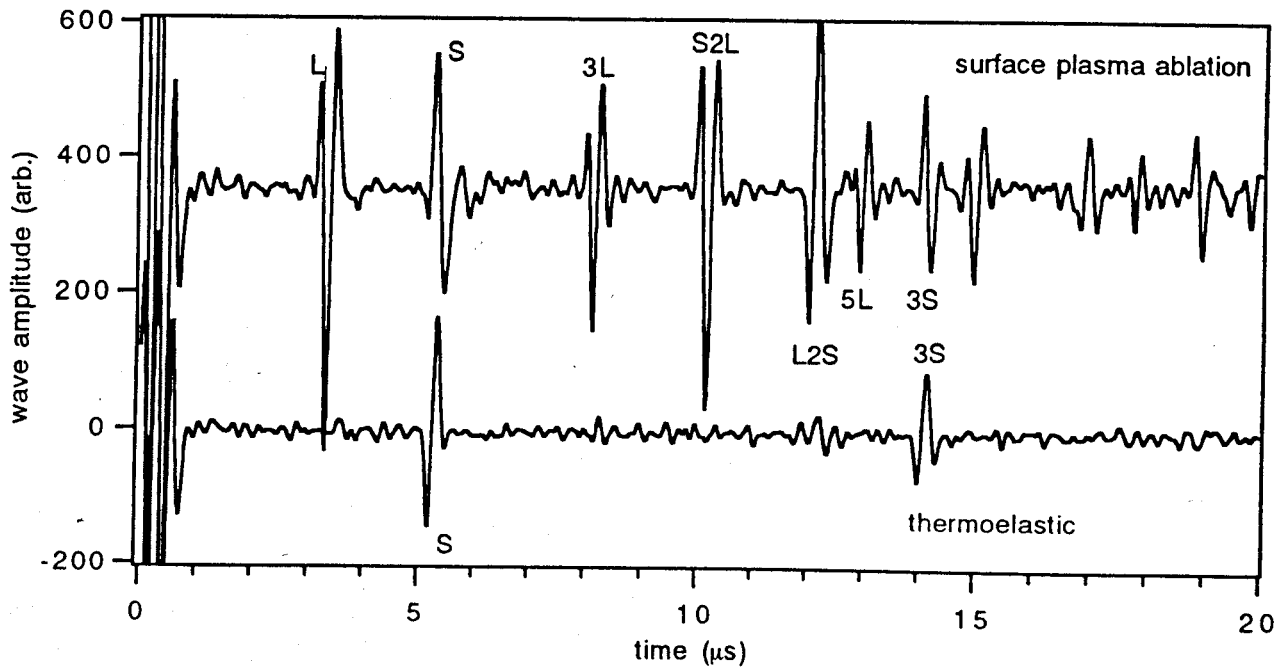

Figure-4.26: Epicentral ultrasound waveforms on mild steel detected by E-EMAT, generated by CO_2 laser at thermoelastic and surface plasma ablation regimes.

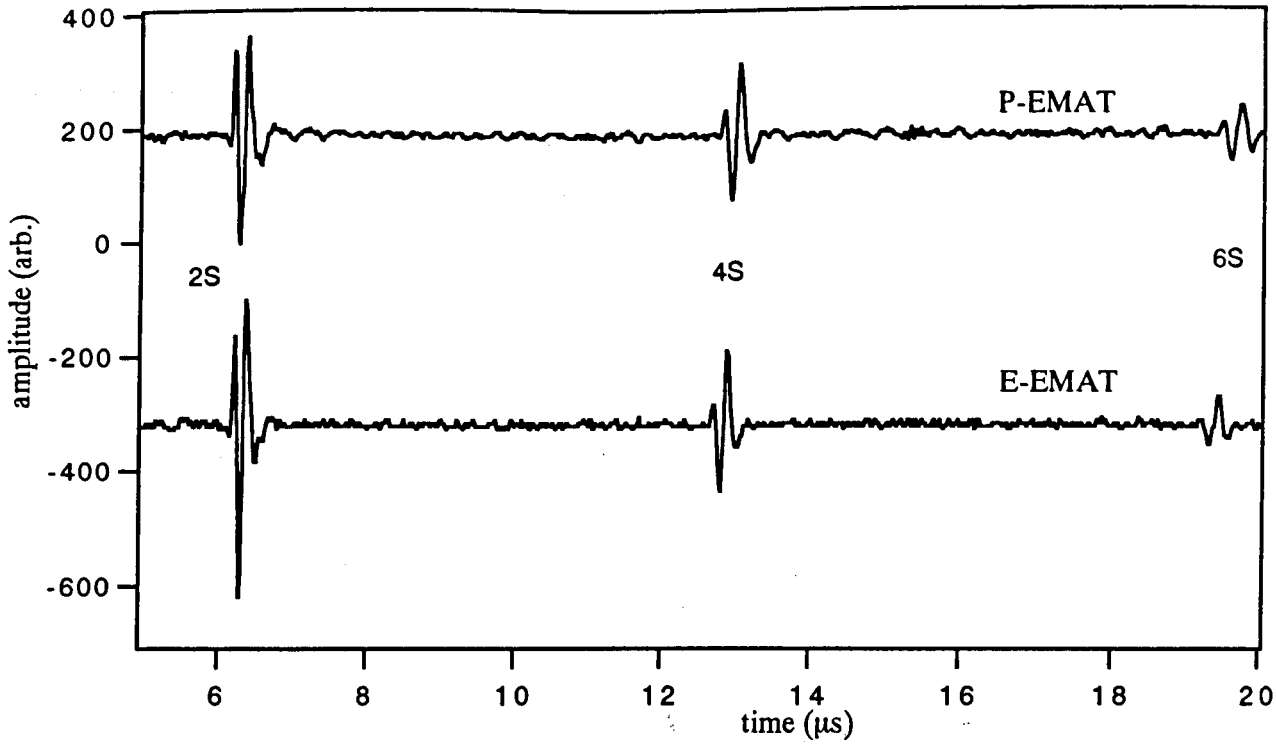

Figure-4.27: Pulse echo shear waveforms in mild steel at 700°C generated by a water cooled P-EMAT and E-EMAT.

CHAPTER-5

Non-Contact Ultrasound Measurements At High Temperatures.

5.0 Introduction

Seamless steel tubes and pipes are widely used in the chemical, oil and gas industries. The service environments of these products are severe and a stringent code of practice and application has to be complied with. The code of practice demands a high commercial quality and dimensional precision. To achieve this, the wall thickness of pipes is one of the most important parameters that needs to be taken into consideration. An accurate measurement of the wall thickness could be used to improve the manufacturing process and allow finer control of the product dimensions. Precise control of the wall thickness is critical to provide high quality products and to minimise wastage both of rejected pipes and the margin needed to maintain a minimum wall thickness.

Conventionally, the wall thickness has been measured only at the finishing line where the pipes are at or near ambient temperature. Measurements are carried out using a conventional ultrasound thickness gauge. In the hot extrusion processes, the wall thickness of the pipes are estimated from the average thickness over the length and have been monitored by using the whole weight and length, (Yamaguchi et al., [1984]). This measurement is also carried out at or near ambient temperature. Therefore seamless pipe production would greatly benefit from a non-contacting ultrasound inspection system that could measure the wall thickness at an early stage on the production line. The system could also be used for temperature measurement, and to interrogate the interior of the solid material; to characterise and monitor the microstructure non-destructively during or after manufacturing and for detection of any flaws that may occur during processing. The system developed as part of this thesis uses a pulsed laser as the ultrasound generator and an EMAT as the receiver, as described in the previous chapter. Laser-EMAT systems have been demonstrated to function up to a temperature of 1100°C on mild steel in a through-

transmission arrangement, (Idris et al., [1994] and Burns et. al., [1988]).

The production of the seamless steel pipe begins with the heating of a steel billet to about 1500°C in a gas or an electric induction furnace. The white hot steel billet is then extruded and pierced on the production line. This process takes place at a translation speed of about $1ms^{-1}$ and rotation of about 500rpm. After the pipe has emerged from the piercer, it undergoes cooling on the production line, the pipes are moving rapidly at about $0.6ms^{-1}$, and remain rotating at the same speed. It would be of the maximum benefit if the system could operate just after the piercing stage where the temperature of the sample under test is about 1200°C, however this is a very demanding test site (see Figure-5.1). The system has to be operated in send-receive arrangement as access to the inside of the pipe is impossible, the measurement has to be carried out from the outside.

In this chapter, the non-contacting ultrasound measurements on mild steel samples at elevated temperature will be described. The measurements were carried out by using a P-EMAT, an electromagnetic EMAT and combinations of pulsed laser- EMAT systems. Send-receive results and on epicentral measurements will be presented. The EMATs were water-cooled to permit high temperature operation.

5.1 Techniques For Ultrasound Measurement At High Temperature

Ultrasound measurement techniques at elevated temperature have been developed elsewhere using conventional piezoelectric transducers (Krautkramer, [1983]), or advanced non-contacting techniques (Parkinson et al., [1977]; Wadley et al., [1986]; Dewhurst et. al., [1988]; Monchalin, [1993] and Idris et al., [1994]). Measurements were carried out using either optical transduction systems, EMATs or the combination of the two. The transit-time carries information about the appropriate elastic rigidity and thus the ultrasound velocity, allowing one to evaluate the mechanical properties of the sample or if

the velocity is known the sample thickness. As the elastic rigidity and ultrasound velocities vary with the temperature, measurement of the ultrasound transit time can also be used to monitor the temperature of the sample by knowing precisely the wave velocity (Wadley et al., [1986]). An accurate transit time measurement in the time domain requires a broad bandwidth (temporally short) ultrasound pulse to be transmitted into the sample under test; this requirement can be satisfied by using a pulsed laser as ultrasound generator. This source can be complemented with an EMAT as wide bandwidth ultrasound detector.

5.2 Non-Contact Ultrasound Measurements On Steel At High Temperature.

A primary aim of this project was to establish the suitability of a water-cooled EMAT receiver to be operated with a laser generator in send-receive arrangement at elevated temperature. The ultrasound was generated by a pulsed laser, either a Nd:YAG or CO_2 laser. In the initial experiments, a series of ultrasound measurements was conducted on mild steel samples to examine the possibility of making thickness measurements using either an EMAT or a laser-EMAT system. The variation of both longitudinal and shear wave velocities with increasing sample temperature has been examined.

In the experiment, the transit time of the ultrasound propagation in the sample was monitored as the sample temperature increased to establish a calibration curve for the temperature dependence of the ultrasound wave velocities as a reference. The data could be obtained by non-contact methods such as laser interferometry or through-transmission using a pulsed laser generator and EMAT receiver as described earlier.

5.3 Experimental Techniques

The sample was mounted onto a sample holder that was pinned to a pair of stainless steel tubes (Figure-5.2a), lying horizontally across a cylindrical furnace. The

samples were normally in the form of plates of dimension 120mm x 100mm with thickness varying from 6mm up to 12.5mm. Thicker samples, up to 50mm thick, were directly pinned onto the stainless steel tube rack as shown in Figure-5.2b. The sample surfaces were initially cleaned of any rust or scale.

The temperature of the sample was measured by a chromel-alumel (Ni/Cr-Ni/Al) K-type thermocouple inserted into a drill hole, a few millimetres deep beneath the sample surface on the opposite face to the EMAT. It was connected to a Digitron digital temperature meter with a precision of $\pm$1°C and absolute accuracy of $\pm$3°C in 1000°C.

The temperature controlled furnace (figure-5.3) has a heating zone with a diameter of 150mm by 325mm long and a maximum operating temperature of 1100°C. In operation, the temperature was increased gradually, firstly up to about 800°C then up to 1100°C. This allowed careful measurement in the region of the Curie temperature of the mild steel. During the experiment, both ends of the furnace were closed using alumina bricks to reduce heat losses.

The alumina brick at the EMAT side was removed and then the EMAT was immediately slid up to the sample to take a measurement. As the cross section area of the E-EMAT covered almost 80% of the cross section area of the furnace (Figure-5.3), the introduction of the EMAT acted in a similar way to the alumina brick preventing a large amount of heat loss. The introduction of the smaller diameter P-EMAT into the furnace however, caused a significant heat loss and therefore an immediate ultrasound measurement needed to be performed. The EMAT was introduced on to the sample surface momentarily and pulled back once the waveform had been captured to ensure that the intense heat did not destroy the EMAT. This took place in a short time interval typically around 1-2 seconds. The temperature of the sample was recorded when the EMAT was introduced onto the sample surface and immediately after the waveform had

been captured. The cooling water flow rate was regulated to ensure that it was sufficient to protect the EMAT from the heat and to avoid excessive cooling of the sample. Since the size of the E-EMAT was almost the same as the sample, the introduction of the EMAT onto the sample surface might well cool the sample and introduced errors in the temperature reading. This effect will be dealt with in more detail in chapter 6. However, to minimise the effect of this error, the laser was fired at a constant time delay after positioning the EMAT on the surface of the sample. The details of the time delay used will also be described in chapter 6.

5.3.1 EMATs in Pulse Echo Mode

The schematic illustration of the experimental set-up is given in figure-4.3. A water-cooled P-EMAT was used as both the generator and the detector of ultrasound. During the measurements, the EMAT was introduced into close contact with the sample surface in the furnace and remained there until an average of 500 waveforms had been captured. The EMAT was then extracted. The captured ultrasound signals were displayed on a Lecroy type 9310 digitising oscilloscope and stored on a computer disk for subsequent analysis. At higher temperatures, the number of waveform averages was reduced and in some cases, in particular at the temperatures above 700°C, only 10 waveforms were captured.

A similar experiment was carried out using the E-EMAT described in detail in chapter-4 (see figure-4.10). The measurements were carried out up to the highest temperature possible, and the EMAT was carefully monitored, to avoid damage. At low temperatures, the recorded waveform was obtained after averaging of 10 waveforms, and the sampling number was reduced to 5 as the temperature exceeded 650°C. Above 700°C, we only recorded single shot waveforms. The waveform sampling number to be captured

by E-EMAT had to be reduced because of its lower repetition rate compared to the P-EMAT. The recorded waveforms were then stored for subsequent analysis.

5.3.2 Measurements Using Pulsed Laser Generator and E-EMAT Receiver

The experimental set up has been described in detail in chapter-4 (see figure-4.11 and figure-4.12). The ultrasound was generated in the weak ablation regime by setting the voltage of the Nd:YAG laser flashlamp at 840V and partially focusing the beam. The degree of ablation could be increased by focusing the beam to a smaller spot allowing both longitudinal and shear wave signals to be detected with reasonable amplitude for accurate transit-time measurements. The water-cooled E-EMAT was used as the receiver for both epicentral and send-receive arrangement.

Before the sample was placed in the furnace, the laser beam and the EMAT were aligned so that an accurate epicentral waveform could be recorded. In send-receive arrangement with both laser and EMAT on the same side of the sample, alignment was crucial for the laser to pass through the central hole in the EMAT and hit the sample. As the temperature of the sample increased, in particular above the Curie temperature of the sample, the intensity of the irradiating beam was increased by increasing the pulse energy to generate a stronger ultrasound source to compensate for the higher ultrasound attenuation exhibited in the sample. When the CO_2 laser with a constant energy output was used as the generator, the laser energy deposited onto the sample surface was altered by varying the aperture diameter of the laser window and/or focusing the beam onto the surface of the sample to alter the strength of the laser source .

5.4 Results and Discussion

5.4.1 EMATs in Pulse Echo Measurements

The temperature dependence of the ultrasound wave velocities in mild steel, measured using the various experimental configurations described earlier, is shown in figure-5.4. For the shear wave, (figure-5.4a), below the Curie temperature T_c, the velocity data was measured from both epicentral and send-receive waveforms, generated and detected by both Nd:YAG and CO_2 laser-EMAT systems. The data was also measured from pulse echo waveforms generated using both types of EMAT. At about T_c and above, this data was measured from the epicentral waveforms, generated by a Nd:YAG laser and detected by E-EMAT since in this temperature range both send-receive and pulse echo ultrasound waveforms were dominated by longitudinal arrivals only. Below T_c, the longitudinal wave velocity (figure-5.4b), was measured from the epicentral ultrasound waveforms, where the detected signals had clear shear and longitudinal arrivals. The measured longitudinal and shear wave velocities for the sample at room temperature are 5975 ± 13 ms^{-1} and $3230 \pm 15ms^{-1}$ respectively. At 700°C, the longitudinal and shear wave velocities are $5485 \pm 23ms^{-1}$ and 2717 ± 19 ms^{-1} respectively. These values are in agreement, within the experimental error, with those obtained by Idris et al., [1994], Papadakis et. al., [1972], Wadley et. al., [1986], McKie, [1987], and Dewhurst et. al., [1988]. Both the temperature-velocity curves show a gradual decrease in velocity with increasing temperature. From about 740°C to approximately 770°C the gradient of the ultrasound velocity-temperature curves increases dramatically, after which the longitudinal wave velocity decreases in a linear manner with a slower rate.

Figure-5.5, shows the pulse echo ultrasound waveforms in a mild steel sample generated by a P-EMAT. The waveforms are dominated by shear wave arrivals corresponding to the path-lengths of 2S, 4S and so on, where S is the shear wave path-

length equal to the thickness of the sample. As the temperature increases, the transit time of the wave arrival increases corresponding to the reduction in the wave velocity. The detected signal amplitude increases gradually with the increasing temperature and at the same time the signal to noise ratio improved. As the temperature approaches the Curie temperature T_c, the amplitude of the shear wave decreases gradually and longitudinal waves begin to appear with an increase in amplitude. At T_c, the waveform is dominated by anomalous longitudinal arrivals, denoted as 4L, 6L etc,. The amplitude of these signals increases dramatically just above T_c. Similar results have been observed by Cole, [1978]; Parkinson et al., [1977] and Lee at .al., [1992] using EMAT for both generation and detection, and Idris et. al., [1994] using a laser-EMAT system.

Figure-5.6 shows the temperature dependence of the pulse echo ultrasound waveforms in mild steel generated by a water-cooled E-EMAT which exhibits similar features to the P-EMAT (figure-5.5). In both cases, the paralysis of the EMAT receiver increases with the increasing temperature preventing some of the 1st. longitudinal arrivals from being seen. The shear wave amplitude increases gradually up to the temperature of 700°C and then decreases rapidly until about 760°C, (figure-5.7). Above this temperature, the waveform is dominated by longitudinal arrivals, the signal amplitude increases dramatically and peaks at about 780°C, close to the Curie temperature of the sample. As the temperature increases further, the signal amplitude reduces rapidly with no discernible signal above 870°C. In parallel with the ultrasonic measurements, the intensity of magnetic field generated on the surface of the sample was monitored. The details of this measurement will be described in Chapter-6. It was observed that the magnetic field at the surface of the sample remained constant at about 1.4T from room temperature up to the temperature 740°C. Above 740°C, the magnetic field intensity decreased rapidly and reached about 0.35T at temperature 770°C. The field remained constant at 0.35T at a

higher temperature and it corresponded to the static field generated by the electromagnet on a non-magnetic metal such as aluminium.

5.4.2 Pulsed Nd:YAG Laser Generator--E-EMAT Receiver

Figure-5.8 shows the temperature dependence of the epicentral ultrasound waveforms in a thick mild steel sample generated by a Nd:YAG laser and detected by a E-EMAT. The ultrasound source was generated in a mild ablative regime. At low temperature the waveforms are dominated by shear wave arrivals with a relatively weak longitudinal signal (Figure-5.9). The amplitude of the shear wave increases with the increasing temperature up to about 700°C after which the amplitude decreases. No shear arrival could be detected above 780°C. The amplitude of the longitudinal wave arrivals are almost constant below T_c. As the temperature approaches T_c, the amplitude increases with a pronounced enhancement just above T_c. The amplitude reduces as the temperature increases further and no discernible signal could be detected at temperature above 860°C even after increasing the source strength.

Figure-5.10 shows the temperature dependence of the send-receive ultrasound waveforms in mild steel generated by the Nd:YAG laser and detected by E-EMAT. At room temperature the waveform is dominated by the shear wave arrivals, however as the temperature increased, the longitudinal wave and the mode converted pulses began to appear. Figure-5.11 shows the temperature dependence of the ultrasound arrivals (in the sample similar to Figure-5.10) at higher temperature. At a temperature of above 820°C, no discernible signals was recorded, however after increasing the laser flashlamp voltage to 870V and focusing the beam, a weak longitudinal arrival was detected. When the temperature was increased further, the receiver exhibited higher noise while the signal amplitude was not affected. The wave amplitudes diminished and no measurements were

possible above 1040°C even when the power density of the incident irradiating laser was increased by increasing the laser flashlamp voltage to 890V.

The temperature dependence of the ultrasound signal amplitude in mild steel generated by Nd:YAG laser and pulsed field EMAT detector is shown in figure-5.12. The curves show that the amplitude of the shear wave increases with temperature and reaches a maximum at a temperature about 600°C then it falls rapidly until about 750°C. It is also observed that the amplitude of the mode converted longitudinal wave increases gradually with increasing temperature above 600°C. At about 750°C the longitudinal wave amplitude increases rapidly and exhibits a sharp peak at 780°C, after which it falls rapidly to a minimum at about 800°C. At a higher temperature, the longitudinal wave amplitude remained low although a higher laser energy density was deposited onto the sample surface.

5.4.3 CO_2 Laser Generator--E-EMAT Receiver.

Figure-5.13 shows the temperature dependence of the epicentral ultrasound waveforms in mild steel. The ultrasound source was generated in the surface plasma ablation regime where the CO_2 laser beam was partially focused. The waveforms are labelled as described earlier. At lower temperatures, the waveforms are dominated by the large shear arrivals, accompanied by weaker longitudinal arrivals and also the mode converted signals. As the temperature increases, amplitudes increase and the shear wave arrival exhibits a peak at 670°C after which it begins to decrease. The longitudinal arrivals begin to change polarity at about 770°C and there is an enhancement of the longitudinal amplitude at 790°C above which its amplitude begins to decrease. The measurements were discontinued at 820°C when no ultrasound signal could be detected even after increasing

the laser power density irradiated onto the sample surface to form an air breakdown source.

Figure-5.14 shows the send-receive ultrasound waveforms in mild steel detected by pulsed field EMAT. The waveforms again vary with temperature in a similar manner to the earlier description (figure-5.8). The ultrasound was generated in a surface ablation regime with partial laser focusing. The waveforms are dominated by the longitudinal arrivals and mode converted arrivals. As the temperature was increased to above 795°C, no acoustic signal could be detected even after increasing the laser energy density. An attempt was made to generate the ultrasound by creating an air breakdown wave on the surface of the sample, however this created signal noise that saturated the receiver system. The generated air blast wave causes reverberation on the EMAT coil and the plasma is also a source of electrical noise and thus paralysed the preamplifier. If we compare the waveforms in figure-5.13 and figure-5.14, it clearly shows that the detected signal in the send-receive arrangement is more prone to the noise than that on epicentre where the sample shields the detector from both electrical and mechanical noise. This arises from the reverberation of the EMAT coil as the high energy laser beam strikes the surface of the sample.

5.4.4 Factors Affecting the Temperature Dependence of the Ultrasound Velocities.

Temperature dependence of ultrasound velocities in mild steel is shown in figure-5.4. Below T_c, the velocity of the shear wave reduces gradually with an increase in the temperature at an average rate of $-0.78 ms^{-1} °C^{-1}$ and drops rapidly at about T_c. The longitudinal wave also reduces in a similar manner (the average of $-0.92 ms^{-1} °C^{-1}$), but then reduces rapidly between 740° - 780°C. At a higher temperature the longitudinal wave velocity reduces more gradually. The reductions of both the longitudinal and shear waves velocities and thus the elastic constants can be explained in three different temperature

ranges where different physical changes occurred.

In ferromagnetic materials such as mild steel at room temperature, the magnetic ordering contributes an additional force to its rigidity. As the temperature increases, thermal agitation gradually disturbs the magnetic ordering. At the Curie temperature, the magnetic interaction between atoms becomes random and the sample becomes paramagnetic. The loss in magnetic order at elevated temperature can be observed on the spontaneous magnetisation- temperature curve of iron, (Figure-5.15). The spontaneous magnetisation is only weakly dependent on the temperature until it reaches $0.75T_c$. Above that the magnetisation decreases rapidly towards zero at T_c. The samples also exhibit a strong magnetostriction effect where the stress field of an ultrasound wave is able to induce both the normal strain and an additional strain associated with the stress induced magnetic domain's reorientation (Mason, [1958]). The relative contribution of these effects to the elastic rigidity and thus the ultrasound velocities will gradually decrease as the spontaneous magnetisation decreases on heating and disappears at T_c .

In the second region, (temperature ranges between 740°C-780°C), the dramatic changes in the wave velocity with the increasing temperature may be attributed to the ferromagnetic to paramagnetic phase transition. The additional decrease in wave velocities arises from the loss of the magnetostriction effect in the material. These become evident as the spontaneous magnetisation reduces rapidly to zero at temperatures approaching T_c. Papadakis et al., [1972] and Wadley et al., [1986] however; associate the reduction in the acoustic wave velocity in a 1% carbon steel alloy with a gradual structural phase transformation from α to γ–phase. In this alloy, there is a two phase region above 723°C where α and γ–phases coexist. The structural phase transformation from body-centered cubic ferrite, (α) phase into a stable face-centered cubic austenite, (γ) phase begins at about 723°C and at the same time the unstable carbide rapidly dissolves. The

transformation completes at about 850°C for the 1%C steel (high carbon steel) and occurs at 910°C in pure iron. Since there is no α and γ phases coexists in pure iron, the large drop in longitudinal wave velocity observed near T_c , is therefore purely due to the magnetic phase transformation (McKie, [1987]). The phase diagram of a mild steel shows that, the α–γ phase transformation complete at temperature above 850°C (Hume-Rothery, [1966]), well beyond the region of rapid velocity change. Since both rapid velocity and magnetisation change occurred in a similar temperature range, (i.e. 740°C-780°C), therefore the change in magnetic property produces a dominant effect on the wave velocity change (and thus the elastic constants) than that caused by the structural changes.

At a higher temperature (above 780°C) when the sample is totally paramagnetic, the change in wave velocity is due to the structural phase transformation which produces gradual changes. This may be caused by an increase in the volume that is associated with the introduction of a carbon atom into the interstitial site of the iron cubic lattice and could be attributed to the different acoustic wave velocity in each metallurgical phase. The velocity in the γ-phase is faster than that in the α-phase and the α–γ phase transformation would tend to result in an increase in velocity.

5.4.5 Factors Affecting the Temperature Dependence of the Ultrasound Amplitude

The temperature dependence of the ultrasound signal amplitude in mild steel detected by an EMAT could have been caused by the changes in the surface and the bulk properties of the sample which will affect ultrasound transduction by laser and EMATs. The generation of ultrasound by laser depends on the laser energy density deposited on the sample surface, the laser wavelength (McKie [1987]), and the condition of the sample surface (Taylor, [1990], Davies et. al., [1993]). For a particular irradiating laser wavelength, e.g. Nd:YAG laser at λ=1.06μm, the generated ultrasound source strength is

dependent on the laser energy density. If we assume that the ultrasound is generated by a weak ablation process at room temperature so that both longitudinal and shear waves are generated in the sample, then as the temperature increases, the degree of ablation increases since the additional energy required to ablate the material is reduced. This results in an increase in longitudinal wave amplitude where more material has been ablated from the surface, increasing the normal recoil forces responsible for the propagation of the longitudinal wave. However, an increase in the sample temperature does not necessarily enhance the amplitude of the shear wave observed at normal incidence. In this experiment, the increase in shear wave amplitude with increasing temperature may be attributed to the transduction characteristic of the EMAT rather than the enhancement of the shear wave generation by laser. An increase in temperature may also alter the surface condition of the sample due to the formation of an oxide layer and this increases the absorptivity of the surface. The irradiating laser beam will ablate this oxide layer and enhance the longitudinal wave amplitude.

In case of a CO_2 laser, operating in surface ablation regime, the generation process is influenced by the surface quality of the sample (Taylor, [1990]). Rough surface quality, due to the presence of either oxide or poor surface polishing, will reduce the threshold of the surface plasma formation where the surface provides a sufficient number of sites for the initiation of the plasma. Surface oxide acts in a similar way to other surface modifying layers, providing a highly absorbent layer which is rapidly vaporised by incident laser radiation. It plays an important role in determining the threshold when generating plasma above the irradiated surface.

At room temperature, EMAT transduction efficiency on mild steel is determined by the material's electrical and magnetic characteristics and is also affected by the presence of a magnetite layer on the sample surface (Parkinson et al., [1977], Edwards et al.,

[1990]). The ultrasound transduction may be the result of complex combined effects of Lorentz force interactions, magnetic and magnetostriction mechanisms. The effect of the magnetite scale on transduction efficiency of the EMAT at room temperature has been discussed in chapter-4. As the temperature increases above room temperature, the pulse echo shear wave amplitude generated by an E-EMAT increases and exhibits a maximum at about 600°C, then the amplitude decreases with increasing temperature (figure-5.7). Enhancement of shear wave amplitude could be due to the magnetostriction effect of the magnetite scale developed during heating. The peak in shear wave amplitude could be due to the Curie temperature of the magnetite at 585°C (Callister, [1991]). A similar result is shown when the EMAT was used as the detector and the ultrasound was generated by pulsed laser. Above this temperature (585°C), however the contribution of the magnetite towards the magnetostriction effect is lost and the remaining magnetostriction effect is contributed by the bulk metal. This effect enhances the EMAT efficiency at higher temperatures. As the temperature approaches T_c (about 760°C) however, the efficiency begins to decrease gradually. At T_c , the transformation from ferromagnetic to paramagnetic takes place resulting in a complete loss of the magnetostriction effect. The ultrasound was therefore detected by the Lorentz force interaction mechanism and this could be the cause of the reduction in the shear wave signal amplitude. At this transition temperature (740°C - 770°C), the magnetic field generated on the sample surface decreases rapidly from about 1.4T down to 0.35T, confirming the phase changes in the material.

The efficiency of ultrasound transduction by an EMAT on mild steel is temperature dependent as the parameters involved are temperature dependent. The transduction efficiency due to the Lorentz force mechanism, at 10MHz, as given by Grubin [1970] in Chapter- 3; is shown in table-5.1. The value dictated here only considers the contribution of the Lorentz force interaction mechanism at a given external applied field B_o. The wave

velocity was extracted from figure-5.4, and the other parameters were taken from Kaye & Laby, [1986]. In a ferromagnetic sample, the magnetic field B_o is temperature dependent. At room temperature, B_o generated by the E-EMAT is about 1.4T, giving the transduction efficiency for a longitudinal wave η of about 5.31×10^{-5}. This corresponds to an insertion loss IL = 10 log(η) = 42dB. At higher temperature, above T_c in particular, B_o is about 0.35T, giving $\eta = 2.49 \times 10^{-7}$ corresponding to IL = 66dB at 800°C. The reduction in Lorentz force transduction efficiency at temperatures above T_c may be due to the loss of magnetisation and the decrease in conductivity leading to an increase in the β factor >1 (see equation 3.5).

As the temperature increases and passes the T_c, the longitudinal wave generated by the pulsed laser and detected by the EMAT exhibits a change in polarity and the signal amplitude is lower if one compares it to that of below T_c. These changes could be related to the ferromagnetic to paramagnetic phase transformation which occurs at T_c. The reduction in signal amplitude could be due to the loss of magnetic properties and hence the magnetostriction effect. The wave was therefore detected by Lorentz force interaction resulting in a reduction in signal amplitude. The change in polarity of the longitudinal wave could be due to the changes in the EMAT transduction mechanism at T_c. A similar phenomenon has also been observed by Idris, [1995], where the polarity of the longitudinal wave detected by EMAT on mild steel changes after the temperature exceeds the Curie temperature. This effect has been reported by Edwards and Palmer [1990], through the comparisons of the ultrasound waveforms on aluminium and mild steel generated using a Nd:YAG laser and detected by a normal motion sensitive EMAT. They observed that the longitudinal wave polarity on the waveforms obtained from a nonmagnetic aluminium alloy and stainless steel is in contrast to that of the magnetic steel.

Well above T_c, when both the bulk and the detection surface of the material are paramagnetic, the detected ultrasound waveform is dominated by relatively weak longitudinal arrivals compared to that in the ferromagnetic phase (Figure-5.11) because the detection is only achieved by the Lorentz force mechanism. The waveforms may or may not have the subsequent echoes and in some samples the pulse shows a slight broadening compared with that at room temperature. These are an indication of the reduction in EMAT transduction efficiency and increase in wave attenuation due to scattering of the high frequency component within the materials caused by the coarse γ-austenitic phase (Scruby et al., [1989]). In mild steel at elevated temperature, this effect has been investigated by Tripathi et al., [1973] who concluded that the increase in ultrasound attenuation was related to the characteristic of the material. They studied the temperature dependence of the ultrasound attenuation in a 1% carbon steel at elevated temperature at 5MHz. The longitudinal wave attenuation remained constant with increasing temperature up to about 700°C, and then increased dramatically with slope changes at 750°C and 900°C. A sharp increase in attenuation at about 750°C was thought to be due to the gradual transformation of the unstable body-centered cubic lattice of the ferrite phase into the face-centered cubic lattice of the austenite (γ) phase. The second change occurred at about 900°C and was due to the completion of the austenite phase transformation. Above this temperature, when the steel was in the austenite phase, the increase in attenuation was caused by the increase in grain size. Bhatia, [1967] and Darbari et al., [1968]; concluded that the sharp increase in ultrasound attenuation at elevated temperature was due to the reduction in the shear and longitudinal wave velocities that was caused by the weakening of the interatomic forces. The attenuation of the shear waves becomes pronounced at temperatures above 500°C and then increases rapidly with increasing temperature, (Papadakis et al., [1972]). They associated these attenuation phenomena with the

magnetisation in the steel, the changes in crystal structure (i.e. during phase transformation from α to γ phase), the solubility of the carbides and scattering from the grains. The scattering due to grain growth after all the carbides are dissolved is the main cause of the ultrasound attenuation at a temperature above 800°C.

5.4.6 The Enhancement of Longitudinal Wave at About the Curie Temperature

Above T_c, the pulse echo ultrasound waveforms generated by a shear wave EMAT are dominated by the longitudinal wave arrivals and a similar phenomenon occurs when a similar EMAT is used to detect ultrasound pulses generated by a pulsed laser, in send-receive arrangement. The amplitude of the longitudinal wave increases dramatically and reaches a maximum at temperatures close to T_c and then rapidly decreases with increasing temperature. Strong excitation of the longitudinal wave at this temperature has been described elsewhere, (Parkinson et al., [1977], Edwards et al., [1994] and Idris et al., [1994]). The enhancement of the longitudinal wave may be attributed to the cooling of a thin skin of the material back into ferromagnetic phase causing a concentration and reorientation of the magnetic field parallel to the surface of the sample or may be due to volume magnetostriction.

Above T_c, the introduction of the water-cooled EMAT close to the surface of the sample causing surface cooling and creates a thin layer which is much colder directly facing the EMAT. If the whole sample is just above T_c, then this layer may be cooled sufficiently to take it below T_c and into the ferromagnetic phase. The magnetic flux will then flow into the surface of the ferromagnetic layer instead of penetrating the bulk of the paramagnetic sample. The reorientation of the magnetic flux parallel to the surface will be ideal for the generation of a longitudinal wave into the bulk of the material. The presence

of the ferromagnetic layer on the surface of the sample, automatically increases the EMAT transduction efficiency (Edwards et al., [1994]).

For a given EMAT probe and cooling rate, the thickness of this layer will depend on the initial temperature of the sample. If the sample temperature is well above T_c, the cooling of the EMAT may have no effect and no signal is detected. As the temperature is lowered towards T_c, a temperature will be reached (T_{max}) where the cooling effect of the EMAT is sufficient to lower the temperature of the thin layer below T_c and into the ferromagnetic phase. As the temperature is reduced further, the thickness of this ferromagnetic layer will increase and therefore the magnetic flux density entrapped will be reduced. When the sample is well below T_c the cooling effect at the surface will produce a surface region with a higher permeability and spontaneous magnetisation and there present the preferential generation of longitudinal wave. This could be the cause of the increase in the longitudinal wave signal amplitude below T_c.

Volume magnetostriction usually occurs at a very high field close to the saturation magnetisation M_s . However near T_c, M_s is below the level of field which can be obtained from the EMAT. The magnetostriction effect which will occur in the thin layer of the ferromagnetic phase where the magnetic flux concentration exist will also contribute to this enhancement. This effect will diminish as the cooling effect by the transducer reduces and the temperature at the surface of the sample exceeds the Curie temperature.

5.4.7 The Transit Time Correction

Above the Curie temperature the ultrasound waveform is dominated by the longitudinal arrivals with weak subsequent echoes. In some samples only the first or the second arrival pulse is seen. This makes the transit time measurement less accurate particularly in thin samples. In such cases where the transit time is measured from the

arrival of the first pulse, the correction due to the electronic delay, size of the ultrasound source and the effective diameter of the receiver, has to be considered. The laser source is effectively a point source and produces a spherical wavefront and the concentric EMAT coil detects the ultrasound echoes over a solid angle determined by the plate thickness and the inner and outer diameter of the coil. If we assume a true point source with an EMAT coil diameter, D and the plate thickness, T, with ultrasound velocity, υ, the arrival time t_c at the coil centre is:-

$$t_c = 2T/\upsilon$$

at the extreme edge of the coil, t_e, is:-

$$t_e = \frac{(4T^2 + D^2)^{\frac{1}{2}}}{\upsilon}$$

The ratio of the arrival times at the edge and the centre of the coil can be used to estimate the worst case of percentage error in thickness. In practice the coil can be considered as being formed from a single turn at an effective diameter half way between the inner and the outer diameter of the coil. For a concentric EMAT coil of outer and internal diameter 18mm and 8mm respectively, the average of an additional wave pathlength traverse across the sample of 10mm thick, to reach the EMAT is about 4.5% of the sample thickness and needs to be subtracted from the ultrasonically measured thickness. If however, the transit time was measured based on the subsequent pulse arrivals, this correction becomes insignificant. The correction due to the thermal expansion of the sample (linear thermal expansion coefficient $1.07 \times 10^{-5}\ C^{-1}$) is equivalent to about 1 % for every 1000°C change in temperature or 0.001% per degree Celcius change and therefore this correction may not be significant.

5.4.8 Ultrasound Measurement at the Steel Mill.

A similar CO_2 laser-EMAT system described earlier was used for non-contact ultrasound measurements on a site similar to the actual production line of the seamless pipe in the Wednesfield plant of British Steel. The experimental set up is shown in figure-5.16. A concentric EMAT was positioned at a 2mm stand off from the rotating sample on biscuit rollers built on the test rig. The rig was built to house the CO_2 laser and the electronics. The laser beam was fully enclosed to comply with the safety regulations and irradiated the test sample from the bottom of the rig.

The sample was a section of an extruded mild steel pipe with outer diameter of 125mm and 15mm wall thickness. Initially it was heated in a gas furnace to a temperature of about 1200°C. However on transferring the sample to the test rig the sample was cooled and its temperature reduced to about 850°C at the commencement of the measurements. The sample temperature was monitored using an optical pyrometer. The ultrasound source was generated with a low energy density that produce ablation of the surface scale. The sample was slowly rotated between shots so that the measurements could be made at different positions on the surface of the sample.

The waveforms detected at different temperatures are shown in figure-5.17. The EMAT detects a discernible waveform after the sample cooled down to a temperature of about 750°C. Ultrasound detection at a higher temperature was hampered by the surface condition of the sample. Prior to the measurement, the sample was heated for 2-3 hours to reach a temperature of about 1200°C, causing a thick oxide scale (up to about 2mm thick) to develop on its surface. Although such oxide layer will increase the laser energy absorption on the sample surface, it reduced the EMAT transduction efficiency due to its poor adhesion to the metal. Above T_c , both the sample and the oxide layer were paramagnetic and the oxide layer exhibited low electrical conductivity.

5.4.9 The Comparison Between the Laser -EMAT Systems.

The limits for high temperature operation of the present non-contact laser/EMAT ultrasound systems are in the range of about 800°C for the EMATs and up to about 1100°C for the laser-EMAT system. In mild steel, this operation was limited by the EMAT performance whereby above these temperatures it was unable to detect any ultrasound signals. Pulsed lasers are excellent ultrasound generators on steel even at elevated temperature, and have been used up to a temperature of 1100°C using Nd:YAG laser, and up to 900°C using CO_2 laser where, in both cases, a permanent magnet EMAT with PCB etched spiral coil was used (Idris, [1995]). In comparison, our send-receive Nd:YAG laser-E-EMAT system that used a wire wound coil, normally can be operated up to a temperature range of 800°C-850°C, even in some cases up to 1000°C.

The operation limit for the CO_2 laser generator and E-EMAT receiver was much lower in the case of send-receive configuration than the through-transmission. At higher temperature, the quantity of the laser energy required to form a surface plasma ablation is much smaller than that at room temperature as the state of the gas molecules in the atmosphere and oxide material at the surface of the sample is already closer to their excitation state. Therefore the plasma may form at a lower energy density and occurs at a point further away from the sample surface inside the electromagnet cavity. This generates inefficient ultrasound source. At elevated temperature, we need to deposit a high laser energy to create a stronger ultrasound source on the surface of the sample to compensate for the high ultrasound attenuation in the material and lower EMAT transduction efficiency. However this leads to the formation of plasma breakdown that will saturate the EMAT response. A similar problem also occurred when using a permanent magnet concentric EMAT as the detector operated on hot steel in send-receive configuration.

The send-receive laser-EMAT system using the Nd:YAG laser has an advantage

over the CO_2 laser at high temperature where the former is capable of creating a strong ultrasound source on the sample surface without paralysing the receiver. The waveform has better signal to noise ratio than the CO_2 system. At high energy density, the Nd:YAG laser leaves a small damage pit on the sample surface but this can be avoided by using the CO_2 laser. However, for thickness measurement of a thick wall pipe, such minute damages can be neglected. The CO_2 laser with the laser wavelength 10.6μm is easier to operate safely in an industrial environment than a Nd:YAG laser but the latter is available in a smaller scale with enclosed beam that could be taken close to the hot sample. The limitation of the laser-EMAT system operated in send-receive arrangement on hot steel is mainly caused by the poor performance of the EMAT receiver at elevated temperature due to low transduction efficiency and saturation of its response when operated with the CO_2 laser.

5.5 Conclusions

It has been demonstrated that the laser-EMAT system in send-receive arrangement offers a versatile technique for a non-contacting ultrasound measurement on hot steel where the sample could be accessed from a single surface. The EMAT was water-cooled and operated in pulsed excitation. Measurements were made up to a temperature of 1040°C using the Nd:YAG laser and around 800°C using the CO_2 laser generator respectively. The pulsed field EMAT also could be used as both the ultrasound generator and detector and was capable of performing non-contacting measurement on hot steel up to a temperature of 850°C. The ultrasound transit time measurements were based on shear wave pulses in the ower temperature range i.e. below 750°C, and it was based on the longitudinal wave pulses at elevated temperature. The system shows an enhancement of the longitudinal wave at temperatures a few degrees above the Curie point of the sample.

5.6 References

Bhatia A. B., Ultrasonics Absorption , (Claarendron Press, Oxford) 1967.

Burns L. R., Alers G. A. and MacLauchlan D. T. Rev. Prog. In Quantitative NDE, ed. Thompson D.O. and Chimenti D.E., **Vol. 7B**, (1988) , (Plenum , New York), pp.1677-1683.

Bozoroth R.M., Ferromagnetism, D Van Nostrand Co. Inc. Canada. (1951), pp.714.

Callister W. D., Materials Science and Engineering-An Introduction, (John Wiley & Son Inc. Canada) 1991.

Cole P. T., Ultrasonic, **Vol. 15**, July (1978), pp.151-155.

Darbari G. S., Singh R. P. and Verma G. S.; J.of Appl. Phys., **Vol.39,** no.5, April (1968), pp.2238-2243.

Dates E.H.F., Atkins M. and Beaton G.V., Ultrasonics, **Vol. 9**, Oct. (1971), pp. 209-214.

Davies S. J., Edwards C., Taylor G.S. and Palmer S.B., J. Phys. D: Appl. Phys. **Vol. 26,** (1993) pp. 329-348

Dewhurst R.J., Edwards C., McKie A.D.W and Palmer S. B., J. Appl. Phys. **Vol. 63,** no. 4, 15 Feb. (1988), pp.1225-1227.

Dobbs E. R.., in Physical Acoustic, ed. W.P Mason and R.N Thruston. **Vol. 7,** (1976), (Academic Press, New York), pp.197-

Edwards C. and Palmer S. B., IEEE Trans. On Magnetics, **Vol. 26,** no. 5, Sept. (1990) pp.2080-2084.

Edwards C., Dixon S., Idris A., Reed J. and Palmer S.B., in Rev. in Prog. of Quantitative Nondestructive Evaluation, Colorado, **Vol. 14B**, (1994), pp.2253-2260

Grubin H. L., IEEE Trans. on Sonic and Ultrasonics, **Vol. SU-17,** No. 4 1970, pp.227-229.

Hume-Rothery W., The Structures of Alloys of Iron--an Elementary Introduction., (Pergamon Press, Oxford), 1966.

Idris A. Edwards C. and Palmer S. B., Nondestr. Test. Eval., **Vol. 11**, (1994), pp.195-213.

Idris A.; Ph D Thesis, Warwick University, 1995

Krautkramer J. and Krautkramer H.: Ultrasonic Testing Of Materials, 3rd. Edition, Springer-Verlag, (1983).

Kaye G. W. C. and Laby T. H., Tables of Physical and Mechanical Constants, (Longman London) 1986.

.Lee S.S and Ahn B.Y., Nondestr. Test. Eval., **Vol. 7**, (1992), pp.253-261.

Mason W.P., Physical Acoustic and the Properties of Solids, pp. 209-224, Princeton, New Jersey, D Van Nostrand & Co., (1958).

McKie A.: Ph D Thesis , University of Hull , (1987)

Monchalin J.P. and Heon R., Materials Evaluation, **Vol. 44**, Sept.(1986), pp.1231-1237.

Monchalin J. P., Rev. Prog. in Quantitative NDE., ed. D. O. Thompson and D.E Chimenti, Vol 12, 1993., pp.495-506.

Papadakis E. P., Lynnworth L. C., Fowler K. A. and Carnevale E. H., J. Acoust. Soc. Am., **Vol. 52**, no. 3, (part 2), (1972), pp.850-857.

Parkinson G. J., Willson D. M., British Journal of NDT, July (1977), pp. 178-184.

Scruby C. B., Ultrasonics, Vol.27, July 1989, pp.195-209

Taylor G. S., PhD Theses, University of Warwick 1990

Tripathi R. C. andVerma G. S., J. Acoust. Soc. Am., **Vol. 53**, no.5, (1973), pp.1344-1345

Wadley H. N. G., Norton S. J., Mauer F. and Droney B., Phill. Trans. R. Proc. Lond. **A 320**, pp.341-361 (1986).

Yamaguchi H., Hashimoto K., Ikishawa H., Kadoki T., Sato I., in Rev. Prog. In Quantitative NDE., ed. D.O. Thompson and D.E Chimenti, **Vol. 3**, Plenum, New York (1984), pp. 734-737

EMAT transduction efficiency due to Lorentz force mechanism in both magnetic and nonmagnetic metals,

$$\eta = \frac{2B_o^2}{\rho \upsilon \mu_o \mu_r \omega \delta (1+\beta^2)}$$

The skin depth, $\delta = (\frac{2}{\mu_o \mu_r \sigma \omega})^{\frac{1}{2}}$

β factor: $\beta^2 = \frac{1}{2}\left(\frac{\omega\delta}{\upsilon}\right)^2$

insertion loss IL (dB)= $10 \log_{10}(\eta)$

Table-5.1

temperature °C	velocity υ (ms^{-1})	μ_r	δ (μm)	β^2	$\eta \times B_o^2$	η at a given B_o /IL(dB)
iron 20	5960	100	17	0.02	3.31×10^{-5}	5.31×10^{-5} B_o=1.35T IL=42dB
800	4,850	1	113	1.13	2.77×10^{-6}	2.494×10^{-7} B_o=0.35T IL=66.5dB
aluminium 20	6300	1	26	0.01	6.24×10^{-5}	7.65×10^{-5} B_o=0.35T IL= 51dB

Table-5.1: Longitudinal wave transduction efficiency by EMAT due to Lorentz force mechanism at 10MHz in iron at 20°C and 800°C and aluminium at 20°C at a given magnetic field intensity generated by E-EMAT

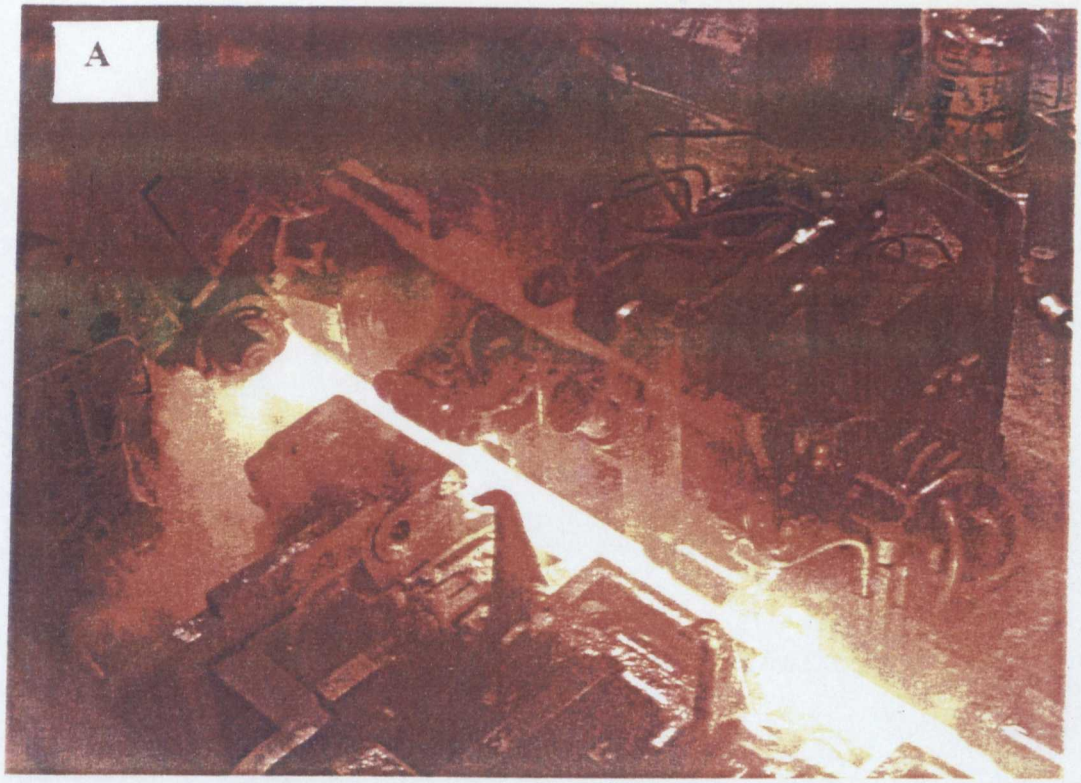

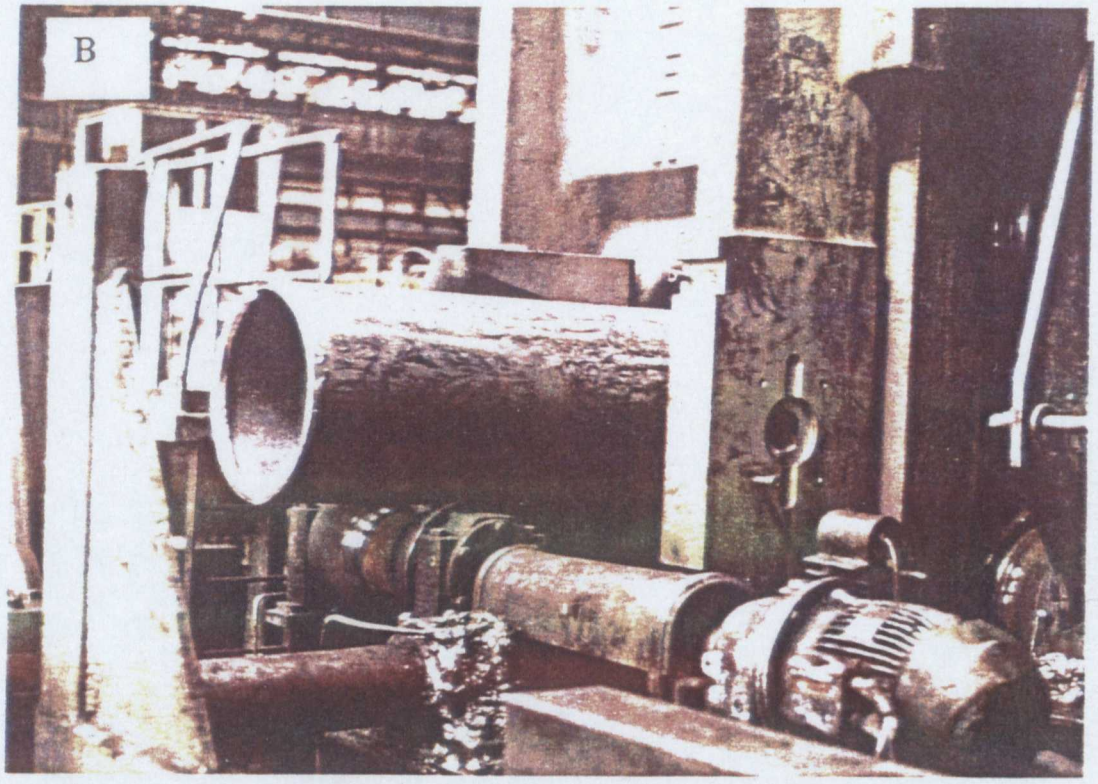

Figure-5.1: The processing environment of seamless steel pipe that requires a non-contact ultrasound inspections . (A)- Extrusion process, (B)-surface condition of the test sample on the production line.

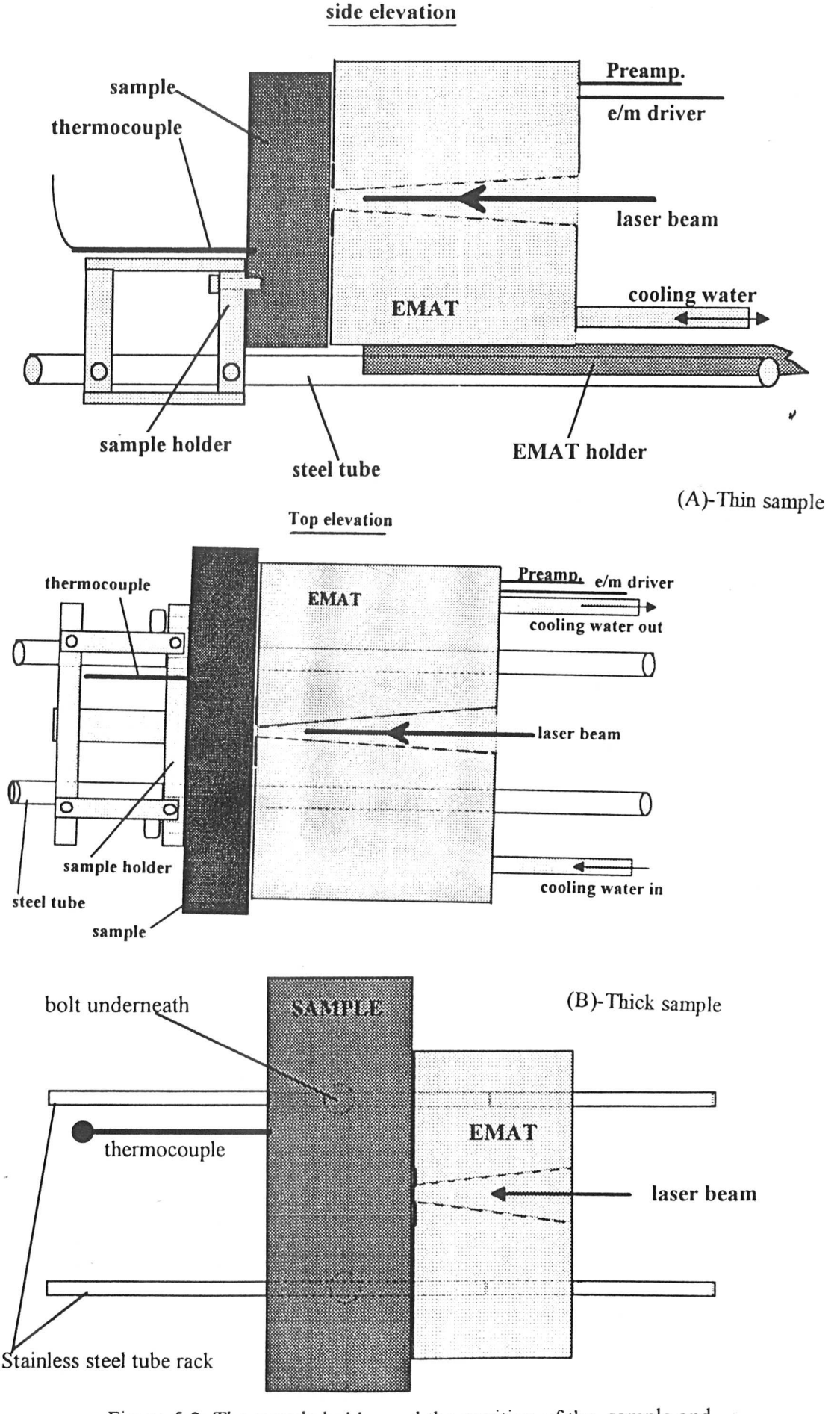

Figure 5.2: The sample holder and the position of the sample and the EMAT, (a) thin sample, (b)-thick sample in send-receive ultrasound measurement.

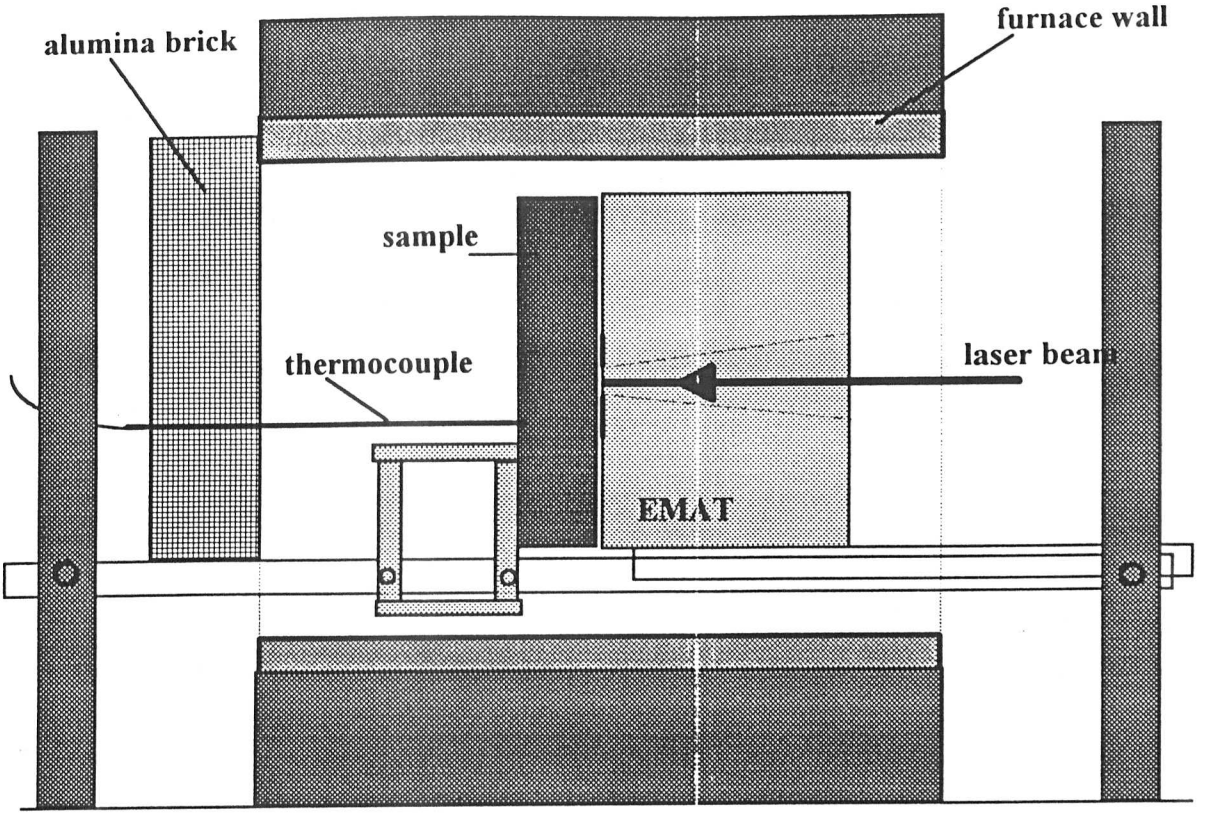

Figure-5.3: The arrangement of the sample and the holder on the sample rack and pulsed field EMAT inside the furnace

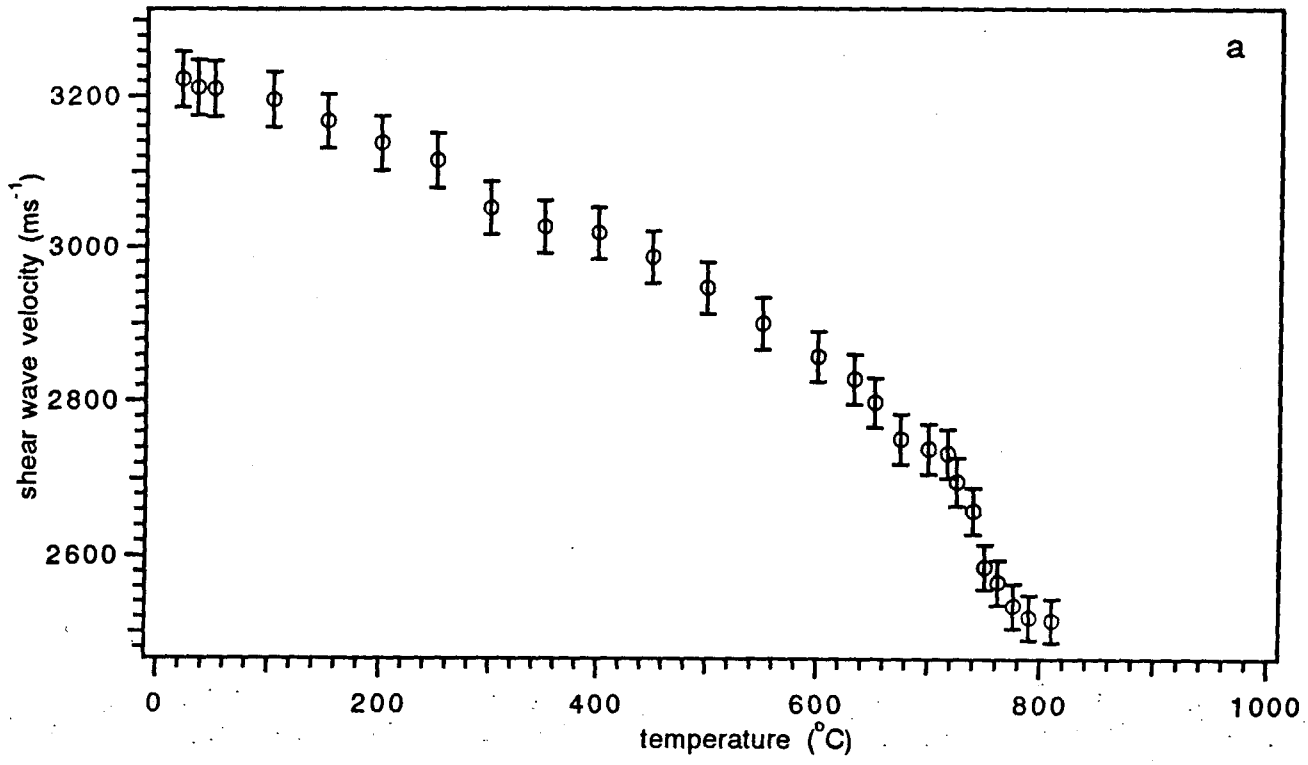

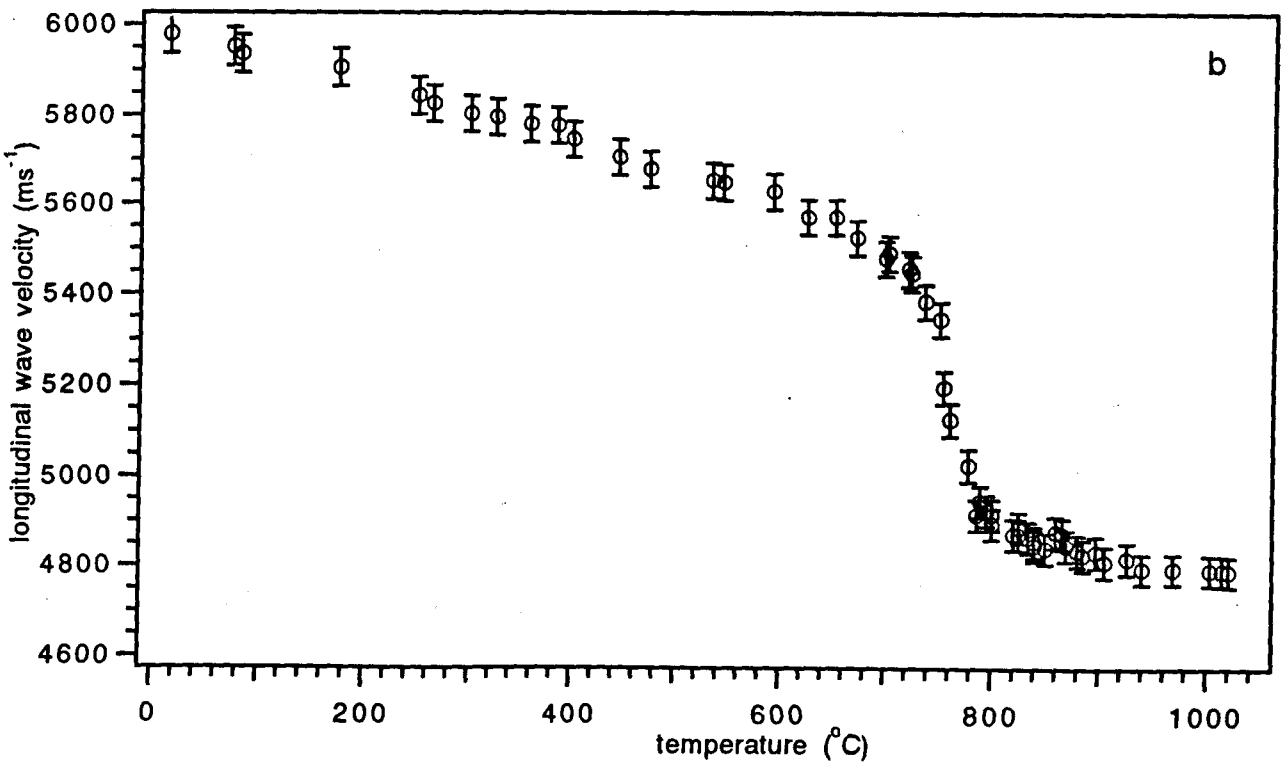

Figure-5.4: Temperature dependence of the ultrasound velocities in mild steel, (a)-shear wave, (b)-longitudinal wave. The data were measured from both the epicentral and send-receive waveforms generated and detected by non-contact laser/EMAT system.

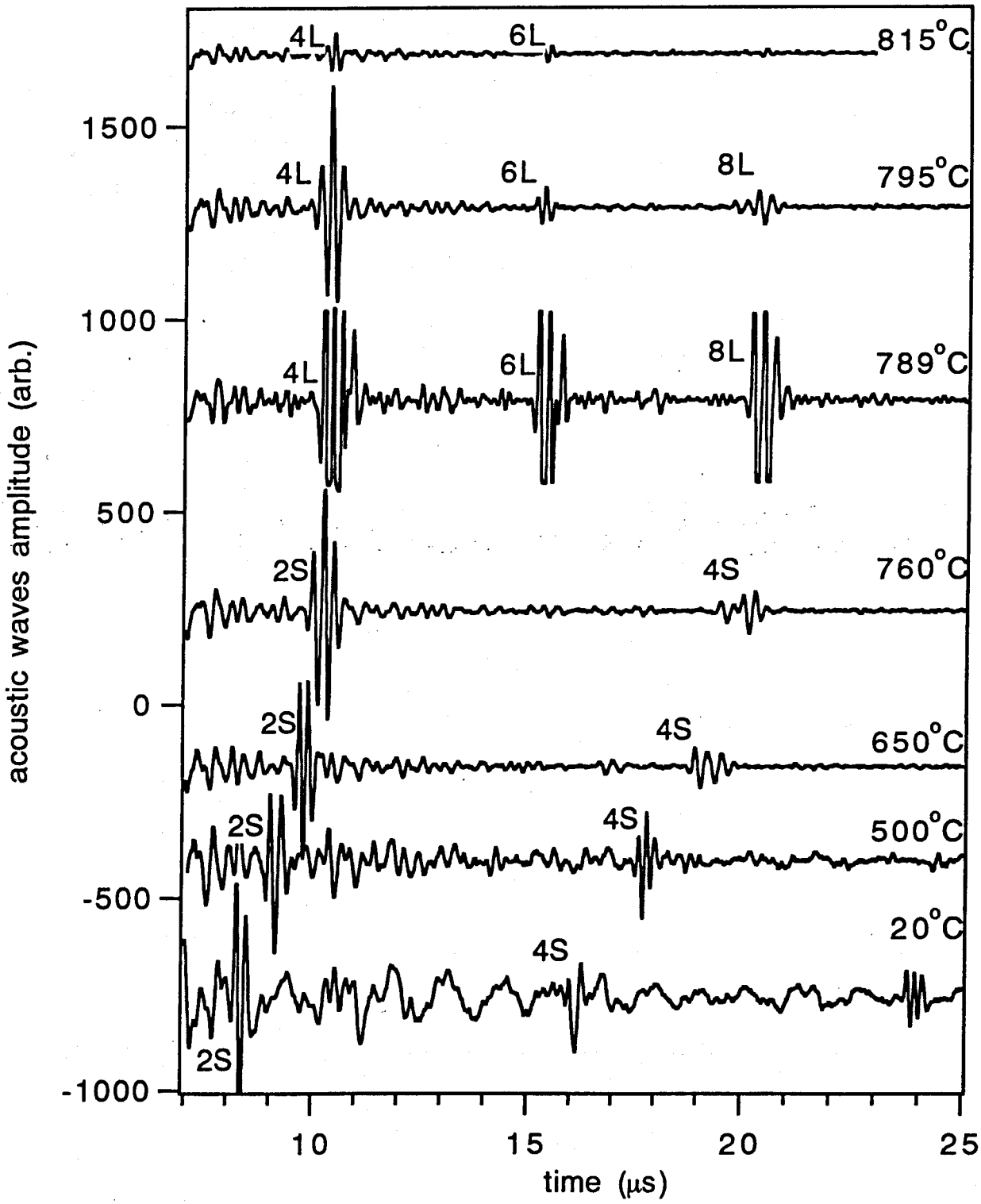

Figure-5.5: Pulse echo ultrasound waveforms in mild steel (12.5mm thick) at elevated temperatures, generated by P-EMAT.

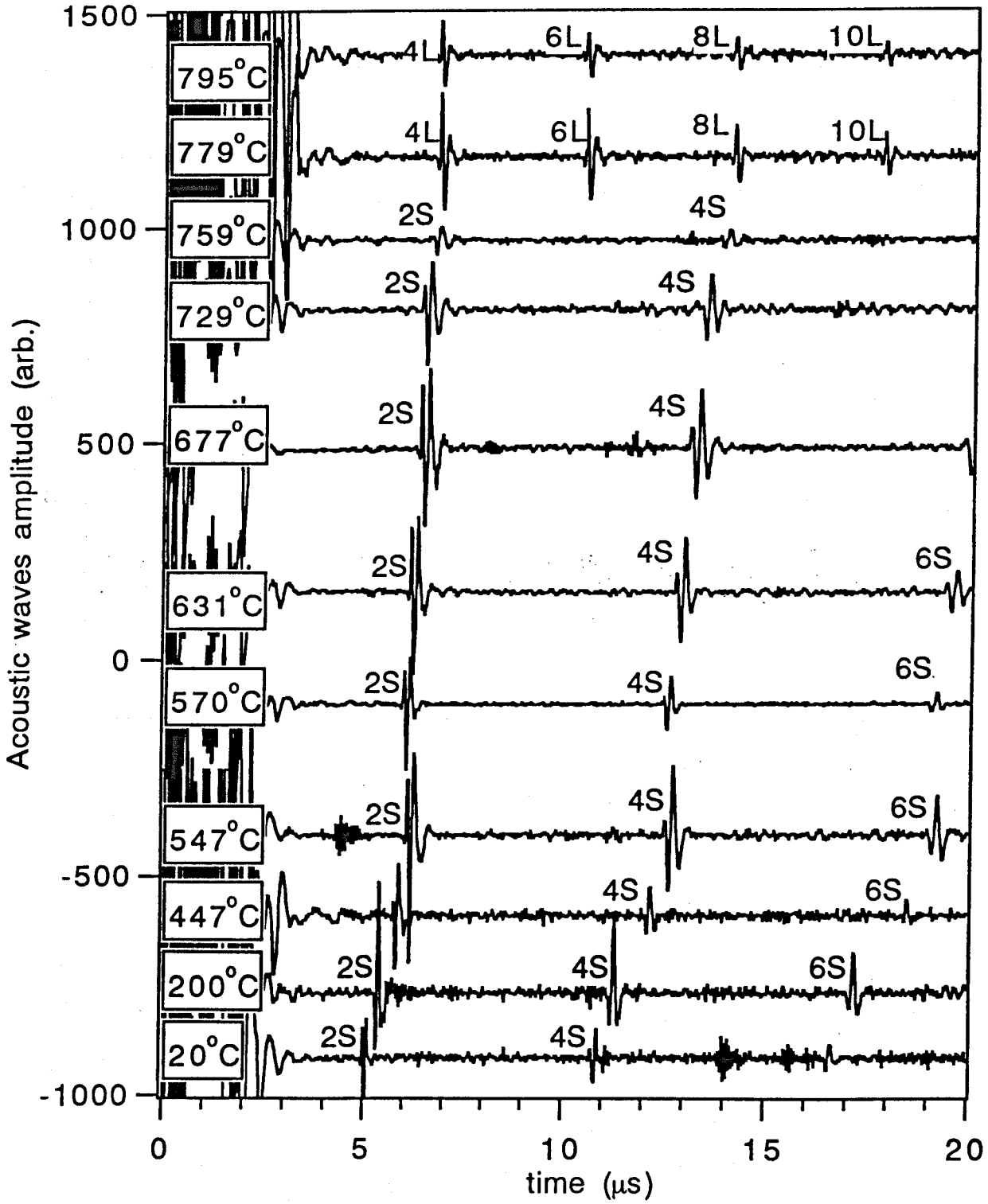

Figure-5.6: Pulse echo ultrasound waveforms in mild steel (10.5mm thick) at elevated temperatures, generated by E-EMAT.

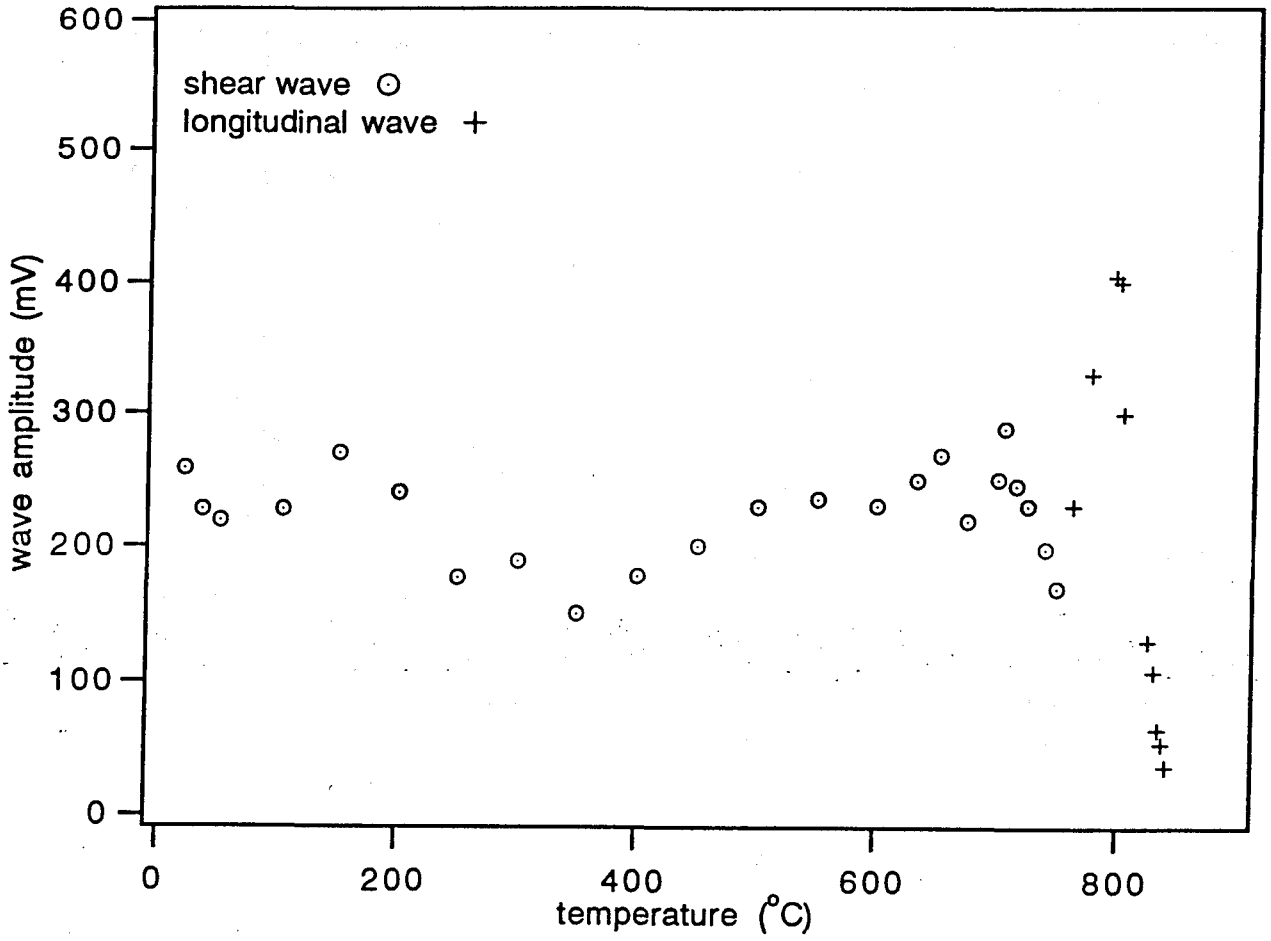

Figure-5.7: Temperature dependence of the pulse echo ultrasound amplitude in mild steel generated by E-EMAT.

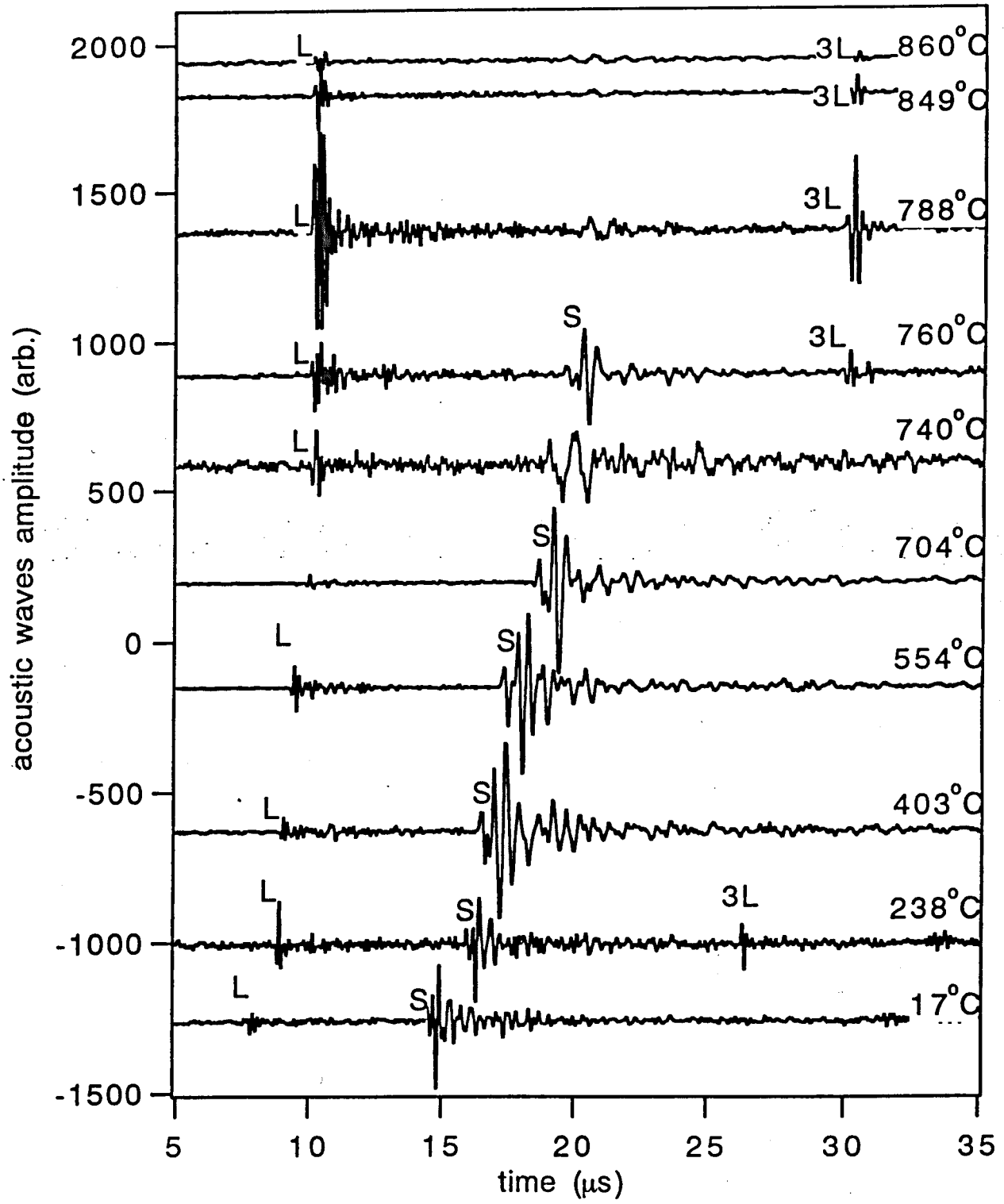

Figure-5.8: Ultrasound waveforms in mild steel (50mm thickness) at elevated temperatures. The ultrasound was generated by Nd:YAG pulsed laser and detected by E-EMAT on epicentre.

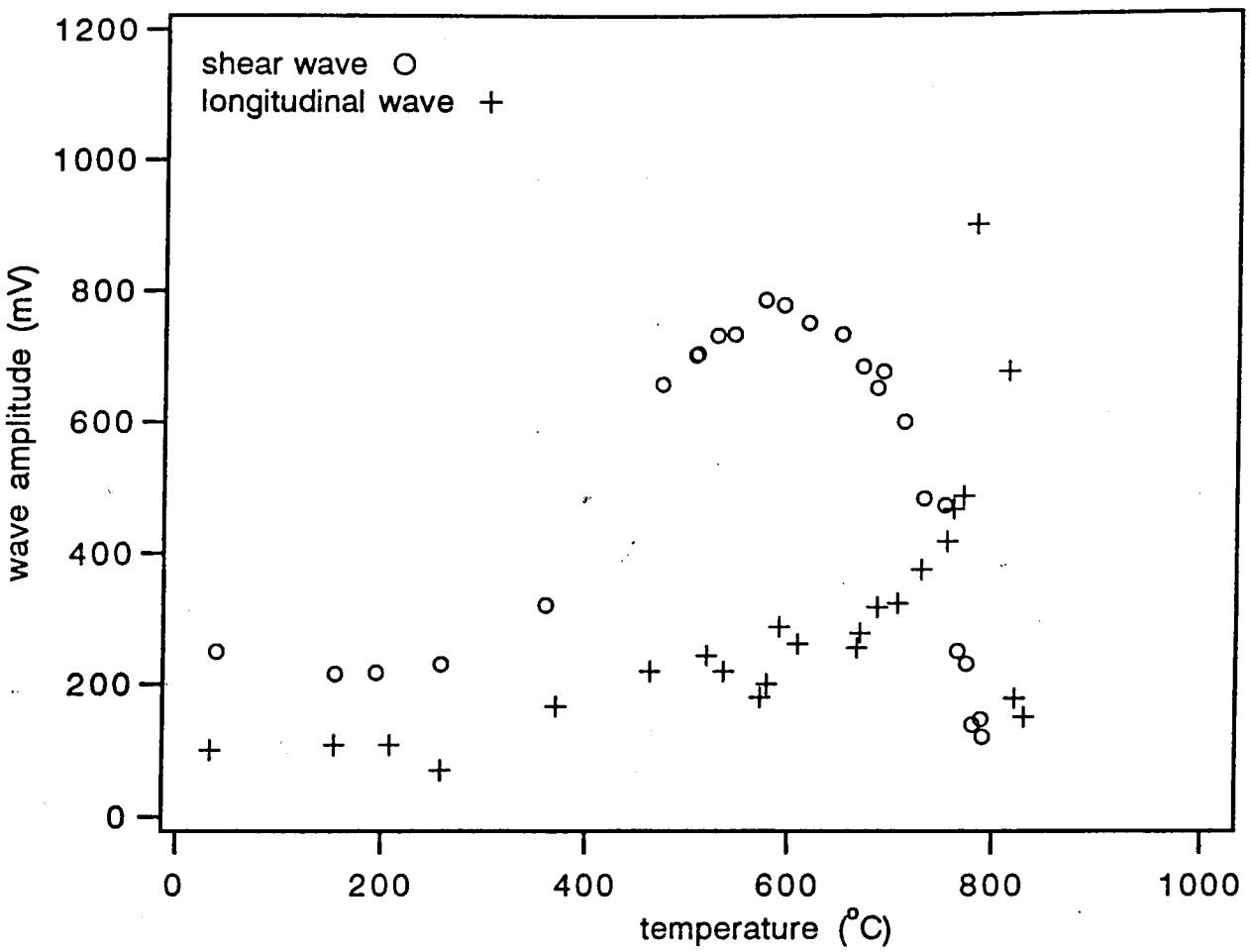

Figure-5.9: Temperature dependence of ultrasound wave amplitude in mild steel generated by a Nd:YAG laser and detected by E-EMAT on epicentre.

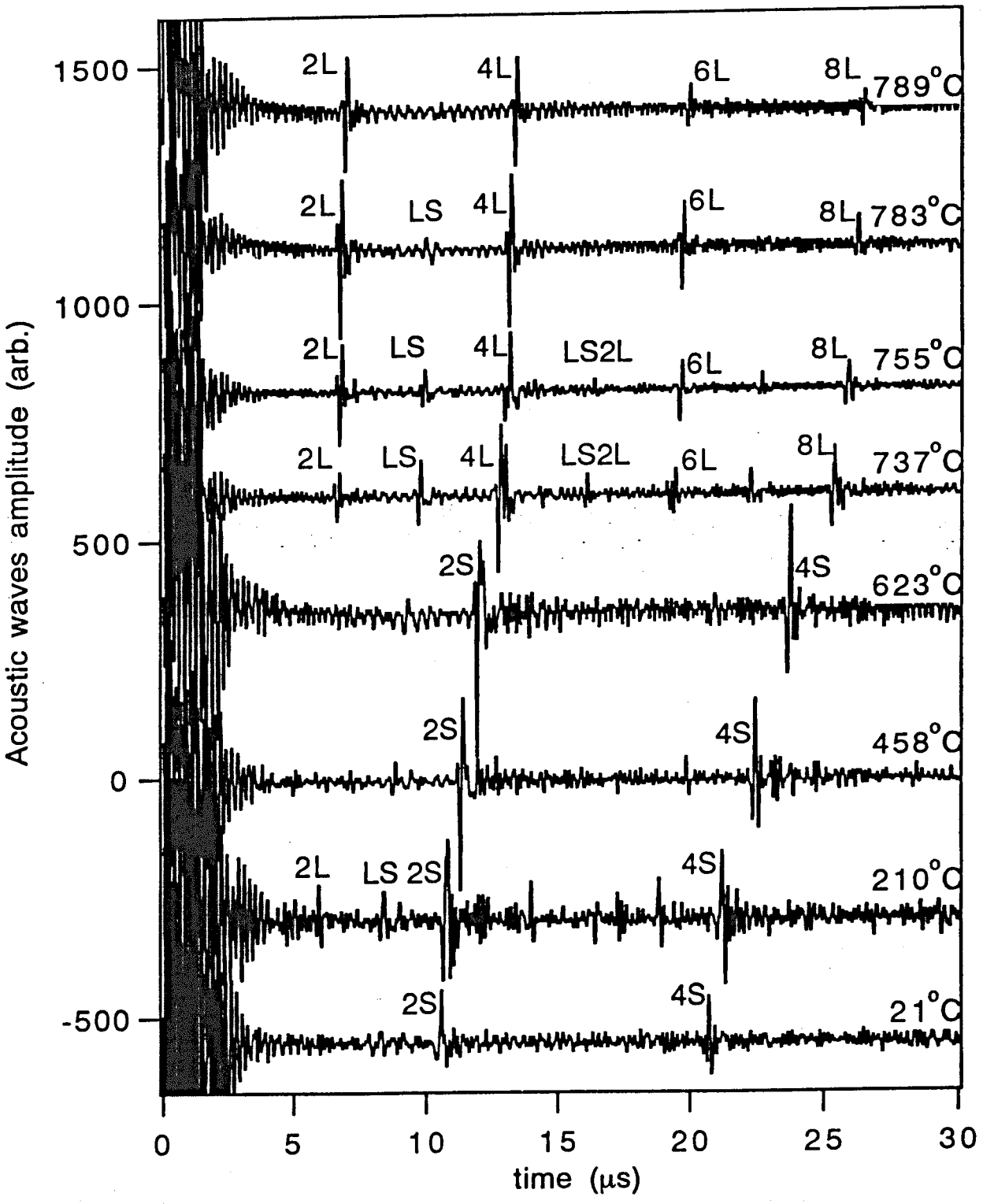

Figure-5.10: Send-receive ultrasound waveforms in mild steel at elevated temperatures generated by Nd:YAG laser and detected by E-EMAT. The ultrasound source was generated in the thermoelastic regime.

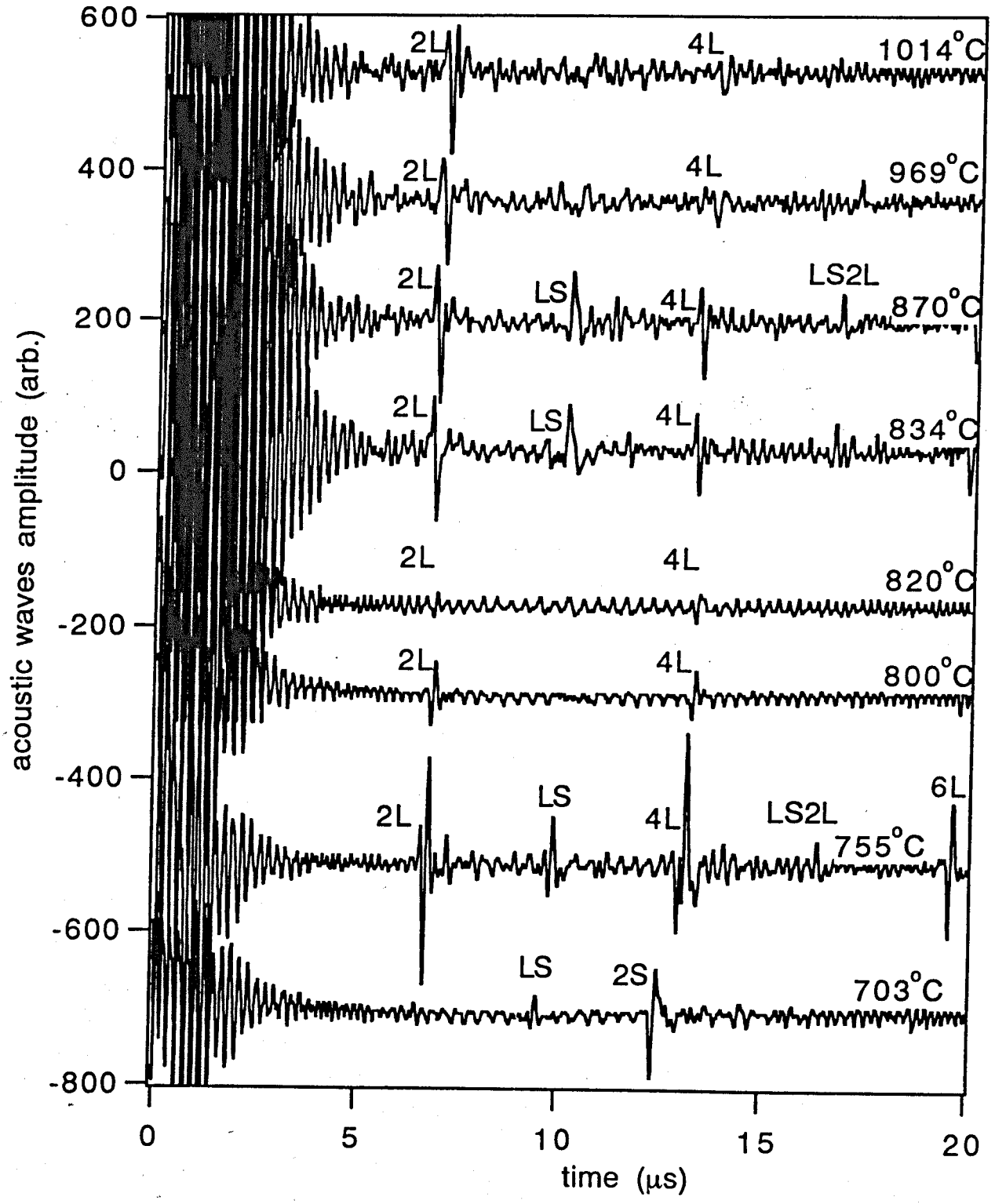

Figure-5.11: Ultrasound signal waveforms in mild steel similar to that in figure-5.10. At temperature above 820°C, the laser energy density was increased to generate an ablative source.

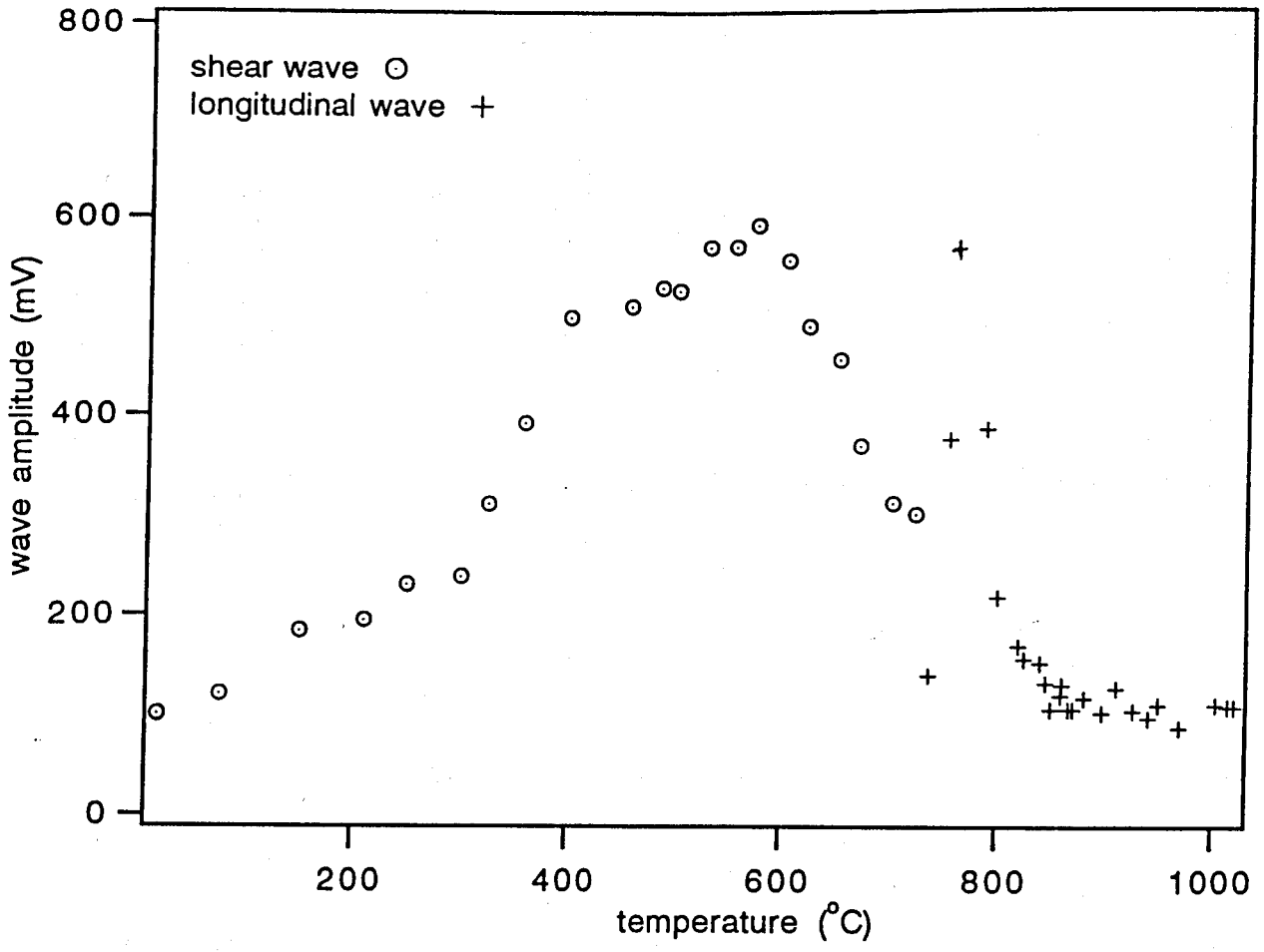

Figure-5.12: Temperature dependence of the send-receive ultrasound wave amplitude in mild steel generated by a Nd:YAG laser and detected by E-EMAT.

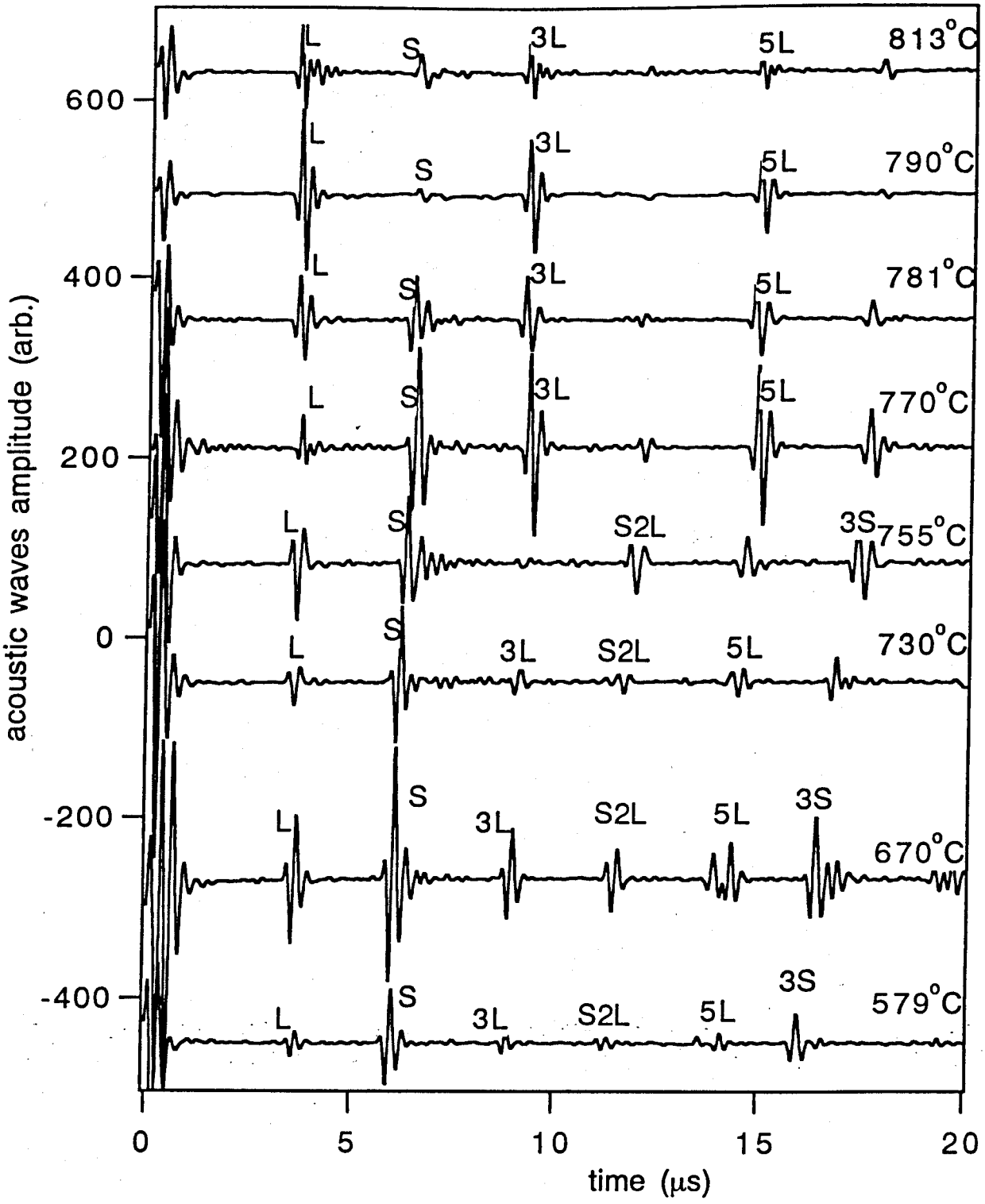

Figure-5.13: Ultrasound waveforms in mild steel (15mm thickness) at elevated temperatures, generated by CO_2 laser and detected by E-EMAT on epicentre.

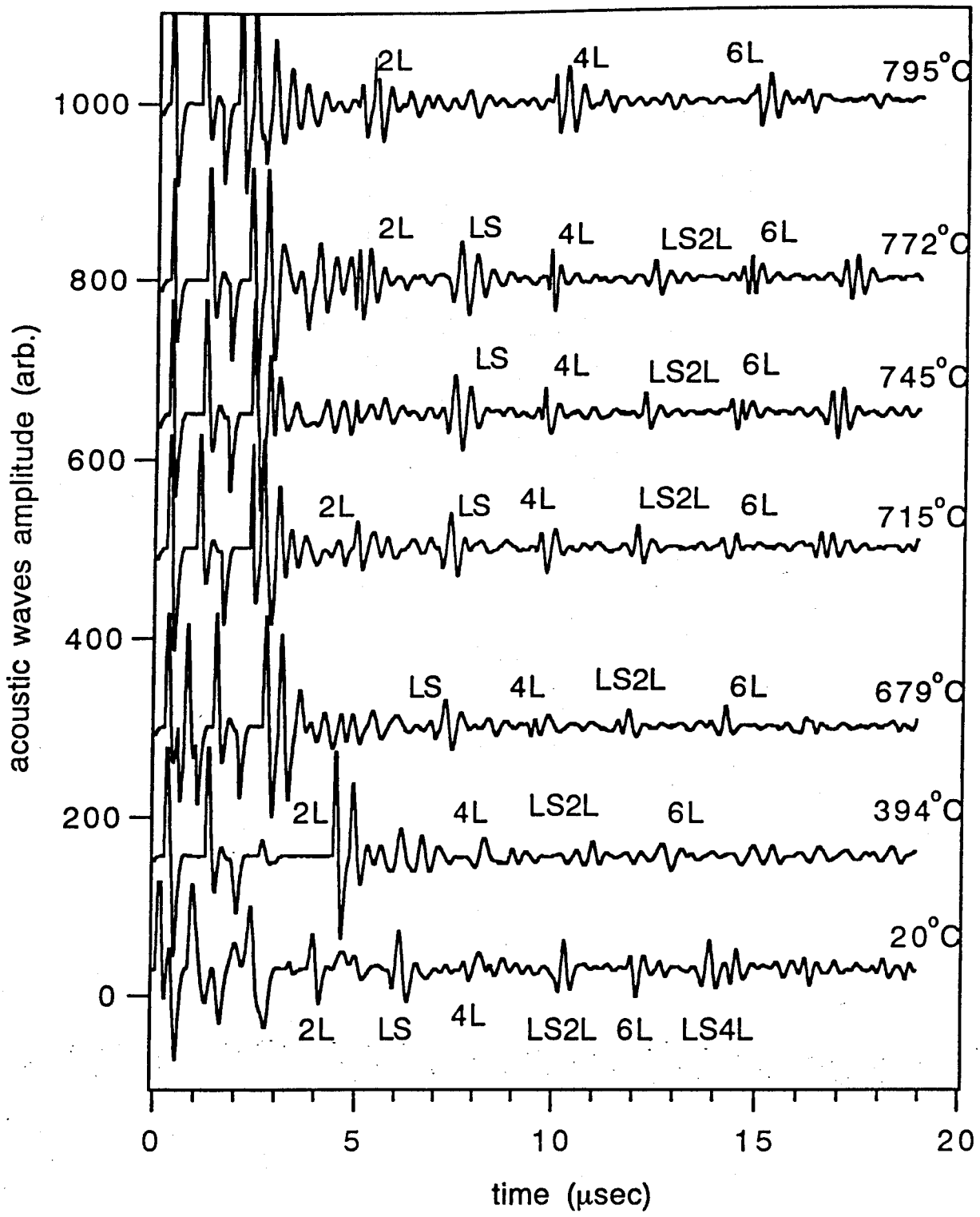

Figure-5.14: Send-receive ultrasound waveforms in mild steel (12.5mm thickness) at elevated temperature, generated by CO_2 laser and detected by E-EMAT.

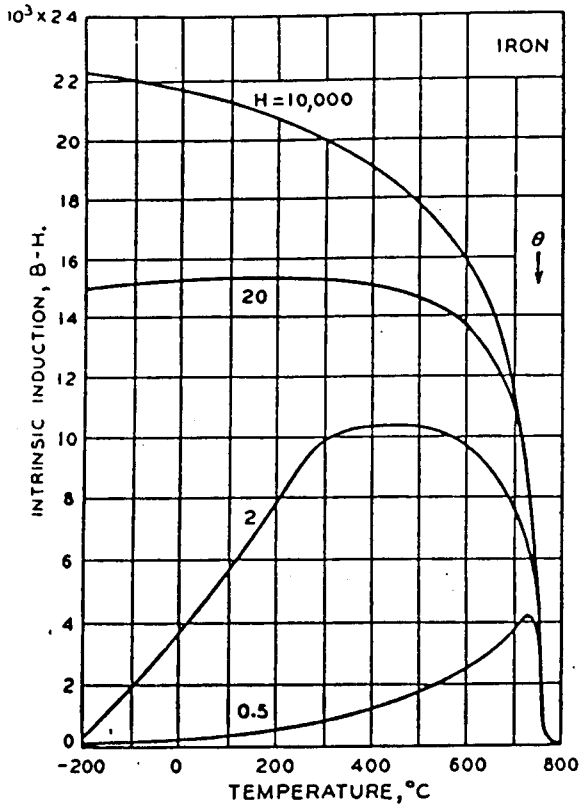

Figure-5.15: Magnetisation (in Gauss)-temperature curve of iron.(After Bozoroth, [1951])

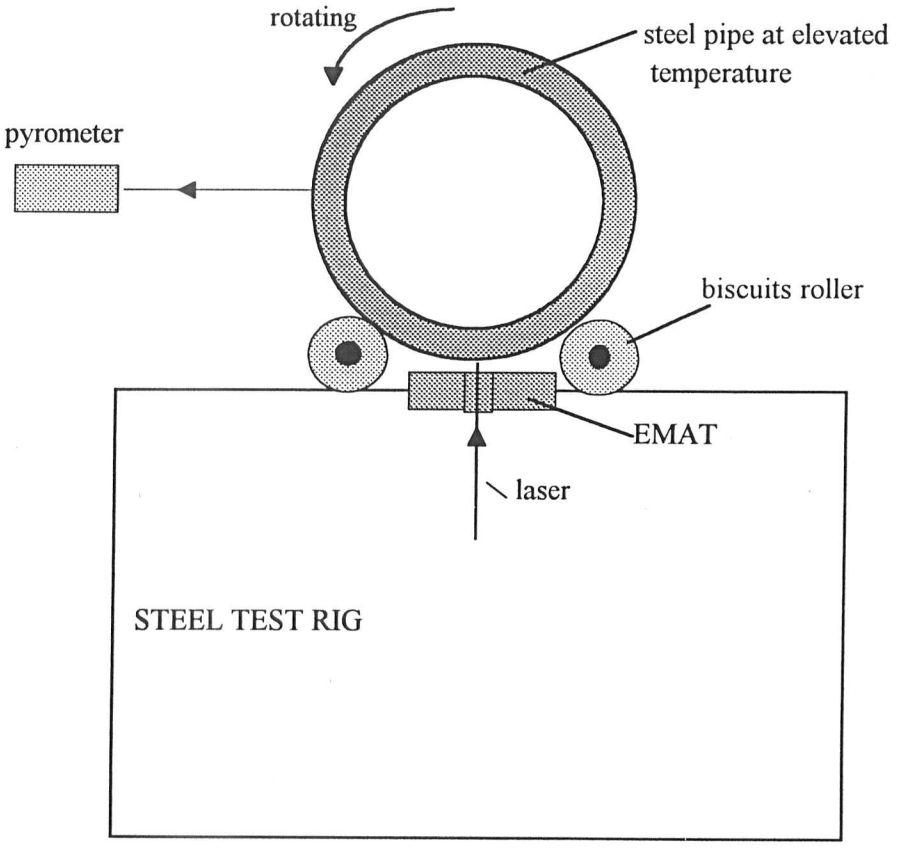

Figure-5.16: Experimental set-up for non-contacting ultrasound measurement on hot steel pipe at the steel mill site using CO_2 laser generator and P-EMAT detector. The laser and the associated peripherals are housed in a test rig.

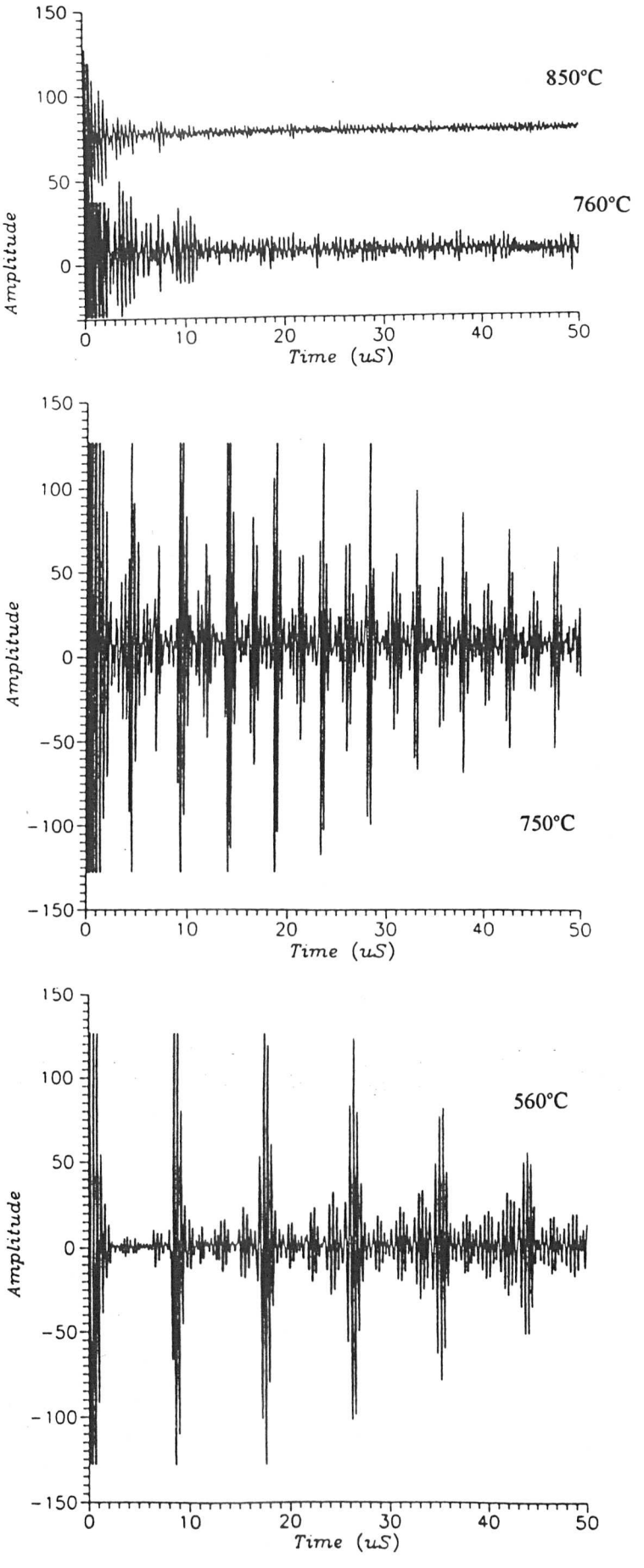

Figure-5.17: Send-receive ultrasound waveforms in mild steel at elevated temperatures, generated by CO_2 laser and detected by a concentric P-EMAT. Measurement was made at the Steel Mill site.

CHAPTER-6

Magnetostriction, Cooling Effect and Magnetisation Measurements

6.0 Introduction

In this chapter, further experimental measurements carried out using the EMAT on mild steel will be discussed. The first part deals with the effect of the static magnetic field on the EMAT efficiency of ultrasound transduction in ferromagnetic metals. This study is essential to gain further understanding of EMAT transduction mechanisms as there is a large variation in sensitivity in different steel samples. The second part will investigate the temperature dependence of EMAT efficiency at elevated temperature, where the amplitude of the magnetic field produced by the E-EMAT will be monitored so that the Curie Temperature can be identified. EMAT operation close to the Curie point will be examined in detail as it gives data relevant to the underlying transduction mechanisms. The corresponding ultrasound waveforms will be discussed. Finally, this chapter will investigate the cooling effect on a sample at elevated temperature caused by momentary contact with a water-cooled EMAT.

6.1 Magnetic Field Dependence of Ultrasound Transduction by EMAT

As already described in Chapter-3, EMAT ultrasound transduction is governed by the static magnetic field B_o, and the electrical and magnetic properties of the sample. For a single coil used in pulse echo on a paramagnetic metal, the transduction is due to a Lorentz force mechanism where the transduction efficiency, as represented by wave amplitude, shows a linear dependence of amplitude versus B_o^2 , passing through the origin (Dobbs, [1976]). However, in ferromagnetic materials the transduction mechanism is more complex, in addition to the Lorentz force mechanism there can also be a magnetostrictive mechanism. As a result there is a nonlinearity in the wave amplitude versus B_o^2 relation.

For the case of a surface wave generated by an EMAT on ferromagnetic materials, the signal amplitude detected by a piezoelectric probe reaches an essentially higher level than that in paramagnetic materials, and this occurs at a lower magnetic field intensity (Thompson, [1976]). The generation efficiency may also be affected by magnetostrictive oxides on the metal surface, for example magnetite. The EMAT transduction efficiency is affected by the oxide layer thickness (Maxfield et.al., [1987]) and its adhesion to the surface of the metal as well as the thermal and metallurgical history of the sample.

In this section, we will investigate the influence of the material properties and the external magnetic field on the efficiency of the shear wave transduction by EMAT in magnetic and non-magnetic metals.

6.1.1 Experimental Technique

Two separate experiments were carried out to study the effect of the static magnetic field B_o, on the shear wave transduction by EMAT on mild steel samples, aluminium was used as a non-magnetic standard. The shear wave signal amplitude was monitored with increasing magnetic field which was generated by either a DC electromagnet or the E-EMAT described in Chapter 4.

6.1.1.1 DC Electromagnet EMAT

The schematic diagram of the experimental set-up is shown in figure-6.1. The EMAT coil was clamped to the surface of the sample which then was inserted between the poles of a Newport Instruments DC electromagnet. The magnetic field was normal both to the EMAT coil and sample surface; the configuration to excite shear waves. The coil was fed with sharp current pulses at a repetition rate up to 10kHz, generated by a modified spike generator (PAR-250) from Par Industries. The same coil was used as the receiver.

The pulse echo signal amplitude was monitored while the energising current of the electromagnet was increased in small increments. The magnetic field was measured using a small Hall effect probe inserted behind the coil. The magnetic field was varied from 0 to 2.0T. The 16mm diameter EMAT coil was a PCB etched spiral coil consisting of 18 turns. It was bonded onto an aluminium plate which could be clamped to the samples, (see figure-6.1). Aluminium and mild steel plate samples of different stock and surface conditions were studied.

6.1.1.2 E-EMAT.

A similar experimental set-up to that shown in figure-4.10 was used. The magnetic field B_o was increased in small increments by using a VARIAC to adjust the voltage in the electromagnet discharge circuit. The pulsed magnetic field generated on the sample surface was measured using a field sensing coil, as described in chapter-4. The amplitude of the EMAT signal output was monitored after taking an average of 100 waveforms to improve the signal to noise ratio.

6.1.2 Results and Discussion

Figure-6.2 shows the magnetic field dependence of the pulse echo ultrasound amplitude for the mild steel and aluminium samples generated by a DC electromagnet EMAT. The aluminium sample shows an initial linear dependence of wave amplitude upon the square of the magnetic field B_o, there is a deviation at high signal amplitudes due to a non-linear response of the preamplifier. A linear relationship in amplitude versus B_o^2 and originating from zero, is consistent with the Lorentz force mechanism (Dobbs, [1976]). Deviations or shifting from this linearity indicate other transduction mechanisms are important such as magnetostrictive effects. In the mild steel sample (K044), the

amplitude-B_o^2 curve shows a linear dependence at high magnetic field strength, although there is a deviation at high signal amplitude arising from a non-linear response of the receiver preamplifier. At lower magnetic field intensity (figure-6.2b), the curve deviates from this linearity indicating a magnetostrictive effect. A similar linear amplitude-B_o^2 relationship at high magnetic field strength is also observed in other samples as shown in figure-6.3 and figure-6.4. These results clearly indicate that, at high magnetic field strength, EMAT transduction in mild steel K044 is dominated by the Lorentz force mechanism as in aluminium. The extrapolation of the line-fit of the amplitude-B^2 curves at high magnetic field pass through the origin. These results are in agreement to those demonstrated by Dobbs, [1976] and Thompson, [1978].

Mild steel samples J221 and 7927 (figure-6.2), however show a non-linear amplitude-B_o^2 relationship even at high magnetic field intensity. This may be due to a magnetostrictive effect being the dominant ultrasound transduction mechanism. Non-linear behaviour at low magnetic fields is exhibited in all of the steel samples as shown in figure-6.2b, figure-6.3 and those samples with a magnetite oxide surface layer as shown in figure-6.4. These figures show that the magnetostrictive effects are exhibited by both the magnetite layer on the sample surface and the underlying metal. Hydrated rust however, does not show any pronounced magnetostrictive effects (figure-6.3b), since the removal of this scale does not alter the amplitude-B_o^2 curve. The non-linear effect in amplitude-B^2 relationship indicates a magnetostrictive effect in the underlying metal.

In the results presented here, the amplitude versus B_o^2 curve varies from one sample to another indicating different EMAT transduction efficiencies for different steels. The EMAT transduction efficiency in mild steel can be classified as good as shown in sample K044, medium as shown by sample 7927, and poor. We found that one of the mild steel samples (British Gas pipeline steel 50D) exhibited a poor ultrasound transduction,

where even after increasing the magnetic field up to 2T, there were no discernible ultrasound signals.

6.1.2.1 Transduction on Clean Sample

EMAT ultrasound transduction efficiency for the Lorentz force mechanism has been modelled by Dobbs, [1976], (see equation-3.5). This solution excludes any acoustic loss exhibited in the materials. It is shown from our measurements that the transduction efficiency on aluminium is about 10dB above that of mild steel (sample K044) as shown in figure-6.2. In mild steel, Lorentz force transduction efficiency was reduced by its high magnetic permeability as well as its density. Ferromagnetic samples also have attenuation arising from the wave interaction with magnetic domains (Mason, [1958]). Based on equation (3.5) however, at room temperature the transduction efficiency in mild steel is about 20dB lower than for aluminium using an equal magnetic field strength. Enhancement in transduction efficiency may arise from the magnetostrictive effects.

6.1.2.2 Effect of Oxide Layer

The presence of black oxide scale, magnetite, on the surface typically enhances the transduction efficiency by 6dB compared with a clean metal surface (Figure-6.3a). The effect of the surface layer however varies from sample to sample. Another type of oxide studied, hydrated rust, did not enhance the transduction efficiency in the sample. This is clearly shown in sample-B taken from a section of a water corroded mild steel pipe, covered with water corroded scale on its surface (Figure-6.3b). A similar result was obtained after the removal of oxide scale.

Figure-6.4 shows the field dependence of pulse echo ultrasound amplitude generated by E-EMAT on mild steel samples. On a clean sample, the wave amplitude-B_o^2

curve increases smoothly with the increasing magnetic field (Figure-6.4a). However in the presence of a thin layer of magnetite on the surface of the sample, the curve exhibits a maximum at low fields with the peak at about $B_o^2 = 0.3T^2$. As the field is increased further, the curve decreases and then again behaves in a linear manner with the increasing field (Figure-6.4b). Figure-6.4c, shows the effect of a thicker magnetite layer on the shear wave EMAT transduction. The wave amplitude-B_o^2 curve increases with the field intensity and reaches a maximum at about $B_o^2 = 0.3T^2$, however as the field increases further, the signal amplitude decreases and exhibits an inflection at $B^2=1.5T^2$ (or B= 1.25T). Above this point the curve exhibits a linear dependence indicating Lorentz force interaction dominating the transduction mechanism. In a normal E-EMAT operation, (i.e. at magnetic field intensity B_o= 1.3T), the shear wave signal amplitude is reduced by about 12 dB compared to that at the maximum. The peak in the signal amplitude-B_o^2 curves may be attributed to the magnetostriction occurring mainly in the magnetite layer.

On a clean mild steel, the contribution of magnetostriction is also present but it has a smaller magnitude compared to that with a magnetite layer. The typical linear magnetostriction coefficient (saturation value) at room temperature for magnetite is of the order of $+40x10^{-6}$ (Jacubovic, [1991]) and for iron (the closest to low carbon mild steel), the coefficient varies with the field intensity as shown in figure-6.6. A minimum in magnetostriction coefficient ($-8x10^{-6}$) occurs at a magnetic field of about 0.35 Tesla, and thereafter, there is a slow lengthening associated with a change in volume, volume magnetostriction. The shape of this curve may depend on the heat treatment and the alloying content of the sample. Since the magnetostriction coefficient of a magnetite layer is much greater than steel, it may dominate the ultrasound transduction at low field ranges. At higher magnetic field intensity, when the material is magnetically saturated and the magnetostrictive effect has been reduced, the amplitude-B_o^2 curve becomes linear and

ultrasound transduction is dominated by the Lorentz force mechanism. In a high magnetic field region, the magnetic permeability of the sample remains constant and thus the β factor (given by equation 3.5.) remains constant and therefore the transduction efficiency is directly proportional to B_o^2.

On a sample with a thick layer of magnetite, the ultrasound signal amplitude began to decrease above $B_o^2 = 0.3T^2$. As the magnetic field is increased, the magnetostrictive-strain coefficient of both the magnetite and the iron are reduced leading to the reduction in the wave amplitude arising from the magnetostrictive mechanism. At the same time, the ultrasound transduction efficiency in the magnetite layer by the Lorentz force mechanism is also reduced due to the reduction of its magnetic permeability and increases in β factor given by equation-3.5. Ultrasound transduction efficiency by the Lorentz force mechanism in the underlying metal is increased with increasing magnetic field as more current reaches its surface. Although the magnetite is a poor electrical conductor ($\sigma \sim 2.5 \times 10^4\ \Omega m^{-1}$ compared to mild steel, $1 \times 10^7 \Omega m^{-1}$), at lower magnetic field intensity, the thick magnetite layer tends to screen the electromagnetic waves from penetrating into the underlying metal due to its high permeability as well as introducing an additional stand-off between the coil and the metal surface. The magnetite screening effect reduces at higher field due to its reduced permeability hence larger skin depth. Since the transduction efficiency in magnetite is much lower than that of iron, the detected wave amplitude begins to increase as the effect due to the increasing field is greater than that of the stand-off. Another possible explanation of a strong magnetostrictive effect from the magnetite layer could be caused by the preferential direction of growth of the magnetite grains on the sample surface. In this case the grains grow in the easy magnetisation direction which is normal to the surface as the sample cools down.

6.2 Cooling Effect Measurement

As the temperature of the sample increases, the flow rate of the cooling water supplied to the EMAT is increased to maintain the EMAT temperature below 100°C. The increase of the water flow rate, may give the EMAT a greater cooling effect on the sample surface, creating a temperature gradient across the sample thickness. As a result, this may introduce errors in the measurement of the ultrasound velocities at elevated temperature. This problem may become more serious when the measurements are made in send-receive arrangement using a large size EMAT receiver with a large temperature gradient between the surface of the sample and the EMAT. Idris, [1995] has demonstrated the cooling effect on the surface of the sample for temperatures up to 500°C. The momentary contact of the water-cooled EMAT on the sample surface introduced a surface cooling with a temperature gradient of 8°C across the sample thickness of 14mm rather than cooling the whole sample. The measurement was recorded after the EMAT had been in contact with the sample for about 8s.

6.2.1 Experimental Technique

In this experiment we adopted a similar technique to that used by Idris, [1995] to measure the cooling effect on the sample at elevated temperature (figure-6.7). The temperature on both sides of the surface of the sample was monitored as the water-cooled EMAT was brought into close contact for a pre-set period. A time delay trigger box with a delay timer setting between 0.7s to 8s was designed, enabling the electromagnet driver to be excited only after the EMAT had been in the measuring position on the surface of the sample for a pre-set time.

The trigger box is manually triggered and this is shown in figure-6.8. The circuit is designed around two of the gates of a CD4001 i.c.. The circuit action is such that its

output is normally lower or at logic level-0 but switches to logic level-1 for a pre-set period as a rising trigger waveform is applied to pin 2 of the i.c.. The period of the output pulse is determined by the values of R_1 and C_1 and for a given value R_1 (1.5MΩ), it is approximately 1s per μF of C_1. The output pulse (100μs width), is initiated at the moment the input trigger signal rises through a threshold level of roughly half of the supply voltage. When the manual push button S_1 is closed, it will cause the capacitor C_2 to discharge through the load R_2 with the time constant $T_2=R_2C_2$, which then will trigger the input signal of pin 2 of the i.c.. T_2 determines the pre-set time delay which can be varied from 0.74s to 8s by varying the value of R_2. The trigger signal is derived from the positive supply rail 9V by a push button switch S_1 and at the same time it acts as the time reference signal which will be used to trigger the oscilloscope. The output signal will trigger the electromagnet driver and thus other related equipment.

The trigger box was clamped on to the EMAT rail (figure-6.9) with its position adjusted so that the push button S_1 would start the sequence at the instant the EMAT was in position in contact with the surface of the sample. The electromagnet was excited manually and its supplied voltage input had to be kept low (about 120-140V of the VARIAC output).

The equipment set-up for the temperature measurement is shown in figure-6.7. The Ni/Cr-Ni/Al thermocouples were used to measure the temperature on both surfaces of the sample. The thermocouple's tip on the EMAT side was inserted into a hole 1.5mm deep on the sample and connected to the temperature preamplifier which was designed to have a sensitivity of approximately $4mV°C^{-1}$. The temperature signal output was then passed through a low pass filter to remove any high frequency noise before the temperature curve was displayed and recorded on a Lecroy 9310 oscilloscope. The other thermocouple was inserted on the opposite surface of the sample on epicentre to the

EMAT. It was connected to a Digitron temperature meter to measure the absolute temperature of the sample. The thermocouple output on the detection side was displayed by one channel of the oscilloscope, triggered by the time reference signal output. When the EMAT was positioned on the surface of the sample, and the press button (figure-6.9) of the delayed trigger switch was closed, it triggered the oscilloscope in roll mode. The delay trigger output was fed to the other channel of the oscilloscope to trigger the oscilloscope to stop and hold the waveform.

The sample was heated up to about 840°C and after it reached a constant temperature the EMAT was introduced to the sample and allowed to come into close contact for pre-set times of 0.74s and 1.95s respectively. After the pre-set time, the EMAT was withdrawn from the surface of the sample so that the heating effect could be monitored.

6.2.2 Results and Discussion

The temperature variation on the surface of the sample in close contact with a water-cooled EMAT is shown in figure-6.10. When the EMAT was introduced onto the surface of the sample at a temperature of 823°C, the temperature was reduced by 5°C after 0.74s. In a second experiment with the sample at 840°C, the temperature was reduced by 15°C after being 1.95s in close contact with the EMAT. Similarly, at a slightly lower temperature (608°C), the corresponding cooling effect on the sample after 4.5s in contact with the EMAT is about 30°C. From the wave velocity curves, the percentage changes in the longitudinal wave transit time and hence the velocity corresponding to these temperature changes are 0.76% at 823°C and 0.85% at 840°C. These values lie within the error of the ultrasound velocities-temperature curves which range from about 1-1.5%. At 823°C, the temperature on the other side of the sample was also monitored and

it was indicated that the temperature remained constant after 0.74s and reduced by 1.6°C after 1.94s in contact with the EMAT. A similar effect occurred at 840°C where the temperature on the other side of the sample reduced by about 1.5°C after 1.94s in contact with the water-cooled EMAT. It was concluded that such a short contact between the surface of the sample and the water-cooled EMAT did not significantly cool the whole sample but only produced a superficial effect

In the experimental results presented in this thesis, the EMAT remained in contact with the sample for a very short period (about 1s), therefore the cooling effect would not significantly alter the wave velocities or the transit times as the cooling only occurred on the surface when in contact with the EMAT. In other measurements, the external delay trigger unit was used so that the ultrasound was generated and detected at a constant pre-set time (at 0.74s) after the EMAT was positioned on the surface of the sample.

6.3 Magnetisation Measurement

The efficiency of the ultrasound transduction by EMATs is linearly proportional to the magnitude of the magnetic field on the surface of the sample. On ferromagnetic materials such as mild steel however, the external magnetic field will magnetise the sample. As the temperature of the sample is increased and approaching T_c, the magnetisation of the sample reduces and tends to zero at the Curie temperature where the sample undergoes the ferromagnetic to paramagnetic transformation. This phase transformation temperature could be estimated from when the EMAT is no longer attracted to the sample, however an accurate Curie temperature could not be determined using this method since the introduction of the EMAT cools down the surface of the sample. An accurate Curie temperature determination of the sample is important since above this transition temperature the ultrasound transduction mechanism by EMAT is only due to the Lorentz

force mechanism.

This section will describe the magnetisation measurements at elevated temperatures using the E-EMAT. The measurements were made by making the sample a part of a closed loop magnetic circuit. The magnetic field induced by the sample could be determined by measuring the induced voltage arising from the time varying field in the gap between the electromagnet pole and the sample, using a single loop sensing coil bonded to the outside of the EMAT coil. The magnetic field intensity was determined by integrating the output of the field sensing coil described in chapter-4. The ultrasound and magnetisation measurements were made simultaneously by non-contacting technique.

6.3.1 Experimental Technique

A similar experimental set-up shown in figure-6.7 was used. The electromagnet was excited manually at a pre set time delay after positioning the E-EMAT on the surface of the sample. In this measurement, the EMAT was introduced into close contact with the surface of the sample for a pre set period of 0.72s as described in section 6.2. of this chapter. The EMAT was pulled out from the sample immediately after the waveform had been captured. A consistent contact of the EMAT and the surface of the sample allowed a consistent cooling effect. The electromagnet was excited at a constant input voltage (130V VARIAC output). The output of the field sensing coil and the ultrasound waveforms generated on the sample at varying temperature were recorded onto the disk for further analysis.

6.3.2 Result and Discussion

Figure-6.11 shows the temperature dependence of the magnetisation measured on the surface of the sample. The magnetic field remained unchanged at about 1.4T up to a

temperature of about 745°C. Above this temperature the magnetic field intensity begins to reduce dramatically down to about 0.35 T at 780°C. As the temperature was increased further, the magnetic field intensity remained constant. The sharp change in the recorded magnetic field occurs at a temperature range 740°C-760°C, representing the transition region from ferromagnetic into paramagnetic phase and the collapse of magnetic ordering in the material at 760°C where the EMAT is no longer attracted to the sample.

Figure-6.12 shows the pulse echo waveforms generated and detected by the EMAT at different temperatures. The shear wave amplitude increases with the increasing temperature but begins to reduce as the temperature approaches T_c and becomes very weak at T_c. As the temperature increases further, the waveform is dominated by the longitudinal wave arrivals where the amplitude increases with temperature as described in chapter-5. The ultrasound measurement was discontinued at a temperature of about 803°C when no discernible signal could be detected.

The temperature variation of the ultrasound wave amplitude which represents the ultrasound transduction efficiency of EMAT on mild steel is shown in figure-6.11. Below T_c , it is indicated that the transduction efficiency is independent of the magnetic field intensity, however at just above this temperature, when the sample is completely paramagnetic, the waveform is dominated by longitudinal wave echoes. The excitation of longitudinal wave is not associated with the low magnetic field generated on the surface of the sample but it is more associated to the phase transition at T_c, the reorientation of the magnetic flux entrapped within a skin layer of the ferromagnetic phase and a strong volume magnetostriction effect as described in chapter-5.

The excitation of a strong longitudinal wave at temperatures just above T_c could arise from the magnetostriction of the paraprocess where this transduction mechanism is most efficient in the region of the transition from paramagnetic to the ferromagnetic state

and vice-versa. Such effects have been studied by Andrianov et al., [1988] in gadolinium, which shows a giant excitation of the longitudinal wave at temperatures just above T_c. As the magnetoelastic coupling parameter, ζ , is small compared to unity over the whole temperature range, the transduction efficiency due to magnetostriction arising from the paraprocess was simplified as (Andrianov et al., [1988]);

$$\eta_m = S.\frac{\zeta\chi}{(1+4\pi\chi)^2}$$

where S is a constant, χ is the magnetic susceptibility ($\chi=\mu_r-1$). In the paramagnetic state, the susceptibility χ is given by the Curie-Weiss relation, $\chi = \frac{\text{constant}}{T-T_c}$. Far above the Curie temperature, the paramagnetic susceptibility $\chi << 1$; hence $\eta_m \alpha \zeta\chi$. As the temperature approaches T_c, and for a fixed value of the magnetic field intensity (in this case B_o is of the order of 0.35T), the magnetisation M changes with temperature monotonically, while the χ increases rapidly. By substituting the susceptibility factor χ into the transduction coefficient η_m above, the temperature dependence of the ultrasound transduction efficiency above T_c in pulse echo arrangement, is given by η_m^2 versus $(T-T_c)$ curve as shown in figure-6.14. The transduction efficiency increases rapidly from zero at T_c with the increasing temperature above T_c and reaches a maximum at about 20°C above T_c. As the temperature is increased further, η_m^2 reduces gradually. Comparing the wave amplitude versus $(T-T_c)$ and η_m^2 versus $(T-T_c)$ curves, the measured wave amplitude reduces monotonically due to the increasing wave attenuation in the material at elevated temperature.

6.4 Conclusions

Ultrasound transduction by EMAT on mild steel arises from both the magnetostrictive and the Lorentz force mechanisms, the former dominates at low magnetic field and the latter at higher field. Magnetite layers of certain thickness also enhance the

transduction efficiency. At high field intensity, thick layers of magnetite may impair the transduction efficiency. The E-EMAT was also capable of monitoring the magnetisation of steel samples at elevated temperature and T_c can be determined accurately from the extrapolation of the magnetisation versus temperature curve that shows a rapid drop in the magnetisation from 1.4T to 0.35T and occurs at about 760°C. The transition from ferromagnetic to paramagnetic state of the sample was accompanied by the excitation of the enhanced longitudinal wave in the vicinity of T_c. The introduction of EMAT to the surface of the sample at elevated temperature did not alter the temperature of the bulk sample and the cooling effect was only superficial.

6.5 References

Andrianov A. V., Buchel'nikov V. D., Vasil'ev A. N., Guidukov Yu. P., Il'yasov R. S. and Shavrov V. G., Sov. Phys. JETP. **Vol. 67** , no.11, November 1988. pp.2331-2337.

Bozoroth R.M., Ferromagnetism , D Van Nostrand Co. Inc. Canada. (1951), pp.714.

Dobbs E. R., in Physical Acoustic ed. W.P Mason, **Vol. 10**, 1976, pp.127-191

Idris A.; Ph D Thesis, Warwick University, 1995

Jacubovich. J.P., Magnetism and Magnetic Materials, (Inst. Of Materials-London) 1991

Mason W. P., Physical Acoustic and the Properties of Solids, (Princeton, New Jersey, D Van Nostrand & Co.) !958.

Maxfield B. W., Kuramoto A. and Hulbert J. K., Material Evaluation, **Vol. 45,** Oct.1987, pp.1166-1183.

Thompson R.B., Appl. Phys. Letters, **Vol. 28**, No.9, May 1976. pp.483-485.

Thompson R.B., IEEE Trans. on Sonics and Ultrason., **Vol.-SU-25**, no. 1, Jan. 1978, pp.7-15.

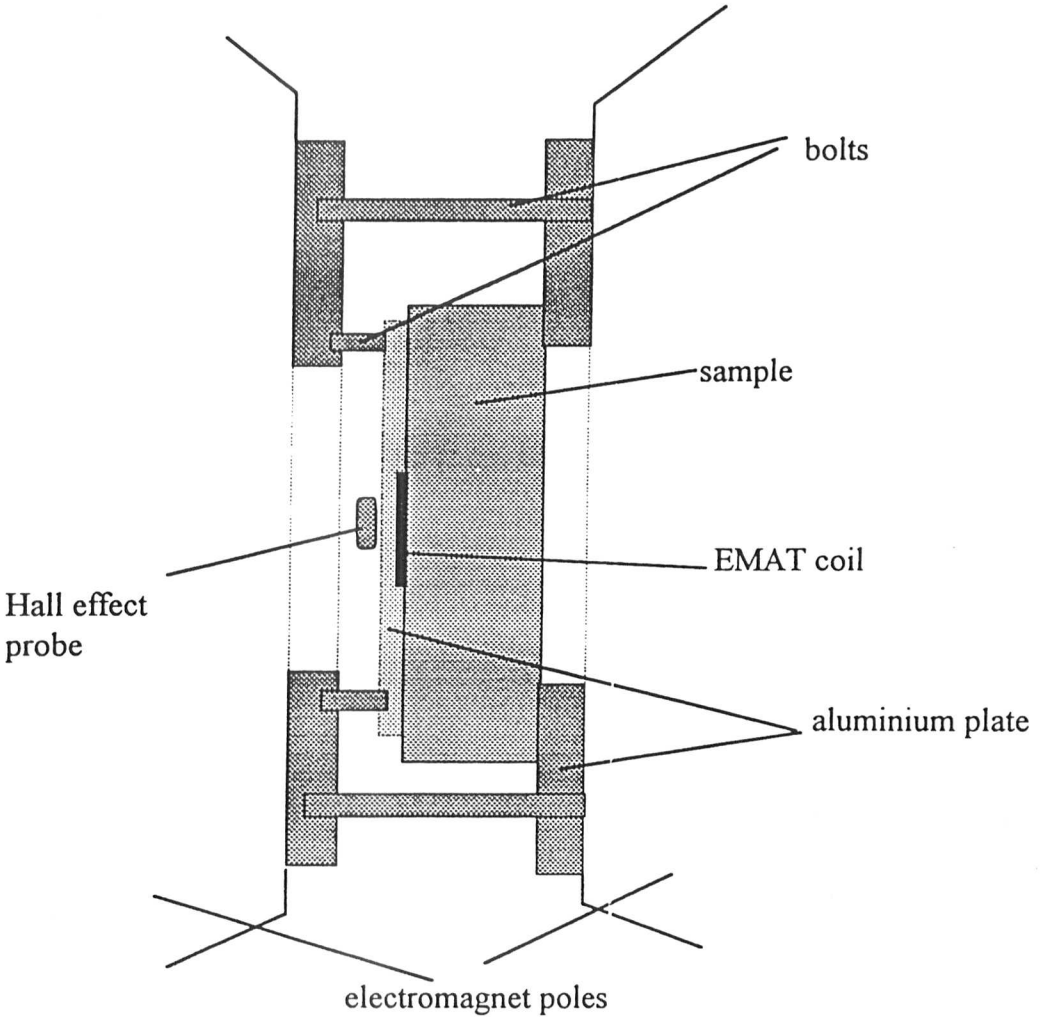

Figure 6.1:Set up for ultrasound transduction by a DC electromagnet EMAT.

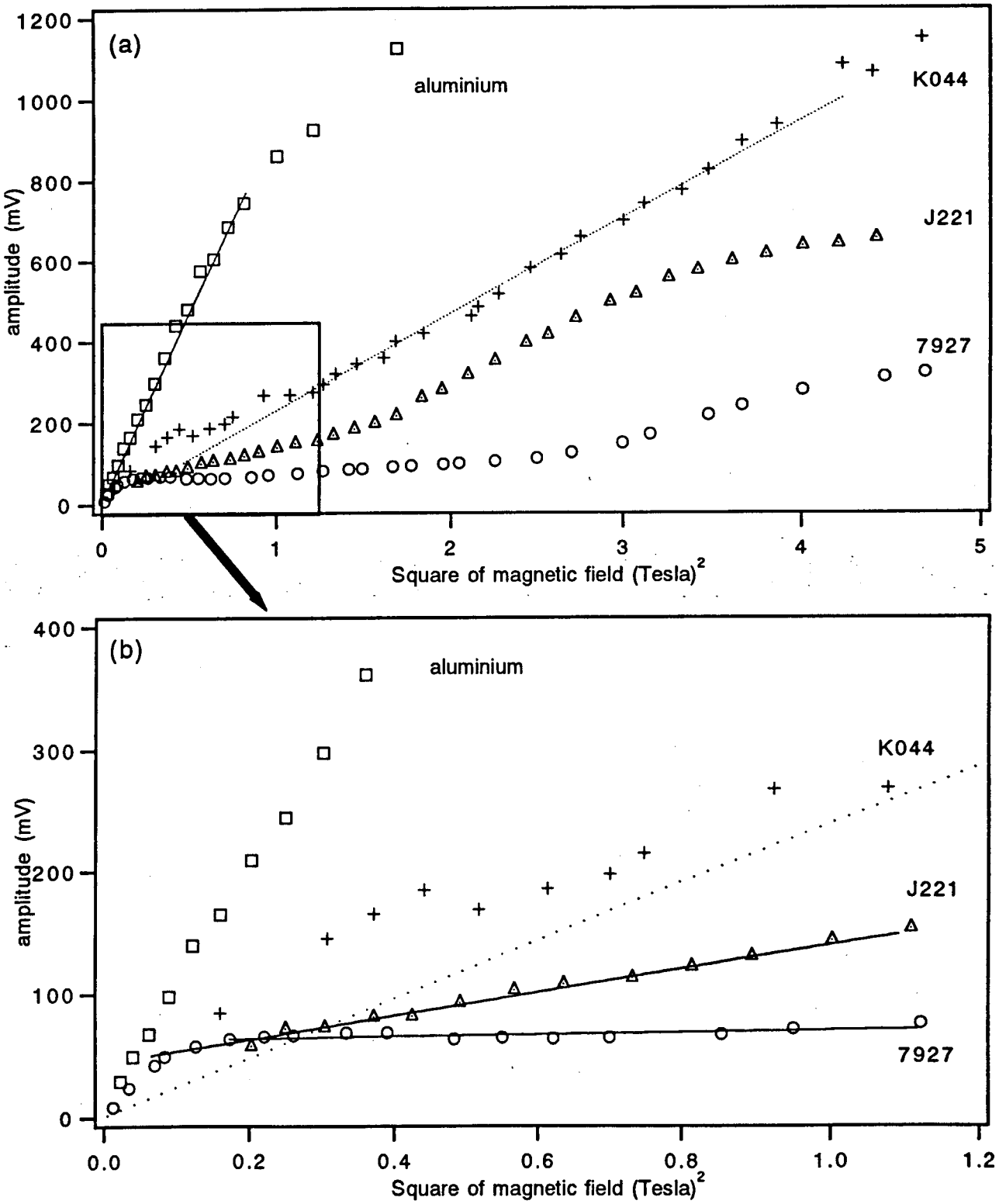

Figure-6.2: Pulse echo shear wave amplitude-B_o^2 variation in aluminium and mild steel samples of different stock generated by an EMAT. The magnetic field $B_o$was generated by a DC electromagnet. The deviation from a linear relationship originating from the origin indicates magnetostrictive transduction.

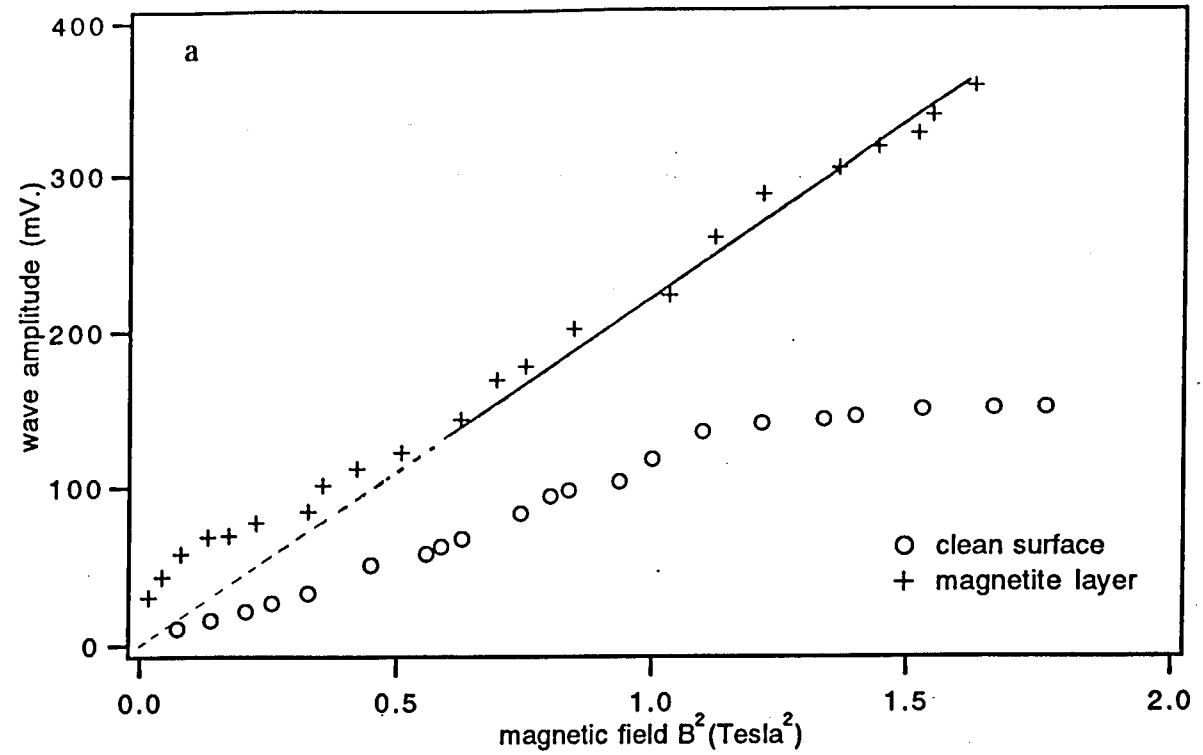

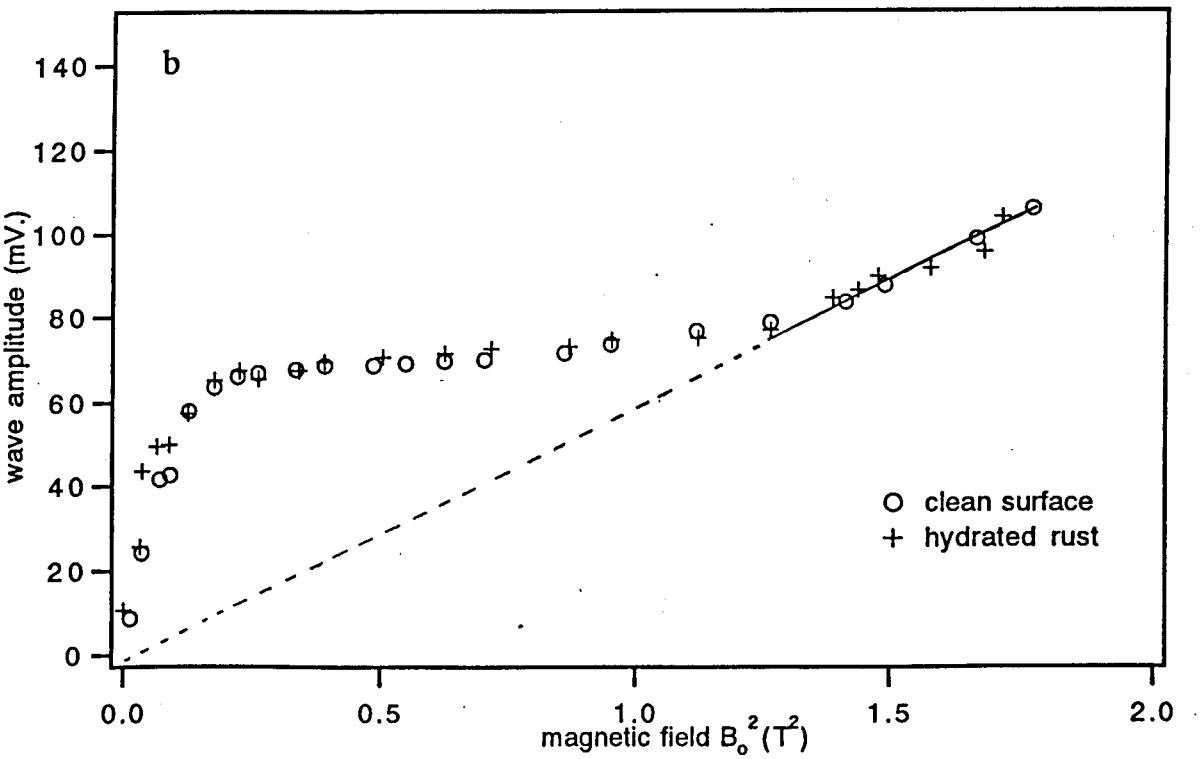

Figure-6.3: Variation of pulse echo ultrasound amplitude excited in mild steel with square magnitude of the magnetic field; indicating the effect of (a)-magnetite layer, (b)-the hydrated or red rust on the ultrasound transduction by an E-EMAT. The line fitting at high magnetic field intensity indicates ultrasound transduction arises from the Lorentz force mechanism.

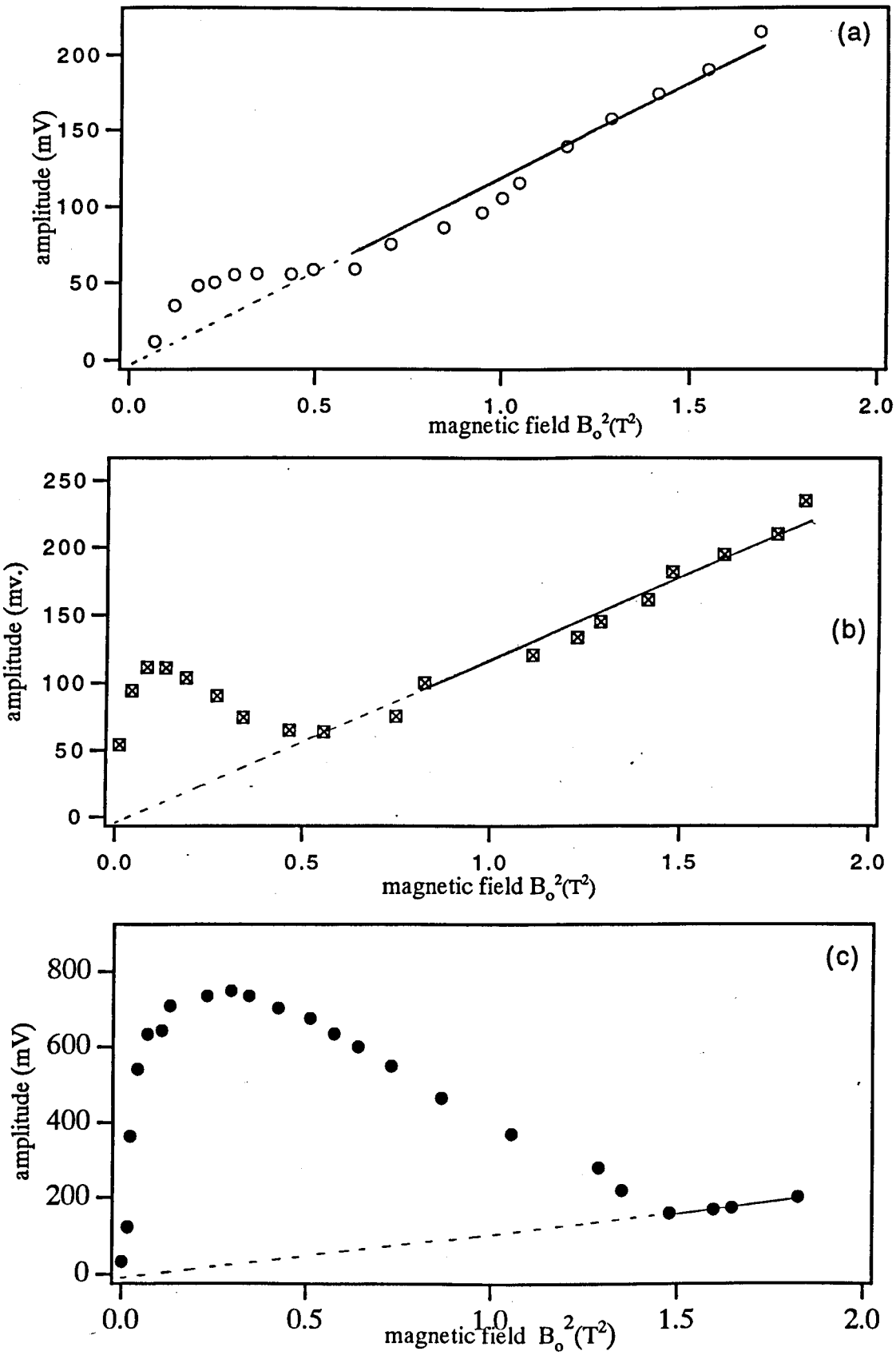

Figure-6.4: Pulse echo shear wave amplitude-B_o^2 variation in mild steel generated by E-EMAT.
(a) Clean surface
(b) Thin layer of magnetite
(c) Thick layer of magnetite

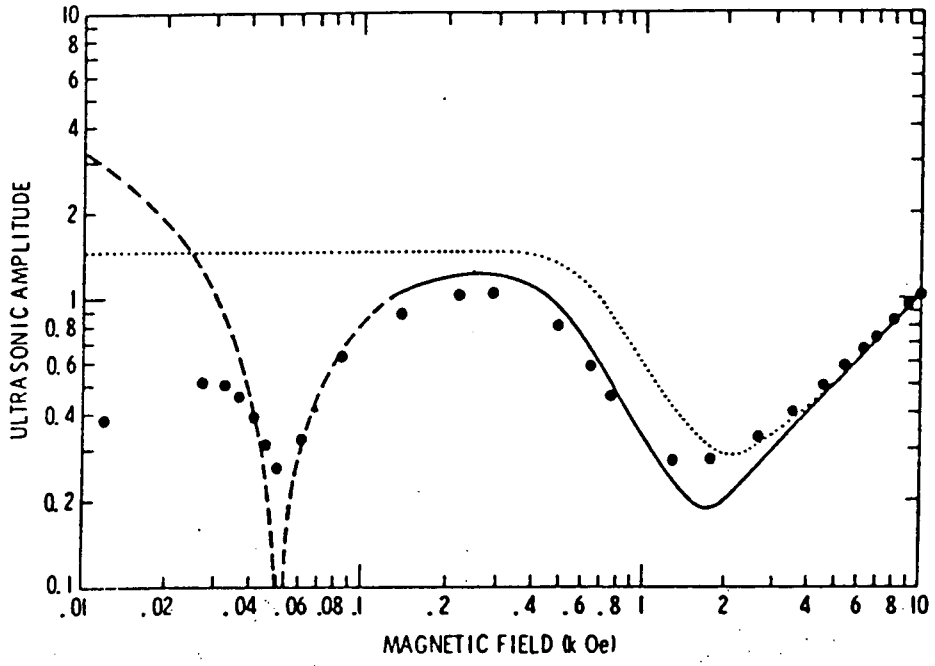

Figure-6.5: Comparison of experimental measurement of ultrasound amplitude in polycrystalline iron generated by EMAT to the theoretical predictions. The dotted theoretical line is the result when magnetic parameters are evaluated from the domain rotation model. The solid line is the result when the magnetic parameters are determined from direct measurements of static response. This line is broken at lower fields indicates the hystereses effects (after Thompson, [1976]).

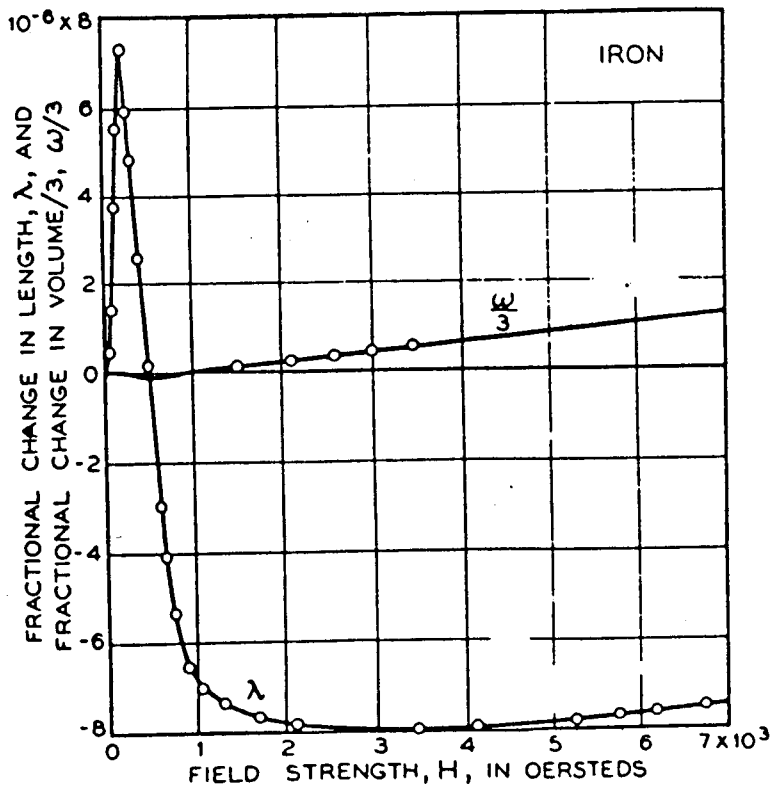

Figure-6.6: Linear and volume magnetostriction of iron.
(After Bozoroth, [1951])

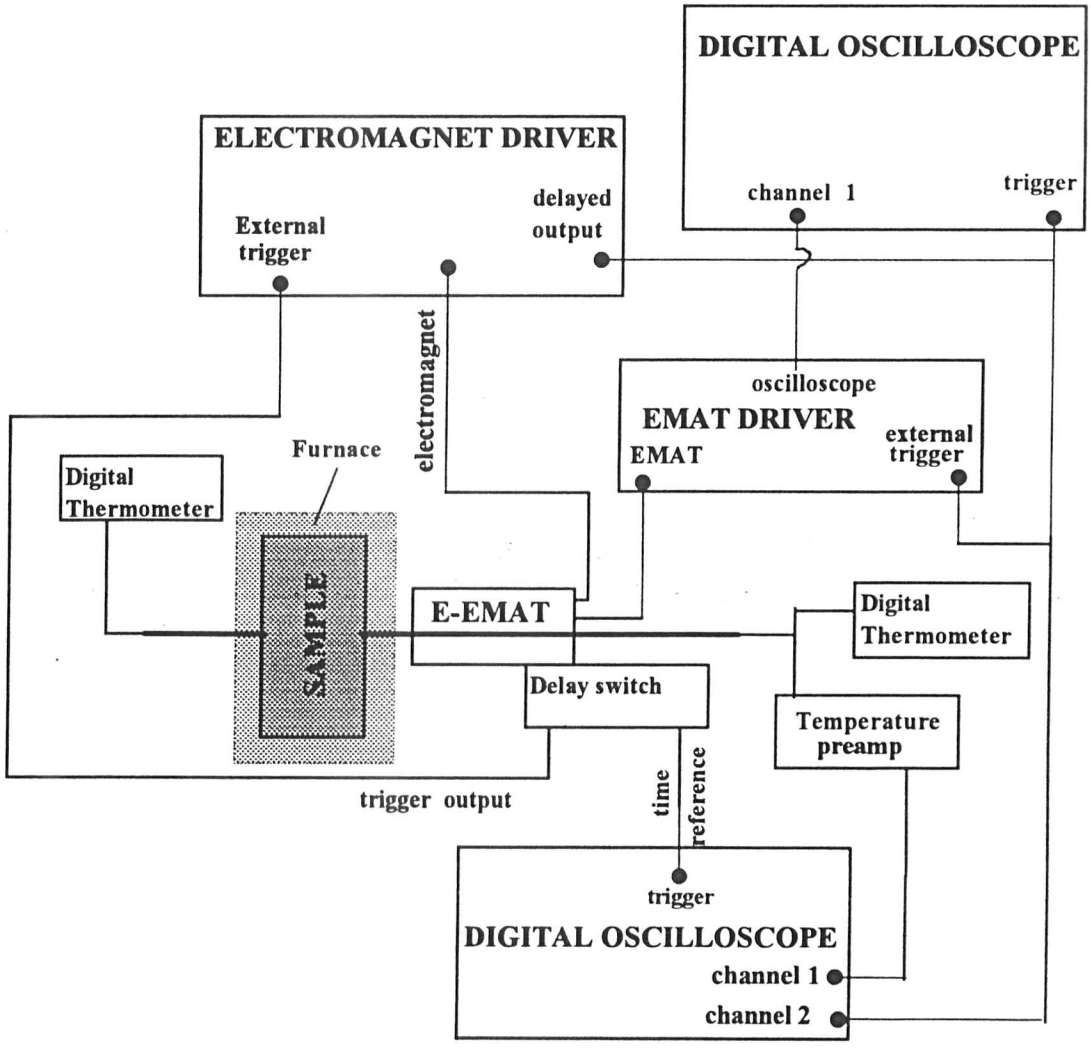

Figure-6.7: Schematic diagram of the experimental set up for ultrasound and sample temperature mesurements due to cooling in contact with a water-cooled E-EMAT.

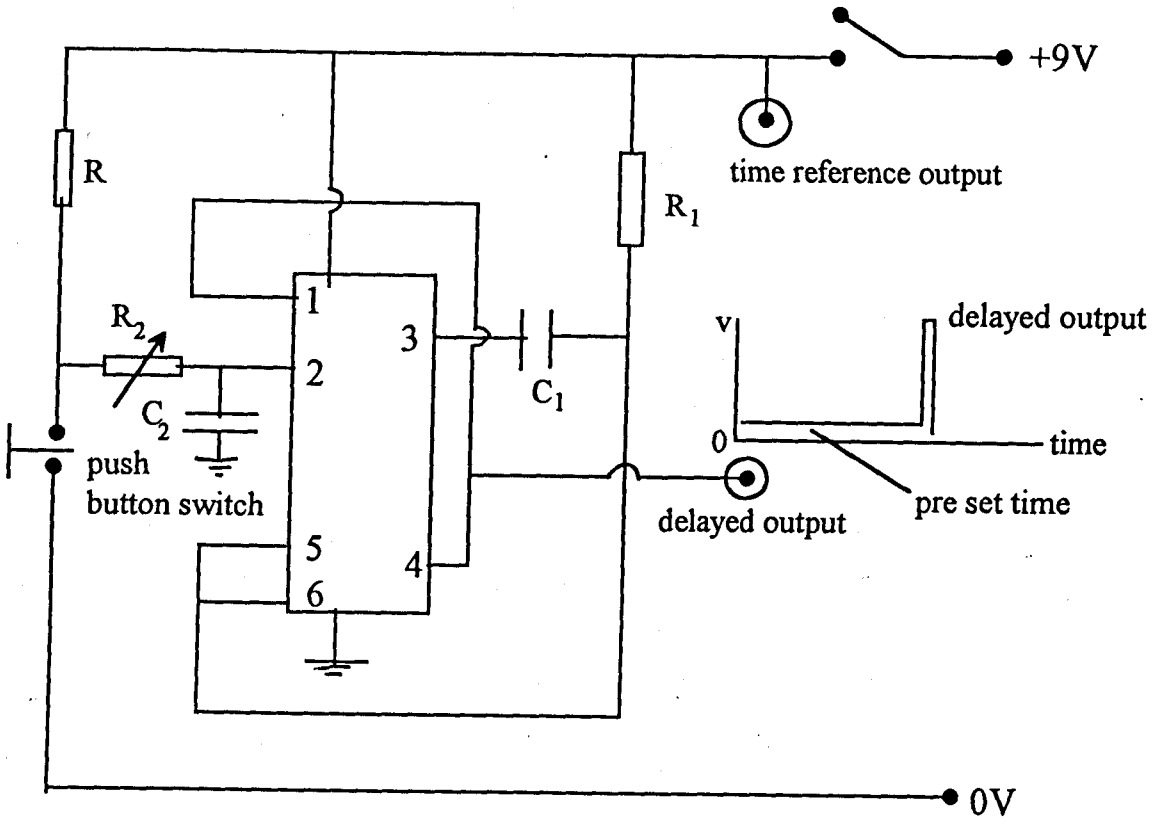

Figure-6.8: Schematic diagram of the delay timer, constructed based on the CD4001 i.c.. R_2 determines the pre set time before the out put triggers the electromagnet driver.

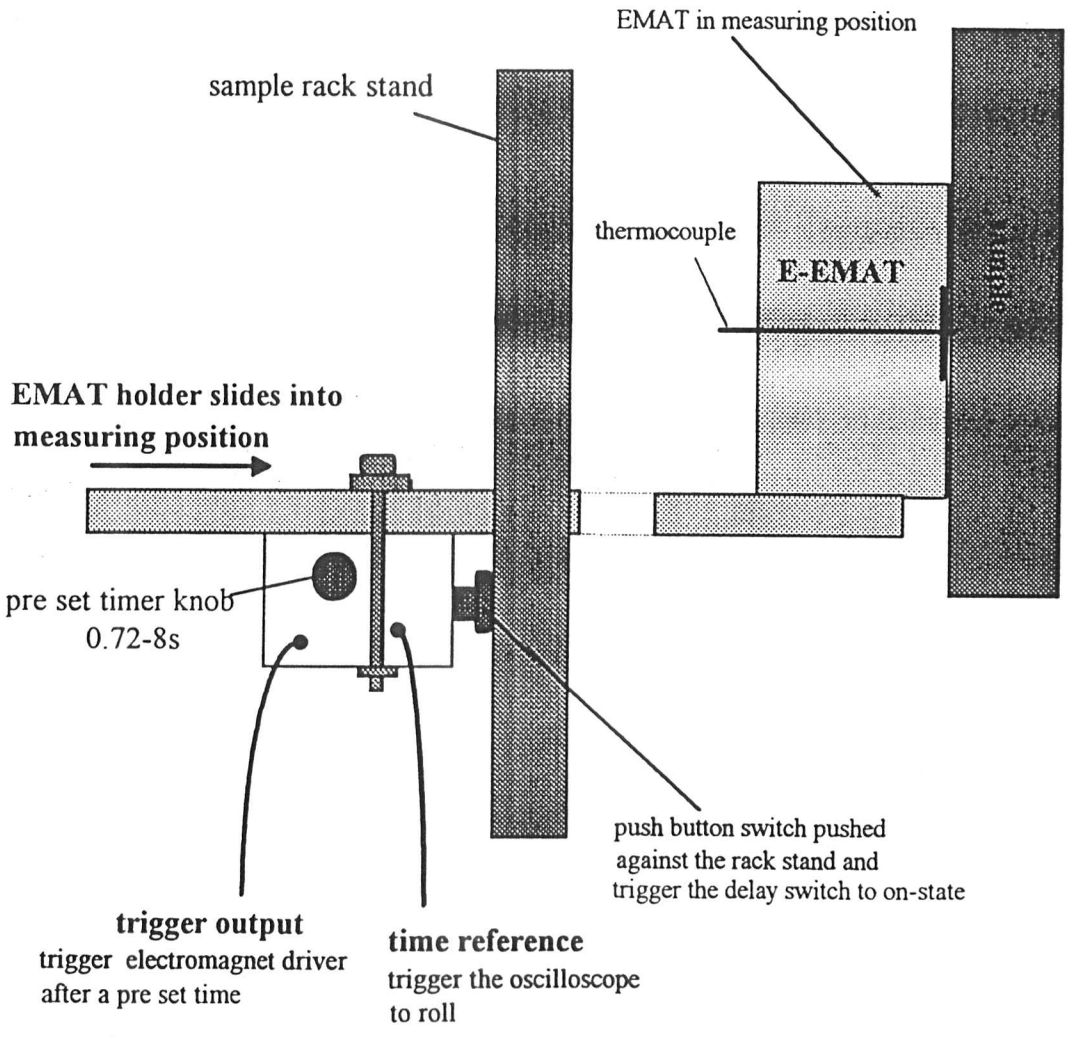

Figure-6.9: The positioning of delay timer switch. When the EMAT is slid into the measuring position, the push button switch is pushed against the sample rack stand and triggers the delay switch to on-state.

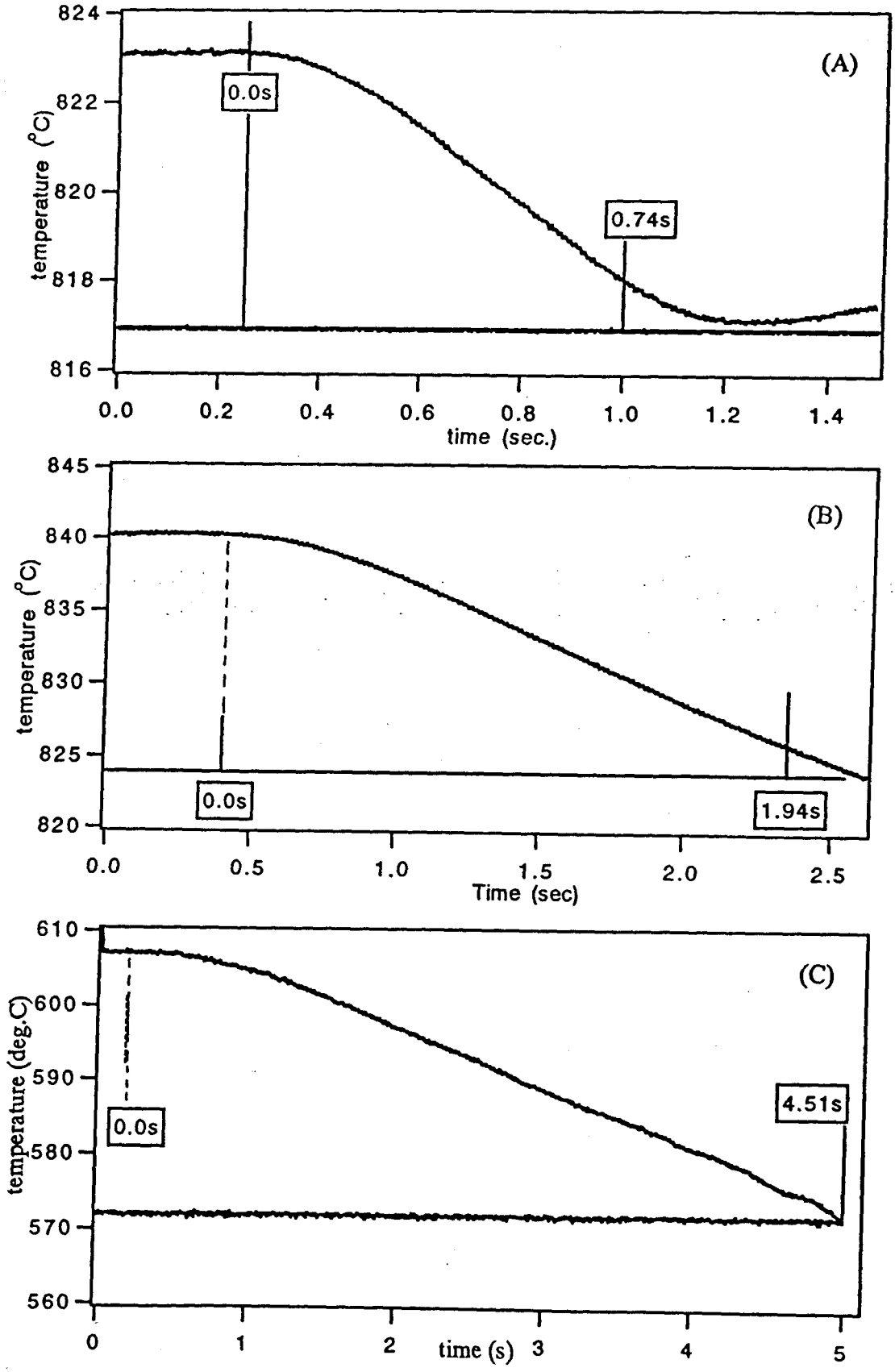

Figure-6.10: Reduction of the surface temperature of the sample after contact with a water-cooled E-EMAT in a pre set time;
(A)-at 823°C after 0.74s
(B)-at 840°C after 1.94s
(C)-at 607°C after 4.51s

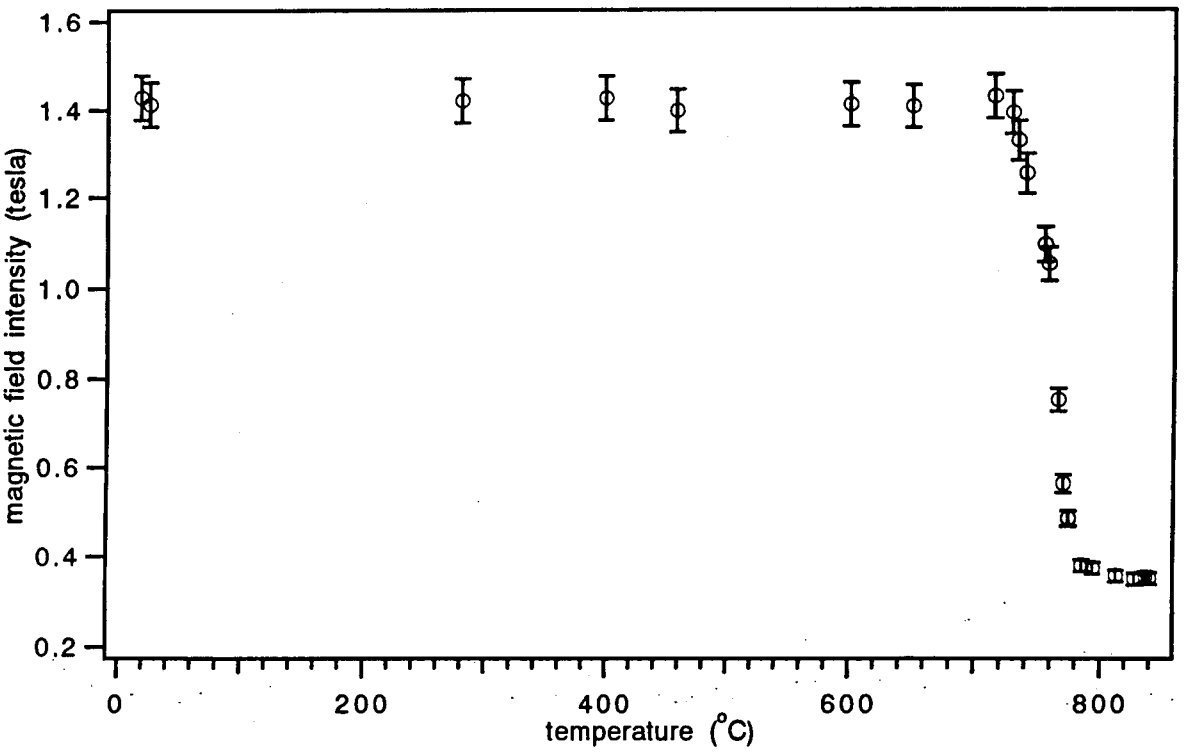

Figure-6.11: Temperature dependence of the magnetic field intensity in mild steel generated by E-EMAT.

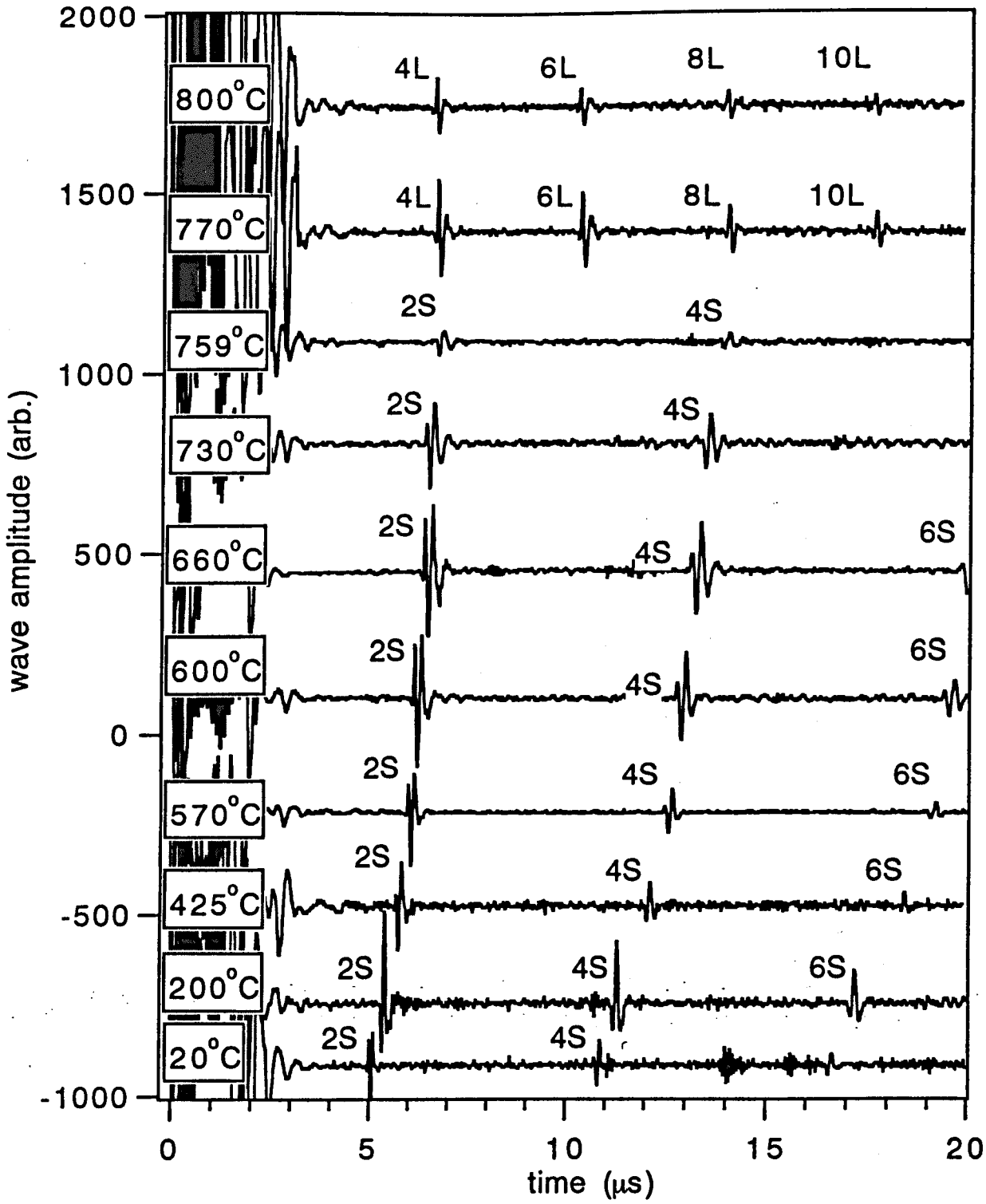

Figure-6.12: Pulse echo ultrasound waveforms in mild steel (10.5mm thickness) at elevated temperatures generated by E-EMAT.

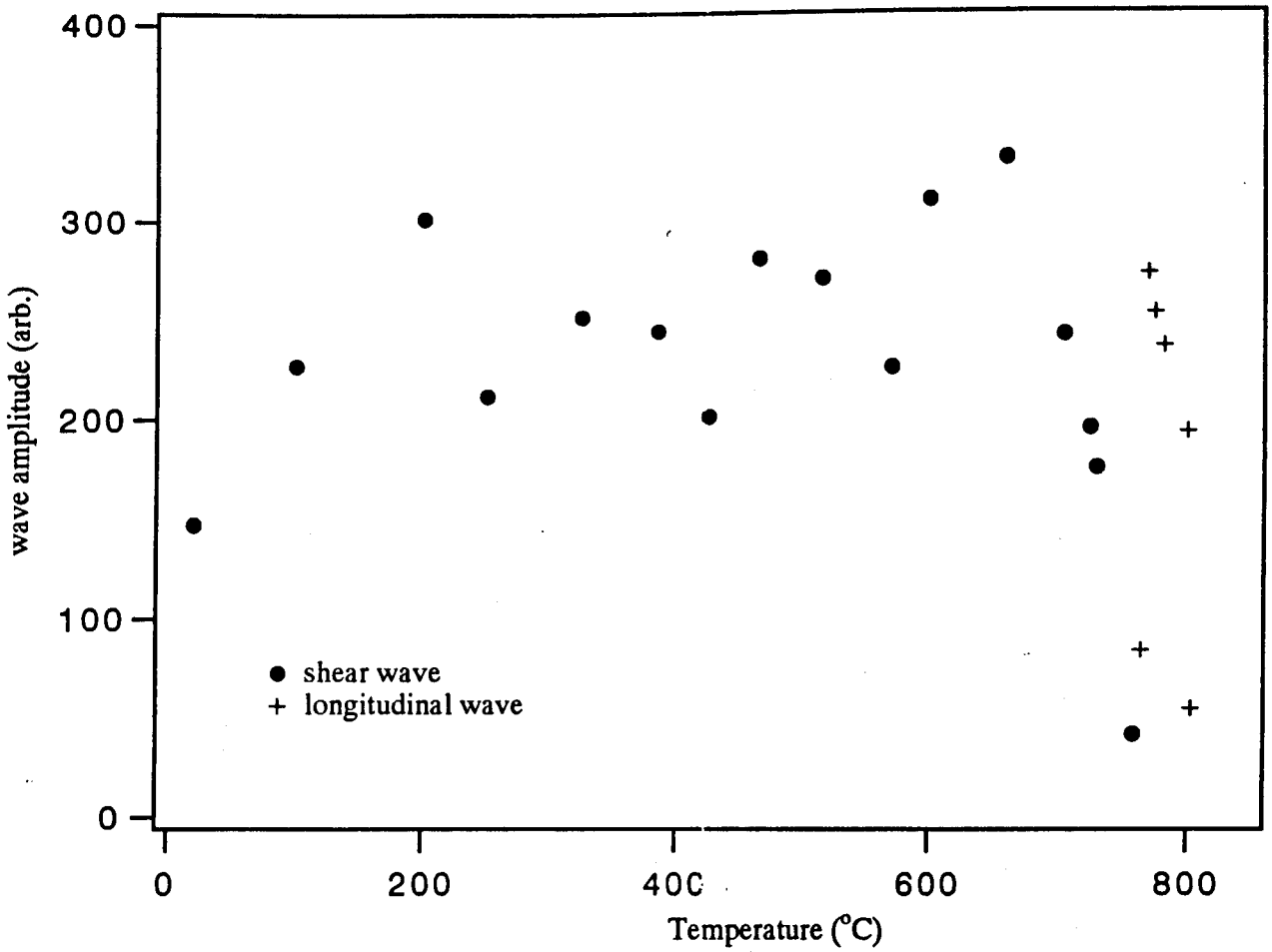

Figure-6.13: Temperature dependence of pulse echo ultrasound amplitude in mild steel generated by E-EMAT

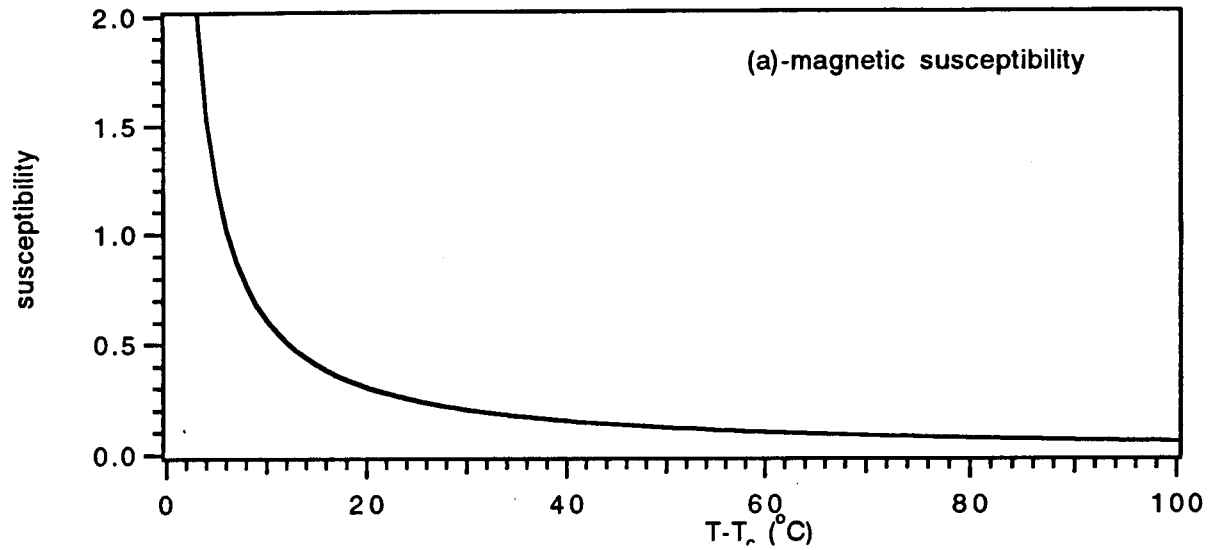

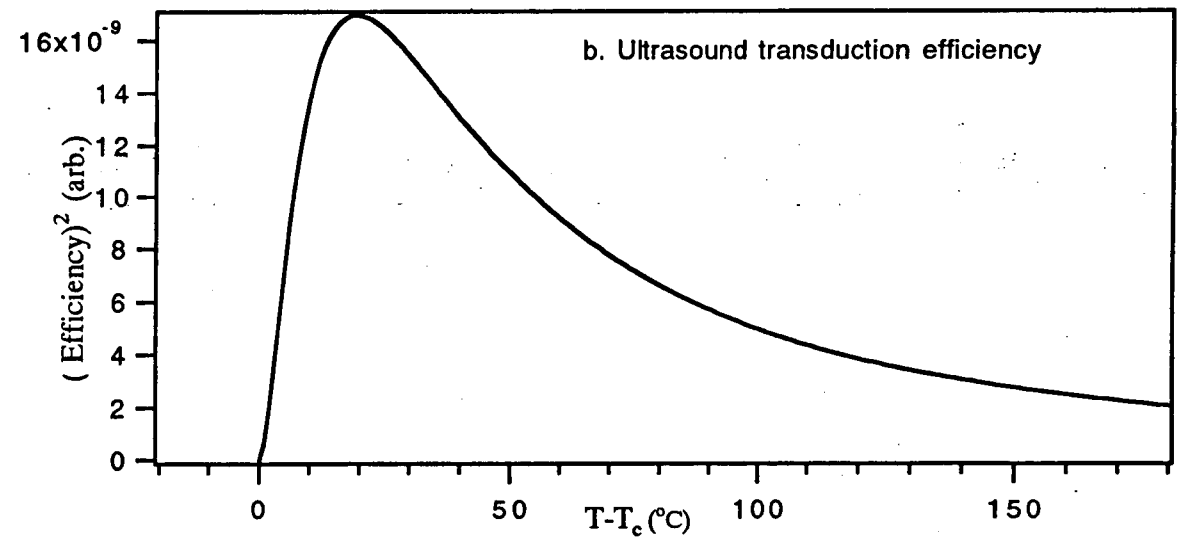

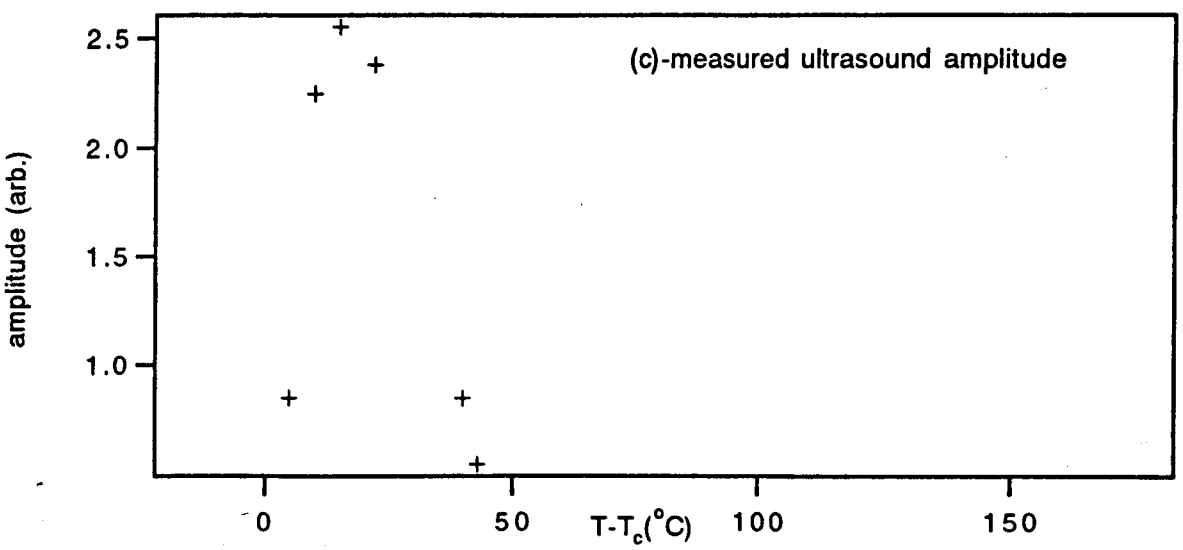

Figure-6.14: Temperature dependence of; (a)-the predicted magnetic susceptibility, (b) predicted ultrasound transduction efficiency due to the paraprocesses and (c)-measured longitudinal wave amplitude generated by E-EMAT on mild steel above the Curie point, T_c.

CHAPTER-7

Conclusions and Future Work

7.0 Introduction

The work in this thesis has demonstrated that non-contact laser/EMAT ultrasound systems, are capable of making non-contacting ultrasound measurements on hot steel. Measurements up to about 1000°C have been achieved using a send-receive laser-EMAT system where a water cooled concentric EMAT detector is positioned on the generation side, showing single sided inspection is feasible. Since no physical contact is needed, there is the potential that the sample could be assessed in a rapid scanning mode. The presence of surface roughness and oxide layers on the sample enhanced the sensitivity of the system, in particular at elevated temperatures. This promises that the non-contact laser-EMAT system developed in this work could be used for ultrasound thickness measurement on moving hot steel; in particular seamless extruded steel pipes on the production line. Measurements could be made on unprepared steel samples without the need of a good surface finish.

The non-contacting ultrasound system is sensitive to both shear and longitudinal waves. The EMAT was designed to generate shear waves and as a detector it is sensitive to both shear and longitudinal waves. The pulsed laser is capable of simultaneously generating both types of bulk wave. In this study, the thickness of steel pipe wall was determined from the transit time of the bulk waves between the sample's walls, using a calibrated ultrasound velocity-temperature dependence chart of the sample measured earlier. Measurements based on the shear wave pulses are most efficient at temperatures below 750°C. At higher temperatures the longitudinal wave gives better results. This is due to transduction nature of the shear wave EMAT on steel.

The ultrasound system comprised of a pulsed laser as the ultrasound generator. In this work we used both the Nd:YAG laser with wavelength $\lambda = 1.06\mu m$, energy output 400mJ, and also a CO_2 laser which has a wavelength, $\lambda = 10.6\mu m$, and 4J energy output. Pulsed lasers are capable of generating both the shear and longitudinal waves simultaneously and the wave amplitudes can be easily controlled by varying the energy density deposited onto the surface of the sample. At low energy density, the pulsed laser generates the shear wave through the thermoelastic mechanism. At a higher energy density or in mild ablation regimes, both shear and longitudinal waves are generated by the laser. In this work, we generated bulk waves in the mild ablation regime at temperatures below T_c, so that we could monitor both the shear and longitudinal waves simultaneously. At about T_c and higher temperatures, where the EMAT transduction efficiency has been reduced and the sample exhibits higher ultrasound attenuation, therefore a stronger ablation source was used so that a stronger ablative ultrasound source could be generated. In this temperature range, the measurements were made on the transit time of the longitudinal wave as the sensitivity of the EMAT for shear wave was very weak.

The EMATs are broad bandwith devices and have to be deployed close to the surface of metallic samples. The magnetic field for its operation could be provided either by a permanent magnet (P-EMAT) or an electromagnet (E-EMAT). These devices could be operated in pulse echo mode on hot steel up to a temperature of about 800°C. A strong enhancement of the longitudinal wave occurs at temperatures just above the Curie point of the sample, and rapidly decays at temperatures far above T_c. This feature is related to the nature of EMAT transduction in ferromagnetic materials at their magnetic phase transition. The EMATs could be used simply as the detector with pulsed laser as generator to much higher temperatures. The thesis also has demonstrated that the magnetic field from the E-EMAT can be easily monitored, non-contact, so that the magnetic state of the sample

could be assessed at elevated temperatures.

7.1 The EMAT Design

The P-EMAT has been demonstrated to be an efficient device for the generation and detection of ultrasound on steel within the above mentioned temperature range. As the system is to be used on ferromagnetic materials, there is a tendency that the ferromagnetic swarf and dirt may stick to the surface of the EMAT and thus reduce its performance. We have suggested the use of a E-EMAT that is capable of generating magnetic fields of above 1T on mild steel and which could be turned-off to avoid any ferromagnetic swarf and dirt accumulating on its surface and deteriorating its performance.

The EMATs were operated in momentary contact with the sample to generate or to detect the ultrasound waveforms and pulled out immediately after the waveform was captured. This was necessary to avoid excessive cooling of samples and also to protect the EMAT. The detection of pulsed echo ultrasound generated with the same EMAT could be made up to a temperature of about 800°C and was limited by the poor ultrasound transduction efficiency and high ultrasound attenuation in the sample.

The EMAT has been evaluated as the receiver to detect ultrasound generated either by the Nd:YAG laser or the CO_2 laser. The measurements were made on epicentre and most importantly in send-receive arrangement. The send-receive Nd:YAG laser-EMAT system has been used for the ultrasound measurement on mild steel up to about 1000°C. Below the Curie point, T_c, the detected waveforms were dominated by shear arrivals. The amplitude of these pulses decreases as the temperature approaches T_c and the longitudinal wave pulses begin to appear and dominate the waveforms at temperatures at and just above T_c. Above T_c, the amplitude of the longitudinal wave pulses decrease dramatically. However by increasing the laser energy incident on the surface of

the sample to generate a stronger ablative source, the signal amplitude could be detected at a reasonable amplitude.

Similar measurements were carried out using the CO_2 laser as the ultrasound generator. The measurements were made in thermoelastic, surface ablation and plasma breakdown regimes. The incidence of sufficiently high laser energy onto the sample surface forms a plasma that comprise particles from the sample surface and /or from the air at the sample surface. The plasma rapidly expands away from the point of its origin and generating a net resultant force normal to the sample surface and hence strong longitudinal waves. The deposition of higher laser energy density onto a small volume of air inside the electromagnet in the vicinity of the sample surface may cause the ionisation of the air which leads to formation of plasma breakdown. The result is the generation of an air blast wave inside the electromagnet that occurred further away from the sample surface. In such a case, resonance could occur and lead to the saturation of the receiver. At high temperatures this problem became severe as the threshold of ionisation of the air inside the electromagnet reduces and the probability of the plasma breakdown occurring further away from the sample increases. The detected waveforms are similar to that generated by the Nd:YAG laser. The measurements were carried out up to about 800°C.

The high temperature operation of the EMAT on hot steel was limited by the loss of transduction efficiency inherent in the material. This could be caused by loss of magnetisation and the magnetostriction effect as well as the decrease in material conductivity and permeability. At low temperatures these effects may reinforce the Lorentz force mechanism in the generation and detection of the ultrasound. On the other hand, above T_c, the ultrasound transduction only originated from the Lorentz force mechanism. At temperatures far above T_c, the wave amplitude was weaker due to the reduction in conductivity and magnetic permeability and the intensity of the operating magnetic field

that impairs the EMAT transduction efficiency as well as increases the ultrasound attenuation in the sample. The measurement was discontinued once the EMAT failed to detect any ultrasound signal. It is suggested that the laser-EMAT system can be used for non-contact ultrasound measurements of steel using shear waves at temperatures below 750°C, since up to this temperature, the system is sensitive to shear waves. At higher temperature however, better measurements can be made using longitudinal waves.

It has been demonstrated that momentary contact between the sample at elevated temperature and the water cooled EMAT does not significantly alter the temperature of the bulk sample and thus the ultrasound velocity in the sample. The cooling effect was superficial and the temperature changes are also insignificant compared to the sample temperature. The change in ultrasound velocity introduced by small changes in sample temperature lies within the error in wave velocity measurement. A disadvantage of the system developed here is that the EMAT could not stay long in the vicinity of the hot sample, in particular at temperatures above 700°C.

7.2 Magnetisation Monitoring

The time varying magnetic field generated by the pulsed electromagnet in the E-EMAT was monitored by a single loop coil bonded beneath the electromagnet pole. The output provides information about the magnetisation of the sample underneath. The magnetic field intensity is about 1.4T when the electromagnet is positioned on the surface of the ferromagnetic sample such as mild steel, and 0.35T on a non-magnetic sample. In mild steel the intensity of the generated magnetic field was below its saturation magnetisation (over 2T), and this leads to the magnetisation-temperature curve showing a step occurring between 740°C to 760°C where the field decreases from 1.4T to 0.35T at T_c. The magnetisation field intensity remains at 0.35T above T_c. The enhancement of the

longitudinal wave just above the Curie point is not fully understood; it may be caused by a redistribution and reorientation of the magnetic flux in a thin ferromagnetic skin layer formed due to cooling by the EMAT or could be due to strong volume magnetostriction near the magnetic phase change.

7.3 Performance of the Laser Generation of Ultrasound System

We have demonstrated that both types of pulsed laser, Nd:YAG laser and CO_2 laser offer versatile techniques for the non-contact generation of ultrasound in hot steel. In the case of the send-receive technique, the Nd:YAG laser has more advantages than the CO_2 laser as it is capable of generating high intensity ultrasound without the risk of saturating the response of the receiver. The passage of the Nd:YAG laser beam through the EMAT did not interfere with the EMAT response. The limitation of the Nd:YAG laser is that it is less eye safe than the CO_2 laser where in the former the beam wavelength lies in the near infra-red range and requires special eye protection whereas the CO_2 laser the beam could be absorbed effectively by a few millimetres of perspex. This makes the CO_2 laser more industrially friendly and as a result it has been used widely in industry.

7.4 Suggested Future Work.

The ultrasound transduction on steel by EMAT is sensitive to electrical , magnetic properties, the microstructure and also surface condition of the sample. In this thesis we have partly studied the transduction of ultrasound on steel by EMAT at elevated temperature where the sample undergoes a magnetic phase transition at the Curie point. We have also studied the ultrasound transduction in ferromagnetic steel at room temperature at low magnetic field where in some samples, the magnetostrictive effect is dominant. This was demonstrated by the deviation of their amplitude-B^2 curves from a

linear relationship. For a purely Lorentz force mechanism, such as exhibited by non-magnetic metals, the amplitude-B^2 curve shows a linear relationship and passes through the origin. The results presented here however do not provide a complete picture of the ultrasound transduction in steel by EMAT. Further characterisation of EMAT transduction on steel is required to improve performance and to realise industrial applications.

Pulsed electromagnetic EMAT (E-EMAT) performance on steel at elevated temperatures could be improved both in its design and the receiver electronics. The electromagnet design could be improved to generate higher magnetic field intensity, using a larger electromagnet and/or passing higher magnetising current. A more powerful power supply to energise the electromagnet is essential. The cooling system of the EMAT could be further improved to allow the EMAT to be in close contact with the hot sample for prolonged periods without the risk of being destroyed. A fine cooling water groove could be made beneath the rf coil on the surface of the electromagnet. The rf coil could also be potted in a high temperature adhesive and protected with a material that could withstand a higher thermal gradient, such as silicon nitride.

Ultrasound generation by CO_2 laser inside the E-EMAT cavity is affected by the presence of dust particles that seed the creation of plasma breakdown of air. This may occur far away from the surface of the sample causing an inefficient generation of ultrasound. This 'seeding' of the plasma becomes more of a problem as the temperature increases. A possible technique which may improve the generation by CO_2 laser inside a confined cavity may be to pre-ionise the sample prior to irradiation such that the electrons seeding could be brought to the sample surface. The pre-ionisation may be created by an initial pulse of ultra violet radiation to excite photoelectrons from the sample and seed the plasma creation on the surface of the sample. Additional pre-amp protection would be

need to prevent electronic paralysis

Send-receive laser-EMAT systems using a Nd:YAG laser as the generator could be made smaller or adapted to a fibre optic laser delivery system and operated at higher repetition rates. The repetition rate of the pulsed magnetic field could be increased by using a larger power supply to energise the electromagnet sufficiently rapidly. The system may also require further refinement to be used for the detection of defects such as porosity, surface cracks, etc., at elevated temperatures. Since EMATs could be designed to generate a steered beam, a send-receive laser-EMAT system could be used to monitor and assess the solidification of weld pool and heat effected zone of the weld metal. The EMAT will detect the ablative laser generated ultrasound on the molten weld metal and reflected from the back wall of the parent metal. In general, laser-EMAT systems could be used as a tool for non-destructive testing of metals at elevated temperature or in other hostile environments.